mgr Karolina Orzeł-Gajowik

Znaczenie mikroRNA w uszkodzeniu bariery krew-mózg w encefalopatii wątrobowej

Rozprawa na stopień naukowy doktora
w dziedzinie nauk medycznych i nauk o zdrowiu
w dyscyplinie nauki medyczne

Promotor: Prof. dr hab. n. med. Magdalena Zielińska

Polska Akademia Nauk

Postępowanie w sprawie nadania stopnia doktora
w Instytucie Medycyny Doświadczalnej i Klinicznej
im. Mirosława Mossakowskiego PAN

Warszawa 2024

Badania finansowane przez:

Narodowe Centrum Nauki (NCN-2015/19/B/NZ4/01902)

Europejski Fundusz Społeczny (EFS-POWR.03.02.00-00-1028/17-00)

Fundusz Badań Własnych IMDiK PAN (FBW 031)

NARODOWE CENTRUM NAUKI

Składam serdeczne podziękowania Pani Profesor dr hab. n. med. Magdalenie Zielińskiej, za nieocenione wsparcie, na każdym kroku mojej pracy. Dziękuję za nieustanne zachęcanie mnie do rozwoju, pomoc w odkrywaniu nowych ścieżek badawczych. Jestem wdzięczna szczególnie za wielokrotne dawanie mi szans na poprawę i doskonalenie mojego warsztatu. Dziękuję za indywidualne podejście, które umożliwiło mi rozwój nie tylko jako naukowca, ale także jako człowieka;

Panu Prof. dr hab. Janowi Albrechtowi za dostarczanie ciekawych dyskusji oraz najnowszej literatury naukowej;

Dr hab. Monice Szelidze za porady metodologiczne, szczególnie uratowanie mojej pierwszej reakcji RT-PCR;

Dr Marcie Obarze-Michlewskiej za wprowadzenie w świat badań behawioralnych, oraz stawianie czoła sceptykom, którzy nie wierzą, że można przeżyć bez steka na talerzu;

Dr n. med. Mariuszowi Popkowi za Twoje nieustające wsparcie, lojalność i przyjaźń. Dziękuję za każde nasze merytoryczne (i te mniej) rozmowy przy kawie, które otwierały przede mną nowe perspektywy i pozwalały spojrzeć na problem z innej strony. Dziękuję za tony samoprzylepnych karteczek i zeszytów, na których mogłam zamieszczać pomysły do niniejszej pracy;

Małgosi Bogacińskiej-Karaś za wprowadzenie w świat hodowli komórkowej, dziękuję Ci, że nawet ręka w gipsie nie spowolniła moich doświadczeń;

Kamili Szumskiej za ciągłą gotowość do pomocy, silny charakter i ciepło, które na swój sposób wprowadzasz do Naszego Zespołu;

Dorocie Rycko, za ludzką życzliwość;

Zuzannie Sulej oraz Joannie Buczkowskiej, za ciepło i dobre słowo;

Dr n. med. Krzysztofowi Milewskiemu, dziękuję za nasze rozmowy, które prowadziły mnie do głębszych refleksji zarówno w sferze zawodowej, jak i prywatnej;

Inez Fręśko, dziękuję za utrzymywanie przez wiele lat rodzinnej atmosfery w Zakładzie;

Dr n. med. Markowi Pawlikowi, za naukę patrzenia na jasną stronę życia;

Moim Mamom, Basi i Justynie, za czułość, ukazanie wielu aspektów życia i walki o nie. Tacie, za pokazanie świata i rozbudzeniu ciekawości;

Kurczakowi, że Osoby takie jak Ty, istnieją;

Tomkowi, współautorowi niniejszej pracy, mojej Osobie, oferującej, niezależnie od okoliczności, swoje wsparcie i nieskończoną cierpliwość.

„Przepraszam, ale jestem naukowcem i moim obowiązkiem jest być sceptycznym”

Sheldon Cooper, *The Bing Bang Theory*, Chuck Lorre i Bill Prady, sezon 2, odcinek 4, CBS, 2009.

Wyniki zamieszczone w rozprawie zostały opublikowane w pracach:

PUBLIKACJA I

Orzeł-Gajowik K., Milewski K, Zielińska M. miRNA-ome plasma analysis unveils changes in blood-brain barrier integrity associated with acute liver failure in rats. Fluids Barriers CNS. 2023 Dec 8;20(1):92. doi: 10.1186/s12987-023-00484-7. PMID: 38066639; PMCID: PMC10709860.

PUBLIKACJA II

Milewski K, Orzeł-Gajowik K., Zielińska M. Mitochondrial Changes in Rat Brain Endothelial Cells Associated with Hepatic Encephalopathy: Relation to the Blood-Brain Barrier Dysfunction. Neurochem Res. 2024 Jun;49(6):1489-1504. doi: 10.1007/s11064-022-03698-7. Epub 2022 Aug 2. Erratum in: Neurochem Res. 2024 Jun;49(6):1505. doi: 10.1007/s11064-022-03780-0. PMID: 35917006; PMCID: PMC11106209.

PUBLIKACJA III

Orzeł- Gajowik K.; Gajowik, T.; Rówienicz, Ł.; Zielińska, M. The Ohm-Azing Custom-Made Transendothelial Electrical Resistance Measuring Device (and Why Is It a Current Sensation?). Sensors and Actuators B: Chemical 2024, 404, 135192, doi: 10.1016/j.snb.2023.135192.

- Złożonego patentu pod numerem P.442747

PUBLIKACJA IV

Orzeł-Gajowik K.; Milewski, K.; Zielińska, M. Insight into microRNAs-Mediated Communication between Liver and Brain: A Possible Approach for Understanding Acute Liver Failure? Int. J. Mol. Sci. 2022, 23, 224. https://doi.org/10.3390/ijms23010224

Wyniki nieopublikowane są podstawą manuskryptu wysłanego do recenzji:

Orzeł-Gajowik K.; Milewski, K.; Obara-Michlewska, M.; Ellert-Miklaszewska, A.; Karpińska, A.; Kwapiszewska, K.; Zielińska, M. Unraveling Hyperammonemia Induced Brain Saga: The Role of miRNA-183-5p in the Endothelial Senescence and Cerebrovascular Density Decline. Free Radical Biology & Medicine (FRBM-D-24-01297).

SPIS TREŚCI

WYKAZ SKRÓTÓW 7
STRESZCZENIE 9
SUMMARY 11
INNOWACYJNOŚĆ ROZPRAWY 12
WSTĘP 13
Klasyfikacja encefalopatii wątrobowej 13
Diagnostyka encefalopatii wątrobowej 14
Patomechanizm obrzęku 15
Efekty toksyczności amoniaku w komórkach śródbłonka 18
HIPOTEZA 20
CEL PRACY 20
MATERIAŁY I METODY 21
Modele 21
Metody 22
Konstrukcja i budowa urządzenia do pomiaru rezystancji monowarstwy komórek 28
OMÓWIENIE WYNIKÓW 29
Ad. Cel szczegółowy 1 29
Ad. Cel szczegółowy 2 29
Ad. Cel szczegółowy 3 30
Ad. Cel szczegółowy 4 31
Ad. Cel szczegółowy 5 32
PODSUMOWANIE WYNIKÓW 34
DYSKUSJA 35
WNIOSKI 41
LITERATURA 42
PUBLIKACJE 59
Wskaźnik oddziaływania 59
Publikacja 1 60
Publikacja 2 79
Publikacja 3 95
Publikacja 4 106
Oświadczenia autorów 162

WYKAZ SKRÓTÓW

ADC	przetwornik analogowo-cyfrowy (ang. analog to digital converter)
ADMA	asymetryczna dwumetyloarginina (ang. asymmetric dimethylarginine)
ALF	ostra niewydolność wątroby (ang. acute liver failure)
ALT	aminotransferaza alaninowa (ang. alanine aminotransferase)
Analiza GO	analiza ontologii genów (ang. gene ontology analysis)
AST	aminotransferaza asparaginianowa (ang. aspartate aminotransferase)
BBB	bariera krew-mózg (ang. blood-brain barrier)
cGMP	cykliczny guanozyno-3′,5′-monofosforan (ang. cyclic guanosine monophosphate)
CPM	liczba zmapowanych odczytów na milion (ang. counts per million)
CSF	płyn mózgowo-rdzeniowy (ang. cerebrospinal fluid)
EB	błękit Evansa (ang. Evans blue)
EDTA	kwas wersenowy (ang. ethylenediaminetetraacetic acid)
EEG	elektroencefalogram (ang. electroencephalogram)
EVs	pęcherzyki zewnątrzkomórkowe (ang. extracellular vesicles)
HE	encefalopatia wątrobowa (ang. hepatic encephalopathy)
FCS	metoda korelacji fluorescencji (ang. fluorescence correlation spectroscopy)
FITC	izotiocyjanian fluoresceiny (ang. fluorescein isothiocyanate)
GLAST	transporter glutaminianu/asparaginianu (ang. glutamate aspartate transporter)
GS	syntetaza glutaminy (ang. glutamine synthetase)
HIEC-6	linia komórek śródbłonka jelita ludzkiego (ang. human intestinal endothelial cells line 6)
Hsp27	białka szoku cieplnego 27 (ang. heat shock protein 27)
i.p.	podanie dootrzewnowe (ang. intraperitoneal)
ICAM-1	międzykomórkowa molekuła adhezyjna-1 (ang. intercellular adhesion molecule 1)
IL	interleukina (ang. interleukin)
JAM	cząsteczka adhezyjna (ang. junctional adhesion molecule)
KEGG	Kyoto Encyclopedia of Genes and Genomes (ang. Kyoto Encyclopedia of Genes and Genomes)
miRNA	mikroRNA (ang. microRNA)
MMP	metaloproteinazy macierzy zewnątrzkomórkowej (ang. matrix metalloproteinases)
MPTP	zjawisko zmiany przepuszczalności błon mitochondrialnych związane z otwarciem megakanałów (ang. mitochondrial permeability transition pore)
NGS	sekwencjonowanie nowej generacji (ang. next-generation sequencing)
NOS	syntaza tlenku azotu (ang. nitric oxide synthase)
NVU	jednostka nerwowo-naczyniowa (ang. neurovascular unit)
OA	octan amonu (ang. ammonium acetate)
PMEC	komórki śródbłonka mikronaczyń mózgu szczura (ang. primary brain microvascular endothelial cells)

PBMEC	pierwotne komórki śródbłonka mikronaczyń mózgu (ang. primary brain microvascular endothelial cells)
RBE4	linia komórek śródbłonka mózgu szczura (ang. rat brain endothelial cell line 4)
ROS	reaktywne formy tlenu (ang. reactive oxygen species)
RT-qPCR	metodą ilościowej reakcji PCR w czasie rzeczywistym (ang. real-time quantitative polymerase chain reaction)
SASP	fenotyp sekrecyjny związany senescencją (ang. senescence-associated secretory phenotype)
SDMA	symetryczna dwumetyloarginina (ang. symmetric dimethylarginine)
SF	fluoresceina sodu (ang. sodium fluorescein)
snRNA	mały jądrowy RNA (ang. small nuclear RNA)
TAA	tioacetamid (ang. thioacetamide)
TEM	transmisyjna mikroskopia elektronowa (ang. transmission electron microscopy)
TJ	połączenia ścisłe (ang. tight junctions)
TNFα	czynnik martwicy nowotworów α (ang. tumor necrosis factor α)
VCAM	cząstka adhezyjna śródbłonka (ang. vascular cell adhesion molecule)
VEGF	czynnik wzrostu śródbłonka naczyniowego (ang. vascular endothelial growth factor)
vWF	czynnik von Willebranda (ang. von Willebrand factor)
WB	metoda Western blot (ang. Western blot)
ZO	białka kompleksu zonula occludens (ang. zonula occludens proteins)
β-gal	β-galaktozydaza (ang. beta-galactosidase)
γGTP	gamma-glutamylotranspeptydaza (ang. gamma-glutamyl transpeptidase)

STRESZCZENIE

Encefalopatia wątrobowa (ang. hepatic encephalopathy; HE) ujawniająca się w wyniku uszkodzeń wątroby stanowi istotny problem epidemiologiczno - ekonomiczny, który dotyczy ~1 miliona mieszkańców krajów UE. Najpoważniejszym objawem klinicznym jest obrzęk mózgu prowadzący w większości przypadków ostrej i w stanach zaostrzenia przewlekłej HE, do zgonu pacjenta. Mechanizm obrzęku mózgu w HE jest głównie następstwem obrzmienia astrocytów, jednak udział czynnika naczyniowego, związanego z dysfunkcją bariery krew-mózg (ang. blood - brain barrier; BBB) wydaje się mieć również istotne znaczenie. Biorąc pod uwagę liczbę współgrających elementów, wiedza dotycząca uszkodzenia i deregulacji składowych BBB wymaga uszczegółowienia.

W przebiegu procesów patologicznych coraz częściej zwraca się uwagę na udział jednoniciowych, niekodujących RNA - mikroRNA (ang. microRNA; miRNA), postawiono więc hipotezę zakładającą, że jedną z przyczyn uszkodzenia BBB w HE są zmiany profilu miRNA.

Celem dysertacji była analiza profilu miRNA w osoczu i korze mózgowej szczurów z hiperamonemią prostą i szczurów z ostrym uszkodzeniem wątroby oraz wykazanie molekularnego podłoża zmian w komórkach śródbłonka naczyniowego mózgu, głównego elementu tworzącego BBB.

Doświadczenia wykonano wykorzystując (1) modele *in vivo* tj. szczurzy model hiperamonemii i szczurzy model ostrego uszkodzenia wątroby (2) modele *in vitro* tj. linię komórek śródbłonka naczyń mózgu szczura (ang. rat brain endothelial cell line; RBE4) i pierwotne hodowle komórek śródbłonka naczyń mózgu szczura (ang. primary brain microvascular endothelial cells; PBMEC), oraz (3) izolowane naczynia mózgu szczura.

Na podstawie analizy profilu miRNA osocza i kory mózgowej szczurów modelowych, zidentyfikowano odpowiednio w modelu hiperamonemii prostej 35 i 128, a w modelu ostrego uszkodzenia wątroby 338 i 345 zmienionych miRNA, zaś analiza bioinformatyczna, wykorzystująca dostępne narzędzia oraz bazy danych wykazała potencjalny związek 2 miRNA z genami kodującymi białka związane strukturalnie i funkcjonalnie z BBB (okludynę, integrynę 1β). W ocenie morfologicznej BBB wykazano uszkodzenia obejmujące zmiany morfologii komórek śródbłonka, korelujące ze zwiększoną przepuszczalnością BBB. W badaniach *in vitro*, w komórkach śródbłonka naczyń mózgowych, analizowano zmiany poziomu ekspresji badanych białek, ze wskazaniem ich znaczenia funkcjonalnego, wykazując udział zidentyfikowanych miRNA-122-5p i miRNA-183-5p w obniżeniu poziomu ekspresji odpowiednio: okludyny i integryny 1β.

Oceniona w modelu OA zmniejszona gęstość naczyń mózgowych sugerowała zmienione unaczynienie mózgu, porównywalne z unaczynieniem mózgu szczurów 12 miesięcznych, sugerując zmiany charakteryzujące starzenie normatywne. Zmieniony fenotyp komórek śródbłonka zweryfikowano w badaniach *in vitro*, wykazując cechy charakterystyczne dla procesu starzenia.

Skonstruowano, wykonano i przetestowano autorski system do pomiaru wartości rezystancji elektrycznej, służący ocenie integralności komórkowych modeli BBB w czasie rzeczywistym. Wartości pomiarów uzyskane w testach komórkowych były niezależne od zmian pH i temperatury, cechowały się wyższą dokładnością i precyzją, dlatego urządzenie wydaje się być odpowiednim narzędziem do badań toksyczności związków / leków w ocenie funkcji barier biologicznych.

Podsumowując, wyniki dysertacji poszerzają wiedzę na temat patomechanizmu uszkodzeń BBB w HE, w szczególności komórek śródbłonka. W kontekście dysfunkcji wątroby, badania wskazują na znaczenie miRNA w komunikacji na osi wątroba-mózg. Wyniki badań dostarczają nowych danych na temat roli miRNA w regulacji funkcji BBB, co może mieć potencjalne zastosowanie w diagnostyce i terapii zaburzeń neurologicznych związanych z chorobami wątroby. Konstrukcja autorskiego systemu do pomiaru rezystancji warstwy komórek, stanowi wartość interdyscyplinarną dysertacji.

SUMMARY

Hepatic encephalopathy (HE) develops, due to liver damage and represents a significant epidemiological and economic burden affecting approximately 1 million EU citizens. Brain edema is the most severe clinical symptom, which, in most cases of acute and overt chronic HE, leads to patient death. The mechanism of brain edema in HE primarily results from astrocyte swelling; however, the contribution of vascular factors related to the impairment of the blood-brain barrier (BBB) function also seems significant. However, knowledge of BBB dysfunction and HE damage is far from being complete, considering the number of interacting elements.

In pathological processes, increasing attention has been paid to the role of single-stranded, non-coding RNAs - microRNAs (miRNAs). Therefore, we formulated a hypothesis that the possible cause of the BBB damage in HE is miRNA profile changes that regulate the BBB. The dissertation aimed to analyze the miRNA profile in plasma and brain cortex of rats with simple hyperammonemia and rats with acute liver failure, and to demonstrate the molecular basis of changes in endothelial cells of brain vessels, the main component of the BBB.

Experiments were conducted using (1) a rat model of hyperammonemia and a rat model of acute HE, (2) *in vitro* models, including a rat brain endothelial cell line (RBE4) and primary brain microvascular endothelial cells (PBMEC), and (3) isolated rat brain vessels. Based on the analysis of the miRNA profile in the plasma and brain cortex of the rat's model, 35 and 128, as well as 338 and 345 altered miRNAs were identified, respectively. Bioinformatic analysis using available tools and information from databases indicated a potential association of 2 altered miRNAs with genes encoding proteins structurally and functionally related to the BBB (occludin, integrin 1β).

Morphological assessment of the BBB showed damage involving changes in endothelial cell morphology correlating with increased BBB permeability, at the cellular level, changes in the expression levels of studied proteins were observed, indicating their functional significance. The involvement of identified miRNA-122-5p and miRNA-183-5p in the reduced expression of occludin and integrin 1β in brain endothelial cells was demonstrated. The decreased density of brain microvessels observed in the acute liver failure model suggested disturbances in brain vascularization comparable to that of 12-month-old rats, indicating changes characteristic of normative aging.

A custom system for resistance measuring was constructed, implemented, and tested, serving to assess the integrity of cellular BBB models in time. The measurement was more accurate and independent of pH and temperature fluctuations, making the device a suitable tool for toxicity studies of compounds/drugs when evaluating biological barrier functions. This result adds interdisciplinary value to the dissertation.

In summary, the research expands our understanding of HE pathomechanism related to BBB damage, particularly endothelial cells. In the context of liver dysfunction, the study highlights the importance of miRNA in liver-brain axis communication. The results provide new insights into the role of miRNAs in regulating BBB function, which may have potential applications in the diagnosis and/or therapy of acute and chronic neurological disorders associated with liver diseases.

INNOWACYJNOŚĆ ROZPRAWY

1. Analiza miRNA osocza i kory czołowej mózgu szczurów z hiperamonemią prostą i ostrym uszkodzeniem wątroby, identyfikująca miRNA, które korelowały z białkami związanymi z dysfunkcją bariery krew-mózg *in vivo* i *in vitro*.
2. Badania funkcjonalne bariery krew-mózg oraz identyfikacja zmian morfologicznych w analizowanych modelach.
3. Wykazanie zmniejszonego unaczynienia mózgu szczura w warunkach hiperamonemii, przypominającego zmiany obserwowane w starzeniu normatywnym oraz zmienionego fenotypu komórek śródbłonka naczyń mózgowych szczura.
4. Wykonanie i przetestowanie nisko-kosztowego, precyzyjnego i konfigurowalnego autorskiego systemu pomiarowego do mierzenia w czasie rzeczywistym wartości rezystancji elektrycznej warstwy komórek śródbłonka/nabłonka tworzących barierę. Urządzenie stanowi efekt interdyscyplinarny rozprawy i jest przedmiotem złożonego wniosku patentowego o numerze zgłoszenia P.442747.

WSTĘP

Encefalopatie hiperamonemiczne to heterogenna etiologicznie grupa schorzeń, spośród których encefalopatia wątrobowa (ang. hepatic encephalopathy; HE) jest diagnozowana najczęściej. HE rozwija się w wyniku dysfunkcji wątroby o różnym nasileniu, w skutek czego dochodzi do systemowej akumulacji szeregu toksyn, przede wszystkim amoniaku [1]. Hiperamonemia definiuje stan metaboliczny organizmu, którego bezpośrednią przyczyną jest patologicznie podwyższone stężenie amoniaku w osoczu, przekraczające wartość 100 μmol/l u noworodków i 50 μmol/l u dzieci i osób dorosłych [2].
Pacjenci z HE doświadczają szerokiego spektrum zaburzeń neuropsychiatrycznych i neurologicznych, w tym halucynacji, labilności emocjonalnej, zaburzeń świadomości i in., po poważny w skutkach obrzęk mózgu i śpiączkę [3,4]. HE jest znacznym obciążeniem ekonomicznym i społecznym, prowadzącym do obniżenia jakości życia pacjentów, w związku ze stopniowym pogorszeniem zdolności wykonywania nawet podstawowych, codziennych czynności [5]. W krajach Europy Zachodniej oraz Stanach Zjednoczonych, u ok. 25% pacjentów z marskością wątroby, rozwija się HE. W krajach rozwijających się, gdzie wirusowe zapalenie wątroby jest w dalszym ciągu rozpowszechnione, częstość występowania HE z powodu zapalenia wątroby pochodzenia wirusowego może sięgać 40-50% [6]. Typ minimalnej HE, w zależności od zastosowanych metod diagnostycznych, rozpoznawany jest u ok. 20% do 80% pacjentów z marskością wątroby, zaś u pacjentów poddanych procedurze zespolenia wrotno-systemowego, częstość występowania HE w ciągu dwóch lat od zabiegu wynosi od 20% do 55% [7].

Klasyfikacja encefalopatii wątrobowej

Wyróżniamy cztery główne typy HE: typ A, B, C oraz typ D (Ryc. 1). Typ A dotyczy ostrej niewydolności wątroby i charakteryzuje się nagłym wystąpieniem objawów i szybkim rozwojem choroby. Główną przyczyną HE typu A jest przedawkowanie leków, zwłaszcza paracetamolu, co stanowi 58% rozpoznanych przypadków oraz zakażenia wirusowe (wirusowe zapalenie wątroby typu A, B, C, E) stanowiące ~10% przypadków [8]. Inne, rzadsze przyczyny obejmują wrodzone deficyty enzymów cyklu mocznikowego, powikłania chorób metabolicznych, chorobę Wilsona, autoimmunologiczne zapalenie wątroby, ostre stłuszczenie wątroby ciężarnych, zespół Budd-Chiariego i in. [9]. Typ B HE rozwija się w wyniku zaistnienia przetoki wrotno-systemowej, do czego może dojść w wyniku chirurgicznego lub spontanicznego zespolenia wrotno-systemowego, bez współwystępującej choroby wątroby [10]. Typ C rozwija się jako konsekwencja marskości wątroby, a wyodrębnić można następujące podtypy: minimalny, epizodyczny i przewlekły [11]. Minimalna HE charakteryzuje się subtelnymi zaburzeniami poznawczymi, gdzie czynnikami sprawczymi są istniejąca lub rozwijająca się marskość wątroby, przewlekłe infekcje wirusowe, alkohol itp. [12]. Typ D odnosi się do zaostrzenia istniejącej choroby i rozpoznawany jest jako dekompensacja w przebiegu marskości wątroby. Typ D został przedstawiony jako odrębna kategoria ze względu na złożone mechanizmy patofizjologiczne oraz gorsze rokowanie pacjentów [13].

Objawy kliniczne HE obejmują zaburzenia poznawcze, zmiany psychiczne oraz deficyty motoryczne [14]. W szczególności, rozwój objawów ma charakter progresywny, od obserwowanych początkowych subtelnych zmian cyklu snu i czuwania, przez zmiany osobowości, takie jak apatia, dezorientacja, zaburzenia pamięci, aż po objawy kończące się śpiączką [15]. Według kryteriów West Haven opracowanych przez WHO wyróżnić można pięć stopni nasilenia choroby.

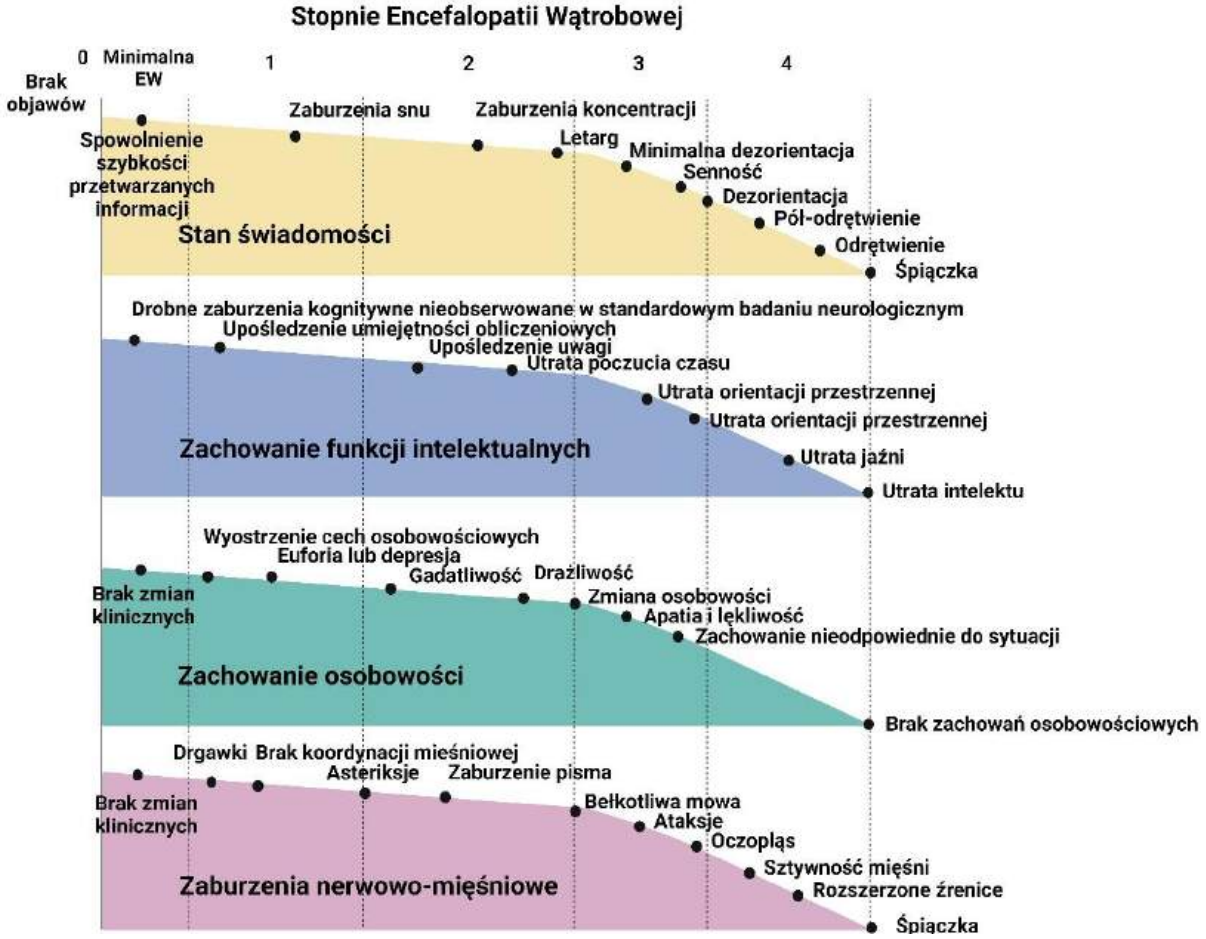

Ryc. 1. Klasyfikacja stopni nasilenia (wg. WHO) wraz z objawami klinicznymi encefalopatii wątrobowej (uaktualniono na podstawie Conn i Lieberthal, 1979) [16].

Diagnostyka encefalopatii wątrobowej

Diagnostyka HE jest złożona i opiera się w znacznym stopniu na ocenie klinicznej i testach psychometrycznych, mających na celu przede wszystkim wykluczenie innych potencjalnych przyczyn determinujących wystąpienie zaburzeń neurologicznych. Ocenie poddawane są m. in. drżenia (ang. asterixis), stopień spowolnienia psychomotorycznego, objawy pozapiramidowe. Objawy kliniczne często są niejednoznaczne i zmienne, dlatego bezwzględnie wykonuje się pomiar stężenia amoniaku we krwi, który determinuje mechanizmy patofizjologiczne HE.

Ośrodkowy układ nerwowy jest wysoce wrażliwy na toksyczne działanie amoniaku ze względu na ograniczoną możliwość jego detoksykacji. W mózgu nie występuje pełen cykl mocznikowy, a jedynym wydajnym mechanizmem detoksykacji amoniaku jest reakcja enzymatyczna katalizowana przez enzym syntetazę glutaminy (ang. glutamine synthetase; EC 6.3.1.2) w wyniku której powstaje glutamina. Proces ten jest mniej efektywny niż cykl mocznikowy w wątrobie, co sprawia, że nawet niewielkie wzrosty stężenia amoniaku mogą prowadzić do jego akumulacji i toksycznego wpływu na neurony [17,18].

Z diagnostycznych badań pomiarowych wykonuje się rejestracje elektroencefalograficzne (ang. electroencephalogram; EEG) wykazujące spowolnienie podstawowej aktywności rytmicznej z falami trójfazowymi i anomaliami przednio-dominującymi, wykonywane do wykluczenia padaczki, sepsy, hiperkapnii czy encefalopatii polekowej. Wykonuje się obrazowanie rezonansem magnetycznym, tomografię komputerową, czy spektroskopię rezonansu magnetycznego mogącą wskazać na wzrost stężenia glutaminy i glutaminianu oraz spadek poziomu mioinozytolu i choliny, jako metabolity charakterystyczne w stanach z rozpoznawanym obrzękiem mózgu [19].
W diagnostyce minimalnej HE kluczową rolę odgrywa ocena neuropsychologiczna [20]. Test psychometryczny obejmujący pięć testów oceniających szybkość psychomotoryczną i zdolności przestrzenne, jest uważany za tzw. złoty standard diagnostyczny minimalnej HE. Poza tym, wykonywany jest test krytycznej częstotliwości migotania, test kontroli hamowania, test skanowania oraz test Stroopa. Pomiar EEG jest uważany za bardziej czuły niż testy psychometryczne w diagnostyce minimalnej HE. Niektóre charakterystyczne zapisy EEG mogą świadczyć o wystąpieniu jawnej postaci HE w ciągu zdefiniowanego okresu czasu (~ 1 rok) [21].
Współczesnym, coraz powszechniej stosowanym narzędziem diagnostycznym minimalnej HE, dostępnym również on-line, jest test EncephalApp Stroop, mierzący zdolność kontrolowania uwagi i szybkość przetwarzania informacji (https://encephalapp.com/).
W dalszym ciagu jednak, badania diagnostyczne wymagają poszerzenia o poszukowania łatwych do wykrycia, stabilnych i swoistych biomarkerów. Sugeruje się, że markery, takie jak mikroRNA (miRNA), mogą znacząco wspomóc diagnostykę HE, ze względu na relatywną stabilność cząsteczek miRNA, wynikającą z ich struktury oraz zdolności do tworzenia kompleksów z białkami, chroniacych je przed degradacją. W związku z tym, część badań nakierowywana jest na poszukiwania miRNA jako nowych biomarkerów HE, definiujących w miarę możliwości, stopień i rodzaj powikłań klinicznych, np. obrzęku mózgu [22].

Patomechanizm obrzęku

Obrzęk mózgu jest najpoważniejszym klinicznym powikłaniem HE typu A i rozwija się u około 25-50% pacjentów z ostrą niewydolnością wątroby [23]. Warto w tym miejscu nadmienić, że obrzęk mózgu jest główną przyczyną śmiertelności wśród tej grupy pacjentów [23-25].
Obrzęk mózgu rozwija się na skutek gromadzenia się wody w przestrzeniach międzykomórkowych i samych komórkach. Obrzęk definiowany jako cytotoksyczny, dotyczy

gromadzenia się wody przede wszystkim w astrocytach, co powoduje ich obrzmienie (tzw. komponenta cytotoksyczna), zaś uszkodzenie i wzrost przepuszczalności BBB (tzw. komponenta naczyniowa) dodatkowo umożliwia przedostawanie się różnych związków, w tym toksycznych dla OUN, z krwi do tkanki mózgowej [26,27].

Cytotoksyczny mechanizm obrzęku mózgu związany jest przede wszystkim z toksycznym działaniem amoniaku i obejmuje różnego rodzaju konsekwencje metaboliczne, zaburzenia energetyki komórek czy zaburzenia sygnalizacyjne [28]. Wysokie stężenie amoniaku w komórkach glejowych mózgu wpływa na homeostazę jonową, szczególnie jonów potasu i wapnia, co przyczynia się do zachwiania równowagi wodnej i elektrolitowej, gromadzenia się wody [29] i deregulacji sygnalizacji wapniowej w astrocytach [30]. Amoniak może bezpośrednio hamować aktywność białkowych wymienników, transporterów czy np. pompy sodowo-potasowej (Na+/K+-ATPaza), co bezpośrednio skutkuje nierównowagą jonową i sprzyja powstawaniu obrzmienia astrocytów [28,31-33]. Jednym z proponowanych mechanizmów obrzęku cytotoksycznego, wydaje się być zwiększona produkcja i akumulacja glutaminy w astrocytach, która jako substancja osmotycznie czynna, sprzyja napływowi wody do komórki [34].

Zgodnie z hipotezą konia trojańskiego [35], wzrost syntezy glutaminy w cytozolu skutkuje jej przedostawaniem się do mitochondriów, gdzie powstający z jej rozkładu amoniak, przyczynia się do dysfunkcji mitochondriów, w tym nadmiernej produkcji wolnych rodników i indukcji zjawiska przepuszczalności błon mitochondrialnych, związanego z otwarciem megakanałów (ang. mitochondrial permeability transition; MPTP). Akumulacji glutaminy w astrocytach sprzyja m.in. zahamowanie aktywnego transportu glutaminy na zewnątrz, co związane jest z deregulacją głównego astrocytarnego transportera dla glutaminy SN1 (aka SNAT3; Slc38a3) [36,37].

Zwierzęce modele ostrej HE w przeważającej większości odwzorowują rozwijający się i obserwowany w klinice obrzęk mózgu [38,39], co umożliwiło częściowe poznanie elementów jego patomechanizmu [1,40].

Składowa naczyniopochodna obrzęku mózgu związana jest bezpośrednio ze zwiększoną przepuszczalnością BBB, co jest w znacznej mierze również wynikiem toksycznego działania amoniaku i innych krążących toksyn, oraz występuje jako konsekwencja współistniejącego ogólnoustrojowego stanu zapalnego oddziałującego na komórki śródbłonka naczyń i/lub pozostałe typy komórek tworzących BBB [41,42]. Analiza morfologiczna *post mortem* mózgu pacjentów z ostrym uszkodzeniem wątroby dostarczyła informacji dokumentujących wakuolizację i powiększenie komórek śródbłonka naczyń, a także rozszerzenie przestrzeni zewnątrzkomórkowych [19], co wykazano także w zwierzęcym modelu ostrej HE [43]. Zmiany te sugerowały zwiększoną przepuszczalność BBB oraz nasilenie transportu pinocytarnego w badanych rejonach mózgu. Ogólnoustrojowy stan zapalny przyczynia się do rozwoju HE [44], co dokumentowały badania korelacyjne: podwyższony poziom interleukiny-6 (IL-6) wiązano z występowaniem minimalnej HE u pacjentów z marskością wątroby [44]. Również TNFα i IL-1β łączono ze zwiększoną przepuszczalnością naczyń i obrzękiem obserwowanym u pacjentów z HE [45]. Wzrost przepuszczalności BBB w badanych modelach był również zależny od analizowanego rejonu mózgu oraz wybranego do badań modelu i stopnia nasilenia HE. Upraszczając, efekt łączono ze wzrostem endocytozy śródbłonka [46]. Wykazywano

wzrost aktywności MMP-9 związany z degradacją białek TJ, co osłabiało integralność poszczególnych elementów strukturalnych BBB [47,48]. Ponadto wykazano, że proces zapalny koreluje z zaburzeniami funkcji poznawczych w modelu przewlekłej HE [49], a środki przeciwzapalne, takie jak ibuprofen, poprawiały aktywność motoryczną. W modelu ostrej HE wywołanej hepatotoksyną AOM, wykazano upośledzenie funkcji poznawczych, w tym zaburzeń pamięci i zdolności uczenia się [50,51]. Dodatkowo, wykazano stopniowe spowolnienie funkcji neurologicznych od 6 godziny po podaniu AOM, w konsekwencji doprowadzając do stanu przypominającego śpiączkę [52].

BBB zapewnia ochronę mózgu przed przedostawaniem się szkodliwych substancji z obwodu, jednocześnie umożliwiając na drodze dyfuzji lub transportu aktywnego, transport składników odżywczych [17]. Strukturę tworzą komórki śródbłonka, wysoce wyspecjalizowane nabłonki płaskie, które wyścielają pojedynczą warstwą ściany włośniczek od wewnątrz. Warstwa glikokaliksu pokrywa komórki śródbłonka od strony światła naczynia [53]. Komórki endotelialne włośniczek OUN charakteryzują się brakiem fenestracji (okienek) w ścianach, większą liczbą mitochondriów wskazującą na duży metabolizm energetyczny, niską aktywnością pinocytarną, zapobiegającą przechodzeniu wielkocząsteczkowych związków organicznych z krwi do CSF (ang. cerebrospinal fluid, CSF), obecnością złącz ścisłych (ang. tight junctions, TJ) oraz selektywną przepuszczalnością dla szeregu związków [54,55]. Za utrzymanie stabilności BBB odpowiadają również połączenia przylegające (ang. adherens junctions) pomiędzy komórkami śródbłonka naczyń mózgowych. Połączenia ścisłe składają się z białek transbłonowych (klaudyna, okludyna), cząstki adhezyjne JAM, łączą się z białkami kompleksu zonula occludens (ZO-1, ZO-2) oraz z cytoszkieletem komórki, w tym z aktyną [56,57]. Połączenia przylegające tworzą m.in. koneksyna 43, kadheryny (np. VE-kadheryna) i kateniny (α, β, δ), które łączą się z cytoszkieletem komórki, wspierając stabilność komórek śródbłonka [58]. W skład BBB wchodzą także białka receptorowe, takie jak integryny, które wiążą komórki z komponentami macierzy zewnątrzkomórkowej (np. kolagenem, fibronektyną, lamininą) oraz dystroglikan, który łączy cytoszkielet komórek śródbłonka z macierzą zewnątrzkomórkową [59]. Integryny są kolejnym elementem stabilizującym system białek tworzących TJ w komórkach śródbłonka, przyczyniając się do utrzymania integralności BBB [60]. Integryny odgrywają rolę w przemieszczaniu się komórek układu immunologicznego przez BBB, np. w warunkach stanu zapalnego [61]. Z pozostałych komórkowych komponentów BBB należy wymienić astrocyty i perycyty, których udział jest szeroko omówiony w licznych pracach przeglądowych [62-66] i szczegółowe omawianie ich znaczenia wykracza poza ramy dysertacji.

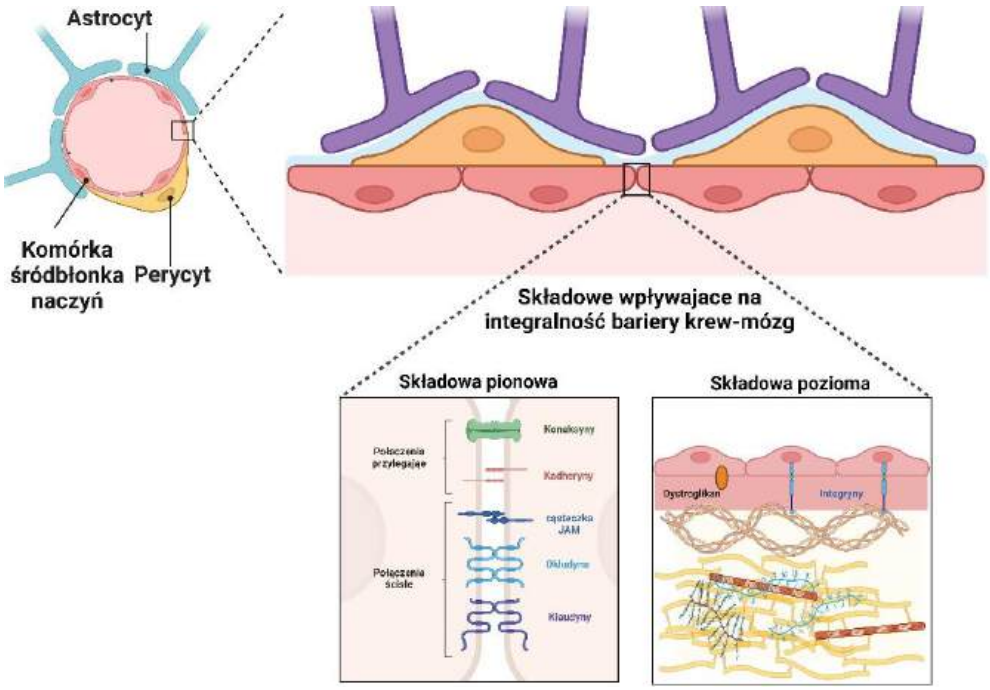

Ryc. 2. Schemat bariery krew-mózg (na podstawie Zoppo i Milner, 2006) [67].

Niektóre doniesienia dokumentowały ogólne zmiany poziomu ekspresji miRNA w zwierzęcych modelach ostrej HE [68-70]. Tylko nieliczne identyfikują specyficzne, krążące miRNA u pacjentów z ostrą HE np., w skutek zatrucia paracetamolem [71], czy z przewlekłą HE, w wyniku poalkoholowego uszkodzenia wątroby [72]. Udział miRNA w kontekście dysfunkcji BBB w HE nie był dotychczas przedmiotem badań.

Efekty toksyczności amoniaku w komórkach śródbłonka

W komórkach śródbłonka naczyń mózgowych, hiperamonemia zmienia transport aminokwasów, m.in. tryptofanu [73], tyrozyny i fenyloalaniny [26,74]. Wykazano, że hiperamonemia wpływa na transport i metabolizm argininy i ornityny, w wyniku czego powstają poliaminy, wywierające działanie hepato- i neuroprotekcyjne [75,76]. Zmiany stężenia ornityny wpływają również na transport metabolitów energetycznych, glukozy i kreatyny [77,78]. W warunkach hiperamonemii dochodzi ponadto do zmian stężenia asymetrycznej dimetyloargininy (ang. symmetric dimethylarginine; SDMA) oraz symetrycznej dimetyloargininy (ang. asymmetric dimethylarginine; SDMA), endogennych inhibitorów syntazy tlenku azotu (ang. nitric oxide synthase; NOS) [79].
W ostatniej dekadzie udokumentowano wywołane działaniem amoniaku, w którym pośredniczy stres oksydacyjny, zmiany fenotypu komórek, scharakteryzowane jako proces starzenia [80]. Proces udokumentowano w astrocytach *in vitro*; poza tym, obecność markerów stresu oksydacyjnego oraz cechy wskazujące na proces starzenia wykazano *post mortem* w tkance mózgowej pacjentów z marskością wątroby [81]. Wykazano, że jednym z przejawów stresu oksydacyjnego są podwyższone stężenie nitrowanej tyrozyny, wzrost poziomu ekspresji białka szoku cieplnego 27 (ang. heat shock protein; hsp) współwystępującego z obniżoną

aktywnością GS i podwyższoną ekspresją transportera glutaminianu/asparaginianu (ang. glutamate aspartate transporter; GLAST) [82]. Zasugerowano, że trwałe upośledzenie funkcji poznawczych pacjentów HE może być skutkiem procesu starzenia obserwowanego w astrocytach [80,83] ze względu na wykazaną korelację, zgodną z wykazaną zależnością pomiędzy procesem starzenia i obniżeniem funkcji poznawczych u osób starszych [82]. Intensywne badania procesu starzenia przez grupę Profesora Dietera Haussingera, nie dotyczyły jednak komórek śródbłonka naczyniowego mózgu w HE.

W procesie starzenia, komórki tracą zdolność do podziału i proliferacji [84], obserwuje się szereg charakterystycznych zmian fenotypowych i funkcjonalnych [85]. Jedną z głównych, jest trwałe zatrzymanie cyklu komórkowego [86]. Komórki nie przechodzą fazy S (zwana syntetyczną) i M (zwana mitotyczną) cyklu komórkowego, co uniemożliwia ich dzielenie się [87]. Zatrzymanie cyklu komórkowego jest często wynikiem aktywacji mechanizmów odpowiedzi na uszkodzenia DNA oraz na stres oksydacyjny, co prowadzi do wzrostu poziomu markerów: p16, p21 oraz p53 [87]. Komórki charakteryzują się fenotypem sekrecyjnym (ang. senescence - associated secretory phenotype; SASP), tworzonym przez m.in. cytokiny, chemokiny, proteazy [88], który może pogłębiać współwystępujący stan zapalny, istotny w rozwoju chorób przewlekłych. Poza tym, komórki w procesie starzenia, wykazują zwiększoną aktywność lizosomalnego enzymu β-galaktozydazy (EC 3.2.1.23) hydrolizującego β-galaktozydy do monosacharydów, powszechnie akceptowany marker procesu [89]. Zróżnicowana, zależna od pH aktywność β-galaktozydazy (optymalna ~ pH 6,0), determinuje identyfikację komórek [90].

Zaburzenia funkcji mitochondriów prowadzą do zwiększonej produkcji reaktywnych form tlenu (ang. reactive oxygen species; ROS) i stresu oksydacyjnego, co sprzyja procesowi starzenia. [91]. Dysfunkcja mitochondriów w komórkach śródbłonka w starzeniu normatywnym została udokumentowana *post mortem* m.in. w tkance mózgowej pacjentów z chorobą Alzheimera [92] oraz 28 miesięcznych myszach [93-95]. Z kolei w badaniach *in vitro* wykazano, że komórki śródbłonka w obecności oligomerów β-amyloidu wykazywały zmieniony, odwzorowujący cechy starzenia fenotyp [96]. Skład SASP śródbłonka obejmuje wysokie stężenia ROS, NO, a także ICAM-1, VCAM i VEGF [97–101]. Komórki śródbłonka mózgu charakteryzowały się zmniejszoną liczbą mitochondriów oraz obniżoną aktywnością enzymów łańcucha oddechowego wynikającą z uszkodzeń białek, skutkującą słabszą efektywnością przenoszenia elektronów i obniżoną produkcją ATP [96,102-104], co w efekcie przełożyło się na indukcję przewlekłego stresu oksydacyjnego. Uważa się, że za redukcję liczby mitochondriów może odpowiadać zbyt aktywny proces autofagii lub obniżony proces biogenezy mitochondriów [105].

HIPOTEZA

Zmiany profilu miRNA w osoczu lub korze mózgowej szczurów w warunkach HE są związane z dysfunkcją BBB na poziomie struktury i funkcji, w szczególności, z tworzącymi ją komórkami śródbłonka naczyń.

CEL PRACY

Celem dysertacji jest analiza profilu miRNA w osoczu i korze mózgowej szczurów z hiperamonemią prostą i szczurów z ostrym uszkodzeniem wątroby oraz wykazanie molekularnego podłoża zmian w komórkach śródbłonka naczyniowego mózgu, głównego elementu tworzącego BBB.

Cele szczegółowe:

1. Analiza profilu ekspresji miRNA w osoczu i w korze czołowej mózgu szczurów z hiperamonemią prostą i ostrym uszkodzeniem wątroby;
2. Analiza morfologiczna i funkcjonalna BBB w badanych modelach *in vivo*;
3. Analiza *in silico* identyfikująca miRNA oraz białka efektorowe w kontekście uszkodzeń BBB oraz weryfikacja na poziomie komórki, z wykorzystaniem modeli BBB *in vitro* (linia komórek śródbłonka naczyń mózgowych szczura; RBE4 oraz pierwotna hodowla komórek śródbłonka mikronaczyń mózgu szczura);
4. Weryfikacja wpływu hiperamonemii na fenotyp komórek śródbłonka naczyń mózgowych szczura *in vitro* i analiza unaczynienia mózgu szczura *in vivo*;
5. Zaprojektowanie, skonstruowanie i przetestowanie autorskiego systemu pomiarowego do mierzenia rezystancji elektrycznej monowarstwy komórkowej, warunkującego właściwe modelowanie BBB *in vitro*.

MATERIAŁY I METODY

Do przeprowadzenia doświadczeń wykorzystano modele *in vivo*, *ex vivo*, *in vitro* oraz analizy *in silico*, a także skonstruowano autorskie urządzenie do pomiaru rezystancji elektrycznej monowarstwy komórek.

Modele

In vivo

Doświadczenia na zwierzętach przeprowadzono zgodnie z wytycznymi Krajowej Komisji Etycznej ds. Doświadczeń na Zwierzętach, na podstawie zezwolenia IV Lokalnej Komisji ds. Doświadczeń na Zwierzętach w Warszawie (zgodnie z pozwoleniami o numerach: 57/2015; 473/2017 oraz 462/2017).

U szczurów rasy Sprague-Dawley o masie ciała 250-300 g. ALF indukowano poprzez dootrzewnową (i.p.) iniekcję hepatotoksyny tioacetamidu (ang. thioacetamide; TAA) w dawce 300 mg/kg co 24 godziny przez 3 dni. Hiperamonemię prostą indukowano przez i.p. podanie octanu amonu (ang. ammonium acetate, OA) w dawce 600 mg/kg co 12 godzin przez 3 dni. Grupa kontrolna otrzymywała 0,3 ml 0,9% NaCl co 24 godziny.

Po dekapitacji izolowano korę mózgową i pobierano krew do probówek z EDTA. Kora mózgowa została wykorzystana do kolejnych etapów doświadczeń oraz do izolacji frakcji mikronaczyń.

In vitro

W badaniach wykorzystano pierwotne hodowle komórek śródbłonka mikronaczyń mózgu (PBMEC) izolowane z kory mózgowej 14 dniowych lub 12 miesięcznych samców szczurów szczepu Sprague-Dawley według opisanego protokołu [106].
Doświadczenia przeprowadzono również na linii komórek śródbłonka mózgu szczura (RBE4), uzyskanej przez unieśmiertelnienie komórek śródbłonka mikronaczyń mózgu szczura za pomocą transfekcji plazmidem zawierającym gen E1A adenowirusa. Komórki linii RBE4 wykazywały fenotyp śródbłonka naczyniowego, brak transformacji nowotworowej oraz ekspresję markerów typowych dla komórek śródbłonka mózgu. W obecności czynników wzrostu, tworzyły trójwymiarowe struktury wykazujące aktywność enzymów związanych z barierą krew-mózg, γ-glutamylotranspeptydazy (EC 2.3.2.2) oraz fosfatazy alkalicznej (EC 3.1.3.1) [107].
Komórki RBE4 i PBMEC inkubowano w 5 mM chlorku amonu i/lub 50 ng/ml TNFα przez 24 godziny. Stężenie podawanego do pożywki chlorku amonu użytego w eksperymencie było 2-3 razy niższe niż poziom wewnątrzkomórkowy mierzony w tkance mózgowej pacjentów z ciężką hiperamonemią [108,109]. W badaniach procesu starzenia, RBE4 hodowano przez 21 dni, wymieniając pożywkę hodowlaną co 3 dni.

Metody

Stężenia amoniaku w osoczu oraz aktywność enzymów wątrobowych: aminotransferazy asparaginianowej (EC 2.6.1.1), aminotransferazy alaninowej (EC 2.6.1.2), oraz γ-glutamylotranspeptydazy mierzono przy użyciu komercyjnego analizatora (Scil Vet, Niemcy).

Stężenia cytokin prozapalnych (TNFα, IL-1α, IL-1β, IL-6 oraz IL-10) oznaczono metodą cytometrii przepływowej, której szczegółowy opis znajduje się w publikacji I.

Przepuszczalność BBB zbadano poprzez wykorzystanie dwóch markerów o niskiej i wysokiej masie cząsteczkowej. Fluoresceina sodu (ang. sodium fluoresceine; SF), dzięki niskiej masie cząsteczkowej, przenika przez uszkodzoną BBB, której przepuszczalność określa się na podstawie intensywności fluorescencji. SF, w dawce 100 mg/ml soli fizjologicznej była podawana dootrzewnowo, a po 45 minutach wykonywano perfuzję solą fizjologiczną. Po dekapitacji, mózgowia były izolowane, ważone i homogenizowane w stosunku 1:10 (w/v) w sterylnym PBS. Homogenaty rozcieńczano, a sygnał mierzono przy długości fali wzbudzenia 480 nm i emisji 538 nm. Przepuszczalność BBB mierzono jako stosunek SF na gram tkanki mózgowej do ilości SF w 1 ml osocza.
Zastosowanym markerem o wysokiej masie cząsteczkowej był błękit Evansa (ang. Evans blue; EB), który wiąże się z albuminą osocza. Kompleks albumina-barwnik nie przenika nienaruszonej bariery. 2% roztwór EB w sterylnej soli fizjologicznej podawano do żyły ogonowej szczurów w dawce 4 ml/kg. Po 2 godzinach szczury perfundowano transkardialnie 200 ml zimnej soli fizjologicznej. Następnie mózgi izolowano, a kora mózgowa była ważona i homogenizowana w 30% kwasie trzy chlorooctowym. Homogenat wirowano przy 10,000 × g przez 20 minut, absorbancję mierzono przy świetle o długości 620 nm, co pozwalało na określenie przepuszczalności BBB jako intensywności fluorescencji EB, wyrażonej w nanogramach na miligram tkanki mózgowej.

Analiza morfologiczna mózgu z uwzględnieniem zmian ultrastruktury BBB u szczurów TAA i OA analizowano za pomocą transmisyjnej mikroskopii elektronowej (ang. transmission electron microscopy; TEM). Preparaty analizowano wykorzystując mikroskop elektronowy LIBRA 120. Dla każdej próbki oceniano od 12 do 24 pól widzenia.

Izolacja naczyń mózgowych. Wyizolowane fragmenty kory mózgowej szczurów homogenizowano w roztworze Ringera, wirowano przy 1500 × g przez 10 minut w temperaturze 4°C. Uzyskany nadsącz zawieszano w świeżym buforze i odwirowywano, etap powtarzano trzykrotnie. Końcowy osad homogenizowano w 10 ml 0,25 M sacharozy i wirowano w gradiencie sacharozy (0,25:1:1,5 M) w 30 000 × g, 30 min i 4°C. Zbierano frakcję zawierającą naczynia.

Izolację całkowitego RNA z kory mózgowej i osocza przeprowadzano za pomocą TRI Reagent lub zestawów miRNeasy i mirVana. Próbki przechowywano w temperaturze -80°C. Kwantyfikacja całkowitego RNA była przeprowadzana spektrofotometrycznie, a 1 μg całkowitego RNA używano do przygotowania biblioteki.

Sekwencjonowanie NGS dla próbek osocza wykonywano przy użyciu systemu DNBSEQ G400 (MGI2000) w trybie SE50 (BGI Company, Shenzen, Chiny). Dla każdej próbki generowano minimum 20 milionów odczytów parowanych końców, a kwantyfikacja obejmowała liczbę surowych odczytów oraz znormalizowany poziom ekspresji w postaci wartości CPM (ang. Counts per milion, liczba zmapowanych odczytów na milion), aby uwzględnić zmienność wielkości biblioteki. Następnie do identyfikacji sekwencji miRNA użyto analizy Quantifier miRDeep2 opartej na bibliotece miRbase2.0. Skrypt Quantifier narzędzia miRDeep2 z domyślnymi parametrami był używany do kwantyfikacji poziomu ekspresji miRNA.

Sekwencjonowanie NGS kory mózgowej było prowadzone przy pomocy platformy NextSeq 500. Średnia liczba odczytów wynosiła 10 milionów odczytów na próbkę; następnie RNA było konwertowane na biblioteki miRNA NGS. Kontrola jakości była przeprowadzana za pomocą Bioanalyzer 2100 (Agilent) lub TapeStation 4200 (Agilent). Na podstawie jakości pomiarów stężenia, biblioteki były łączone w równomolarnych proporcjach. Surowe dane NGS były zdemultipleksowane, a pliki FASTQ dla każdej próbki były generowane przy użyciu oprogramowania bcl2fastq (Illumina Inc.).

Poziomy ekspresji miRNA oraz mRNA dla okludyny i integryny β1 mierzono w osoczu, korze mózgu oraz komórkach RBE4 i PBMEC metodą ilościowej reakcji polimerazy w czasie rzeczywistym (RT-qPCR) z użyciem odpowiednich sond (Tab. 1). Wykonano analizę poziomu ekspresji mRNA genów *Opa1*, *Mfn1*, *Fis1* oraz *Mff*, związanych z mitochondrialnymi procesami fuzji i fragmentacji. Z wykorzystaniem metody RT-qPCR, zweryfikowano poziom mRNA genu kodującego p16 oraz p21. Kontrolą endogenną miRNA był U6 snRNA (snRNA), natomiast dla ww. białek, β-aktyna. Względne poziomy ekspresji obliczono przy użyciu metody 2-ΔΔCt.

Tab. 1. Sondy TaqMan wykorzystane w reakcji Real-Time PCR.

Nazwa miRNA/genu	Numer katalogowy	Producent
miRNA-183-5p	QG-339306_YP00206030	Qiagen, Hilden, Germany
miRNA-122-5p	QG-339306_YP00205664	Qiagen, Hilden, Germany
snRNA U6	QG-339306_YP02119464	Qiagen, Hilden, Germany
p21	Rn00589996_m1	Thermo Fisher Scientific, Waltham, MA, USA
p16	Rn00580664_m1	Thermo Fisher Scientific, Waltham, MA, USA
Opa1	Rn00592200_m1	Thermo Fisher Scientific, Waltham, MA, USA
Mfn1	Rn00594496_m1	Thermo Fisher Scientific, Waltham, MA, USA
Fis1	Rn01480911_m1	Thermo Fisher Scientific, Waltham, MA, USA
Mff	Rn01400790_m1	Thermo Fisher Scientific, Waltham, MA, USA
Itgβ1	Rn00566727_m1	Thermo Fisher Scientific, Waltham, MA, USA
Ocln	Rn00580064_m1	Thermo Fisher Scientific, Waltham, MA, USA
β-actin	Rn00667869	Thermo Fisher Scientific, Waltham, MA, USA

Metodę Western blotting (WB) zastosowano, wykorzystując homogenaty kory mózgu szczurów modelowych oraz lizaty komórek RBE4 i PBMEC zgodnie z metodami opisanymi w publikacji I.

Wykonano analizę immunocytochemiczną do pomiaru fluorescencji białek w korze mózgowej, frakcji mikronaczyń, a także pęcherzyków zewnątrzkomórkowych oraz PBMEC, w celu potwierdzenia poprawności przeprowadzonej izolacji i hodowli. Zbadano również wpływ transfekcji mimic-miRNA-183-5p na fluorescencję białka p53 i β-galaktozydazy w komórkach linii RBE4. Listę przeciwciał przedstawia Tab. 2.

Tab. 2. Przeciwciała 1^{o} wykorzystane w metodzie WB oraz immunocytochemicznej.

Nazwa przeciwciała 1^{o}	Stężenie przeciwciała	Numer katalogowy	Producent
CD-31	1:400	ab28364	Abcam, Cambridge, UK
vWF	1:400	ab6994	Abcam, Cambridge, UK
Okludyna	1:300	91131	Cell Signalling, Inc. Denver, MA, USA
Integryna β1	1:200	4706	Cell Signalling, Inc. Denver, MA, USA
β-Galaktozydaza	1:400	ab616	Abcam, Cambridge, UK
p53	1:400	ab131442	Abcam, Cambridge, UK
CD-9	1:400	ab223052	Abcam, Cambridge, UK
ZO-1	1:400	33-9100	Thermo Fisher Scientific, Waltham, MA, USA

Analiza gęstości mikronaczyń mózgu, poprzez pomiar intensywności immunofluorescencji markera mikronaczyń, czynnika von Willebranda (ang. von Willebrand Factor; vWF), w komórkach śródbłonka. Procedurę opisano dokładniej w publikacji III.

Analiza proliferacji komórek linii RBE4 inkubowanych w 5 mM amoniaku badano za pomocą komercyjnie dostępnego urządzenia HoloMonitor M4 (Phase Holographic Imaging, PHI AB, Lund, Szwecja). Komórki wysiano w gęstości 1 x 10^5 na płytki 6 dołkowe i inkubowano przez 24 godziny z amoniakiem. Płytka hodowlana została zamontowana w urządzeniu i umieszczona w inkubatorze. Obrazowanie w trybie poklatkowym przeprowadzano w regularnych odstępach czasu (co 10 minut) przez okres 24 godzin, przy zachowaniu stałych warunków środowiskowych (temperatura, poziom CO_2). Zarejestrowane obrazy holograficzne przetworzono za pomocą oprogramowania HoloStudio (PHI, AB). Zastosowano algorytmy kontrastu fazowego w celu zwiększenia widoczności struktur komórkowych. Komórki identyfikowano i liczono automatycznie za pomocą wbudowanych narzędzi rozpoznawania w oprogramowaniu. Stopy proliferacji obliczano, porównując liczbę komórek w różnych punktach czasowych, analizując tempo podziału i wzrostu komórek w całym okresie obrazowania.

Aktywność β- galaktozydazy (β-gal), markera starzenia komórkowego, analizowano przy użyciu mikroskopu świetlnego. Komórki przepłukano PBS, utrwalano przez 15 minut

w temperaturze pokojowej, ponownie przepłukano, a następnie inkubowano w roztworze β-galaktozydazy z X-Gal przez noc w temperaturze 37°C w inkubatorze bez CO_2. W wyniku reakcji zaobserwowano niebieski precypitat, co wskazujący na aktywność β-gal. Komórki wykazujące fenotyp starzenia komórkowego obserwowano pod mikroskopem optycznym (Nikon DIAPHOT 300) i liczono w trzech losowych polach widzenia.

Stężenia TNF-α, ICAM-1, V-CAM i VEGF mierzono metodą immunoenzymatyczną w komórkach inkubowanych w 5 mM amoniaku lub 20 nM mimic-miRNA-183-5p przez 24 godziny. Do analizy wykorzystano również medium hodowlane pochodzące z 3 tygodniowej hodowli RBE4. Anality mierzono za pomocą wstępnie skonfigurowanych paneli immunologicznych ProcartaPlex (Cat. No. PX010-10420-901 Thermo Fisher Scientific, Waltham, USA). Komórki inkubowano zgodnie z opisem w sekcji Materiały i Metody, następnie wirowano przy 10,000 × g przez 7 minut, a nadsącz pożywki bez komórek zebrano i przechowywano w temperaturze -80°C. Następnie na płytkę ProcartaPlex dodano 50 µl nadsączu pożywek hodowlanych oraz standardów. Stężenie analitów mierzono za pomocą instrumentu do multipleksowania MAGPIX (Luminex, TX, USA) z oprogramowaniem XPonent. Stężenie analitów było wyznaczane na podstawie wcześniej wyznaczonej krzywej standardowej dla każdego z oznaczanych związków. Świeżą pożywkę hodowlaną użyto jako kontroli zerowej.

Oceniono integralność komórek RBE4 poprzez określenie przepuszczalności monowarstwy dla fluoresceiny izotiocyjanianu dekstranu (ang. fluorescein isothiocyanate; FITC) o masie 40 kDa przy fali wzbudzenia 485 nm, emisji 520 nm. FITC-dekstran, ze względu na swoją wysoką masę cząsteczkową, nie jest przenoszony na drodze aktywnego transportu.

Integralność komórkowego modelu BBB zbadano poprzez pomiar przez-śródbłonkowego oporu elektrycznego (ang. transendothelial electrical resistance; TEER) za pomocą specjalnie zaprojektowanego urządzenia, którego model opisano szczegółowo w publikacji IV. Pomiar rezystancji elektrycznej warstwy komórek śródbłonka, hodowanych na półprzepuszczalnej membranie, charakteryzuje integralność i szczelność bariery komórkowej. Niska wartość oporu, świadczy o uszkodzeniu TJ i osłabieniu funkcji bariery. Pomiar za pomocą skonstruowanego autorskiego urządzenia jest nieinwazyjny i może być wielokrotnie powtarzany, co pozwala na monitorowanie dynamiki zmian w odpowiedzi na zmieniające się czynniki eksperymentalne. Opór elektryczny rejestrowano automatycznie co 5 minut przez 24 godziny. Wartości pomiarów, wyrażone w omach (Ω), obliczano jako różnicę oporu komórek w insertach hodowlanych i wartość oporu insertów bez komórek. Przy użyciu urządzenia analizowano adhezję komórek do kolagenu I, zgodnie z metodologią opisaną przez Lajkó i in. [56]. Wartości wyrażone w Ω obliczano jako różnicę między początkowym oporem komórek, a wartością oporu po 24 godzinach inkubacji. Wyniki normalizowano względem insertów niepokrywanych.

Zbadano także potencjał błony mitochondrialnej za pomocą metody opartej na sondzie fluorescencyjnej JC-10, zgodnie z protokołem producenta.

Stężenie ROS w komórkach śródbłonka mierzono przy użyciu sondy fluorescencyjnej 2′,7′-dichlorofluoresceiny octanu, fluorescencję komórek mierzono za pomocą fluorescencyjnego czytnika mikropłytek FLUOstar OMEGA (BMG Labtech, Ortenberg, Niemcy) przy długości fali wzbudzenia 485/20 nm. i długości fali emisji 528/20 nm., zgodnie z opisem w publikacji II.

Transfekcję komórek PBMEC oraz linii RBE4 przeprowadzono przy użyciu syntetycznych miRNA: mimic-miRNA-183-5p i mimic-miRNA-122-5p, jak również kontroli negatywnej (Tab. 3). Komórki wysiano na 6 dołkową płytkę hodowlaną w gęstości $3{,}3 \times 10^5$ oraz transfekowano odpowiednimi sekwencjami (Tab. 3.). Transfekcję przeprowadzono przy użyciu odczynnika do transfekcji HiPerFect zgodnie z instrukcjami producenta, stosując stężenie 5 μM lub 20 μM przez 24 godziny.

Tab. 3. Sekwencje mimic-miRNA zastosowane w technice transfekcji komórkowej.

Nazwa miRNA	Sekwencja mimic-miRNA	Numer katalogowy	Producent
miRNA-122-5p	5′-UGGAGUGUGACAAUGGUGUUUG-3′	33173YM00470430-ADA	Qiagen, Hilden, Germany
miRNA-183-5p	5′-UAUGGCACUGGUAGAAUUCACU-3′	339173YM00471390-ADA	Qiagen, Hilden, Germany
Kontrola negatywna	5′-UCACCGGGUGUAAAUCAGCUUG-3′	339173YM00479902-ADA	Qiagen, Hilden, Germany

Pęcherzyki zewnątrzkomórkowe (ang. extracellular vesicles; EVs) izolowano z medium hodowlanego linii komórkowej RBE4. Komórki hodowano na 100 mm^2 szalkach hodowlanych w gęstości 10^6 Pożywki z hodowli komórkowej zebrano i poddano wirowaniu przy 200 × g przez 10 minut, a następnie ponownemu wirowaniu przy 500 × g przez 10 minut w temperaturze 4°C. Otrzymane próbki odwirowano przy 2000 × g przez 20 minut w celu usunięcia resztek komórkowych, a następnie odwirowano przy 100 000 × g przez 75 minut w temperaturze 4°C. Osad przepłukano dejonizowaną solą fizjologiczną buforowaną fosforanami a następnie poddano dodatkowemu wirowaniu przy 100 000 × g przez 75 minut w temperaturze 4°C. Następnie usunięto uzyskany nadsącz, a osad ponownie zawieszono w 1 ml dejonizowanej soli fizjologicznej buforowanej fosforanami i przechowywano w temperaturze -80°C.

Ilościową ocenę, w tym pomiar korelacji fluorescencji, przeprowadzono na izolowanych i fluorescencyjnie wybarwionych EVs, potwierdzając obecność obiektów o średnim promieniu hydrodynamicznym 11,6 nm. Metoda korelacji fluorescencji (ang. fluorescence correlation spectroscopy; FCS) jest techniką optyczną używaną do badania dynamiki molekularnej w roztworach na poziomie pojedynczych cząsteczek, mierząc fluktuacje intensywności fluorescencji. Wyniki FCS pozwoliły na określenie współczynnika dyfuzji oraz promienia hydrodynamicznego egzosomów, co było kluczowe dla potwierdzenia poprawności metody izolacji EVs.

Analiza *in silico*: wyniki NGS analizowano wykorzystując trzy bazy danych: miRDB v5, TargetScan7.1 i TarBase v.8. Korzystając z narzędzia MirTarget w miRDB, przewidywano geny docelowe miRNA, uwzględniając tylko te z wynikiem docelowym powyżej 60. TargetScan7.1 służył do predykcji biologicznych celów miRNA poprzez wyszukiwanie obecności konserwatywnych miejsc 8mer, 7mer i 6mer, pasujących do regionu miRNA. TarBase v.8 dostarczał eksperymentalnie potwierdzone cele miRNA.

Przedstawiona w pracy I analiza koncentrowała się na genach wielokrotnie raportowanych we wszystkich trzech bazach danych, które były związane ze strukturą lub funkcją BBB. Wyniki pochodzące z narzędzia MirTarget zostały wykorzystane do odfiltrowania mniej prawdopodobnych genów docelowych, co pozwoliło skupić się na najbardziej prawdopodobnych interakcjach miRNA-cel. Po zidentyfikowaniu specyficznych genów regulowanych przez wybrane miRNA, określono ich potencjalny wpływ na funkcje biologiczne. Przeprowadzono analizę ścieżek za pomocą narzędzia String Tool w celu zweryfikowania potencjalnego udziału wybranych genów w szersze spektrum procesów biologicznych. Analiza ścieżek Kyoto Encyclopedia of Genes and Genomes (KEGG), w połączeniu z grupowaniem genów wykazała interakcje o prawdopodobieństwie większej niż minimalna wymagana wartość (0,15), w wyniku czego uwzględniono jedynie te ścieżki w przewidywaniach. Ustalono próg interakcji na poziomie 0,9, co stanowi najwyższą ocenę pewności uzyskanego wyniku.

Łączna analiza danych NGS pochodzących z kory mózgowej i surowicy obejmowała identyfikację 306 miRNA, które wykazywały zmiany ekspresji w obu tkankach. MiRNA zostały poddane analizie przy użyciu baz danych, takich jak TarBase, miRDB i TargetScan, aby przewidzieć potencjalne geny docelowe regulowane przez wybrane miRNA. W wyniku tej analizy zidentyfikowano 852 potencjalnych celów genowych. Następnie przeprowadzono analizę z wykorzystaniem narzędzia ShinyGO genów docelowych, uwzględniając ich funkcje biologiczne oraz udział w szlakach metabolicznych. Statystyczna istotność była zachowana poprzez zastosowanie progu oczekiwana proporcji błędów (ang. false discovery ratio; FDR) wynoszącego 0,05, zgodnie z zaleceniami autorów baz danych [110].

Przeprowadzono systematyczny przegląd literatury w bazach danych MEDLINE poprzez strony PubMed oraz Elsevier Scopus, obejmujące oryginalne prace opublikowane od 1 stycznia 2011 roku do 1 lipca 2021 roku. Skupiono się na wynikach pochodzących od pacjentów z ostrą niewydolnością wątroby (ang. acute liver failure; ALF) oraz badaniach ekspresji miRNA, wykorzystując słowa kluczowe, oparte na przeglądzie literatury i medycznych hasłach przedmiotowych. Zastosowano kompleksową strategię wyszukiwania, którą podsumowano na Rysunku 1 w publikacji V. Dane wyodrębniono niezależnie, stosując zdefiniowane kryteria kwalifikacji. Aby ujednolicić dane, wykluczono badania z niejednoznaczną diagnozą pacjentów, przykładowo: w przebiegu przewlekłej choroby wątroby lub obecnością wielu czynników współwystępujących z ALF.

Po zidentyfikowaniu wielokrotnie raportowanych zmienionych miRNA w próbkach surowicy i osocza, przeanalizowano raporty o zmienionych profilach miRNA wątroby i moczu. Na koniec, zweryfikowano specyficzność oraz funkcjonalne implikacje miRNA dla patogenezy ALF, przeprowadzając przewidywanie genów docelowych i szlaków regulowanych przez wybrane miRNA.

Geny docelowe miRNA i ścieżki biologiczne analizowano za pomocą dostępnych narzędzi internetowych DIANA [111]. Narzędzie Micro-T oparte na bazie danych miRBase użyto do identyfikacji potencjalnych genów docelowych miRNA oraz ścieżek. TargetScan wykorzystano do badania przewidywania potencjalnych genów docelowych i demonstrowania relacji między nimi. Analiza ścieżek MiRPath v3.0 została przeprowadzona w celu weryfikacji zaangażowania wybranych genów w ścieżki biologiczne zgodnie z KEGG.
Spis wszystkich wykorzystanych baz danych znajduje się w Tabeli 4.
Szczegółowe opisy metodologii i wyników analiz są szczegółowo opisane w publikacji V.

Tab. 4. Bazy danych wykorzystane do analizy *in silico*.

Baza danych	Cel analizy	Źródło
miRDB v5	Predykcja celów miRNA	[112]
TargetScan 7.1	Predykcja celów miRNA	[113]
TarBase v8	Predykcja celów miRNA	[114]
miRBase	Identyfikacja sekwencji miRNA	[115]
KEGG (Kyoto Encyclopedia of Genes and Genomes)	Analiza ścieżek biologicznych	[116]
ShinyGO	Analiza funkcjonalna genów docelowych	[110]
STRING	Analiza interakcji białkowych	[117]

Konstrukcja i budowa urządzenia do pomiaru rezystancji monowarstwy komórek

Urządzenie do pomiaru rezystancji elektrycznej zostało zaprojektowane w celu dokładnej oceny integralności barier komórkowych, takich jak bariery śródbłonkowe i nabłonkowe. Podstawa konstrukcyjna urządzenia jest wykonana z laminatu epoksydowego wzmocnionego włóknem szklanym, co zapewnia zarówno lekkość, jak i wytrzymałość konstrukcji. Górna powierzchnia ramki jest pokryta warstwą miedzi, która pełni funkcję ekranu elektromagnetycznego, chroniąc urządzenie przed zakłóceniami zewnętrznymi. Dolna powierzchnia ramki posiada miedziane ścieżki, które są odpowiedzialne za przesyłanie sygnałów z elektrod pomiarowych do głównego układu przetwarzania. Elektrody pomiarowe zostały wykonane ze srebra, które charakteryzuje się wysoką przewodnością elektryczną oraz odpornością na korozję. Elektrody mają kształt długich, cienkich cylindrów o średnicy 1 mm i długości 20 mm. Są one przymocowane do płytki drukowanej pod kątem prostym do jej powierzchni, co zapewnia ich stabilność oraz precyzyjne ustawienie w insertach hodowlanych. Centralna elektroda pomiarowa jest umieszczona wewnątrz insertu, a zewnętrzna elektroda znajduje się pomiędzy insertem a dołkiem w płytce hodowlanej. Urządzenie korzysta z procesora z rodziny C2000 (TMS320F28369D). Procesor kontroluje przetwornik analogowo-cyfrowy (ang. analog to digital converter; ADC), który przetwarza sygnały elektryczne z elektrod na dane cyfrowe. Proces autokalibracji odbywa się zarówno po uruchomieniu urządzenia, jak i przed każdą serią pomiarów. Opis powyższej konstrukcji urządzenia jest szczegółowo przedstawiony w publikacji III.

OMÓWIENIE WYNIKÓW

Ad. Cel szczegółowy 1

Wykorzystane w badaniach szczurze modele zwierzęce hiperamonemii prostej (OA) i ostrego toksycznego uszkodzenia wątroby (TAA), opracowane wcześniej w Zakładzie Neurotoksykologii [118,119], weryfikowano pod względem zgodności i odtwarzalności ustalonych wcześniej parametrów: stężenia amoniaku, aktywności enzymów wątrobowych: AST, ALT i GGTP oraz stężenia cytokin prozapalnych TNFα, IL-1α, IL-1β, IL-6, IL-10 w osoczu; uszkodzenie wątroby weryfikowano histopatologicznie. W odniesieniu do modelu OA wprowadzono modyfikację procedury poprzez zastosowanie dwukrotnego podania octanu amonu w odstępie 12 godz. w dawce 600 mg/kg m.c. przez 3 dni.
Wykonano jakościowe i ilościowe profilowanie miRNA w osoczu i korze mózgowej szczurów w obu modelach, wykazując różnice pomiędzy ustalonymi profilami. W osoczu szczurów OA oznaczono 35 zmienionych miRNA, z których 34 wykazywały obniżony poziom ekspresji. W osoczu szczurów TAA zidentyfikowano 128 statystycznie zmienionych miRNA, z tego 125 wykazywało wzrost, natomiast 3 miRNA miały obniżony poziom ekspresji. W modelu OA stwierdzono zmieniony poziom ekspresji 35 miRNA (ekspresja 12 miRNA była podwyższona, 23 miRNA obniżona). Zaobserwowano znaczącą zbieżność (83%) profili miRNA w badanych modelach (Publikacja 1, Ryc. 2). Wykorzystując narzędzia bioinformatyczne miRTarget na podstawie danych z bazy miRDB wykazano, że 127 miRNA zmienionych w osoczu szczura TAA może wpływać na ekspresję 205 genów kodujących białka związane strukturalnie lub funkcjonalnie z BBB, a tym samym potencjalnie indukować zmiany zarówno w morfologii i funkcji elementów BBB (Publikacja 1, Ryc. 3).
W korze mózgowej szczurów OA wykazano 338 zmienionych miRNA. Spośród nich, 187 wykazywały spadek, natomiast 151 wzrost poziomu ekspresji. W modelu TAA zidentyfikowano 345 statystycznie zmienionych miRNA, w tym: 176 wskazywały obniżenie, a 169 wzrost poziomu ekspresji. Na podstawie analizy porównawczej grup OA i TAA, zidentyfikowano 335 wspólnych miRNA, w tym 3 miRNA swoiste dla OA, natomiast 10 miRNA dla TAA (dane niepublikowane, manuskrypt na etapie recenzji).

Ad. Cel szczegółowy 2

Wyniki analizy obrazowej wykonanej metodą mikroskopii elektronowej wykazały subtelne zmiany morfologii komórek śródbłonka naczyń tworzących BBB u szczurów OA. W mózgu szczurów TAA obserwowano wyraźne pofałdowania błony komórkowej komórek śródbłonka oraz nacieki zapalne w obszarach okołonaczyniowych (Publikacja 1, Ryc. 2A).
Wyniki analizy ultrastrukturalnej ponadto dostarczyły informacji dokumentujących wyraźne zmienioną morfologię mitochondriów w komórkach śródbłonka. W obu modelach mitochondria były powiększone, wskazując na obrzęk, przy jednoczesnym wyraźnym ich wydłużeniu, co udokumentowano pomiarami morfometrycznymi (Publikacja 1, Ryc. 2A).
Statystycznie istotny wzrost przepuszczalności BBB dla związków egzogennych o niskiej masie cząsteczkowej - fluoresceiny sodu (376 Da) oraz tendencję wzrostową w przypadku podania związku o wyższej masie cząsteczkowej - błękitu Evansa (69 kDa) wykazano

w modelu TAA. Nie obserwowano wyraźnych zmian przepuszczalności BBB w modelu OA. (Publikacja 1, Ryc. 2B).

Ad. Cel szczegółowy 3

Aby zidentyfikować geny docelowe miRNA, przeprowadzono analizę *in silico* przy użyciu trzech baz danych: miRDB, TargetScan oraz TarBase. MiRDB wykorzystuje algorytmy do przewidywania celów miRNA na podstawie analizy danych eksperymentalnych, TargetScan identyfikuje potencjalne cele miRNA na podstawie sekwencji konserwatywnych w różnych gatunkach, a TarBase przedstawia zweryfikowane eksperymentalnie interakcje miRNA-gen. Dzięki połączeniu wyników uzyskanych z tych trzech baz danych, zidentyfikowano dziewięć genów docelowych związanych z funkcjonowaniem BBB w grupie TAA. Wykorzystując narzędzie bioinformatyczne String, przeanalizowano funkcje biologiczne przewidywanych genów docelowych. String pozwala na tworzenie sieci interakcji białkowych oraz identyfikację szlaków biologicznych, w których uczestniczą zidentyfikowane geny. Analiza GO (ang. gene ontology) oraz KEGG Pathways wskazały dziewięć procesów biologicznych związanych z funkcjonowaniem BBB, w tym w związanych z integrynami, połączeniami międzykomórkowymi oraz specyficznymi integralnymi składnikami błony komórkowej.
Wśród wytypowanych, miRNA-122-5p i miRNA-183-5p wyróżniały się jako potencjalnie kluczowe miRNA determinujące zmiany BBB w modelu TAA. Wskazano, że miRNA-122-5p potencjalnie reguluje poziom ekspresji okludyny, białka kluczowego dla utrzymania szczelności TJ. Z kolei miRNA-183-5p zidentyfikowano jako regulator integryny β1, białka determinującego m.in. adhezję komórek i interakcje komórka-macierz zewnątrzkomórkowa. Analiza qRT-PCR potwierdziła także wzrost poziomu ekspresji miRNA-122-5p oraz miRNA-183-5p w mózgu szczurów TAA (Publikacja 1, Ryc. 3).
Powyższe analizy zweryfikowano eksperymentalnie. Badania *in vitro* wykazały, że traktowanie komórek amoniakiem i TNFα prowadziło do wzrostu poziomu ekspresji miRNA-122-5p, i obniżało poziom mRNA dla okludyny i integryny β1 (Publikacja 1, Ryc. 4B oraz Ryc. 6A). Z kolei transfekcja komórek RBE4, sekwencjami miRNA-122-5p powodowała obniżenie poziomu okludyny, a transfekcja miRNA-183-5p poziomu integryny β1 oraz hamowała adhezję komórek do kolagenu I (Publikacja 1, Ryc. 7).
W izolowanych naczyniach mózgowych szczurów TAA zaobserwowano zmniejszenie intensywności fluorescencji okludyny i integryny β1 w porównaniu z grupą kontrolną (Publikacja 1, Ryc. 5C). Obniżenie immunofluorescencji białek było wyraźne zarówno w izolowanych naczyniach mózgowych, jak i w skrawkach tkankowych kory przedczołowej szczurów (Publikacja 1, Ryc. 5B).
Analiza obrazów w mikroskopie konfokalnym wykazała, że komórki śródbłonka naczyń mózgowych szczurów poddane działaniu amoniaku i/lub TNF wykazywały zmniejszoną intensywność okludyny, co wskazuje na degradację TJ. Podobnie, zmniejszona intensywność barwienia integryny β1 sugerowała osłabienie interakcji komórkowych i adhezji z macierzą zewnątrzkomórkową (Publikacja 1, Ryc.6 B).

Ad. Cel szczegółowy 4

W modelu OA szczura wykazano zmniejszenie gęstości naczyń w korze mózgowej, co oceniano i kwantyfikowano na podstawie pomiaru intensywności fluorescencji czynnika von Willebranda, powszechnie stosowanego markera naczyń. Zmniejszenie gęstości unaczynienia było zbieżne i porównywalne z obniżoną intensywnością fluorescencji obserwowaną u szczurów 12 miesięcznych (Manuskrypt na etapie recenzji).

Na podstawie przeprowadzonej analizy *in silico* zidentyfikowano 306 miRNA, których ekspresja była zmieniona zarówno w próbkach kory mózgowej i surowicy szczurów w modelu OA. Zidentyfikowano regulowane 852 geny docelowe. Następnie, geny przypisano do zdefiniowanych procesów fizjologicznych przy użyciu analizy ShinyGO, która wykazała, że miRNA-183-5p reguluje 117 genów związanych z procesami starzenia komórkowego. Z uwagi na fakt, że następne w kolejności miRNA-200-3p regulowało jedynie 17 genów, miRNA-183-5p wybranych do dalszych badań. W wyniku opisanej analizy, wskazano miRNA-183-5p jako potencjalny czynnik, który może być zaangażowany w wywołane patofizjologicznymi stężeniami jonów amonowych zmiany fenotypu komórek śródbłonka mózgu szczura (dane niepublikowane, manuskrypt na etapie recenzji). W kolejnych badaniach *in vitro* przeprowadzonych na komórkach linii RBE4 oraz pierwotnej hodowli komórek śródbłonka mikronaczyń PBMEC traktowanych amoniakiem o stężeniu 5 mM, wykazano fenotyp charakterystyczny dla procesu starzenia komórkowego (dane niepublikowane, manuskrypt na etapie recenzji). Obserwowano m.in. zwiększoną aktywność enzymu β-galaktozydazy, wzrost poziomu ekspresji mRNA p16 i p21 oraz zwiększoną intensywność fluorescencji białka p53 (dane niepublikowane, manuskrypt na etapie recenzji). Komórki linii RBE4 w obecności amoniaku wykazywały obniżoną proliferację, co jest zgodne z wcześniejszymi obserwacjami przeprowadzonymi w Zakładzie Neurotoksykologii IMDiK PAN [120]. Wykazano wzrost poziomu miRNA-183-5p w komórkach RBE4 i PBMEC traktowanych amoniakiem, jak również w pęcherzykach zewnątrzkomórkowych izolowanych z medium hodowlanego komórek (dane niepublikowane, manuskrypt na etapie recenzji). Zmiany wskazujące na proces starzenia komórkowego obserwowano następnie w komórkach RBE4 i PBMEC transfekowanych sekwencjami mimic-miRNA-183-5p. Zarówno w komórkach śródbłonka naczyń mózgu szczura traktowanych amoniakiem, jak i w komórkach transfekowanych mimic-miRNA-183-5p, obserwowano zmieniony fenotyp wydzielniczy (sekrecyjny) tzw. czynniki fenotypu starzenia (SASP), tj.: ICAM-1, TNF-α, V-CAM i VEGF (dane niepublikowane, manuskrypt na etapie recenzji). Wzrost wewnątrz-komórkowego poziomu wolnych rodników tlenowych, obniżony potencjał błony mitochondrialnej oraz spadek potencjału antyoksydacyjnego wraz ze zmianami poziomu ekspresji mRNA genów kodujących białka odpowiedzialne za procesy fuzji i podziału, z przesunięciem dynamiki zmian w kierunku rozszczepienia, wykazano na komórkach RBE4 traktowanych amoniakiem lub TNFα (Publikacja 2, Ryc. 2 oraz Ryc. 3). Równolegle, w korze mózgowej szczurów OA obserwowano wzrost poziomu ekspresji genów kontrolujących fuzję mitochondriów (*Opa1*, *Mfn1*), podczas gdy w modelu TAA był wyraźny spadek, zaś wzrost poziomu ekspresji mRNA genu *Fis1*, kontrolującego rozszczepienie mitochondriów, sugerując wyjście z fenotypu starzenia (Publikacja 2, Ryc. 4).

Ad. Cel szczegółowy 5

Zaprojektowano i wykonano urządzenie do pomiaru rezystancji warstwy komórek, co uznawane jest przesłankę dokumentującą integralność bariery komórkowej, np. komórkowych modeli BBB. Urządzenie tworzą innowacyjne komponenty, dostosowane do potrzeb elektrody i przyjazne dla użytkownika oprogramowanie, co umożliwia dokładne pomiary integralności bariery komórkowej. Urządzenie testowano wykorzystując linię komórkową RBE4, komórki śródbłonka naczyń mózgu szczura, PMEC, pierwotną hodowlę komórek śródbłonka naczyń mózgu szczura, PBMEC oraz linię komórkową ludzkiego nabłonka jelitowego, HIEC. Urządzenie, wykazywało stabilne wartości pomiarów oporu, a komórki traktowane chlorkiem amonu w stężeniu 5 mM manifestowały niższe wartości, w porównaniu do komórek kontrolnych, co potwierdzono również pomiarem przepuszczalności monowarstwy komórek z użyciem barwnika fluoresceiny sodu oraz mikroskopią konfokalną (Publikacja 3, Tab. 1, Ryc. 6). Pomiar fluorescencji z mikroskopii konfokalnej pozwolił na porównanie poziomu ekspresji białka ZO-1 między badanymi grupami.

Wyniki udokumentowały precyzję pomiarów w odniesieniu do weryfikowanego zakresu biologicznego (różne typy analizowanych komórek) (Publikacja 3, Tab. 1). Ponadto testowano inercję urządzenia: brak wpływu temperatury i pH na otrzymywane wartości pomiaru, co umożliwia długoterminowe, monitorowanie stabilności bariery komórkowej (Publikacja 3, Ryc. 5).

W pracy przeglądowej (Publikacja 4) dokonano analizy dostępnych danych opublikowanych w pracach z obszaru doniesień klinicznych, dotyczących analiz miRNA osocza, i wykorzystano je do oceny potencjału miRNA w komunikacji między wątrobą a mózgiem, w kontekście badanego w dysertacji schorzenia. Istotą systematycznego przeglądu literatury było zrozumienie, w jaki sposób miRNA mogą determinować funkcje BBB i odzwierciedlać uszkodzenia związane z ALF. Założono, że identyfikacja specyficznych miRNA, których poziom wykazywano jako zmieniony we krwi pacjentów z ALF, może prowadzić do opracowania nowych, szybkich i mniej inwazyjnych testów diagnostycznych. Ponadto, jednoznaczne wskazanie na konkretne miRNA mogące determinować komunikację na osi wątroba-mózg mogło dostarczyć nowej wiedzy dotyczącej patomechanizmu HE typu A.

Przeprowadzony systematyczny przegląd literatury objął wyniki pochodzące z 21 prac, w których zawarto wyniki pochodzące od 852 pacjentów z ostrym uszkodzeniem wątroby wskutek przedawkowania acetaminofenu, zakażeń wirusowych, zatruciem toksycznym - grzybami, autoimmunologicznego zapalenia wątroby oraz innych czynników etiologicznych nieznanego pochodzenia (Publikacja 4, Ryc. 1). Zidentyfikowano 205 istotnie zmienionych miRNA w osoczu, spośród których, a 25 istotnie zmienionych miRNA powtarzało się we wszystkich pracach (Publikacja 4, Ryc. 2).

Wybrane zmienione miRNA poddano analizie in silico pod kątem ich specyficznego pochodzenia tkankowego i potencjału do regulacji szlaków molekularnych związanych z funkcjonowaniem BBB. Analiza wykazała udział wskazanych miRNA w procesach kluczowych dla utrzymania integralności BBB i w konsekwencji właściwego funkcjonowania OUN. Wskazane szlaki KEGG dotyczyły procesów: Focal adhesion (hsa:04520), Adherens junctions (hsa:045020), Tight junctions (hsa04530), Gap junctions (hsa04550) (Publikacja 4,

Ryc. 6). Wytypowane szlaki sugerują, że ich deregulacja może być związana z dysfunkcją BBB w przebiegu HE. Zidentyfikowane, 25 istotnie zmienione miRNA osocza, szczególnie te o wysokiej specyficzności tkankowej dla wątroby lub mózgu, mogą służyć jako biomarkery do wczesnej diagnostyki, prognozowania, i w przyszłości być może zweryfikowania możliwych interwencji terapeutycznych w stanach chorobowych wynikających z uszkodzenia wątroby. Na podstawie przeanalizowanych danych, przedstawiono równolegle interesującą zależność między poziomem ALT i AST i miRNA-122-5p (Publikacja 4, Ryc. 3). Wzrost miRNA-122-5p korelował z aktywnością enzymów ALT i AST w surowicy, co wskazywało pośrednio na możliwość wykorzystania miRNA-122-5p jako markera dysfunkcji i oceny stopnia uszkodzenia wątroby.

Należy podkreślić, że prace, na których oparto przegląd literaturowy, nie zawierały jednolitych informacji klinicznych. Ograniczeniem przede wszystkim był brak szczegółowych informacji dotyczących wystąpienia lub ewentualnej oceny stopnia obrzęku mózgu. Chociaż przegląd literatury pozwolił na wyłonienie miRNA potencjalnie związanych z uszkodzeniem BBB, brak jednoznacznego wskazania na korelację z danymi klinicznymi stanowi ograniczenie ogólnego znaczenia pracy. Dalsza weryfikacja i korelacja miRNA z uszkodzeniami BBB/obrzękiem w ALF, obejmująca kompleksową ocenę kliniczną pacjentów oraz diagnostykę obrzęku mózgu pozostają celami przyszłych badań.

PODSUMOWANIE WYNIKÓW

Dotychczasowa wiedza na temat złożonego i wieloczynnikowego patomechanizmu HE głównie definiuje rolę kluczowych czynników patogennych (m.in. amoniaku, stanu zapalnego). W dysertacji wykorzystano intensywnie rozwijane techniki wysokoprzepustowe, umożliwiające m.in. identyfikację jednoniciowych miRNA, i założono, że mogą być przydatne w identyfikacji klinicznie najpoważniejszego powikłania ostrej HE, jakim jest obrzęk mózgu, obejmujący uszkodzenia BBB w tym, zmiany śródbłonka naczyń mózgowych.

W projekcie przeprowadzono analizę sekwencjonowania miRNA osocza i kory czołowej mózgu zwierząt z wywołaną hiperamonemią prostą i ostrym uszkodzeniem wątroby, co umożliwiło wytypowanie miRNA, które korelowano z obserwowanym uszkodzeniem BBB. Uszkodzenia obejmowały zmiany morfologii komórek śródbłonka oraz zwiększoną przepuszczalność, zaś na poziomie komórki, zmiany poziomu ekspresji badanych białek, ze wskazaniem ich znaczenia funkcjonalnego.

Zmniejszona gęstość naczyń mózgowych sugerowała zaburzenia w unaczynieniu mózgu, porównywalne z unaczynieniem mózgu obserwowanym u szczurów 12 miesięcznych, sugerując, że charakter zmian w warunkach hiperamonemii częściowo odzwierciedla zmiany charakteryzujące starzenie normatywne.

Wytypowane miRNA ze względu na charakter cząsteczek (potencjalny biomarker) mogą stanowić interesujący punkt wyjścia do uwzględnienia znaczenia krążących miRNA w diagnostyce klinicznej, a być może stać się inspiracją do podjęcia prób przyszłych interwencji farmakologicznych nakierowanych na identyfikację lub kontrolę obrzęku mózgu - z selektywnym uwzględnieniem komponenty naczyniowej.

Wartością interdyscyplinarną dysertacji jest zaprojektowany i zbudowany autorski system do pomiaru rezystancji elektrycznej monowarstwy komórek śródbłonka, powstały na potrzeby badań *in vitro*, wykorzystywane do oceny szczelności i integralności komórkowego modelu BBB.

Na podstawie przeglądu literatury obejmującej dostępne dane kliniczne dotyczące analizy miRNA w osoczu pacjentów z ostrą niewydolnością wątroby, i przeprowadzonej analizie *in silico* wskazano, że 15 miRNA, w tym: miRNA-1247-5p, -125b-5p, -375, -194-5p, -221-3p, -122-5p, -320a, -320b, -320c, -148a-3p, -103a-3p, -107, -30a-5p, -23b-3p, oraz -24-3p posiadają potencjał diagnostyczny mogący służyć weryfikacji uszkodzeń BBB, do tej pory nie opisany w kontekście komunikacji między wątrobą a mózgiem.

DYSKUSJA

Złożony i wieloczynnikowy patomechanizm HE stanowi wyzwanie ukierunkowanych terapii skupiających się na poszczególnych objawach klinicznych, pojawiających się w przebiegu lub w stanach zaostrzenia choroby. Najpoważniejszą konsekwencją kliniczną HE jest obrzęk mózgu, z często współwystępującym uszkodzeniem BBB. W przebiegu zarówno przewlekłej, jak i ostrej HE u pacjentów dokumentowano zmiany strukturalne BBB [40,121–123]. Dysfunkcję BBB na poziomie struktury i funkcji dokumentowały również badania przeprowadzane na modelach zwierzęcych [124–130].
Jednak w dalszym ciągu szczegółowa wiedza, dotycząca uszkodzenia i dysfunkcji poszczególnych elementów BBB w HE, poza identyfikacją kluczowych czynników sprawczych uszkodzeń BBB, takich jak amoniak czy stan zapalny, jest niepełna, mając na względzie liczbę współgrających elementów.
W przebiegu procesów patologicznych, coraz częściej uwaga badaczy koncentruje się na znaczeniu jednoniciowych, niekodujących RNA - mikroRNA (miRNA), które regulują ekspresję genów na poziomie potranskrypcyjnym. Pomimo pojawiających się w literaturze badań wskazujących na rolę niektórych miRNA (np.: miRNA-29, miRNA-146, miRNA-155, miRNA-15a, miRNA-126) w regulacji funkcji BBB, a także ich udziału w patomechanizmach różnych chorób OUN, szczegółowe znaczenie miRNA w uszkodzeniu BBB w HE, z wyszczególnieniem stanu hiperamonemii bez uszkodzenia wątroby, jak dotąd nie udokumentowano.

Na wyniki przedstawionych w dysertacji badań składają się określenie profilu miRNA osocza i kory mózgowej, wraz z analizą struktury i funkcji BBB w szczurzym modelu ostrej niewydolności wątroby oraz hiperamonemii. Na podstawie analizy *in silico* i badań *in vitro* wykazano, że miRNA-122-5p oraz miRNA-183-5p, poprzez udział w regulacji ekspresji białek wchodzących w skład połączeń ścisłych między komórkami lub okludyny i integryny β1, mogą być zaangażowane w patomechanizm uszkodzenia BBB, a bardziej szczegółowo - zmiany w komórkach śródbłonka naczyń mózgowych.

Wykazane zmiany morfologii komórek śródbłonka, tj. powiększenie komórek, pofałdowania błony komórkowej, wraz z obrzękiem i zmienionym kształtem mitochondriów, sugerują dysfunkcję BBB. U szczurów z wywołaną podaniem galaktozaminy ostrą HE, i myszy AOM, wykazano zwiększoną przepuszczalność dla EB [129,131]. W mysim modelu ostrej HE wykazano degradację połączeń ścisłych oraz białek macierzy zewnątrzkomórkowej [132,133], a także rozszczelnienie BBB [128,134-136].

W naszych badaniach, zmiany morfologiczne komórek śródbłonka w modelu TAA korelowały ze zwiększoną przepuszczalnością komórek dla SF, ale nie dla EB. Wynik ten sugeruje subtelne uszkodzenie BBB, jednak w konsekwencji na tyle istotne, że mogące mieć implikacje dla przenikania toksyn do mózgu i pogłębiania się objawów neurologicznych. W innych badaniach udokumentowano, że w modelu TAA, testy behawioralne dokumentowały zmniejszoną aktywność lokomotoryczną, zaburzenia koordynacji ruchowej oraz zaburzenia poznawcze, w tym deficyty pamięci i zdolności uczenia się [137,138]. Podanie acetaminofenu z kolei powodowało wyraźne objawy neurologiczne, takie jak obniżenie aktywności

spontanicznej, deficyty eksploracyjne i zdolności poznawcze, po utratę odruchu rogówkowego [139-141]. Z kolei szczury w modelu podwiązania przewodu żółciowego, prezentowały zmniejszoną aktywność społeczną oraz zmiany strukturalne mózgu odwzorowujące zmiany obserwowane u pacjentów z HE [142,143].

W modelu OA nie stwierdzono zmian morfologicznych oraz zmian przepuszczalności BBB, co sugeruje, że podwyższony poziom amoniaku nie jest w naszym modelu wystarczający do wywołania uszkodzenia [144,145]. Nie można jednak wykluczyć, że może mieć tu znaczenie zarówno stężenie podawanego OA, jak i czas ekspozycji.

Wyniki mogą również sugerować udział innych czynników, przykładowo: ogólnoustrojowego stanu zapalnego, krążących kwasów żółciowych, transformującego czynnika wzrostu beta 1, lub deregulacji innych cytokin, stresu oksydacyjnego, które w sposób addytywny do amoniaku mogą przyczyniać się do uszkodzenia BBB [120,146–149].

Sekwencjonowanie nowej generacji wykazało istotne różnice w profilu miRNA osocza szczurów TAA i OA. W modelu TAA zidentyfikowano 128 zmienionych miRNA, natomiast w modelu OA stwierdzono ich 35. Kilka wcześniejszych badań wytypowało miRNA powiązane z HE, których kierunek zmian został potwierdzony także w niniejszej pracy [150-155]. Prace te jednak, raportują również inne miRNA, co może wynikać z odmiennej patofizjologii zastosowanych modeli badawczych oraz metod analizy [156]. Wykonana w ramach niniejszej pracy analiza *in silico* zidentyfikowanych miRNA polegająca na przetwarzaniu danych biologicznych, w tym sekwencji RNA i białek, za pomocą komputerowych algorytmów, wskazała miRNA-122-5p i miRNA-183-5p jako mogące regulować białka okludynę i integrynę β1.
Okludyna jest białkiem transbłonowym, wchodzącym w skład TJ komórek śródbłonka naczyń mózgowych, stanowiących integralną część BBB, chroniąc przed niekontrolowanym przepływem substancji między krwią a tkankami mózgu [157]. Jej struktura obejmuje cztery transmembranowe domeny oraz część cytoplazmatyczną, która wiąże się z innymi białkami strukturalnymi i sygnalizacyjnymi w kompleksie TJ [158]. Integryna β1 jest białkiem receptorowym obecnym na powierzchni komórek śródbłonka, które uczestniczy w adhezji komórek do macierzy zewnątrzkomórkowej oraz bierze udział w sygnalizacji międzykomórkowej. Współuczestniczy w regulacji interakcji między komórkami śródbłonka i otaczającym środowiskiem [159]. Integryna β1 jest zaangażowana w przekazywanie sygnałów mechanicznych, prowadząc do odpowiedzi biochemicznej, co jest istotne np. dla adaptacji naczyń krwionośnych do warunków fizjologicznych i patologicznych [160].
W dysertacji wskazano, że miRNA-122-5p może wpływać bezpośrednio na jedno z białek strukturalnych BBB, i w ten sposób przyczyniać się do dysfunkcji BBB. MiRNA-122-5p jest swoisty dla wątroby; jego nadekspresja w modelu TAA wiąże się z uszkodzeniem wątroby wskutek działania hepatotoksycznego TAA. Wykazano, że miRNA-122-5p jest uwalniane w mikropęcherzykach, tj. egzosomach, które chronią je przed degradacją i umożliwiają transport do innych komórek [161]. Inny mechanizm opiera się na wiązaniu miRNA-122 do białek argonauta (AGO), zwłaszcza AGO2 [162]. Powstające stabilne kompleksy mogą być uwalniane z komórek, co umożliwia miRNA-122 przedostawanie się do krwiobiegu i dotarcie

do komórek docelowych. Dodatkowo, miRNA-122 może być przenoszone przez lipoproteiny wysokiej gęstości, które również chroni je przed degradacją [163–165].

Wyniki badań *in vitro* wykazały, że transfekcja mimic-miRNA-122-5p komórek śródbłonka, spowodowała znaczną redukcję poziomu mRNA okludyny. Warto zauważyć, że w naszych doświadczeniach transfekcja mimic-miRNA-122 nie prowadziła do wzrostu przepuszczalności monowarstwy komórek śródbłonka naczyń, modelu *in vitro* BBB. Prawdopodobnie świadczy to o złożonym mechanizmie kontroli transkrypcji okludyny, zależnym od innych czynników. Badania wskazały na udział szeregu czynników transkrypcyjnych w regulacji procesu [166,167]. Ponadto zidentyfikowano szlaki sygnalizacyjne z czynnikami Raf1, GSK-3, EGFR i PKC, również regulujące proces transkrypcji [167–170].

Drugi z wytypowanych zmienionych miRNA, miRNA-183-5p należy do klastra zlokalizowanego na chromosomie 7q32.2, który obejmuje również miRNA-96 i miRNA-182. miRNA-183-5p jest związany z regulacją apoptozy i proliferacją komórkową [3,43]. Analiza *in silico* wskazała, że może on regulować należącą do białek adhezyjnych integrynę β1. W naszych badaniach transfekcja komórek śródbłonka mimic-miRNA-183-5p powodowała obniżenie poziomu mRNA integryny β1 i redukowała adhezję komórek do podłoża, implikując zmiany na styku komórka-macierz zewnątrzkomórkowa.

Wydaje się, że zmieniony profil miRNA osocza po selekcji odpowiednich miRNA, może być wykorzystany jako potencjalny marker uszkodzenia BBB w HE, jednak pełne wykorzystanie tej wiedzy wymaga bardziej szczegółowych badań. Identyfikacja specyficznych miRNA, takich jak miRNA-122-5p i miRNA-183-5p, może w przyszłości być pomocna w opracowaniu nowych strategii diagnostycznych, umożliwiających wczesne wykrycie i monitorowanie uszkodzenia BBB w HE. Ponadto, wskazane miRNA mogą stanowić potencjalne cele terapeutyczne.

Oczywistym ograniczeniem, które należy uwzględnić rozważając znaczenie omawianych wyników jest fakt, że analizy dotyczą modeli zwierzęcych, co może utrudniać bezpośrednie wykorzystanie efektów badań i ich przełożenie na warunki kliniczne. Chociaż prezentowane dane wskazują na udział w regulacji wybranych białek BBB, w badaniach nie analizowano roli pozostałych komponentów komórkowych BBB, których udział w kontroli właściwego działania BBB jest nie do przecenienia. Jednostka nerwowo-naczyniowa jest układem złożonym z neuronów, komórek glejowych (w tym astrocytów), komórek śródbłonka, perycytów i elementów macierzy pozakomórkowej. Udokumentowano, że wszystkie wymienione elementy biorą udział w utrzymaniu homeostazy mózgu, co może dokumentować kontrola przepływu krwi w odpowiedzi na potrzeby metaboliczne neuronów [171,172].
Poza tym, jedną z istotnych funkcji komórek śródbłonka naczyń mózgu wobec astrocytów, głównego celu działania amoniaku, jest funkcja ochronna, regulująca środowisko wewnętrzne, poprzez kontrolę aktywnego transportu substancji do mózgu i usuwanie produktów zbędnych [173]. Prawidłowo funkcjonujące, tworzące BBB komórki śródbłonka, chronią astrocyty przed toksycznymi metabolitami. Komórki śródbłonka wydzielają czynniki neuroprotekcyjne,

przykładowo NO, który reguluje przepływ krwi i zmniejsza ryzyko wystąpienia procesów zapalnych [174], zaś działając rozszerzająco na naczynia krwionośne, poprawia perfuzję mózgu, w tym dostarczanie tlenu i substancji odżywczych. Pod wpływem stresu oksydacyjnego i stanu zapalnego, funkcjonowanie komórek śródbłonka jest ograniczone, zaś stres oksydacyjny uszkadzając struktury białkowe i lipidowe, pogarsza działanie BBB [174].

Proces starzenia komórkowego - senescencja, to stan trwałego zatrzymania wzrostu komórki, do którego dochodzi w odpowiedzi na różne stresory, takie jak uszkodzenia DNA, stres oksydacyjny, skracanie telomerów czy aktywacja onkogenów. Komórki pozostające w procesie starzenia są metabolicznie aktywne i prezentują charakterystyczny profil sekrecyjny. Ten charakterystyczny zestaw czynników, określany jako SASP, obejmuje cytokiny, chemokiny, proteazy i czynniki wzrostu. Komórki będące w stanie spoczynku (ang. quiescent cells) cechują się zatrzymanymi podziałami komórkowymi, ale w określonych warunkach mogą ponownie wejść w cykl komórkowy, odpowiadając na odpowiednie sygnały [175]. Stan spoczynku jest istotny przy regulacji rezerw komórkowych w tkankach w przebiegu procesów regeneracyjnych. Z definicji może być odwracalny i charakteryzuje się niską aktywnością metaboliczną oraz brakiem wyraźnych markerów uszkodzenia DNA czy stresu oksydacyjnego [176]. Wyniki zawarte w dysertacji, dokumentują, że hiperamonemia zmienia BBB, w szczególności w kontekście subtelnych zmian w obrębie mikronaczyń mózgu tworzonych przez komórki śródbłonka. Wykazaliśmy, że w komórkach linii RBE4 traktowanych amoniakiem dochodzi do wzrostu produkcji ROS oraz wyraźnie obniżonego potencjału antyoksydacyjnego. Ponadto, spadek proliferacji komórek oraz analiza markerów starzenia wskazywała na zmieniony fenotyp komórek wskutek działania amoniaku, zgodny z opisywanym w literaturze fenotypem starzenia [93,177,178].

Na podstawie analizy profilu istotnie zmienionych miRNA osocza oraz kory mózgowej szczurów OA, miRNA-183-5p, wykazywał związek z procesami implikującymi starzenie komórkowe. Istotny statystycznie wzrost poziomu ekspresji wytypowanego miRNA wykazano w komórkach śródbłonka mózgu szczurów traktowanych amoniakiem oraz w izolowanych z medium hodowlanego, pęcherzykach zewnątrzkomórkowych. Na poziomie molekularnym wydaje się, że miRNA-183-5p może być jednym z mechanizmów odpowiedzialnych za ten proces w warunkach hiperamonemii. Transfekcja komórek śródbłonka mimik-miRNA-183-5p odwzorowała fenotyp starzenia, co może potwierdzać to założenie.

Co ciekawe, w szczurzym modelu OA, na podstawie oceny intensywności fluorescencji markera von Willebranda w tkance mózgowej zwierząt wykazano obniżenie gęstości naczyń, porównywalne ze zmianami obserwowanymi u szczurów 12 miesięcznych. Wyniki te sugerują, że hiperamonemia może sprzyjać indukcji lub przyspieszać proces starzenia naczyń mózgowych, co może mieć implikacje dla zrozumienia mechanizmów zachodzących w procesie neurodegeneracji. W kontekście patologii związanych z podwyższonym stężeniem amoniaku, wykazano u osób starszych częstsze występowanie marskości wątroby w porównaniu z młodszymi pacjentami [179]. Ponadto, współwystępowanie przewlekłej niewydolności wątroby i marskości wątroby u osób starszych może prowadzić do szybkiego postępu choroby, niewydolności wątroby czy raka wątrobowokomórkowego [180].

W przebiegu marskości wątroby, starzenie może modulować zmiany neurologiczne, obniżające jakość życia, w tym funkcje poznawcze i wykonawcze. Za przyczyny sprawcze uważa się przewlekły stan zapalny, aktywację mikrogleju czy zmiany neurotransmisji GABA-ergicznej [181]. Znaczenie miRNA w regulacji najważniejszych procesów komórkowych jest wciąż przedmiotem zainteresowania; nawet niewielka zmiana poziomu ekspresji może powodować znaczące skutki biologiczne poprzez np. kontrolę wielu różnych miRNA (najczęściej w jednym szlaku regulacyjnym), czy bezpośrednio modulować szereg odpowiedzi [182].

MiRNA jest przedmiotem zaledwie kilku przeglądów literatury obejmujących dane kliniczne, a dotyczących zarówno ostrych, jak i przewlekłych HE. W pracach [183,184], proponowano miRNA-122-5p jako biomarker wczesnego wykrywania uszkodzeń wątroby wywołanych zatruciem lekami czy wskutek infekcji HBV. Autorzy sugerowali, że zmiany miRNA-122-5p mogą stanowić bardziej specyficzny marker uszkodzenia wątroby, niż tradycyjne analizy biochemiczne obejmujące oznaczanie enzymów wątrobowych. Z kolei w innej pracy, wytypowane miRNA (podwyższony poziom miRNA-138, miRNA-143, miRNA-34a, miRNA-122 i miRNA-221 oraz obniżony poziom miRNA-29a) oznaczane w różnych stadiach włóknienia wątroby były przedstawione jako regulatory patogenezy włóknienia wątroby, i według autorów, nieinwazyjne biomarkery diagnostyczne procesu [185].
W kontekście ostrej HE i uszkodzeń BBB obserwowanych w przebiegu obrzęku mózgu, udział miRNA nie był przedmiotem badań. W związku z tym, podjęto się systemowej analizy literatury, którą przeprowadzono korzystając z dwóch głównych baz danych MEDLINE i Elsevier Scopus, wykluczając badania dotyczące przewlekłych chorób wątroby lub problemów wieloczynnikowych, takich jak historia alkoholowa, przeszczep wątroby lub ciąża. W pracy systematycznie przeszukano bazy danych, obejmując oryginalne publikacje z okresu od 1 stycznia 2011 do 1 lipca 2021 roku, koncentrujące się na pacjentach z ostrą niewydolnością wątroby (ALF) i badaniach ekspresji miRNA. Dane zostały niezależnie wyselekcjonowane przez autorów, według ustalonych *a priori* kryteriów kwalifikowalności. Spośród 205 zmienionych we krwi miRNA, 25 z nich wskazano jako powtarzające się, co czyniło je potencjalnymi kandydatami do stworzenia panelu diagnostycznego ostrej HE. Wytypowane miRNA zidentyfikowano w próbkach od pacjentów głównie po zatruciu paracetamolem. miR-122-5p był najczęściej raportowany, wykazując znacząco wyższe wartości w grupie pacjentów, i silnie korelował z wartościami enzymów wątrobowych, ALT i AST. Dla wyselekcjonowanych 25 miRNA, zidentyfikowano łącznie 94 istotnie zmienionych ścieżek KEGG, związanych z adhezją komórkową - Focal adhesion (hsa04510), połączeniami międzykomórkowymi - Adherens junctions (hs04520), interakcją receptora z macierzą zewnątrzkomórkową - ECM-receptor interaction (hsa04512), cząsteczkami adhezyjnymi komórek - Cell adhesion molecules (hsa04514) oraz połączeniami szczelinowymi: Gap junctions (hsa04540). Wymienione ścieżki wydają się istotne dla utrzymania strukturalnej i funkcjonalnej integralności BBB.
W pracy przeanalizowano specyficzne tkankowo wzorce ekspresji miRNA, korzystając z Human miRNATissueAtlas [186]. Wyniki obejmowały miRNA specyficzne dla wątroby: miRNA-122-5p, miRNA-21-5p, miRNA-320c i miRNA-148a. Poziom ekspresji miRNA-

125b-5p w mózgu był znacznie wyższy niż w wątrobie, co sugerowało jego mózgową specyficzność. Badanie wykazało, że w normalnych warunkach miRNA specyficzne dla wątroby, takie jak miRNA-122-5p, oraz miRNA specyficzne dla mózgu, takie jak miRNA-125b-5p, są obecne na stosunkowo niskich poziomach w osoczu. Jednak ich znaczący wzrost we krwi pacjentów z HE typu A, sugeruje uszkodzenie tkanki i podkreśla ich potencjał diagnostyczny w określeniu uszkodzeń, odpowiednio dla wątroby, i mózgu. Dane literaturowe, sugerowały także, że rodzina miRNA-183, w skład której wchodzi miRNA-182, miRNA-183-5p i miRNA-96, ulega wysokiej ekspresji w tkance nerwowej [187].
Ograniczeniem przeprowadzonej analizy literatury jest brak w pracach dostępnych danych klinicznych, równolegle wskazujących na obecność obrzęku mózgu u pacjentów. Brak tych informacji nie pozwolił jednoznacznie potwierdzić i korelować wyłonione zmienione miRNA z uszkodzeniami BBB w ostrej HE.
Pomimo dostarczonych w niniejszej dysertacji, danych łączących miRNA-183-5p z uszkodzeniem BBB wykazanym w modelach *in vivo* i *in vitro*, przeprowadzona analiza *in silico* nie dostarczyła wystarczających przesłanek do uznania miRNA-183-5p za jeden z potencjalnych biomarkerów uszkodzenia BBB w ostrej HE. Należy wziąć pod uwagę, że wszystkie analizy informatyczne opierają się wyłącznie na dostępnych bazach danych, które wykorzystywane są w danej analizie. Dostępne bazy mogą nie posiadać pełnych wpisów i informacji dla wszystkich możliwych interakcji miRNA, szczególnie jeśli chodzi o nowo odkryte, lub mniej badane miRNA. Używane algorytmy predykcyjne mogą różnić się pod względem czułości i specyficzności. Różnice w modelach obliczeniowych i wadze przypisywanej różnym typom dowodów (np. miejsc wiązania, walidacja eksperymentalna) mogą prowadzić do zmienności w przewidywanych celach. Wzorce ekspresji i sieci regulacyjne miRNA mogą być zależne od kontekstu. Zatem, miRNA-183-5p może pełnić rolę w specyficznych, patologicznych warunkach, takich jak towarzyszące HE uszkodzenie BBB, które nie są odpowiednio identyfikowane w ogólnych zbiorach danych używanych do predykcji *in silico*. Predykcje te, często wymagają wnikliwej walidacji eksperymentalnej, aby potwierdzić ich biologiczne znaczenie. Nasze badania, dostarczają dowodów, wskazując na udział miRNA-183-5p w obniżeniu poziomu ekspresji integryny β1, korelując tę obserwację ze zmienioną integralnością BBB w szczurzym modelu ostrego uszkodzenia wątroby, jak i z obniżoną adhezją w hodowanych komórkach śródbłonka naczyń mózgowych.

Warto podkreślić, że poznanie mechanizmów uszkodzeń BBB może mieć również znaczenie w kontekście mechanizmów związanych z regeneracją komórek śródbłonka [188,189]. Pomimo, że komórki endotelialne mogą się odnawiać, procesy, które prowadzą do ich uszkodzenia, są złożone i wymagają kompleksowego poznania, w szczególności określenia czynników wspomagających lub hamujących regenerację komórek śródbłonka [190-192]. Proces regeneracji, nie zawsze oznacza pełne przywrócenie funkcji, co może wpływać na stan i efektywność BBB, warto pamiętać, że przewlekłe narażenie na toksyny często prowadzi do kumulacji uszkodzeń, przekraczających zdolności regeneracji [193].

WNIOSKI

1. Na podstawie analizy sekwencjonowania miRNA osocza i kory czołowej mózgu szczurów z hiperamonemią prostą i z ostrym uszkodzeniem wątroby, oraz analizy *in silico*, zidentyfikowano miR-122-5p oraz miR-185-5p, których potencjalną rolę w dysfunkcji BBB zweryfikowano w badaniach *in vivo* i *in vitro*.
2. W mózgach szczurów z ostrym uszkodzeniem wątroby udokumentowano zmiany na poziomie ultrastruktury komórek śródbłonka naczyń mózgowych, najbardziej istotnej komponenty strukturalnej BBB, wskazujące na obrzęk tych komórek, dodatkowo obrzęk mitochochondriów i uszkodzenia błony cytoplazmatycznej w obrębie powierzchni sąsiadujących ze sobą (tj. złączy ścisłych).
3. Udokumentowano, zależną od amoniaku i związaną z miR-183-5p zmianę fenotypu komórek śródbłonka naczyń mózgowych szczura, charakterystyczną dla procesu starzenia komórkowego, co poza spadkiem poziomu ekspresji integryny β1, sugerującym zmienioną interakcję w obrębie komórki i macierzy zewnątrzkomórkowej, może być elementem nieprawidłowości w unaczynieniu mózgu.
4. Zaprojektowano, wykonano i przetestowano autorskie urządzenie pomiarowe, umożliwiające ocenę rezystancji warstwy komórek, warunkującą właściwą funkcję komórkowych modeli BBB, co stanowi wartość interdyscyplinarną dysertacji.

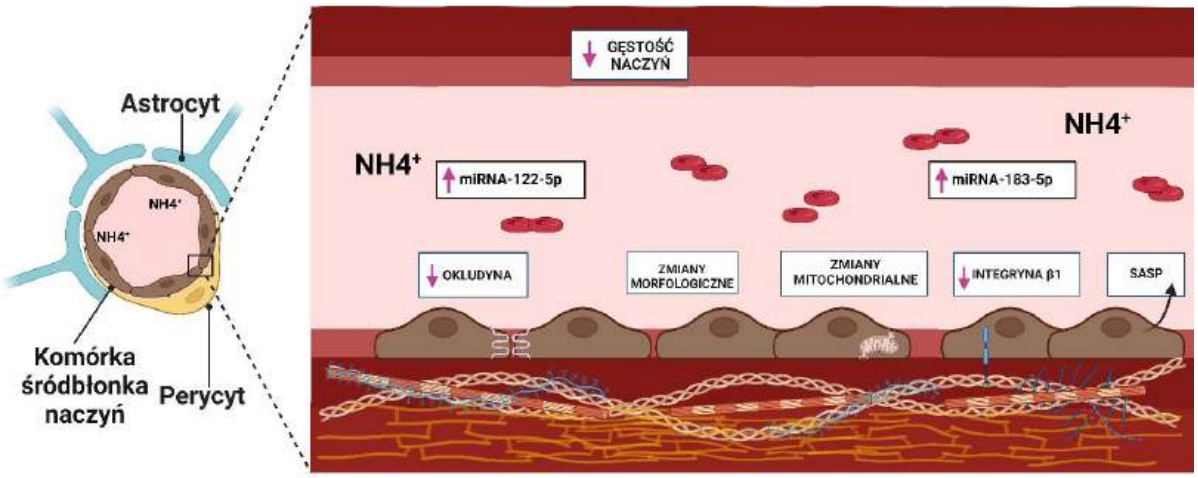

Ryc. 3. Graficzne przedstawienie wniosków.

LITERATURA

1. Zieve, L. Pathogenesis of Hepatic Encephalopathy. *Metabolic Brain Disease* **1987**, *2*, 147–165, doi:10.1007/BF00999607.

2. Raina, R.; Bedoyan, J.K.; Lichter-Konecki, U.; Jouvet, P.; Picca, S.; Mew, N.A.; Machado, M.C.; Chakraborty, R.; Vemuganti, M.; Grewal, M.K.; et al. Consensus Guidelines for Management of Hyperammonaemia in Paediatric Patients Receiving Continuous Kidney Replacement Therapy. *Nat Rev Nephrol* **2020**, *16*, 471–482, doi:10.1038/s41581-020-0267-8.

3. Frontera, J.A.; Kalb, T. Neurological Management of Fulminant Hepatic Failure. *Neurocrit Care* **2011**, *14*, 318–327, doi:10.1007/s12028-010-9470-y.

4. Zeneroli, M.L.; Ventura, E.; Baraldi, M.; Penne, A.; Messori, E.; Zieve, L. Visual Evoked Potentials in Encephalopathy Induced by Galactosamine, Ammonia, Dimethyldisulfide, and Octanoic Acid. *Hepatology* **2007**, *2*, 532S-538S, doi:10.1002/hep.1840020504.

5. Suraweera, D.; Sundaram, V.; Saab, S. Evaluation and Management of Hepatic Encephalopathy: Current Status and Future Directions. *Gut and Liver* **2016**, *10*, 509–519, doi:10.5009/gnl15419.

6. Bajaj, J.S.; Cordoba, J.; Mullen, K.D.; Amodio, P.; Shawcross, D.L.; Butterworth, R.F.; Morgan, M.Y. Review Article: The Design of Clinical Trials in Hepatic Encephalopathy - an International Society for Hepatic Encephalopathy and Nitrogen Metabolism (ISHEN) Consensus Statement: Review: ISHEN Consensus Statement for Hepatic Encephalopathy Trials. *Alimentary Pharmacology & Therapeutics* **2011**, *33*, 739–747, doi:10.1111/j.1365-2036.2011.04590.x.

7. Elsaid, M.I.; Rustgi, V.K. Epidemiology of Hepatic Encephalopathy. *Clinics in Liver Disease* **2020**, *24*, 157–174, doi:10.1016/j.cld.2020.01.001.

8. Fontana, R.J. Acute Liver Failure Including Acetaminophen Overdose. *Medical Clinics of North America* **2008**, *92*, 761–794, doi:10.1016/j.mcna.2008.03.005.

9. Rajaram, P.; Subramanian, R. Management of Acute Liver Failure in the Intensive Care Unit Setting. *Clinics in Liver Disease* **2018**, *22*, 403–408, doi:10.1016/j.cld.2018.01.013.

10. Vilstrup, H.; Amodio, P.; Bajaj, J.; Cordoba, J.; Ferenci, P.; Mullen, K.D.; Weissenborn, K.; Wong, P. Hepatic Encephalopathy in Chronic Liver Disease: 2014 Practice Guideline by the American Association for the Study Of Liver Diseases and the European Association for the Study of the Liver: Vilstrup et Al. *Hepatology* **2014**, *60*, 715–735, doi:10.1002/hep.27210.

11. Romero-Gómez, M. Pharmacotherapy of Hepatic Encephalopathy in Cirrhosis. *Expert Opinion on Pharmacotherapy* **2010**, *11*, 1317–1327, doi:10.1517/14656561003724721.

12. Ganesan, S.; Kumar Subramaniam, A.; Kandasamy, N.; Radhakrishnan, V. A STUDY OF USEFULNESS OF PSYCHOMETRIC TESTS IN DIAGNOSIS OF MINIMAL HEPATIC ENCEPHALOPATHY IN PATIENTS WITH CIRRHOSIS OF LIVER. *jemds* **2016**, *5*, 5889–5893, doi:10.14260/jemds/2016/1329.

13. Weiss, N.; Rosselli, M.; Mouri, S.; Galanaud, D.; Puybasset, L.; Agarwal, B.; Thabut, D.; Jalan, R. Modification in CSF Specific Gravity in Acutely Decompensated Cirrhosis and Acute on Chronic Liver Failure Independent of Encephalopathy, Evidences for an Early Blood-CSF Barrier Dysfunction in Cirrhosis. *Metab Brain Dis* **2017**, *32*, 369–376, doi:10.1007/s11011-016-9916-9.

14. Perazzo, J.C. Hepatic Encephalopathy: An Approach to Its Multiple Pathophysiological Features. *WJH* **2012**, *4*, 50, doi:10.4254/wjh.v4.i3.50.

15. Salgado, M.; Cortes, Y. Hepatic Encephalopathy: Diagnosis and Treatment. *Compend Contin Educ Vet* **2013**, *35*, E1-9; quiz E10.

16. Conn, H.O.; Lieberthal, M.M. *The Hepatic Coma Syndromes and Lactulose*; Williams & Wilkins: Baltimore, 1979; ISBN 978-0-683-02100-4.

17. Felipo, V.; Butterworth, R.F. Neurobiology of Ammonia. *Progress in Neurobiology* **2002**, *67*, 259–279, doi:10.1016/S0301-0082(02)00019-9.

18. Blaya, D.; Pose, E.; Coll, M.; Lozano, J.J.; Graupera, I.; Schierwagen, R.; Jansen, C.; Castro, P.; Fernandez, S.; Sidorova, J.; et al. Profiling Circulating microRNAs in Patients with Cirrhosis and Acute-on-Chronic Liver Failure. *JHEP Reports* **2021**, *3*, 100233, doi:10.1016/j.jhepr.2021.100233.

19. Kato, M.; Hughes, R.D.; Keays, R.T.; Williams, R. Electron Microscopic Study of Brain Capillaries in Cerebral Edema from Fulminant Hepatic Failure. *Hepatology* **1992**, *15*, 1060–1066, doi:10.1002/hep.1840150615.

20. Weissenborn, K.; Ennen, J.C.; Schomerus, H.; Rückert, N.; Hecker, H. Neuropsychological Characterization of Hepatic Encephalopathy. *Journal of Hepatology* **2001**, *34*, 768–773, doi:10.1016/S0168-8278(01)00026-5.

21. Schiff, S.; Casa, M.; Di Caro, V.; Aprile, D.; Spinelli, G.; De Rui, M.; Angeli, P.; Amodio, P.; Montagnese, S. A Low-cost, User-friendly Electroencephalographic Recording System for the Assessment of Hepatic Encephalopathy. *Hepatology* **2016**, *63*, 1651–1659, doi:10.1002/hep.28477.

22. Cisilotto, J.; Do Amaral, A.E.; Rosolen, D.; Rode, M.P.; Silva, A.H.; Winter, E.; Da Silva, T.E.; Fischer, J.; Matiollo, C.; Rateke, E.C.D.M.; et al. MicroRNA Profiles in Serum Samples from Acute-On-Chronic Liver Failure Patients and miR-25-3p as a Potential Biomarker for Survival Prediction. *Sci Rep* **2020**, *10*, 100, doi:10.1038/s41598-019-56630-5.

23. Bernal, W.; Hyyrylainen, A.; Gera, A.; Audimoolam, V.K.; McPhail, M.J.W.; Auzinger, G.; Rela, M.; Heaton, N.; O'Grady, J.G.; Wendon, J.; et al. Lessons from Look-Back in Acute Liver Failure? A Single Centre Experience of 3300 Patients. *Journal of Hepatology* **2013**, *59*, 74–80, doi:10.1016/j.jhep.2013.02.010.

24. Nguyen, J.H. Blood–Brain Barrier in Acute Liver Failure. *Neurochemistry International* **2012**, *60*, 676–683, doi:10.1016/j.neuint.2011.10.012.

25. Goldbecker, A.; Buchert, R.; Berding, G.; Bokemeyer, M.; Lichtinghagen, R.; Wilke, F.; Ahl, B.; Weissenborn, K. Blood–Brain Barrier Permeability for Ammonia in Patients with

Different Grades of Liver Fibrosis Is Not Different from Healthy Controls. *J Cereb Blood Flow Metab* **2010**, *30*, 1384–1393, doi:10.1038/jcbfm.2010.22.

26. Cui, W.; Sun, C.-M.; Liu, P. Alterations of Blood-Brain Barrier and Associated Factors in Acute Liver Failure. *Gastroenterology Research and Practice* **2013**, *2013*, 1–7, doi:10.1155/2013/841707.

27. Wei, X.-E.; Zhang, Y.-Z.; Li, Y.-H.; Li, M.-H.; Li, W.-B. Dynamics of Rabbit Brain Edema in Focal Lesion and Perilesion Area after Traumatic Brain Injury: A MRI Study. *Journal of Neurotrauma* **2012**, *29*, 2413–2420, doi:10.1089/neu.2010.1510.

28. Rose, C.; Kresse, W.; Kettenmann, H. Acute Insult of Ammonia Leads to Calcium-Dependent Glutamate Release from Cultured Astrocytes, an Effect of pH. *Journal of Biological Chemistry* **2005**, *280*, 20937–20944, doi:10.1074/jbc.M412448200.

29. Häussinger, D.; Dhiman, R.K.; Felipo, V.; Görg, B.; Jalan, R.; Kircheis, G.; Merli, M.; Montagnese, S.; Romero-Gomez, M.; Schnitzler, A.; et al. Hepatic Encephalopathy. *Nat Rev Dis Primers* **2022**, *8*, 43, doi:10.1038/s41572-022-00366-6.

30. Thrane, A.S.; Rappold, P.M.; Fujita, T.; Torres, A.; Bekar, L.K.; Takano, T.; Peng, W.; Wang, F.; Rangroo Thrane, V.; Enger, R.; et al. Critical Role of Aquaporin-4 (AQP4) in Astrocytic Ca $^{2+}$ Signaling Events Elicited by Cerebral Edema. *Proc. Natl. Acad. Sci. U.S.A.* **2011**, *108*, 846–851, doi:10.1073/pnas.1015217108.

31. Norenberg, M.D.; Jayakumar, A.R.; Rama Rao, K.V.; Panickar, K.S. New Concepts in the Mechanism of Ammonia-Induced Astrocyte Swelling. *Metab Brain Dis* **2007**, *22*, 219–234, doi:10.1007/s11011-007-9062-5.

32. Rama Rao, K.V.; Jayakumar, A.R.; Tong, X.; Alvarez, V.M.; Norenberg, M.D. Marked Potentiation of Cell Swelling by Cytokines in Ammonia-Sensitized Cultured Astrocytes. *J Neuroinflammation* **2010**, *7*, 66, doi:10.1186/1742-2094-7-66.

33. Tofteng, F.; Hauerberg, J.; Hansen, B.A.; Pedersen, C.B.; Jørgensen, L.; Larsen, F.S. Persistent Arterial Hyperammonemia Increases the Concentration of Glutamine and Alanine in the Brain and Correlates with Intracranial Pressure in Patients with Fulminant Hepatic Failure. *J Cereb Blood Flow Metab* **2006**, *26*, 21–27, doi:10.1038/sj.jcbfm.9600168.

34. Rama Rao, K.V.; Norenberg, M.D. Glutamine in the Pathogenesis of Hepatic Encephalopathy: The Trojan Horse Hypothesis Revisited. *Neurochem Res* **2014**, *39*, 593–598, doi:10.1007/s11064-012-0955-2.

35. Albrecht, J.; Norenberg, M.D. Glutamine: A Trojan Horse in Ammonia Neurotoxicity. *Hepatology* **2006**, *44*, 788–794, doi:10.1002/hep.21357.

36. Hamdani, E.H.; Popek, M.; Frontczak-Baniewicz, M.; Utheim, T.P.; Albrecht, J.; Zielińska, M.; Chaudhry, F.A. Perturbation of Astroglial Slc38 Glutamine Transporters by NH_4^+ Contributes to Neurophysiologic Manifestations in Acute Liver Failure. *The FASEB Journal* **2021**, *35*, doi:10.1096/fj.202001712RR.

37. Zielińska, M.; Albrecht, J.; Popek, M. Dysregulation of Astrocytic Glutamine Transport in Acute Hyperammonemic Brain Edema. *Front. Neurosci.* **2022**, *16*, 874750, doi:10.3389/fnins.2022.874750.

38. Jayakumar, A.R.; Ruiz-Cordero, R.; Tong, X.Y.; Norenberg, M.D. Brain Edema in Acute Liver Failure: Role of Neurosteroids. *Archives of Biochemistry and Biophysics* **2013**, *536*, 171–175, doi:10.1016/j.abb.2013.03.007.

39. Rama Rao, K.V.; Verkman, A.S.; Curtis, K.M.; Norenberg, M.D. Aquaporin-4 Deletion in Mice Reduces Encephalopathy and Brain Edema in Experimental Acute Liver Failure. *Neurobiology of Disease* **2014**, *63*, 222–228, doi:10.1016/j.nbd.2013.11.018.

40. Cudalbu, C.; Taylor-Robinson, S.D. Brain Edema in Chronic Hepatic Encephalopathy. *Journal of Clinical and Experimental Hepatology* **2019**, *9*, 362–382, doi:10.1016/j.jceh.2019.02.003.

41. Butterworth, R.F. Neurosteroids in Hepatic Encephalopathy: Novel Insights and New Therapeutic Opportunities. *The Journal of Steroid Biochemistry and Molecular Biology* **2016**, *160*, 94–97, doi:10.1016/j.jsbmb.2015.11.006.

42. Jayakumar, A.R.; Rama Rao, K.V.; Norenberg, M.D. Neuroinflammation in Hepatic Encephalopathy: Mechanistic Aspects. *Journal of Clinical and Experimental Hepatology* **2015**, *5*, S21–S28, doi:10.1016/j.jceh.2014.07.006.

43. Matkowskyj, K.A.; Marrero, J.A.; Carroll, R.E.; Danilkovich, A.V.; Green, R.M.; Benya, R.V. Azoxymethane-Induced Fulminant Hepatic Failure in C57BL/6J Mice: Characterization of a New Animal Model. *American Journal of Physiology-Gastrointestinal and Liver Physiology* **1999**, *277*, G455–G462, doi:10.1152/ajpgi.1999.277.2.G455.

44. Labenz, C.; Toenges, G.; Huber, Y.; Nagel, M.; Marquardt, J.U.; Schattenberg, J.M.; Galle, P.R.; Labenz, J.; Wörns, M. Raised Serum Interleukin-6 Identifies Patients with Liver Cirrhosis at High Risk for Overt Hepatic Encephalopathy. *Aliment Pharmacol Ther* **2019**, *50*, 1112–1119, doi:10.1111/apt.15515.

45. De Souza Machado, F.; Marinho, J.P.; Abujamra, A.L.; Dani, C.; Quincozes-Santos, A.; Funchal, C. Carbon Tetrachloride Increases the Pro-Inflammatory Cytokines Levels in Different Brain Areas of Wistar Rats: The Protective Effect of Acai Frozen Pulp. *Neurochem Res* **2015**, *40*, 1976–1983, doi:10.1007/s11064-015-1693-z.

46. Sears, E.S.; McCandless, D.W.; Chandler, M.D. Disruption of the Blood-brain Barrier in Hyperammonemic Coma and the Pharmacologic Effects of Dexamethasone and Difluoromethyl Ornithine. *J of Neuroscience Research* **1985**, *14*, 255–261, doi:10.1002/jnr.490140210.

47. Seo, H.B.; Kang, B.K.; Kim, J.H.; Choi, Y.W.; Hong, J.W.; Choi, B.T.; Shin, H.K. Partially Purified Components of Uncaria Sinensis Attenuate Blood Brain Barrier Disruption after Ischemic Brain Injury in Mice. *BMC Complement Altern Med* **2015**, *15*, 157, doi:10.1186/s12906-015-0678-4.

48. Hawkins, B.T.; Lundeen, T.F.; Norwood, K.M.; Brooks, H.L.; Egleton, R.D. Increased Blood–Brain Barrier Permeability and Altered Tight Junctions in Experimental Diabetes in the

Rat: Contribution of Hyperglycaemia and Matrix Metalloproteinases. *Diabetologia* **2006**, *50*, 202–211, doi:10.1007/s00125-006-0485-z.

49. Cauli, O.; López-Larrubia, P.; Rodrigues, T.B.; Cerdán, S.; Felipo, V. Magnetic Resonance Analysis of the Effects of Acute Ammonia Intoxication on Rat Brain. Role of NMDA Receptors. *Journal of Neurochemistry* **2007**, *103*, 1334–1343, doi:10.1111/j.1471-4159.2007.04878.x.

50. Li, D.; Yu, S.; Lin, L.; Guo, J.; Huang, S.; Wu, X.; You, H.; Cheng, X.; Zhang, Q.; Zeng, Y.; et al. Deficiency of Leucine-Rich Repeat Kinase 2 Aggravates Thioacetamide-Induced Acute Liver Failure and Hepatic Encephalopathy in Mice. *J Neuroinflammation* **2024**, *21*, 123, doi:10.1186/s12974-024-03125-4.

51. McMillin, M.; Grant, S.; Frampton, G.; Petrescu, A.D.; Williams, E.; Jefferson, B.; Thomas, A.; Brahmaroutu, A.; DeMorrow, S. Elevated Circulating TGFβ1 during Acute Liver Failure Activates TGFβR2 on Cortical Neurons and Exacerbates Neuroinflammation and Hepatic Encephalopathy in Mice. *J Neuroinflammation* **2019**, *16*, 69, doi:10.1186/s12974-019-1455-y.

52. Popek, M.; Bobula, B.; Sowa, J.; Hess, G.; Polowy, R.; Filipkowski, R.K.; Frontczak-Baniewicz, M.; Zabłocka, B.; Albrecht, J.; Zielińska, M. Cortical Synaptic Transmission and Plasticity in Acute Liver Failure Are Decreased by Presynaptic Events. *Mol Neurobiol* **2018**, *55*, 1244–1258, doi:10.1007/s12035-016-0367-4.

53. Reitsma, S.; Slaaf, D.W.; Vink, H.; Van Zandvoort, M.A.M.J.; Oude Egbrink, M.G.A. The Endothelial Glycocalyx: Composition, Functions, and Visualization. *Pflugers Arch - Eur J Physiol* **2007**, *454*, 345–359, doi:10.1007/s00424-007-0212-8.

54. Saunders, N.R.; Daneman, R.; Dziegielewska, K.M.; Liddelow, S.A. Transporters of the Blood–Brain and Blood–CSF Interfaces in Development and in the Adult. *Molecular Aspects of Medicine* **2013**, *34*, 742–752, doi:10.1016/j.mam.2012.11.006.

55. Engelhardt, B. Development of the Blood-Brain Barrier. *Cell and Tissue Research* **2003**, *314*, 119–129, doi:10.1007/s00441-003-0751-z.

56. Wittchen, E.S.; Haskins, J.; Stevenson, B.R. Protein Interactions at the Tight Junction. *Journal of Biological Chemistry* **1999**, *274*, 35179–35185, doi:10.1074/jbc.274.49.35179.

57. Zheng, X.; Xu, C.; Smith, A.O.; Stratman, A.N.; Zou, Z.; Kleaveland, B.; Yuan, L.; Didiku, C.; Sen, A.; Liu, X.; et al. Dynamic Regulation of the Cerebral Cavernous Malformation Pathway Controls Vascular Stability and Growth. *Developmental Cell* **2012**, *23*, 342–355, doi:10.1016/j.devcel.2012.06.004.

58. Chaudhry, K.K.; Shukla, P.K.; Mir, H.; Manda, B.; Gangwar, R.; Yadav, N.; McMullen, M.; Nagy, L.E.; Rao, R. Glutamine Supplementation Attenuates Ethanol-Induced Disruption of Apical Junctional Complexes in Colonic Epithelium and Ameliorates Gut Barrier Dysfunction and Fatty Liver in Mice. *The Journal of Nutritional Biochemistry* **2016**, *27*, 16–26, doi:10.1016/j.jnutbio.2015.08.012.

59. Masaki, T.; Matsumura, K. Biological Role of Dystroglycan in Schwann Cell Function and Its Implications in Peripheral Nervous System Diseases. *Journal of Biomedicine and Biotechnology* **2010**, *2010*, 1–17, doi:10.1155/2010/740403.

60. Engelhardt, B. β_1 -Integrin/Matrix Interactions Support Blood–Brain Barrier Integrity. *J Cereb Blood Flow Metab* **2011**, *31*, 1969–1971, doi:10.1038/jcbfm.2011.98.

61. Marchetti, L.; Engelhardt, B. Immune Cell Trafficking across the Blood-Brain Barrier in the Absence and Presence of Neuroinflammation. *Vascular Biology* **2020**, *2*, H1–H18, doi:10.1530/VB-19-0033.

62. Yao, Y.; Chen, Z.-L.; Norris, E.H.; Strickland, S. Astrocytic Laminin Regulates Pericyte Differentiation and Maintains Blood Brain Barrier Integrity. *Nat Commun* **2014**, *5*, 3413, doi:10.1038/ncomms4413.

63. Bonkowski, D.; Katyshev, V.; Balabanov, R.D.; Borisov, A.; Dore-Duffy, P. The CNS Microvascular Pericyte: Pericyte-Astrocyte Crosstalk in the Regulation of Tissue Survival. *Fluids Barriers CNS* **2011**, *8*, 8, doi:10.1186/2045-8118-8-8.

64. Daneman, R.; Zhou, L.; Kebede, A.A.; Barres, B.A. Pericytes Are Required for Blood–Brain Barrier Integrity during Embryogenesis. *Nature* **2010**, *468*, 562–566, doi:10.1038/nature09513.

65. Takata, F.; Dohgu, S.; Matsumoto, J.; Takahashi, H.; Machida, T.; Wakigawa, T.; Harada, E.; Miyaji, H.; Koga, M.; Nishioku, T.; et al. Brain Pericytes among Cells Constituting the Blood-Brain Barrier Are Highly Sensitive to Tumor Necrosis Factor-α, Releasing Matrix Metalloproteinase-9 and Migrating in Vitro. *J Neuroinflammation* **2011**, *8*, 106, doi:10.1186/1742-2094-8-106.

66. Toth, A.E.; Klepe, A.; Lipka, D.V.; Goldeman, C.; Brodin, B.; Nielsen, M.S. SorLA in Astrocytes Regulates Blood-Brain Barrier Integrity. *Front. Drug. Deliv.* **2023**, *2*, 1082689, doi:10.3389/fddev.2022.1082689.

67. Del Zoppo, G.J.; Milner, R. Integrin–Matrix Interactions in the Cerebral Microvasculature. *ATVB* **2006**, *26*, 1966–1975, doi:10.1161/01.ATV.0000232525.65682.a2.

68. Vemuganti, R.; Silva, V.R.; Mehta, S.L.; Hazell, A.S. Acute Liver Failure-Induced Hepatic Encephalopathy Is Associated with Changes in microRNA Expression Profiles in Cerebral Cortex of the Rat. *Metab Brain Dis* **2014**, *29*, 891–899, doi:10.1007/s11011-014-9545-0.

69. Yamaura, Y.; Nakajima, M.; Takagi, S.; Fukami, T.; Tsuneyama, K.; Yokoi, T. Plasma MicroRNA Profiles in Rat Models of Hepatocellular Injury, Cholestasis, and Steatosis. *PLoS ONE* **2012**, *7*, e30250, doi:10.1371/journal.pone.0030250.

70. Baker, L.A.; Lee, K.C.L.; Palacios Jimenez, C.; Alibhai, H.; Chang, Y.-M.; Leckie, P.J.; Mookerjee, R.P.; Davies, N.A.; Andreola, F.; Jalan, R. Circulating microRNAs Reveal Time Course of Organ Injury in a Porcine Model of Acetaminophen-Induced Acute Liver Failure. *PLoS ONE* **2015**, *10*, e0128076, doi:10.1371/journal.pone.0128076.

71. Starkey Lewis, P.J.; Dear, J.; Platt, V.; Simpson, K.J.; Craig, D.G.N.; Antoine, D.J.; French, N.S.; Dhaun, N.; Webb, D.J.; Costello, E.M.; et al. Circulating microRNAs as Potential Markers of Human Drug-Induced Liver Injury. *Hepatology* **2011**, *54*, 1767–1776, doi:10.1002/hep.24538.

72. Hornby, R.J.; Starkey Lewis, P.; Dear, J.; Goldring, C.; Park, B.K. MicroRNAs as Potential Circulating Biomarkers of Drug-Induced Liver Injury: Key Current and Future Issues for Translation to Humans. *Expert Review of Clinical Pharmacology* **2014**, *7*, 349–362, doi:10.1586/17512433.2014.904201.

73. James, J.H.; Hodgman, J.M.; Funovics, J.M.; Yoshimura, N.; Fischer, J.E. Brain Tryptophan, Plasma Free Tryptophan and Distribution of Plasma Neutral Amino Acids. *Metabolism* **1976**, *25*, 471–476, doi:10.1016/0026-0495(76)90080-9.

74. Smith, A.R.; Rossi-Fanelli, F.; Ziparo, V.; James, J.H.; Perelle, B.A.; Fischer, J.E. Alterations in Plasma and CSF Amino Acids, Amines and Metabolites in Hepatic Coma: *Annals of Surgery* **1978**, *187*, 343, doi:10.1097/00000658-197803000-00024.

75. Sikorska, H.; Cianciara, J.; Wiercińska-Drapało, A. [Physiological functions of L-ornithine and L-aspartate in the body and the efficacy of administration of L-ornithine-L-aspartate in conditions of relative deficiency]. *Pol Merkur Lekarski* **2010**, *28*, 490–495.

76. Seiler, N. Ammonia and Alzheimer's Disease. *Neurochemistry International* **2002**, *41*, 189–207, doi:10.1016/S0197-0186(02)00041-4.

77. Albrecht, J.; Bender, A.S.; Norenberg, M.D. Ammonia Stimulates the Release of Taurine from Cultured Astrocytes. *Brain Research* **1994**, *660*, 288–292, doi:10.1016/0006-8993(94)91301-3.

78. Faff, L.; Reichenbach, A.; Albrecht, J. Ammonia-Induced Taurine Release from Cultured Rabbit M[illegible]ller Cells Is an Osmoresistant Process Mediated by Intracellular Accumulation of Cyclic AMP. *J. Neurosci. Res.* **1996**, *46*, 231–238, doi:10.1002/(SICI)1097-4547(19961015)46:2<231::AID-JNR11>3.0.CO;2-5.

79. Czarnecka, A.; Milewski, K.; Zielińska, M. Asymmetric Dimethylarginine and Hepatic Encephalopathy: Cause, Effect or Association? *Neurochem Res* **2017**, *42*, 750–761, doi:10.1007/s11064-016-2111-x.

80. Görg, B.; Karababa, A.; Shafigullina, A.; Bidmon, H.J.; Häussinger, D. Ammonia-Induced Senescence in Cultured Rat Astrocytes and in Human Cerebral Cortex in Hepatic Encephalopathy: Hepatic Encephalopathy and Senescence. *Glia* **2015**, *63*, 37–50, doi:10.1002/glia.22731.

81. Saksena, S.; Rai, V.; Saraswat, V.A.; Rathore, R.S.; Purwar, A.; Kumar, M.; Thomas, M.A.; Gupta, R.K. Cerebral Diffusion Tensor Imaging and *in Vivo* Proton Magnetic Resonance Spectroscopy in Patients with Fulminant Hepatic Failure. *J of Gastro and Hepatol* **2008**, *23*, doi:10.1111/j.1440-1746.2007.05158.x.

82. Görg, B.; Qvartskhava, N.; Bidmon, H.-J.; Palomero-Gallagher, N.; Kircheis, G.; Zilles, K.; Häussinger, D. Oxidative Stress Markers in the Brain of Patients with Cirrhosis and Hepatic Encephalopathy. *Hepatology* **2010**, *52*, 256–265, doi:10.1002/hep.23656.

83. Butz, M.; May, E.S.; Häussinger, D.; Schnitzler, A. The Slowed Brain: Cortical Oscillatory Activity in Hepatic Encephalopathy. *Archives of Biochemistry and Biophysics* **2013**, *536*, 197–203, doi:10.1016/j.abb.2013.04.004.

84. Herranz, N.; Gil, J. Mechanisms and Functions of Cellular Senescence. *Journal of Clinical Investigation* **2018**, *128*, 1238–1246, doi:10.1172/JCI95148.

85. Campisi, J.; d'Adda Di Fagagna, F. Cellular Senescence: When Bad Things Happen to Good Cells. *Nat Rev Mol Cell Biol* **2007**, *8*, 729–740, doi:10.1038/nrm2233.

86. Ma, J.; Hu, X.; Liao, C.; Xiao, H.; Zhu, Q.; Li, Y.; Liu, Z.; Tao, A.; He, Z.; Xu, C.; et al. Gypenoside L Inhibits Proliferation of Liver and Esophageal Cancer Cells by Inducing Senescence. *Molecules* **2019**, *24*, 1054, doi:10.3390/molecules24061054.

87. Ogrodnik, M. Cellular Aging beyond Cellular Senescence: Markers of Senescence Prior to Cell Cycle Arrest *in Vitro* and *in Vivo*. *Aging Cell* **2021**, *20*, e13338, doi:10.1111/acel.13338.

88. Huang, W.; Hickson, L.J.; Eirin, A.; Kirkland, J.L.; Lerman, L.O. Cellular Senescence: The Good, the Bad and the Unknown. *Nat Rev Nephrol* **2022**, *18*, 611–627, doi:10.1038/s41581-022-00601-z.

89. Zhao, L.-D.; Bie, L.-Y.; Hu, L.; Zhu, Z.-H.; Meng, X.-H.; Cong, L.-L.; Zhang, S.; Ma, N.; Xiao, J.-H. IGF-1 Induces Cellular Senescence in Rat Articular Chondrocytes via Akt Pathway Activation. *Exp Ther Med* **2020**, *20*, 1–1, doi:10.3892/etm.2020.9177.

90. De Mera-Rodríguez, J.A.; Álvarez-Hernán, G.; Gañán, Y.; Martín-Partido, G.; Rodríguez-León, J.; Francisco-Morcillo, J. Is Senescence-Associated β-Galactosidase a Reliable in Vivo Marker of Cellular Senescence During Embryonic Development? *Front. Cell Dev. Biol.* **2021**, *9*, 623175, doi:10.3389/fcell.2021.623175.

91. Wallace, D.C. A Mitochondrial Paradigm of Metabolic and Degenerative Diseases, Aging, and Cancer: A Dawn for Evolutionary Medicine. *Annu. Rev. Genet.* **2005**, *39*, 359–407, doi:10.1146/annurev.genet.39.110304.095751.

92. Wang, Y.; Wu, J.; Wang, J.; He, L.; Lai, H.; Zhang, T.; Wang, X.; Li, W. Mitochondrial Oxidative Stress in Brain Microvascular Endothelial Cells: Triggering Blood-Brain Barrier Disruption. *Mitochondrion* **2023**, *69*, 71–82, doi:10.1016/j.mito.2023.01.007.

93. Kiss, T.; Nyúl-Tóth, Á.; Balasubramanian, P.; Tarantini, S.; Ahire, C.; DelFavero, J.; Yabluchanskiy, A.; Csipo, T.; Farkas, E.; Wiley, G.; et al. Single-Cell RNA Sequencing Identifies Senescent Cerebromicrovascular Endothelial Cells in the Aged Mouse Brain. *GeroScience* **2020**, *42*, 429–444, doi:10.1007/s11357-020-00177-1.

94. Kulovic-Sissawo, A.; Tocantins, C.; Diniz, M.S.; Weiss, E.; Steiner, A.; Tokic, S.; Madreiter-Sokolowski, C.T.; Pereira, S.P.; Hiden, U. Mitochondrial Dysfunction in Endothelial Progenitor Cells: Unraveling Insights from Vascular Endothelial Cells. *Biology* **2024**, *13*, 70, doi:10.3390/biology13020070.

95. Ungvari, Z.; Labinskyy, N.; Gupte, S.; Chander, P.N.; Edwards, J.G.; Csiszar, A. Dysregulation of Mitochondrial Biogenesis in Vascular Endothelial and Smooth Muscle Cells

of Aged Rats. *American Journal of Physiology-Heart and Circulatory Physiology* **2008**, *294*, H2121–H2128, doi:10.1152/ajpheart.00012.2008.

96. Dominic, A.; Banerjee, P.; Hamilton, D.J.; Le, N.-T.; Abe, J. Time-Dependent Replicative Senescence vs. Disturbed Flow-Induced Pre-Mature Aging in Atherosclerosis. *Redox Biology* **2020**, *37*, 101614, doi:10.1016/j.redox.2020.101614.

97. Childs, B.G.; Gluscevic, M.; Baker, D.J.; Laberge, R.-M.; Marquess, D.; Dananberg, J.; Van Deursen, J.M. Senescent Cells: An Emerging Target for Diseases of Ageing. *Nat Rev Drug Discov* **2017**, *16*, 718–735, doi:10.1038/nrd.2017.116.

98. Chandrasekaran, A.; Idelchik, M.D.P.S.; Melendez, J.A. Redox Control of Senescence and Age-Related Disease. *Redox Biology* **2017**, *11*, 91–102, doi:10.1016/j.redox.2016.11.005.

99. Sato, Y.; Kanno, S.; Oda, N.; Abe, M.; Ito, M.; Shitara, K.; Shibuya, M. Properties of Two VEGF Receptors, Flt-1 and KDR, in Signal Transduction [a]. *Annals of the New York Academy of Sciences* **2000**, *902*, 201–207, doi:10.1111/j.1749-6632.2000.tb06314.x.

100. Liu, Y.; Bloom, S.I.; Donato, A.J. The Role of Senescence, Telomere Dysfunction and Shelterin in Vascular Aging. *Microcirculation* **2019**, *26*, e12487, doi:10.1111/micc.12487.

101. Mabrouk, N.; Ghione, S.; Laurens, V.; Plenchette, S.; Bettaieb, A.; Paul, C. Senescence and Cancer: Role of Nitric Oxide (NO) in SASP. *Cancers* **2020**, *12*, 1145, doi:10.3390/cancers12051145.

102. Higashi, Y.; Noma, K.; Yoshizumi, M.; Kihara, Y. Endothelial Function and Oxidative Stress in Cardiovascular Diseases. *Circ J* **2009**, *73*, 411–418, doi:10.1253/circj.CJ-08-1102.

103. Parodi-Rullán, R.; Sone, J.Y.; Fossati, S. Endothelial Mitochondrial Dysfunction in Cerebral Amyloid Angiopathy and Alzheimer's Disease. *JAD* **2019**, *72*, 1019–1039, doi:10.3233/JAD-190357.

104. Kluge, M.A.; Fetterman, J.L.; Vita, J.A. Mitochondria and Endothelial Function. *Circulation Research* **2013**, *112*, 1171–1188, doi:10.1161/CIRCRESAHA.111.300233.

105. Hall, A.M.; Schuh, C.D. Mitochondria as Therapeutic Targets in Acute Kidney Injury: *Current Opinion in Nephrology and Hypertension* **2016**, *25*, 355–362, doi:10.1097/MNH.0000000000000228.

106. Ruck, T.; Bittner, S.; Epping, L.; Herrmann, A.M.; Meuth, S.G. Isolation of Primary Murine Brain Microvascular Endothelial Cells. *JoVE* **2014**, 52204, doi:10.3791/52204.

107. Roux, F.; Durieu-Trautmann, O.; Chaverot, N.; Claire, M.; Mailly, P.; Bourre, J. -M.; Strosberg, A.D.; Couraud, P. -O. Regulation of Gamma-glutamyl Transpeptidase and Alkaline Phosphatase Activities in Immortalized Rat Brain Microvessel Endothelial Cells. *Journal Cellular Physiology* **1994**, *159*, 101–113, doi:10.1002/jcp.1041590114.

108. Hindfelt, B. ON MECHANISMS IN HYPERAMMONEMIC COMA—WITH PARTICULAR REFERENCE TO HEPATIC ENCEPHALOPATHY. *Annals of the New York Academy of Sciences* **1975**, *252*, 116–123, doi:10.1111/j.1749-6632.1975.tb19148.x.

109. Hindfelt, B. The Distribution of Ammonia between Extracellular and Intracellular Compartments of the Rat Brain. *Clinical Science* **1975**, *48*, 33–37, doi:10.1042/cs0480033.

110. Ge, S.X.; Jung, D.; Yao, R. ShinyGO: A Graphical Gene-Set Enrichment Tool for Animals and Plants. *Bioinformatics* **2020**, *36*, 2628–2629, doi:10.1093/bioinformatics/btz931.

111. Vlachos, I.S.; Paraskevopoulou, M.D.; Karagkouni, D.; Georgakilas, G.; Vergoulis, T.; Kanellos, I.; Anastasopoulos, I.-L.; Maniou, S.; Karathanou, K.; Kalfakakou, D.; et al. DIANA-TarBase v7.0: Indexing More than Half a Million Experimentally Supported miRNA:mRNA Interactions. *Nucleic Acids Research* **2015**, *43*, D153–D159, doi:10.1093/nar/gku1215.

112. Chen, Y.; Wang, X. miRDB: An Online Database for Prediction of Functional microRNA Targets. *Nucleic Acids Research* **2020**, *48*, D127–D131, doi:10.1093/nar/gkz757.

113. Agarwal, V.; Bell, G.W.; Nam, J.-W.; Bartel, D.P. Predicting Effective microRNA Target Sites in Mammalian mRNAs. *eLife* **2015**, *4*, e05005, doi:10.7554/eLife.05005.

114. Tastsoglou, S.; Alexiou, A.; Karagkouni, D.; Skoufos, G.; Zacharopoulou, E.; Hatzigeorgiou, A.G. DIANA-microT 2023: Including Predicted Targets of Virally Encoded miRNAs. *Nucleic Acids Research* **2023**, *51*, W148–W153, doi:10.1093/nar/gkad283.

115. Griffiths-Jones, S. miRBase: microRNA Sequences, Targets and Gene Nomenclature. *Nucleic Acids Research* **2006**, *34*, D140–D144, doi:10.1093/nar/gkj112.

116. Kanehisa, M. KEGG: Kyoto Encyclopedia of Genes and Genomes. *Nucleic Acids Research* **2000**, *28*, 27–30, doi:10.1093/nar/28.1.27.

117. Szklarczyk, D.; Kirsch, R.; Koutrouli, M.; Nastou, K.; Mehryary, F.; Hachilif, R.; Gable, A.L.; Fang, T.; Doncheva, N.T.; Pyysalo, S.; et al. The STRING Database in 2023: Protein–Protein Association Networks and Functional Enrichment Analyses for Any Sequenced Genome of Interest. *Nucleic Acids Research* **2023**, *51*, D638–D646, doi:10.1093/nar/gkac1000.

118. Hilgier, W.; Olson, J.E. Brain Ion and Amino Acid Contents During Edema Development in Hepatic Encephalopathy. *Journal of Neurochemistry* **1994**, *62*, 197–204, doi:10.1046/j.1471-4159.1994.62010197.x.

119. Hilgier, W.; Olson, J.E.; Albrecht, J. Relation of Taurine Transport and Brain Edema in Rats with Simple Hyperammonemia or Liver Failure. *J. Neurosci. Res.* **1996**, *45*, 69–74, doi:10.1002/(SICI)1097-4547(19960701)45:1<69::AID-JNR6>3.0.CO;2-F.

120. Skowrońska, M.; Albrecht, J. Alterations of Blood Brain Barrier Function in Hyperammonemia: An Overview. *Neurotox Res* **2012**, *21*, 236–244, doi:10.1007/s12640-011-9269-4.

121. Claeys, W.; Van Hoecke, L.; Lefere, S.; Geerts, A.; Verhelst, X.; Van Vlierberghe, H.; Degroote, H.; Devisscher, L.; Vandenbroucke, R.E.; Van Steenkiste, C. The Neurogliovascular Unit in Hepatic Encephalopathy. *JHEP Reports* **2021**, *3*, 100352, doi:10.1016/j.jhepr.2021.100352.

122. Shaik, I.H.; Miah, M.K.; Bickel, U.; Mehvar, R. Effects of Short-Term Portacaval Anastomosis on the Peripheral and Brain Disposition of the Blood–Brain Barrier Permeability

Marker Sodium Fluorescein in Rats. *Brain Research* **2013**, *1531*, 84–93, doi:10.1016/j.brainres.2013.07.040.

123. Vairappan, B.; Sundhar, M.; Srinivas, B.H. Resveratrol Restores Neuronal Tight Junction Proteins Through Correction of Ammonia and Inflammation in CCl4-Induced Cirrhotic Mice. *Mol Neurobiol* **2019**, *56*, 4718–4729, doi:10.1007/s12035-018-1389-x.

124. Donahoe, J.P.; Giambrone, J.; Fletcher, O.J.; Kleven, S.H. In Vivo Function Tests of the Effect of Tilorone and Niridazole on Cell-Mediated Immunity in Chickens. *Am J Vet Res* **1977**, *38*, 2013–2017.

125. Laursen, H.; Schrø, H.; Westergaard, E. THE EFFECT OF PORTOCAVAL ANASTOMOSIS ON THE PERMEABILITY TO HORSERADISH PEROXIDASE OF CEREBRAL VESSELS OF THE RAT. *Acta Pathologica Microbiologica Scandinavica Section A Pathology* **1975**, *83A*, 266–268, doi:10.1111/j.1699-0463.1975.tb01384.x.

126. Zaki, A.E.O.; Wardle, E.N.; Canalese, J.; Ede, R.J.; Williams, R. Potential Toxins of Acute Liver Failure and Their Effects on Blood-Brain Barrier Permeability. *Experientia* **1983**, *39*, 988–991, doi:10.1007/BF01989765.

127. Horowitz, M.E.; Schafer, D.F.; Molnar, P.; Jones, E.A.; Blasberg, R.G.; Patlak, C.S.; Waggoner, J.; Fenstermacher, J.D. Increased Blood-Brain Transfer in a Rabbit Model of Acute Liver Failure. *Gastroenterology* **1983**, *84*, 1003–1011.

128. Lv, S.; Song, H.-L.; Zhou, Y.; Li, L.-X.; Cui, W.; Wang, W.; Liu, P. Tumour Necrosis Factor-α Affects Blood-Brain Barrier Permeability and Tight Junction-Associated Occludin in Acute Liver Failure: Blood-Brain Barrier in Liver Failure. *Liver International* **2010**, *30*, 1198–1210, doi:10.1111/j.1478-3231.2010.02211.x.

129. Yamamoto, S.; Nguyen, J.H. TIMP-1/MMP-9 Imbalance in Brain Edema in Rats With Fulminant Hepatic Failure. *Journal of Surgical Research* **2006**, *134*, 307–314, doi:10.1016/j.jss.2005.11.588.

130. Bémeur, C.; Qu, H.; Desjardins, P.; Butterworth, R.F. IL-1 or TNF Receptor Gene Deletion Delays Onset of Encephalopathy and Attenuates Brain Edema in Experimental Acute Liver Failure. *Neurochemistry International* **2010**, *56*, 213–215, doi:10.1016/j.neuint.2009.11.010.

131. Cauli, O.; López–Larrubia, P.; Rodrigo, R.; Agusti, A.; Boix, J.; Nieto–Charques, L.; Cerdán, S.; Felipo, V. Brain Region-Selective Mechanisms Contribute to the Progression of Cerebral Alterations in Acute Liver Failure in Rats. *Gastroenterology* **2011**, *140*, 638–645, doi:10.1053/j.gastro.2010.10.043.

132. Sharief, M.K.; Thompson, E.J. In Vivo Relationship of Tumor Necrosis Factor-α to Blood-Brain Barrier Damage in Patients with Active Multiple Sclerosis. *Journal of Neuroimmunology* **1992**, *38*, 27–33, doi:10.1016/0165-5728(92)90087-2.

133. Chastre, A.; Bélanger, M.; Nguyen, B.N.; Butterworth, R.F. Lipopolysaccharide Precipitates Hepatic Encephalopathy and Increases Blood–Brain Barrier Permeability in Mice with Acute Liver Failure. *Liver International* **2014**, *34*, 353–361, doi:10.1111/liv.12252.

134. Gove, C.D.; Hughes, R.D.; Ede, R.J.; Williams, R. Regional Cerebral Edema and Chloride Space in Galactosamine-Induced Liver Failure in Rats. *Hepatology* **1997**, *25*, 295–301, doi:10.1002/hep.510250207.

135. Shimojima, N.; Eckman, C.B.; McKinney, M.; Sevlever, D.; Yamamoto, S.; Lin, W.; Dickson, D.W.; Nguyen, J.H. Altered Expression of Zonula Occludens-2 Precedes Increased Blood–Brain Barrier Permeability in a Murine Model of Fulminant Hepatic Failure. *Journal of Investigative Surgery* **2008**, *21*, 101–108, doi:10.1080/08941930802043565.

136. McMillin, M.; Frampton, G.; Tobin, R.; Dusio, G.; Smith, J.; Shin, H.; Newell-Rogers, K.; Grant, S.; DeMorrow, S. TGR 5 Signaling Reduces Neuroinflammation during Hepatic Encephalopathy. *Journal of Neurochemistry* **2015**, *135*, 565–576, doi:10.1111/jnc.13243.

137. Milewski, K.; Hilgier, W.; Fręśko, I.; Polowy, R.; Podsiadłowska, A.; Zołocińska, E.; Grymanowska, A.W.; Filipkowski, R.K.; Albrecht, J.; Zielińska, M. Carnosine Reduces Oxidative Stress and Reverses Attenuation of Righting and Postural Reflexes in Rats with Thioacetamide-Induced Liver Failure. *Neurochem Res* **2016**, *41*, 376–384, doi:10.1007/s11064-015-1821-9.

138. Zimmermann, C.; Ferenci, P.; Pifl, C.; Yurdaydin, C.; Ebner, J.; Lassmann, H.; Roth, E.; Hörtnagl, H. Hepatic Encephalopathy in Thioacetamide-Induced Acute Liver Failure in Rats: Characterization of an Improved Model and Study of Amino Acid-Ergic Neurotransmission. *Hepatology* **1989**, *9*, 594–601, doi:10.1002/hep.1840090414.

139. Vigo, M.B.; Pérez, M.J.; De Fino, F.; Gómez, G.; Martínez, S.A.; Bisagno, V.; Di Carlo, M.B.; Scazziota, A.; Manautou, J.E.; Ghanem, C.I. Acute Acetaminophen Intoxication Induces Direct Neurotoxicity in Rats Manifested as Astrogliosis and Decreased Dopaminergic Markers in Brain Areas Associated with Locomotor Regulation. *Biochemical Pharmacology* **2019**, *170*, 113662, doi:10.1016/j.bcp.2019.113662.

140. Ilic, S.; Drmic, D.; Zarkovic, K.; Kolenc, D.; Coric, M.; Brcic, L.; Klicek, R.; Radic, B.; Sever, M.; Djuzel, V.; et al. High Hepatotoxic Dose of Paracetamol Produces Generalized Convulsions and Brain Damage in Rats. A Counteraction with the Stable Gastric Pentadecapeptide BPC 157 (PL 14736). *J Physiol Pharmacol* **2010**, *61*, 241–250.

141. Isobe-Harima, Y.; Terai, S.; Miura, I.; Segawa, M.; Murata, T.; Itamoto, K.; Taura, Y.; Shinoda, K.; Sakaida, I. A New Hepatic Encephalopathy Model to Monitor the Change of Neural Amino Acids and Astrocytes with Behaviour Disorder. *Liver International* **2008**, *28*, 117–125, doi:10.1111/j.1478-3231.2007.01589.x.

142. Braissant, O.; Rackayová, V.; Pierzchala, K.; Grosse, J.; McLin, V.A.; Cudalbu, C. Longitudinal Neurometabolic Changes in the Hippocampus of a Rat Model of Chronic Hepatic Encephalopathy. *Journal of Hepatology* **2019**, *71*, 505–515, doi:10.1016/j.jhep.2019.05.022.

143. Leke, R.; Oliveira, D.L.; Forgiarini, L.F.; Escobar, T.D.C.; Hammes, T.O.; Meyer, F.S.; Keiding, S.; Silveira, T.R.; Schousboe, A. Impairment of Short Term Memory in Rats with Hepatic Encephalopathy Due to Bile Duct Ligation. *Metab Brain Dis* **2013**, *28*, 187–192, doi:10.1007/s11011-012-9347-1.

144. Braissant, O. Ammonia Toxicity to the Brain: Effects on Creatine Metabolism and Transport and Protective Roles of Creatine. *Molecular Genetics and Metabolism* **2010**, *100*, S53–S58, doi:10.1016/j.ymgme.2010.02.011.

145. Häberle, J.; Burlina, A.; Chakrapani, A.; Dixon, M.; Karall, D.; Lindner, M.; Mandel, H.; Martinelli, D.; Pintos-Morell, G.; Santer, R.; et al. Suggested Guidelines for the Diagnosis and Management of Urea Cycle Disorders: First Revision. *J of Inher Metab Disea* **2019**, *42*, 1192–1230, doi:10.1002/jimd.12100.

146. Galea, I. The Blood–Brain Barrier in Systemic Infection and Inflammation. *Cell Mol Immunol* **2021**, *18*, 2489–2501, doi:10.1038/s41423-021-00757-x.

147. McMillin, M.A.; Frampton, G.A.; Seiwell, A.P.; Patel, N.S.; Jacobs, A.N.; DeMorrow, S. TGFβ1 Exacerbates Blood–Brain Barrier Permeability in a Mouse Model of Hepatic Encephalopathy via Upregulation of MMP9 and Downregulation of Claudin-5. *Laboratory Investigation* **2015**, *95*, 903–913, doi:10.1038/labinvest.2015.70.

148. Popek, M.; Bobula, B.; Orzeł-Gajowik, K.; Zielińska, M. The Effect of TGF-B1 Reduced Functionality on the Expression of Selected Synaptic Proteins and Electrophysiological Parameters: Implications of Changes Observed in Acute Hepatic Encephalopathy. *IJMS* **2022**, *23*, 1081, doi:10.3390/ijms23031081.

149. Chiang, J.Y.L. Bile Acid Metabolism and Signaling. In *Comprehensive Physiology*; Terjung, R., Ed.; Wiley, 2013; pp. 1191–1212 ISBN 978-0-470-65071-4.

150. Krauskopf, J.; De Kok, T.M.; Schomaker, S.J.; Gosink, M.; Burt, D.A.; Chandler, P.; Warner, R.L.; Johnson, K.J.; Caiment, F.; Kleinjans, J.C.; et al. Serum microRNA Signatures as "Liquid Biopsies" for Interrogating Hepatotoxic Mechanisms and Liver Pathogenesis in Human. *PLoS ONE* **2017**, *12*, e0177928, doi:10.1371/journal.pone.0177928.

151. Yang, X.; Salminen, W.F.; Shi, Q.; Greenhaw, J.; Gill, P.S.; Bhattacharyya, S.; Beger, R.D.; Mendrick, D.L.; Mattes, W.B.; James, L.P. Potential of Extracellular microRNAs as Biomarkers of Acetaminophen Toxicity in Children. *Toxicology and Applied Pharmacology* **2015**, *284*, 180–187, doi:10.1016/j.taap.2015.02.013.

152. Antoine, D.J.; Dear, J.W.; Lewis, P.S.; Platt, V.; Coyle, J.; Masson, M.; Thanacoody, R.H.; Gray, A.J.; Webb, D.J.; Moggs, J.G.; et al. Mechanistic Biomarkers Provide Early and Sensitive Detection of Acetaminophen-induced Acute Liver Injury at First Presentation to Hospital. *Hepatology* **2013**, *58*, 777–787, doi:10.1002/hep.26294.

153. Dubin, P.H.; Yuan, H.; Devine, R.K.; Hynan, L.S.; Jain, M.K.; Lee, W.M.; the Acute Liver Failure Study Group Micro-RNA-122 Levels in Acute Liver Failure and Chronic Hepatitis C: miR-122 in Acute Liver Failure and Hepatitis C. *J. Med. Virol.* **2014**, *86*, 1507–1514, doi:10.1002/jmv.23987.

154. John, K.; Hadem, J.; Krech, T.; Wahl, K.; Manns, M.P.; Dooley, S.; Batkai, S.; Thum, T.; Schulze-Osthoff, K.; Bantel, H. MicroRNAs Play a Role in Spontaneous Recovery from Acute Liver Failure: HEPATOLOGY, Vol. XX, No. X, 2014. *Hepatology* **2014**, *60*, 1346–1355, doi:10.1002/hep.27250.

155. Russo, M.W.; Steuerwald, N.; Norton, H.J.; Anderson, W.E.; Foureau, D.; Chalasani, N.; Fontana, R.J.; Watkins, P.B.; Serrano, J.; Bonkovsky, H.L. Profiles of Mi RNA s in Serum in Severe Acute Drug Induced Liver Injury and Their Prognostic Significance. *Liver International* **2017**, *37*, 757–764, doi:10.1111/liv.13312.

156. Zhang, H.; Zhang, W.; Yu, G.; Li, F.; Hui, Y.; Cha, S.; Chen, M.; Zhu, W.; Zhang, J.; Guo, G.; et al. Comprehensive Analysis of lncRNAs, miRNAs and mRNAs in Mouse Hippocampus With Hepatic Encephalopathy. *Front. Genet.* **2022**, *13*, 868716, doi:10.3389/fgene.2022.868716.

157. Du, Y.; Duan, Y.; Zhang, S. The Role of Occludin in Vascular Endothelial Protection. In *Endothelial Dysfunction - A Novel Paradigm*; Abukabda, A., Fonner, C., Eds.; IntechOpen, 2023 ISBN 978-1-80356-626-9.

158. Huang, J.; Ge, S.; Wang, Y.; Du, R.; Wang, Y.; Yin, T.; Wang, G. Expression of Endothelial Tight Junction Protein Occludin under Mechanical Factors after Stent Implantation. *Molecular & Cellular Biomechanics* **2019**, *16*, 138–139, doi:10.32604/mcb.2019.07305.

159. Halder, S.K.; Delorme-Walker, V.D.; Milner, R. B1 Integrin Is Essential for Blood–Brain Barrier Integrity under Stable and Vascular Remodelling Conditions; Effects Differ with Age. *Fluids Barriers CNS* **2023**, *20*, 52, doi:10.1186/s12987-023-00453-0.

160. Liu, S.; Leask, A. Integrin B1 Is Required for Maintenance of Vascular Tone in Postnatal Mice. *J. Cell Commun. Signal.* **2012**, *6*, 175–180, doi:10.1007/s12079-012-0170-6.

161. Lou, G.; Song, X.; Yang, F.; Wu, S.; Wang, J.; Chen, Z.; Liu, Y. Exosomes Derived from miR-122-Modified Adipose Tissue-Derived MSCs Increase Chemosensitivity of Hepatocellular Carcinoma. *J Hematol Oncol* **2015**, *8*, 122, doi:10.1186/s13045-015-0220-7.

162. Sheu-Gruttadauria, J.; Pawlica, P.; Klum, S.M.; Wang, S.; Yario, T.A.; Schirle Oakdale, N.T.; Steitz, J.A.; MacRae, I.J. Structural Basis for Target-Directed MicroRNA Degradation. *Molecular Cell* **2019**, *75*, 1243-1255.e7, doi:10.1016/j.molcel.2019.06.019.

163. Jopling, C.L. Regulation of Hepatitis C Virus by microRNA-122. *Biochemical Society Transactions* **2008**, *36*, 1220–1223, doi:10.1042/BST0361220.

164. Ghoshal, B.; Bertrand, E.; Bhattacharyya, S.N. Non-Canonical Ago Loading of EV-Derived Exogenous miRNA Generates Foreign miRNPs on Endosomes to Arbitrate Gene Expression in Recipient Cells 2020.

165. Vickers, K.C.; Palmisano, B.T.; Shoucri, B.M.; Shamburek, R.D.; Remaley, A.T. MicroRNAs Are Transported in Plasma and Delivered to Recipient Cells by High-Density Lipoproteins. *Nat Cell Biol* **2011**, *13*, 423–433, doi:10.1038/ncb2210.

166. Sade, H.; Holloway, K.; Romero, I.A.; Male, D. Transcriptional Control of Occludin Expression in Vascular Endothelia: Regulation by Sp3 and YY1. *Biochimica et Biophysica Acta (BBA) - Gene Regulatory Mechanisms* **2009**, *1789*, 175–184, doi:10.1016/j.bbagrm.2009.01.006.

167. Wang, Z.; Wade, P.; Mandell, K.J.; Akyildiz, A.; Parkos, C.A.; Mrsny, R.J.; Nusrat, A. Raf 1 Represses Expression of the Tight Junction Protein Occludin via Activation of the Zinc-Finger Transcription Factor Slug. *Oncogene* **2007**, *26*, 1222–1230, doi:10.1038/sj.onc.1209902.

168. Severson, E.A.; Kwon, M.; Hilgarth, R.S.; Parkos, C.A.; Nusrat, A. Glycogen Synthase Kinase 3 (GSK-3) Influences Epithelial Barrier Function by Regulating Occludin, Claudin-1 and E-Cadherin Expression. *Biochemical and Biophysical Research Communications* **2010**, *397*, 592–597, doi:10.1016/j.bbrc.2010.05.164.

169. Chen, F.; Hori, T.; Ohashi, N.; Baine, A.-M.; Eckman, C.B.; Nguyen, J.H. Occludin Is Regulated by Epidermal Growth Factor Receptor Activation in Brain Endothelial Cells and Brains of Mice with Acute Liver Failure. *Hepatology* **2011**, *53*, 1294–1305, doi:10.1002/hep.24161.

170. Weiler, F.; Marbe, T.; Scheppach, W.; Schauber, J. Influence of Protein Kinase C on Transcription of the Tight Junction Elements ZO-1 and Occludin. *Journal Cellular Physiology* **2005**, *204*, 83–86, doi:10.1002/jcp.20268.

171. Hartmann, D.A.; Underly, R.G.; Watson, A.N.; Shih, A.Y. A Murine Toolbox for Imaging the Neurovascular Unit. *Microcirculation* **2015**, *22*, 168–182, doi:10.1111/micc.12176.

172. Presa, J.L.; Saravia, F.; Bagi, Z.; Filosa, J.A. Vasculo-Neuronal Coupling and Neurovascular Coupling at the Neurovascular Unit: Impact of Hypertension. *Front. Physiol.* **2020**, *11*, 584135, doi:10.3389/fphys.2020.584135.

173. Abbott, N.J. Astrocyte–Endothelial Interactions and Blood–Brain Barrier Permeability*. *Journal of Anatomy* **2002**, *200*, 629–638, doi:10.1046/j.1469-7580.2002.00064.x.

174. Borgerding, R.A.; Murphy, S. Expression of Inducible Nitric Oxide Synthase in Cerebral Endothelial Cells Is Regulated by Cytokine-Activated Astrocytes. *Journal of Neurochemistry* **1995**, *65*, 1342–1347, doi:10.1046/j.1471-4159.1995.65031342.x.

175. Rodgers, J.T.; King, K.Y.; Brett, J.O.; Cromie, M.J.; Charville, G.W.; Maguire, K.K.; Brunson, C.; Mastey, N.; Liu, L.; Tsai, C.-R.; et al. mTORC1 Controls the Adaptive Transition of Quiescent Stem Cells from G0 to GAlert. *Nature* **2014**, *510*, 393–396, doi:10.1038/nature13255.

176. Lemons, J.M.S.; Feng, X.-J.; Bennett, B.D.; Legesse-Miller, A.; Johnson, E.L.; Raitman, I.; Pollina, E.A.; Rabitz, H.A.; Rabinowitz, J.D.; Coller, H.A. Quiescent Fibroblasts Exhibit High Metabolic Activity. *PLoS Biol* **2010**, *8*, e1000514, doi:10.1371/journal.pbio.1000514.

177. Luo, W.; Li, J.; Li, Z.; Lin, T.; Zhang, L.; Yang, W.; Mai, Y.; Liu, R.; Chen, M.; Dai, C.; et al. HO-1 Nuclear Accumulation and Interaction with NPM1 Protect against Stress-Induced Endothelial Senescence Independent of Its Enzymatic Activity. *Cell Death Dis* **2021**, *12*, 738, doi:10.1038/s41419-021-04035-6.

178. Lee, I.; Piao, S.; Kim, S.; Nagar, H.; Choi, S.; Kim, M.; Vu, G.-H.; Jeon, B.-H.; Kim, C.-S. IDH2 Deficiency Promotes Endothelial Senescence by Eliciting miR-34b/c-Mediated Suppression of Mitophagy and Increased ROS Production. *Antioxidants* **2023**, *12*, 585, doi:10.3390/antiox12030585.

179. Lin, Y.-Y.; Hsu, C.-W.; Chu, S.-J.; Tsai, S.-H. Features of Computed Tomography in a Passive Congestive Liver. *Intern. Med.* **2007**, *46*, 1763–1764, doi:10.2169/internalmedicine.46.0297.

180. Bajaj, J.S.; Ahluwalia, V.; Steinberg, J.L.; Hobgood, S.; Boling, P.A.; Godschalk, M.; Habib, S.; White, M.B.; Fagan, A.; Gavis, E.A.; et al. Elderly Patients Have an Altered Gut-Brain Axis Regardless of the Presence of Cirrhosis. *Sci Rep* **2016**, *6*, 38481, doi:10.1038/srep38481.

181. Liu, R.; Ahluwalia, V.; Kang, J.D.; Ghosh, S.S.; Zhou, H.; Li, Y.; Zhao, D.; Gurley, E.; Li, X.; White, M.B.; et al. Effect of Increasing Age on Brain Dysfunction in Cirrhosis. *Hepatol Commun* **2019**, *3*, 63–73, doi:10.1002/hep4.1286.

182. Montgomery, R.L.; Van Rooij, E. Therapeutic Advances in MicroRNA Targeting. *Journal of Cardiovascular Pharmacology* **2011**, *57*, 1–7, doi:10.1097/FJC.0b013e3181f603d0.

183. Schueller, F.; Roy, S.; Vucur, M.; Trautwein, C.; Luedde, T.; Roderburg, C. The Role of miRNAs in the Pathophysiology of Liver Diseases and Toxicity. *IJMS* **2018**, *19*, 261, doi:10.3390/ijms19010261.

184. Cione, E.; Abrego Guandique, D.M.; Caroleo, M.C.; Luciani, F.; Colosimo, M.; Cannataro, R. Liver Damage and microRNAs: An Update. *CIMB* **2022**, *45*, 78–91, doi:10.3390/cimb45010006.

185. Tadokoro, T.; Morishita, A.; Masaki, T. Diagnosis and Therapeutic Management of Liver Fibrosis by MicroRNA. *IJMS* **2021**, *22*, 8139, doi:10.3390/ijms22158139.

186. Keller, A.; Gröger, L.; Tschernig, T.; Solomon, J.; Laham, O.; Schaum, N.; Wagner, V.; Kern, F.; Schmartz, G.P.; Li, Y.; et al. miRNATissueAtlas2: An Update to the Human miRNA Tissue Atlas. *Nucleic Acids Research* **2022**, *50*, D211–D221, doi:10.1093/nar/gkab808.

187. Amini-Farsani, Z.; Asgharzade, S. The Impact of miR-183/182/96 Gene Regulation on the Maturation, Survival, and Function of Photoreceptor Cells in the Retina. *J of Comparative Neurology* **2020**, *528*, 1616–1625, doi:10.1002/cne.24833.

188. Evans, C.E.; Iruela-Arispe, M.L.; Zhao, Y.-Y. Mechanisms of Endothelial Regeneration and Vascular Repair and Their Application to Regenerative Medicine. *The American Journal of Pathology* **2021**, *191*, 52–65, doi:10.1016/j.ajpath.2020.10.001.

189. Vanhoutte, P.M. Regeneration of the Endothelium in Vascular Injury. *Cardiovasc Drugs Ther* **2010**, *24*, 299–303, doi:10.1007/s10557-010-6257-5.

190. Liu, M.; Zhang, L.; Marsboom, G.; Jambusaria, A.; Xiong, S.; Toth, P.T.; Benevolenskaya, E.V.; Rehman, J.; Malik, A.B. Sox17 Is Required for Endothelial

Regeneration Following Inflammation-Induced Vascular Injury. *Nat Commun* **2019**, *10*, 2126, doi:10.1038/s41467-019-10134-y.

191. Ramasamy, S.K.; Kusumbe, A.P.; Adams, R.H. Regulation of Tissue Morphogenesis by Endothelial Cell-Derived Signals. *Trends in Cell Biology* **2015**, *25*, 148–157, doi:10.1016/j.tcb.2014.11.007.

192. Steinmetz, M.; Nickenig, G.; Werner, N. Endothelial-Regenerating Cells: An Expanding Universe. *Hypertension* **2010**, *55*, 593–599, doi:10.1161/HYPERTENSIONAHA.109.134213.

193. Fiedler, L.R.; Wojciak-Stothard, B. The DDAH/ADMA Pathway in the Control of Endothelial Cell Migration and Angiogenesis. *Biochemical Society Transactions* **2009**, *37*, 1243–1247, doi:10.1042/BST0371243.

PUBLIKACJE

Wskaźnik oddziaływania

Wskaźnik oddziaływania (ang. impact factor, IF), wchodzący w skład rozprawy doktorskiej:

Warszawa, 09.07.2024

PUBLIKACJA I

Orzeł-Gajowik K., Milewski K, Zielińska M. miRNA-ome plasma analysis unveils changes in blood-brain barrier integrity associated with acute liver failure in rats. Fluids Barriers CNS. 2023 Dec 8;20(1):92. doi: 10.1186/s12987-023-00484-7. PMID: 38066639; PMCID: PMC10709860. **IF=5,9**

PUBLIKACJA II

Milewski K, Orzeł-Gajowik K., Zielińska M. Mitochondrial Changes in Rat Brain Endothelial Cells Associated with Hepatic Encephalopathy: Relation to the Blood-Brain Barrier Dysfunction. Neurochem Res. 2024 Jun;49(6):1489-1504. doi: 10.1007/s11064-022-03698-7. Epub 2022 Aug 2. Erratum in: Neurochem Res. 2024 Jun;49(6):1505. doi: 10.1007/s11064-022-03780-0. PMID: 35917006; PMCID: PMC11106209. **IF=3,7**

PUBLIKACJA III

Orzeł- Gajowik K.; Gajowik, T.; Rówienicz, Ł.; Zielińska, M. The Ohm-Azing Custom-Made Transendothelial Electrical Resistance Measuring Device (and Why Is It a Current Sensation?). Sensors and Actuators B: Chemical 2024, 404, 135192, doi: 10.1016/j.snb.2023.135192. **IF=8,0**

PUBLIKACJA IV

Orzeł-Gajowik K.; Milewski, K.; Zielińska, M. Insight into microRNAs-Mediated Communication between Liver and Brain: A Possible Approach for Understanding Acute Liver Failure? *Int. J. Mol. Sci.* 2022, *23*, 224. https://doi.org/10.3390/ijms23010224 **IF=5,6**

Publikacja 1

Orzeł-Gajowik *et al. Fluids and Barriers of the CNS* (2023) 20:92
https://doi.org/10.1186/s12987-023-00484-7

Fluids and Barriers of the CNS

RESEARCH Open Access

miRNA-ome plasma analysis unveils changes in blood–brain barrier integrity associated with acute liver failure in rats

Karolina Orzeł-Gajowik[1], Krzysztof Milewski[1,2] and Magdalena Zielińska[1*]

Abstract

Background Hepatic encephalopathy (HE) symptoms associated with liver insufficiency are linked to the neurotoxic effects of ammonia and other toxic metabolites reaching the brain via the blood–brain barrier (BBB), further aggravated by the inflammatory response. Cumulative evidence documents that the non-coding single-stranded RNAs, micro RNAs (miRs) control the BBB functioning. However, miRs' involvement in BBB breakdown in HE is still underexplored. Here, we hypothesized that in rats with acute liver failure (ALF) or rats subjected to hyperammonemia, altered circulating miRs affect BBB composing proteins.

Methods Transmission electron microscopy was employed to delineate structural alterations of the BBB in rats with ALF (thioacetamide (TAA) intraperitoneal (ip.) administration) or hyperammonemia (ammonium acetate (OA) ip. administration). The BBB permeability was determined with Evans blue dye and sodium fluorescein assay. Plasma MiRs were profiled by Next Generation Sequencing (NGS), followed by in silico analysis. Selected miRs, verified by qRT-PCR, were examined in cultured rat brain endothelial cells. Targeted protein alterations were elucidated with immunofluorescence, western blotting, and, after selected miR mimics transfection, through an in vitro resistance measurement.

Results Changes in BBB structure and increased permeability were observed in the prefrontal cortex of TAA rats but not in the brains of OA rats. The NGS results revealed divergently changed miRNA-ome in the plasma of both rat models. The in silico analysis led to the selection of miR-122-5p and miR-183-5p with their target genes occludin and integrin β1, respectively, as potential contributors to BBB alterations. Both proteins were reduced in isolated brain vessels and cortical homogenates in TAA rats. We documented in cultured primary brain endothelial cells that ammonia alone and, in combination with TNFα increases the relative expression of NGS-selected miRs with a less pronounced effect of TNFα when added alone. The in vitro study also confirmed miR-122-5p-dependent decrease in occludin and miR-183-5p-related reduction in integrin β1 expression.

Conclusion This work identified, to our knowledge for the first time, potential functional links between alterations in miRs residing in brain endothelium and BBB dysfunction in ALF.

Keywords Acute liver failure, Hyperammonemia, Blood–brain barrier, Micro RNA

*Correspondence:
Magdalena Zielińska
mzielinska@imdik.pan.pl
Full list of author information is available at the end of the article

Introduction

Hepatic encephalopathy (HE) is a debilitating neuropsychiatric condition resulting from impaired liver function. Clinical manifestation of HE ranges from mild psychiatric and neurological disturbances in chronic HE, and, brain edema often leading to coma at the acute HE stage, making the disease a significant threat to the healthcare system [1, 2]. The pathophysiology of HE encompasses brain intoxication as a result of inefficient blood clearance of a plethora of toxic when are in excess, metabolites (i.e., ammonia, aromatic amino acids, mercaptans, manganese, benzodiazepines, or xenobiotics) [3]. Accumulated data also strengthens a synergy of inflammation in HE pathology, leading to disease progression [4] beyond the sole and dominant role of harmful ammonia.

The blood–brain barrier (BBB) controls the exchange of diverse biological substances from the blood to the brain. The BBB disruption, particularly changes in junctional proteins' structures composed of tight junction (TJ) proteins, integrins, annexins, etc., is a directly documented pathological event promoting cerebral edema, a leading cause of a fatal outcome in acute HE [5–7]. Structural BBB abnormalities were reported in the cerebral cortex of patients who died due to ALF [8], but also in patients suffering from chronic liver insufficiency, namely liver cirrhosis [9]. While morphological changes of BBB reported in ALF animal models are significant but similar to what was observed in *post-mortem* human tissues, available results differ regarding the BBB failure characteristics, referring to animal species, implemented HE model (toxins/surgical procedure), and severity related to the HE duration, as critical factors of reported diversity of BBB changes, the molecular mechanisms contributing to BBB impairment, are still lacking many details. The BBB disturbances encompassing decomposition of BBB structural elements, uncontrolled influx of different substances thru transporters/channels leading to increased BBB permeability were reported in most of reproducible ALF animal models. Inconsistencies were noticed in a grade of BBB disturbances and BBB structural proteins (e.g., zonula occludens 2, occludin, claudin 5) changes which implicate that alterations may even precedes permeability changes, suggesting that TJ disruption might occur before BBB permeability changes. Additionally, studies published till now mostly focused on astrocytes and astrocytic swelling while other cell types such as the endothelial cells and pericytes, composing BBB in the brain are involved in the pathogenesis of HE. Additionally, at the molecular level, mechanistic details of TJ elements disruption involving microRNAs (miRs) action is yet to be determined.

MiRs, small non-coding RNA sequences, can negatively regulate protein levels by suppressing gene expression. Emerging evidence has suggested circulating non-coding RNAs' diagnostic and therapeutic values in pathologies linked with liver diseases, including ALF [10, 11]. Various miRs were recently proposed as possible biomarkers and regulatory factors in numerous CNS disorders expanding miRs' contributing role in the control of the functioning of BBB-composing endothelial cells [12–14].

In this study, we hypothesize that BBB dysfunction in rat models of ALF results at least in part from an altered pattern of circulating miRs and that alterations affecting specific miRs impact proteins engaged in BBB integrity. To verify this, we performed Next Generation Sequencing (NGS) of plasma in two rat models: (i) ALF induced by the ip. administration of hepatotoxin thioacetamide (TAA) and (ii) primary hyperammonemia, induced by ammonium acetate (OA) ip. injection. Notably, both models present elevated plasma ammonia concentrations, as a common denominator. While the OA model is beneficial for investigating hyperammonemia, it may not completely imitate the acute nature of the illness found in patients. In turn, TAA-induced liver injury frequently causes a twofold increase in blood ammonia levels [15, 16] and generates a variety of systemic and neuroinflammatory alterations.

We assessed our hypothesis using two approaches. The first, descriptive, comprises the examination of the BBB ultrastructure by transmission electron microscopy (TEM) and evaluation of the BBB permeability to low, and high-weight markers. Further, in silico identification and selection of specific genes regulated by established and validated miRs, was followed by the analysis of identified targets' biological function. The second approach was mechanistic and aimed at analyzing the phenotype of cultured endothelial cells (rat brain endothelial cell line and isolated brain microvascular endothelial cells) and their functioning upon treatment with ammonia and/or TNFα, the key factors involved in the pathomechanism of HE.

Methods

Animal models and biochemical analysis

Fifty-three 8–10-week-old male Sprague Dawley rats with an initial body weight of 250–300 g, from the outbred animal colony re-supplied by the Animal House of Mossakowski Medical Research Institute, Warsaw, Poland (Approval No. 57/2015 (14 May 2015 from the 4th Local Ethics Committee for Animal Experimentation, Warsaw, Poland, as compliant with Polish Law) were randomized to the experimental groups (Scheme 1). All efforts have been made to reduce the number of animals and minimize their suffering. The study complies with the ARRIVE (Animal Research: Reporting In Vivo

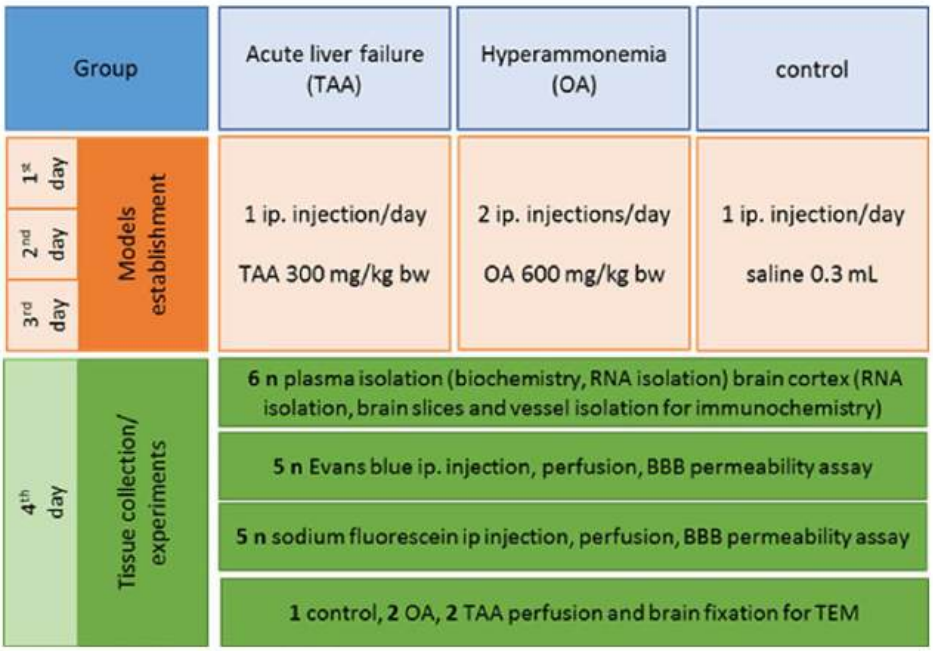

Scheme 1 Graphical representation of the research design

Experiments) guidelines (study design, experimental procedures, housing and husbandry, statistical methods) guidelines for reporting animal research. Animals were given free access to water and standard rodent chow and housed in constant temperature, humidity, and 12 h light-dark cycling.

Acute liver failure (ALF) was induced by thioacetamide (TAA) intraperitoneal (ip.) injections in doses of 300 mg per kg at 24-h intervals for 3 days. The control (sham) group received 0.3 mL of 0.9% NaCl. Hyperammonemia was induced by ip. administration of ammonium acetate (OA) in a dose of 600 mg per kg at 12 h intervals for 3 days. Rats were sacrificed by decapitation and the brains were quickly removed, and the cerebral cortex was isolated. The blood was collected in EDTA tubes, incubated at room temperature for 20 min, and centrifuged at 1500×*g* for 10 min at room temperature for plasma separation.

The blood plasma ammonia level and liver enzymes (aspartate aminotransferase; AST, alanine aminotransferase; ALT, and γ-glutamyl transpeptidase; GGTP) activities were measured by a commercial analyzer (Scil Vet, Germany). Levels of proinflammatory cytokines were evaluated using LEGENDplex™ Rat Inflammation Panel (BioLegend, San Diego, USA) directly according to manufacturer instructions. Data acquisition (300 events for each cytokine) was performed using a BD FACSCanto II flow cytometer with BD FACSDiva Software and FCAP Array software, version 3.0 (BD Biosciences, San Jose, USA).

Rat brain capillaries isolation

After decapitation, brains were extracted, cerebral cortices isolated, and homogenized in Ringer's solution then centrifuged at 1500×*g* for 10 min at 4 °C. The pellet was re-suspended in fresh buffer and centrifuged; the washing step was repeated three times under the same conditions. The final pellet was homogenized in 10 mL of 0.25 M sucrose and centrifuged in a discontinuous sucrose gradient (0.25:1:1.5 M sucrose) (30,000×*g*, 30 min, and 4 °C). The fraction with microvessels was collected and transferred to the Eppendorf tube.

Cell cultures and miRs' transfection

Primary brain microvascular endothelial cells (PBMEC) were isolated from the vesicles of the brain cortex of 14-day-old Sprague-Dawley male rats from the animal colony of Mossakowski Medical Research Institute, Polish Academy of Sciences, directly according to the protocol [17]. Briefly, after decapitation, brains were isolated, and cortices tissue was dissected under sterile conditions. The homogenized tissue was enzymatically and mechanically dissociated with 1 mL of 10 × Trypsin and Type IV Collagenase solution at 37 °C for ~ 30 min. Obtained

pellets after following centrifugation and cleaning steps (800×*g* for 5 min, ~20 °C; 1500×*g* for 15 min ~ 20 °C; 800×*g* for 15 min), and the supernatant was discarded. Cells were seeded on a 6-well plate coated with collagen I (Corning, NY, USA) and cultured in Dulbecco's Modified Eagle's Medium (DMEM) containing 20% FBS and supplemented with 1.0 ng/mL basic fibroblast growth factor (bFGF) and 20.0 µg/mL bovine sodium heparin. In the first 2 days, puromycin was added to the culture medium to inhibit neuron and astrocyte growth. The medium was changed the next day, and then every 2–3 days.

Rat brain endothelial cells (RBE4) were cultured in 24-transwell plates, 60 mm, or 100 mm dishes (Corning, NY, USA) coated with collagen type I. Cells were cultured on the MEM/Ham's F10 medium with Glutamax (Gibco, Thermo Fisher Scientific, Waltham, USA) with the addition of 10% of heat-inactivated FBS, 1.0 ng/mL bFGF, and gentamicin (Gibco, Thermo Fisher Scientific, Waltham, USA) at 37 °C in a humidified atmosphere of 95% air and 5% CO_2 and used after 14–21 days when cells displayed endothelial phenotype and minimum 90% of the surface confluence.

The PBMEC and RBE4 cells were treated with 5 mM ammonium chloride ("ammonia") or 10 ng/mL TNFα (rat recombinant, Sigma-Aldrich, Saint Louis, USA) which were added into the cell culture medium for 24 h.

For transfection experiments, RBE4 cells were seeded at density $3{,}3\times10^5$ and were transfected with the following sequences: 5′-UGGAGUGUGACAAUGGUG UUUG-3′ for mimic miR-122-5p (Qiagen; Cat. No. 33173YM00470430-ADA) and 5′-UAUGGCACUGGU AGAAUUCACU-3′ for mimic miR-183-5p (Qiagen; Cat. No. 339173YM00471390-ADA) or negative control 5′-UCACCGGGUGUAAAUCAGCUUG-3′ (Qiagen; Cat. No. 339173YM00479902-ADA). Transfection was performed using the HiPerFect transfection reagent (Qiagen, Hilden, Germany) according to the manufacturer's instructions, using 5 µM or 20 µM mimic concentration for 24 h. For cell adhesion experiments RBE4 cells were seeded at density 1×10^5 on a 6-well plate coated with collagen I.

RNA extraction and next generation sequencing

Total RNA was extracted from 200 µL rat plasma using the miRNeasy Serum/Plasma Advanced Kit (Qiagen, Hilden, Germany). Samples were thawed on ice and centrifuged at 12,000×*g* for 5 min to remove any cellular debris. For each sample, 200 µL of plasma was mixed with 1 mL of Qiazol followed by extraction steps directly according to the manufacturer's instructions. Finally, RNA was eluted in 10 µL of nuclease-free water and stored at −80 °C to await further analysis. Quantification of total RNA was made spectrophotometrically with a NanoDrop 2000 (Thermo Fisher Scientific, Waltham, USA) and 1 µg of total RNA was used for library preparation. NGS procedure was carried out by the BGI company (Shenzhen, China) using DNBSEQ G400 (MGI2000) system in SE50 mode. A minimum of 20 million paired-end reads were generated per sample. Quantification includes the raw read count, as well as normalized expression level as CPM values (counts per million reads mapped) to account for the variability in the library size. Next, miRDeep2 Quantifier analysis based miRbase 2.0 library was used to identify miR sequences. The quantification of the miR expression level was carried out using the Quantifier script of the miRDeep2 tool applying the default parameters. MiRs with a false discovery rate (FDR) p-value determined by DESeq2 below 0.05 were considered as differentially expressed (up/downregulated).

Quantitative RT-PCR

Reverse transcription and cDNA synthesis were performed using TaqMan Advanced miRNA cDNA Synthesis Kit (Invitrogen, ThermoFisher Applied Biosystems™, A28007) according to the manufacturer's protocol. The levels of miR expression were measured by quantitative RT-PCR with a miRCURY LNA SYBR Green PCR Kit (Qiagen, Hilden, Germany, Cat No. 339345) with appropriate miRCURY LNA miRNA PCR Assay primers: rno-miR-183-5p (Qiagen, Hilden, Germany, Cat No. QG-339306_YP00206030) and rno-miR-122-5p (Qiagen, Hilden, Germany Cat No. QG-339306_YP00205664). The snRNA U6 was used as a normalization control (Qiagen, Hilden, Germany Cat No. QG-339306_YP02119464). The assay was conducted using the Applied Biosystems 7500 Sequence Detection System (Applied Biosystems, Foster City, CA, USA) according to the manufacturer's instructions. The relative expression levels of miRNAs were calculated using the $2^{-\Delta\Delta Ct}$.

Western blot analysis

To evaluate the occludin and integrin β1 protein content in rat cerebral cortex Western blot analysis was used. Triton Lysis Buffer (20 mM Tris pH 6.8, 137 mM NaCl, 2 mM EDTA, 1% Triton X-100, 0.5 mM DTT, 1 mM PMSF) containing Protease Inhibitor Cocktail (Sigma-Aldrich, Germany) and Phosphatase Inhibitor Cocktail (Sigma-Aldrich, Germany) was used to homogenize brain tissue. The homogenate was centrifuged at 12,000×*g* for 20 min at 4 °C. On a 10% SDS-polyacrylamide gel, equal amounts of protein (30 µg) were separated and deposited onto a nitrocellulose membrane. After overnight incubation with an anti-occludin antibody (1:200, Cell Signalling, Inc., Cat. No. 91131) or integrin β1 (1:200, Cell Signalling, Inc., Cat. No. 4706) the membranes were washed, treated with HRP-conjugated anti-rabbit IgG

(1:2000; Sigma-Aldrich, Germany), and developed with West-Pico Chemiluminescence Substrate (Pierce, Rockford, USA). After stripping, the blots were treated for 1 h with an anti-GAPDH antibody.

Bioinformatics analysis

To evaluate the biological impact of the differentially expressed miRs on target genes, we used three different databases: miRDB v5 (http://mirdb.org/miRDB, TargetScan7.1 (https://www.targetscan.org/vert_80/), and TarBase v.8 (https://dianalab.e-ce.uth.gr/html/diana/web/index.php?r=tarbasev8%2Findex). We selected a set of targets linked to BBB structure or function, repetitively reported in all three databases. Next, based on the miRDB tool MirTarget, we predict the most probable miR target genes (miRs with targets with a score < 60 were not taken into further analysis according to miRDB authors' recommendations). Next, we associated data with NGS results considering differently expressed miRNAs but with the lowest p-value, resulting in the most altered miRs with target genes of the highest probability.

After establishing specific genes regulated by selected miRs, we identified the potential of selected genes on biological functions. The String Tool pathways analysis was performed to verify the probable contribution of selected genes to a broader spectrum of processes. We examined the involvement of selected genes in the biological processes as well as KEGG Pathways in combination with gene clustering. The String Tool pathways analysis showed interactions with a confidence score greater than the minimum needed (0.15) as a result only those networks are included in the prediction. The probability that a predicted link between proteins in the same metabolic map in the KEGG database is represented by the confidence score. Following this, we set the required interaction score of 0.9 the highest confidence interaction.

Immunohistochemical and immunofluorescent staining

RBE4 and PBMEC cells were seeded onto collagen I-coated coverslips at a density of 3×10^2 cells/well and cultured for 5–7 days. Cells were fixed with 4% paraformaldehyde/PBS and permeabilized with 0.25% Triton X-100/PBS. Secondly, were incubated with antibodies against CD-31 (1:400, ab28364 Abcam, Cambridge, UK), vWF (1:400, ab6994, Abcam, Cambridge, UK) overnight at 4 °C and then exposed to secondary antibody Alexa Fluor 488 goat anti-rabbit IgG (H+L) (1:1000, Thermo Fisher Scientific, Waltham, MA, USA, Cat. No. A11008).

After 24 h incubation with ammonia and/or TNFα, cells were rinsed with PBS. Cultured cells, brain cortex slices, and isolated brain microvessels were fixed with 4% paraformaldehyde/PBS and permeabilized with 0.25% Triton X-100/PBS. Secondly, were incubated with antibodies against occludin (1:200, Cell Signalling, Inc., Cat. No. 91131) or integrin β1 (1:200, Cell Signalling, Inc., Cat. No. 4706) and CD-31 (1:400, ab28364 Abcam, Cambridge, UK) overnight at 4 °C, and then exposed to secondary antibody Alexa Fluor 488 goat anti-rabbit IgG (H+L) (1:1000, Thermo Fisher Scientific, Waltham, MA, USA, Cat. No. A11008) and Alexa Fluor 546 goat anti-rabbit IgG (H+L) (1:1000, Thermo Fisher Scientific, Waltham, MA, USA, Cat. No. A11008). The nuclei were labeled with Hoechst 33258 (Thermo Fisher Scientific, Waltham, MA, USA, Cat. No. H1398). Images were acquired in a confocal laser scanning microscope LSM780 (Zeiss, Jena, Germany) and processed using the ZEN 2012 (Zeiss, Jena, Germany). To quantify fluorescence intensity, the pictures were subjected to a scaling process to achieve a magnification factor of 20. Additionally, the images were normalized to ensure consistent exposure duration across all samples. A total of eight to ten regions of interest were quantified using ImageJ (Fiji) software, with background fluorescence subtracted from both control and examined sections.

Transendothelial electrical resistance and cells adhesion

The transendothelial electrical resistance (TEER) was measured by a custom-made device, developed for in vitro experiments. RBE4 cells were seeded at a density of 6×10^5, cultured in transwell chambers with 0.4 mm polycarbonate filters (Corning Costar, Corning, NY, United States) at 37 °C in a humidified atmosphere of 95% air and 5% CO_2. Before treatment with the ammonia and TNFα, TEER was measured every 5 min. for 1 h in all inserts. After the treatment, the TEER in 24-well was measured every 5 min. for 24 h. Each day of the experiment was followed by the medium exchange. TEER value was expressed in Ω, and calculated by subtracting the resistance of a transwell without cells from a well with cells.

Using a custom-made device cell adhesion to collagen I was evaluated using the adapted methodology described by Lajkó et al. [18]. The adhesion was measured in 4-h time intervals. The Ω values were obtained as a variation of the initial values of seeded cells to values within 24 h of cell attachment. Results were normalized to uncoated transwell.

Evans blue and sodium fluorescein permeability assay

2% Evans blue (EB; Sigma-Aldrich, Saint Louis, USA) in sterile saline was injected into the tail vein in rats (4 mL/kg. After 2 h circulation, rats were transcardially perfused with 200 mL of ice-cold saline, and the brains were quickly removed. The isolated brain cerebral

cortices were weighed, homogenized in 30% trichloro acid (TCA), and centrifuged at 10,000×*g* for 20 min. The absorbance of the supernatants was measured at 620 nm, using a Pharmacia LKB Ultrospec III spectrophotometer (Uppsala, Finland), and BBB permeability was calculated as a fluorescent intensity. Results were calculated using EB as a standard and expressed as nanograms per milligram of tissue brain tissue. Sodium fluorescein (SF; 100 mg in 1 ml saline; Sigma-Aldrich, Saint Louis, USA) was injected ip., and after 45 min rats were perfused with saline. After decapitation, cerebral cortices were removed, weighed, and homogenized 1:10 (w/v) in sterile PBS. Samples were precipitated with ethanol (1:3 v/v) followed by centrifugation at 3000×*g* for 10 min. The supernatants were diluted and analysed in a spectrofluorometer FLUOstar Omega (BMG Labtech, Ortenberg, Germany) using an excitation wavelength of 480 nm and an emission wavelength of 538 nm. The BBB permeability was measured as the ratio of SF in a gram of brain tissue to the amount of SF in 1 ml of plasma and present in a percentage.

Transmission electron microscopy

One control, two OA, and two TAA rats were anesthetized and perfused through the ascending aorta with 2% paraformaldehyde and 2.5% glutaraldehyde in 0.1 M cacodylate buffer, pH 7.4. The cerebral cortex was fixed in the same solution for 20 h (at 4 °C) and placed in 1% OsO_4 for 6 h. Afterward, the samples were dehydrated by ethanol solutions of increasing concentration (30%–10 min, 50%–10 min, 70%–24 h, 90%–10 min, 96%–10 min, anhydrous EtOH–10 min, finally acetone–10 min) and saturated with epone. Epone was polymerized in blocks at 60 °C for 24 h in an incubator (Agar Scientific, Stansted, England). The polymerized samples were cut into ultrathin sections (70 nm thick) with an RMC MTX ultramicrotome (Boeckeler Instruments, Tucson, Arizona, USA), placed onto copper nets, and analyzed in a LIBRA 120 transmission electron microscope (Zeiss, Oberkochen, Germany). Photographs were taken with a Slow-Scan CCD camera (ProScan, Germany), using the EsiVision Pro 3.2 software. We evaluated 12–24 fields of view from each sample.

Statistical analysis

Data were analyzed and visualized using Prism 7 (GraphPad Software Inc., La Jolla, USA). Results were presented as mean ± SD. The statistical significance between various groups or treatments was measured by unpaired t-test or one-way ANOVA with Dunnett's post hoc test. In all experiments, p-value < 0.05 was considered to be statistically significant, ***p < 0.001, **p < 0.01, *p < 0.05, without asterisks means no significance.

Results

TAA treatment generates severe hepatic injury

Both animal models were previously described and are routinely used in our laboratory and by other groups to study different aspects of HE [19–21]. The levels of ALT and AST were significantly increased in the TAA group acknowledging liver injury. Ammonia levels were markedly increased in both OA and TAA rats (Table 1). Determination of systemic inflammation revealed notable inter-individual variation in the plasma cytokines level. Significantly increased plasma levels of Il-6, IL-10, and Il-1β were measured in TAA rats. Enhanced TNFα levels, noticed in 50% of the TAA group of animals, presented a tendency toward an increase. In turn, the OA group did not present marks of inflammation except for the elevation of Il-1β (Table 1).

Differences and similarities of structural and functional changes of the BBB induced by TAA and OA

Ultrastructural changes of the BBB were verified by TEM imaging. Unchanged microvascular endothelial cells and astrocytes with unaltered structures were observed in the control and OA rat brain prefrontal cortex (Fig. 1A; left and middle panels). In turn, endothelial cells of TAA rat brain microvessels were noticeably swollen with distinct disruption of the cytoplasmic membrane (Fig. 1A; right panel). In the peripheral zone, astrocytic endfeet with swollen mitochondria were also observed (Fig. 1A; right panel).

The BBB permeability was evaluated using a high-weight EB and a low-weight SF, dye. We did not observe any difference in the brain concentration of EB between studied experimental groups (Fig. 1B). In turn, SF concentration in the TAA brain was significantly higher, as compared to the control by ~ 500%, along with an unaltered level in the OA group (Fig. 1B). Taken together, we documented that TAA-induced ALF, unlike OA, causes structural BBB abnormalities and BBB permeability increase for low molecular weight molecules.

Table 1 Biochemistry and cytokines concentration in rat plasma

	Control	OA	TAA
Ammonia (μmol/L)	62 ± 7	93 ± 11**	139 ± 11***
AST (units/L)	163 ± 17	175 ± 47	1958 ± 851***
ALT (units/L)	64 ± 6	70 ± 10	442 ± 154***
GGTP (units/L)	1.7 ± 0.3	1.9 ± 0.7	2.1 ± 0.4
TNFα (pg/mL)	0.039 ± 0.103	0.009 ± 0.024	5.435 ± 10.150
IL-1α (pg/mL)	4.970 ± 7.678	6.034 ± 4.177	59.648 ± 42.246
IL-1β (pg/mL)	n.d.	0.427 ± 1.131***	1.874 ± 6.215***
IL-6 (pg/mL)	95 ± 106	n.d.	10,022 ± 1355***
IL-10 (pg/mL)	n.d.	n.d.	1592 ± 3313***

Results are mean ± SD. n = 6; **p < 0.01, ***p < 0.001 vs. control

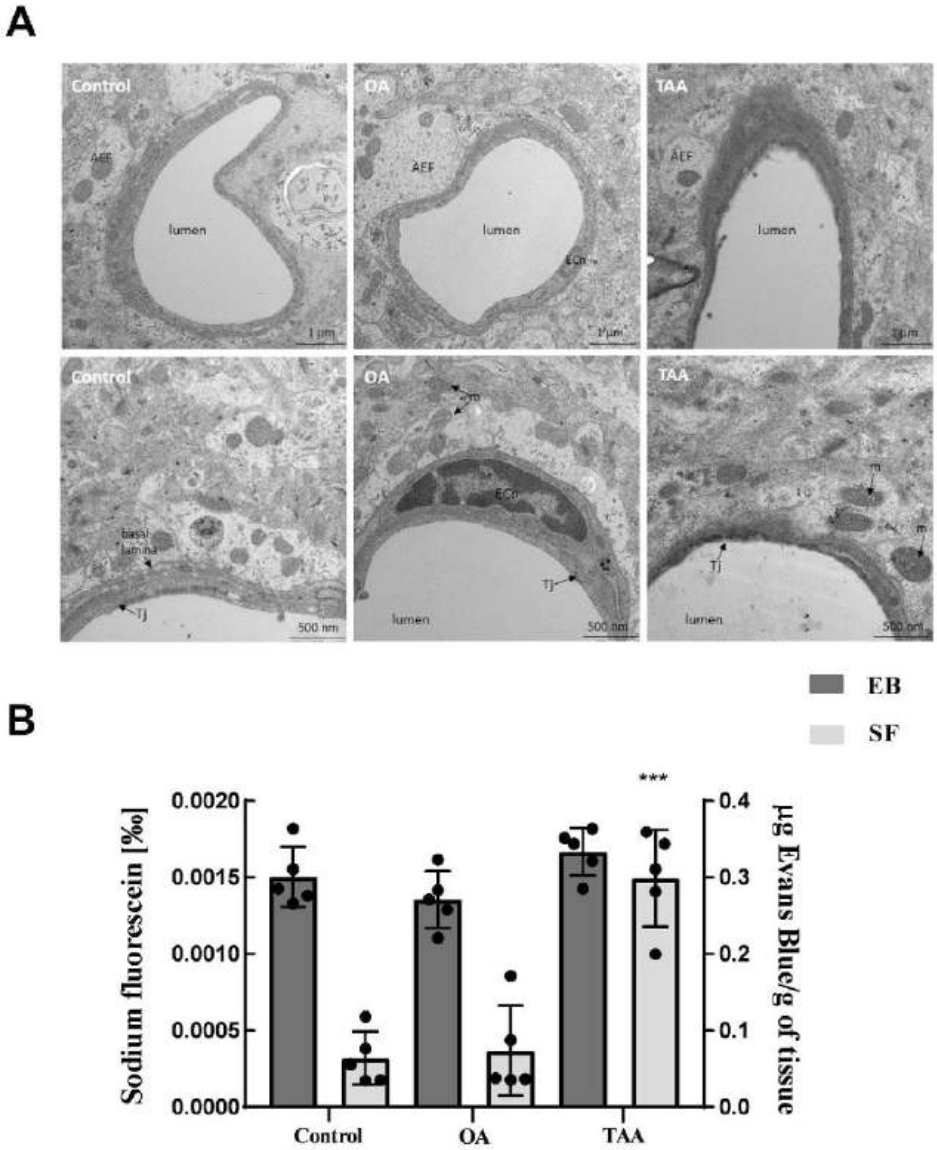

Fig. 1 The effect of OA and TAA administration on the rat BBB structure and permeability. **A** TEM images of the microvessels in rat brain prefrontal cortex of the control, OA, and TAA rat. *j* tight junctions, *m* mitochondria, *ECn* endothelial cell nuclei, *AEF* astrocyte endfeet. Scale bars are posted under individual images. **B** BBB permeability for Evans blue (EB; black bars) and sodium fluorescein (SF; grey bar). The results are the mean ± SD. n = 5; ***p < 0.0001 vs. control, one-way ANOVA, Dunnett's post hoc test

Plasma miRNA expression changes differ between OA and TAA rats

We profiled miRNAs isolated from the plasma of six controls, OA, and TAA-administered rats. The NGS analyses yielded 76×10^6 quality-filtered and processed reads across all samples with a mean count of 4.9×10^6 per sample (Additional file 1: Tables S1, S2). The Pearson correlation analysis revealed one outlier sample in the control group which was in consequence removed from further analysis.

We identified 488 circulating mature miRs across all plasma samples (Additional file 1: Tables S1, S2). Differential expression (DE) analysis revealed significant variation between experimental groups, thus in the

OA group, 35 differentially expressed miR (12 upregulated, and 23 downregulated) were identified (Fig. 2C). In turn, more pronounced changes were analyzed in the TAA group: number of 128 miRs were differentially expressed, of which 125 were upregulated and 3 were downregulated (Fig. 2A). The results comparison of both models revealed high (83%) sharing of the upregulated miRNA observed in OA rats with TAA group (Fig. 2C). The results correspond well to the current knowledge that a systemic, high ammonium concentration (hyperammonemia) is a dominant factor in the course of ALF [22] reproduced well in the TAA rat model (Table 1) [20, 23]. Interestingly, in both models, the most pronounced change was miRNA let-7c-5p increase (twofold in the OA and ~ fourfold in the TAA) (Fig. 2C, Additional file 1: Tables S1, S2).

In silico analysis of differentially expressed miRs and their target genes

Target genes for DE miR were predicted using three different online-available databases: miRDB, TargetScan, and TaRBase. Due to substantial differences in the obtained matches (Additional file 1: Tables S3, S4) only fully overlapped results, in all three databases, were qualified as the most relevant. As a result, nine target genes related to the BBB function were found in the TAA group (Fig. 3A, Additional file 1: Table S3), while no overlapped target was identified in the OA group (Fig. 3A, Additional file 1: Table S4). In consequence, for further analysis only TAA group was taken into consideration. Next, we evaluated the obtained data using the following criteria: low DE analysis p-value obtained in NGS (< 0.001) along with high gene target score (> 60) Displayed targets possess target prediction scores, which are rated by the new computational target prediction system. As a consequence, the search results were sorted by prediction score, additionally, rates fewer than 60 did not proceed in the study. Therefore, our analysis identified miR-122-5p and miR-183-5p as the most relevant and pointed to their potential targets: occludin and integrin β1 respectively, as the most promising for further evaluation.

We looked at the functionality of predicted gene targets by Gene Ontology (GO) analysis in terms of biological processes. Using String bioinformatics tool we identified predicted genes in nine biological processes associated with the BBB functioning: (GO:0005911 Cell-cell junction, GO:0005923 Bicellular tight junction, GO:0008305 Integrin complex, GO:0005887 Integral component of the plasma membrane, GO:0030054 Cell junction, GO:0005886 Plasma membrane, GO:0016328 Lateral plasma membrane, GO:0044291 Cell-cell contact zone as well as in 3 KEGG Pathways: rno04530 Tight Junction, rno04512 ECM–receptor interaction and rno04514 Cell adhesion molecules (Fig. 3B). The occludin was associated with six GO pathways, while integrin β1with seven from nine GO pathways (Fig. 3B).

KEEG analysis selected three from nine predicted target genes (occludin, integrin β1, and claudin 11) indicating their involvement in Tight junction, ECM receptor interaction, and Cell adhesion molecules pathways (Fig. 3B).

Our results pointed out miR-122-5p and miR-183-5p with their target genes, occludin, and integrin β1, as elements potentially involved in BBB alterations observed in the TAA rat brain.

RT-PCR analysis of miR-122-5p and miR-183-5p expression ex vivo and in vitro

Following the results of the NGS analysis documenting the upregulation of both miR of interest in the plasma of TAA rats, we verified their expression level using qRT-PCR analysis. A significant ~ 250% increase and unchanged expression level of the miR-122-5p and miR-183-5p, respectively, in TAA rat plasma, was observed (Fig. 4A, left panel). Since miR-183-5p is predominantly expressed in the brain (Additional file 1: Fig. S1), in parallel, we examined the miR-183-5p expression level in the prefrontal cortex of TAA rats. The revealing analysis documents the onefold increase of this miRNA in the TAA rat brain homogenate (Fig. 4A, right panel).

Next, we verified the potential of key pathogenic factors of HE (ammonia and/or TNFα) to affect miR-122-5p and miR-183-5p expression changes. Using the primary rat brain microvascular endothelial cells (PBMEC) tunnelled to mimic endothelium in vivo, first, we documented culture purity and characteristic PBMEC features that resembled fairly well native endothelium (Additional file 1: Fig. S3). We showed that ammonia, TNFα, or their combination, increase the relative expression of both miRs, with a less pronounced effect of TNFα added alone (Fig. 4B).

The effect of TAA treatment on occludin and integrin β1 levels in the rat brain cortex homogenate and isolated brain cortex microvessels

Next, we studied both proteins amount in the TAA prefrontal cortex homogenates (Fig. 5A), and immunofluorescence intensity in brain slices of the prefrontal cortex (Fig. 5B) as well as in brain microvessels (Fig. 5C) isolated from the TAA rats. A marked decrease in both occludin and integrin β1 was observed in this preparation.

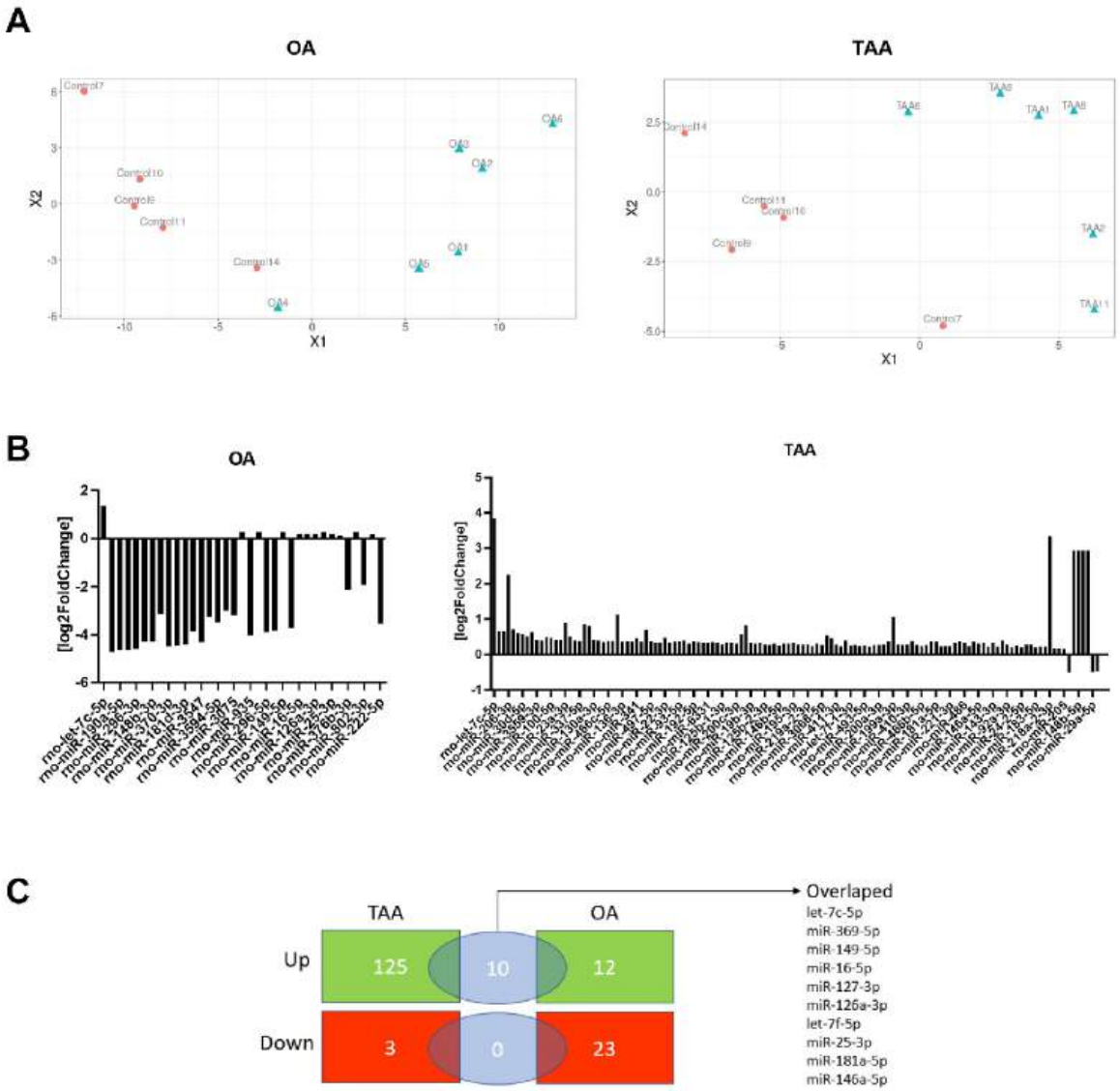

Fig. 2 The effect of OA and TAA on miR levels in the rat plasma. **A** Multidimensional scaling plot of miR profiles of individual animals. **B** Bar plot of differentially expressed miR expressed as log2 fold changes (control vs. OA; left plot and control vs. TAA; right plot). **C** Venn diagram of differentially expressed miRNA in rat plasma showing several upregulated (green) and downregulated miRNA (red) in the studied animal models

In vitro study of miR-122-5p and miR-183-5p involvement in ammonia/TNF-α-induced occludin and integrin β1 changes

The RBE4 cells used in further experiments are suited for the analysis of multiple BBB properties. In this experiment, RBE4 cells treated with ammonia, TNFα, or a combination of both factors, demonstrate a decrease in the occludin level with reduced intensity in occludin immunostaining (Fig. 6A, B, left panels). In RBE4 cells treated with TNFα and cells treated with ammonia and TNFα, the protein level of integrin β1 and immunostaining intensity was reduced (Fig. 6A, B, right panels).

In the following experiment, transfection of RBE4 cells with miR-122-5p mimic reduced the expression level of occludin by approximately threefold (Fig. 7A, left

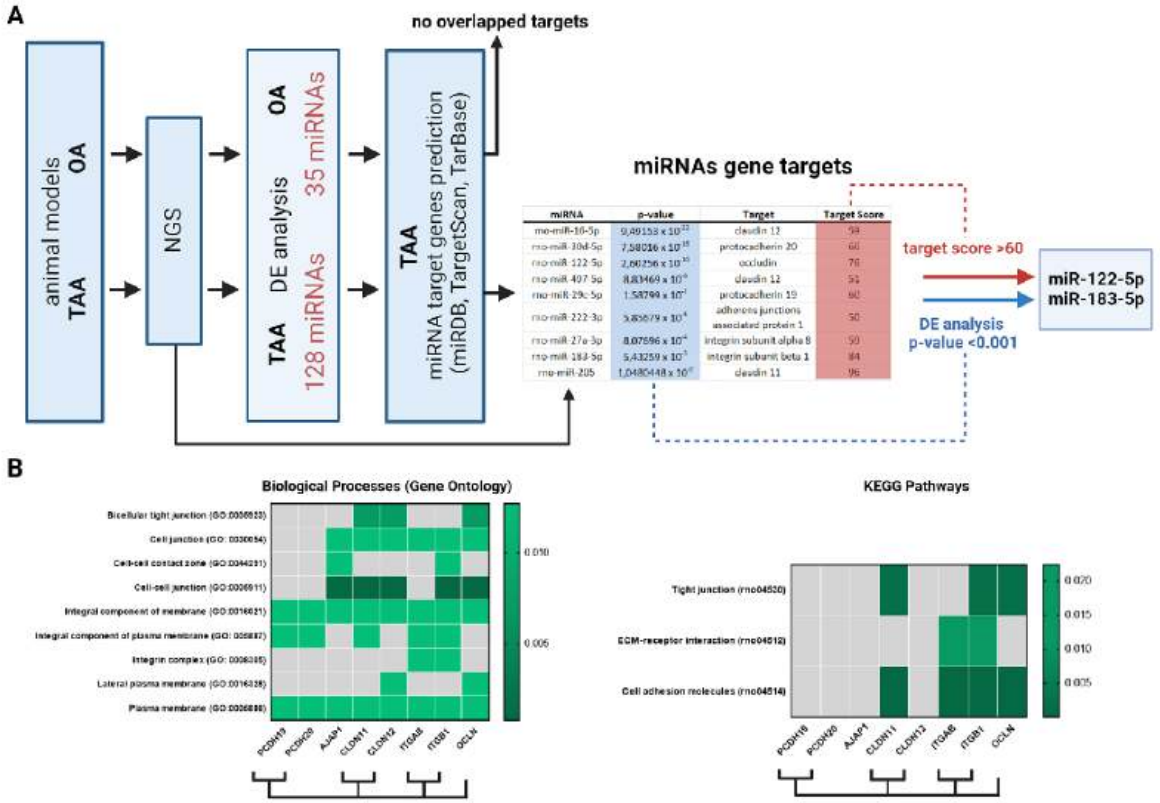

Fig. 3 In silico analysis of differentially expressed plasma miRNA. **A** Flow chart of the miRNA target prediction analysis. **B** Heatmap presenting results of the Gene Ontology (GO) pathway analysis of nine predicted target genes (left panel). Heatmap of the KEGG Pathways analysis of nine predicted target genes (right panel)

panel). Parallelly, RBE4 cell transfection with miR-183-5p mimic significantly decreased the expression of integrin β1 (Fig. 7B, right panel). Since occludin is a key element of TJ proteins [24] and contributes to proper BBB function, we further evaluated the effect of miR-122-5p mimic transfection on the tightness of RBE4 cell monolayer, BBB in vitro model, by transendothelial electrical resistance (TEER) measurement. The unchanged value of resistance of RBE4 cells monolayer was observed (Fig. 7B, left panel), implicating the complexity of TJ protein(s) assembly functioning. In turn, cells transfected with mimic miR-183-5p present a significant reduction of cell adhesion to collagen I (15% and 30% reduction, respectively; Fig. 7B, right panel), interpreted as disturbances in integrin β1-mediated interaction within cellular components of BBB and the extracellular matrix elements [25].

Discussion

Our study implicates, to our knowledge for the first time, a role of specifically identified miRs in BBB impairment associated with acute HE. First, BBB morphological evaluation by electron microscopy revealed BBB structural alterations with noticeable BBB leakage in the TAA model of ALF with less pronounced changes in the pure hyperammonemia animal model. Second, NGS analysis of plasma from both animal models identified miR-122-5p and miR-183-5p with their targets: occludin and integrin β1 respectively, among target genes related to the BBB structural and functional changes. The identified targets were decreased in TAA rat brain homogenates and microvessels isolated from rat brains in the TAA model, but much less so in simple hyperammonemia. Finally, the verification of selected miRs in cultured endothelial cells treated with critical factors for the pathology of HE, ammonia, and/or TNFα documented at the molecular level miRs' effects in the endothelium. The study unraveled that miR-185-5p via integrin β1 decline, disturbs integrin β1-mediated interaction within cellular BBB components and the extracellular matrix elements, thus limiting the ability of BBB to execute and control proper biological phenotype.

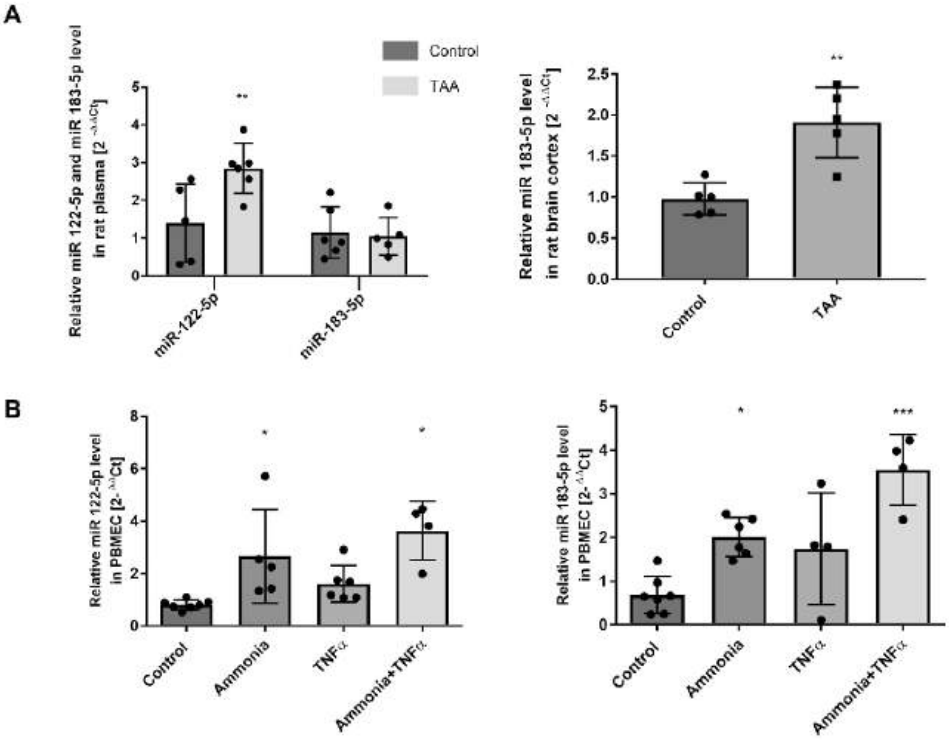

Fig. 4 miR-183-5p and miR-122-5p expression analysis. **A** The expression of miR-122-5p and miR-183-5p in the TAA rat plasma and miR-183-5p expression in the TAA rat brain prefrontal cortex. The results are the mean ± SD. n = 5; **p < 0.001 vs. control, unpaired t-test. **B** The expression of miR-122-5p and miR-183-5p in primary rat brain microvascular endothelial cells treated with ammonia and/or TNFα. The results are the mean ± SD. n = 4; *p < 0.05 vs. control, ***p < 0.001 vs. control, one-way ANOVA, Dunnett's post hoc test

BBB structural and functional changes were documented in acute, chronic, and acute-upon-chronic disease stages in humans [26–28]. Of note, BBB leakage was also documented in both acute and chronic HE models [15, 29] also in animal models of chronic liver diseases [30–32] However, the complexity of the pathogenic events underlying HE that take place all along the liver - brain axis [32–34] limits the progress in translational studies to prevent BBB dysfunction associated with impaired liver function. The present study illustrates a potentially effective venue towards this end.

We analyze BBB permeability in vivo using two markers: Evans blue (EB), the most commonly used vascular permeability marker which, readily binds to plasma albumin forming a permeability marker suitable for detecting significant BBB leakage. Contrary, low molecular weight (376 Da) dye, SF, enables the detection of relatively more subtle alterations [33]. Using these approaches, we documented that TAA-induced ALF, but not OA, causes structural BBB abnormalities and increases for low molecular weight molecules. Concurrently to the TAA model, limited disturbances related to BBB function in OA rats suggest that an elevated ammonia level alone is not sufficient to cause the BBB disruption in vivo, implicating the contribution of systemic inflammation associated with liver failure. Indeed, ammonia-cytokine synergy in causing brain dysfunction has been repeatedly documented (reviewed in ref. [18]). Human cerebrovascular endothelial cells increase ammonia uptake when exposed to TNFα in vitro [34]. Worth noting, that the expression levels of genes coding enzymes involved in oxidative stress were elevated in cultured astrocytes exposed to both cytokines and ammonia [35]. Down the same valley, chronic hyperammonemia-induced peripheral inflammation with microglia activation and increased proinflammatory cytokines in the hippocampus. Alterations were associated with impaired spatial learning and alleviated by anti-TNFα or sulforaphane treatment [36, 37]. Importantly, the role of inflammatory factors in BBB disruption has been widely documented in other neurological syndromes [38].

Kato and colleagues described swollen astrocytic endfeet, increased number of vacuoles and vesicles in endothelial cells and pericytes, basal lamina enlargement,

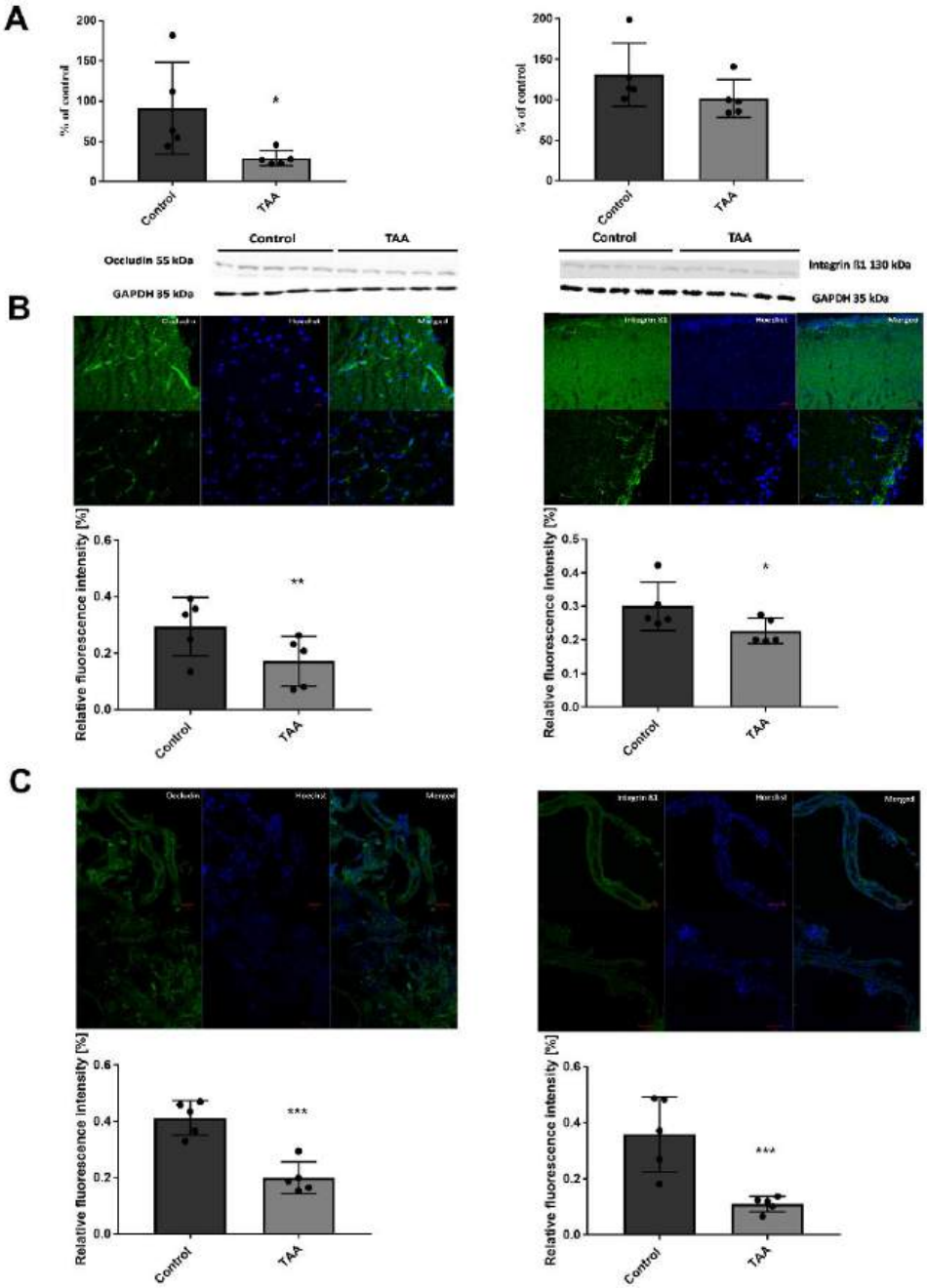

Fig. 5 The effect of TAA treatment on occludin and integrin β1 protein level in the rat brain cortex. **A** Protein level of occludin and integrin β1 in the prefrontal cortex of TAA rat brain. The results are the mean ± SD. n = 5; *p < 0.05 vs. control, unpaired t-test. **B** The immunostaining of occludin (left panel, green) and integrin β1 (right panel, green) in isolated brain cortex, nuclei stained with Hoechst (blue). **C** The immunostaining of occludin (left panel, green) and integrin β1 (right panel, green) in brain cortex microvessels, nuclei stained with Hoechst (blue). The results are the mean ± SD.

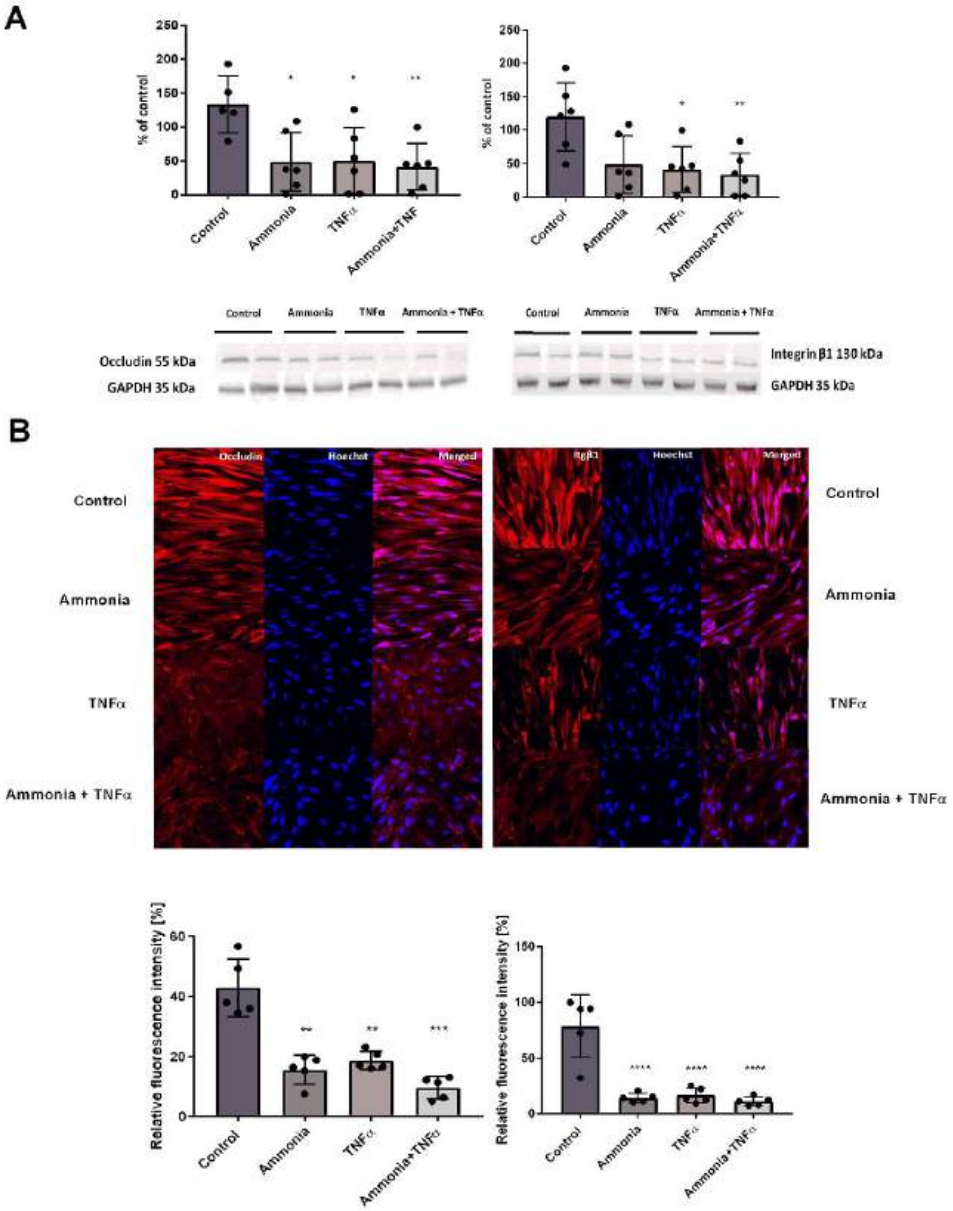

Fig. 6 The effect of ammonia and TNFα on occludin and integrin β1 in a rat brain endothelial cell line (RBE4). **A** Protein level of occludin and integrin β1 with representative immunoblots. **B** Confocal microscopy analysis of occludin immunofluorescence (left panel, red), integrin β1 (right panel, red) in RBE4 cells treated or not with ammonia and TNFα. DAPI staining (blue). The results are the mean ± SD; n = 5; *p < 0.05 vs. control, **p < 0.01 vs. control, ***p < 0.01 vs. control, ****p < 0.01 vs. control, one-way ANOVA, and Dunnett's post hoc test. The results are the mean ± SD. n = 5; *p < 0.05 vs. control, one-way ANOVA, Dunnett's post hoc test

and intact TJs in post-mortem sections of the brains of ALF patients, thereby documenting BBB structural changes [8]. Additionally, a metabolic study carried out on HE patients revealed ammonia easier entry into the brains of HE patients than in healthy volunteers [39]. A recent study showed that the factors abundant in HE patients' plasma, enhanced transendothelial leukocyte migration through the in vitro model of BBB, interpreted as elevated permeabilization of the BBB [40].

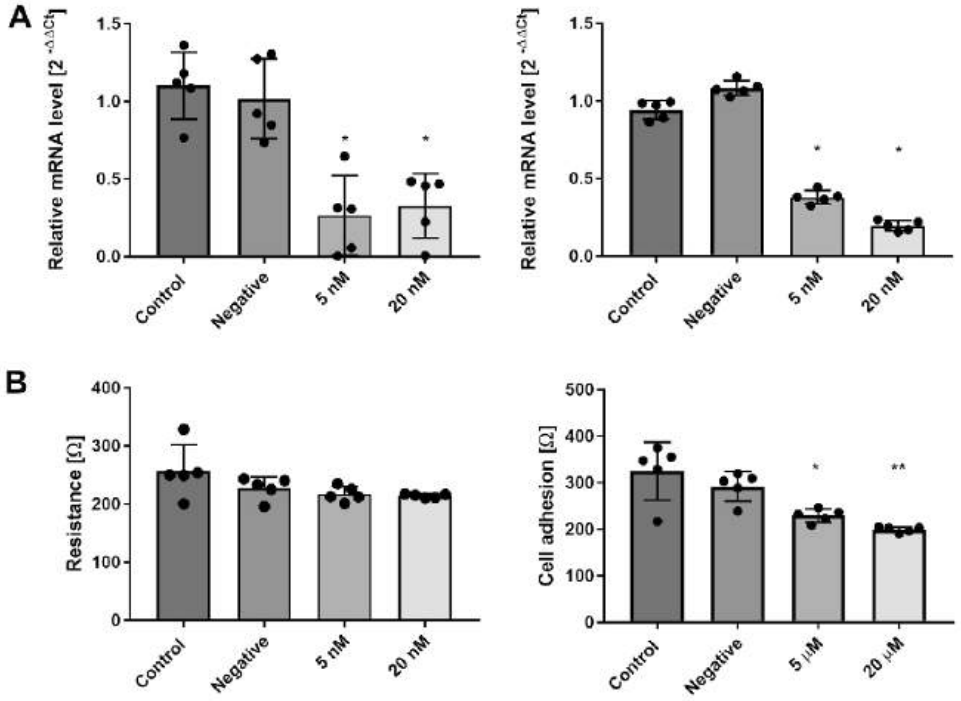

Fig. 7 The effect of transfection with miR-122-5p mimic and miR-183-5p mimic on occludin and integrin β1. **A** The effect of transfection with miR 122-5p mimic and miR 183-5p mimic on the mRNA expression level of occludin (left panel) and integrin β1 (right panel), respectively. The results are the mean ± SD. n = 5, *p < 0.05 vs. control, one-way ANOVA, Dunnett's post hoc test. **B** The effect of transfection with miR-122-5p mimic and miR-183-5p mimic on transendothelial electrical resistance measurement (left panel), and cell adhesion to collagen 1 (right panel). The results are the mean ± SD. n = 5; *p < 0.05 vs. control, **p < 0.01 vs. control, one-way ANOVA, and Dunnett's post hoc test

At the preclinical level, the BBB increased permeability was observed in the hepatotoxic HE model, induced by azoxymethane (AOM), correlating with the progression of liver injury and systemic inflammation [41]. The BBB opening at the symptomatic stage contributed to the neurological decline, as was presented previously [42]. It was documented, that the TAA model leads to cerebral edema as assessed by MRI, though the mechanism has not been elucidated in detail [43]. In the comparative study, the administration of hepatotoxin, TAA increased BBB permeability, measured by EB binding in brain tissue [15]. Complementary, the in vitro experiments using the BBB cellular model in co-culture of brain endothelial cells and astrocytes, documented monolayer increased permeability to AOM but not TAA, indicating direct drug toxicity [15]. Importantly, it was documented that liver injury and resulting inflammation work in concert with the BBB disruption [15]. Our work revealed that enhanced proinflammatory response is noticed in the TAA-injected rats. An enhanced BBB permeability was recently described in the mice model of TAA-induced ALF [15]. Of note, in the bile duct ligation (BDL) rat model of chronic HE, increased BBB permeability to SF and FITC-dextran in multiple brain regions, including the cerebral cortex, were also detected [44]. Regarding HE animal models, in acetaminophen-induced ALF mice increased BBB permeability positively correlates with blood TNFα level, a pleiotropic cytokine and key mediator of inflammation that regulates numerous physiological functions including the development of autoimmunity; the BBB changes in this model were found prevented by anti-TNFα-IgG administration [45]. Moreover, deactivation of the circulating TNFα by TNFα antibody administration increases expression of occludin and zonula occludens1 and decreases BBB permeability for EB day in brains of mice with ALF induced by D-galactosamine and lipopolysaccharide (LPS) administration [46]. Worth noting in this context is that brain endothelial cells do not produce TNFα nor IL-6 in a healthy microenvironment, but rapidly react to challenges (e.g., LPS stimulation), which induces endothelial TNFα and IL-6 production [47].

Less is known about the exact molecular mechanisms underlying BBB permeability increase in HE patients and HE animal models. With the development of bioinformatics tools, the impact of miR in different biological processes control is gradually discovered, however,

very limited experimental data documents miRs' role regarding BBB dysfunction reported in the course of HE.

Increasing evidence points to miR expression changes in body fluids and tissues from both HE patients [11, 48–51] and animal models [52–56] but only a few studies used NGS or other large-scale methods showing whole miRNome changes [57, 58].

In the presented work, we performed NGS profiling of miRs isolated from the plasma of OA and TAA rats, revealing notable differences between experimental groups. We found 35 differently expressed miR in the OA group and 128 in the TAA rat plasma. These analyses allowed us to prove the impact of ammonia on miR expression. Worth noting that the majority of the miRNA upregulated in the OA group (83%) were also increased in TAA indicating an analogous effect of the hyperammonaemia in both models.

The pathomechanism of HE is complex, but increased ammonia concentration in the blood remains the most distinctive event [59, 60]. However, the direct association between HE severity and ammonia level is not certain and has been frequently questioned [61–63]. The direct impact of ammonia on miR expression changes is not fully revealed despite a few reported miRNome dysregulation in clinical studies conducted on patients suffering from acute HE, mostly due to paracetamol over-dose [49, 51, 64–68], or chronic HE: most of the cases were associated with hyperammonaemia [69–71].

Since the impact of relevant changes in altered miR depends on their gene targets, bioinformatic tools serve to select and further investigate miR to predict final functional outcomes [72]. Nevertheless, miR target prediction should be interpreted with caution. Available bioinformatic tools use different algorithms and commercial programs as well as consecutively upgraded databases. Moreover, identified novel sequences added to the databases determine the prediction scores [73–75].

We performed predictive in silico analysis of the gene targets of the differently expressed miR obtained via NGS. We used three different databases: miRDB v5, TargetScan7.1, and TarBase v.8, and selected exclusively overlapped targets as the most certain. Further, we applied a functional prediction method using Gene Ontology (GO) and KEGG Pathways analysis that identified entire biological pathways statistically significantly enriched for selected miR targets [53] to potentiate the overall impact of the analysis, being aware that a single miR regulates hundreds of genes [76].

Our analysis selected miR-122-5p and miR-183-5p from dysregulated miR in a TAA rat plasma and identified occludin and integrin β1 respectively, as their most confirmed targets involved in biological processes associated with the BBB functioning. Noteworthy, we did not obtain output results of our in silico analysis for miR differently expressed in the OA group which is in line with observed unaltered BBB integrity in those animals. These results also indirectly strengthen the hypothesis of the miR-122-5p and miR-183-5p involvement in BBB disturbances described in TAA rats, which we verified in subsequent experiments.

Using the in vitro BBB model, we documented the contribution of selected miR to the reduction of the expression of their targets, the endothelium-located BBB components, occludin, and integrin β1. Consistently we showed that in cultured primary endothelial cells, treatment with ammonia and ammonia with TNFα treatment upregulated miR-122-5p.

The brain microvascular endothelial cells are primary components of the BBB regulating the BBB permeability by junctional proteins' structures composed of TJ proteins, integrins, annexins, etc., which cooperate with basement membrane components [77]. We used an RBE4 cell line that preserves an endothelial phenotype and presents a structural composition inherent to the in situ BBB, including the presence of TJ and adherence junction proteins [78]. Using this in vitro system, we tested the hypothesis that miR-122-5p affects BBB permeability by regulating the expression of occludin, a main structural protein of TJs presenting a protective effect on different cell barriers [79]. The transfection of RBE4 cells with a miR-122-5p mimic reduced the expression level of occludin by ~threefold. In our experimental setting, we did not document functionally the impact of occludin on cells' monolayer tightness. This observation is in line with both in vitro and in vivo studies documenting that occludin controls the passage of macromolecules of ~10–70 kDa through mice epithelium without affecting transepithelial resistance [80]. Beyond its structural roles, occludin also plays signaling roles at the BBB; however, molecular details of this process are incompletely understood [81, 82]. Moreover, altered physiological conditions (e.g., ammonia, and cytokines) may differentially affect the organization of occludin isoforms within plasma membrane lipid rafts. Thus, a detailed investigation of protein interactions of particular occludin isoforms will reveal how different signaling and regulatory molecules modulate occludin oligomeric assemblies to promote changes in TJ integrity at the BBB in the setting of ALF. Interestingly in this context, it was also shown that miR-122-5p containing exosomes secreted from LPS-induced neutrophils regulates beyond brain microvascular endothelial cells proliferation and apoptosis, as well as cell monolayer permeability [10].

miR-122 is the most abundant miR in hepatic tissue, constituting the majority of total miR (about 70%) [57]. Reduction of miR-122-5p was observed in the liver of

rats receiving low doses of TAA (50 mg/kg of b.w.) for 14 days [83] and also after a short 24 h exposition to a higher (150 mg/kg of b.w.) TAA dose [84]. The authors do not conclude if this phenomenon relies on hepatocyte loss and transfer of miR-122-5p from liver tissue to the blood or if it is a regulatory effect. One of the proposed roles of miR-122-5p for endothelium function is its involvement in the regulation of cationic amino acid transporter 1 (CAT-1) expression [85]. Amino acid L-arginine is transported via CAT-1 and is used as a substrate for endothelial production of nitric oxide. An inverse correlation between plasma levels of miR-122-5p and expression of CAT-1 was reported in a large group of patients with essential hypertension [86]. In the study carried out on TAA rat liver tissue, miR-122-5p reduction was reported to parallel CAT-1 expression upregulation [84]. Indeed, our previous work documented the absence of changes in CAT-1 expression in rats with simple hyperammonemia [37] which is compatible with the unchanged plasma level of miR-122-5p in the OA rats. However, the mechanistic nature of the link between the two events requires further investigation.

Cell-adhesion-related pathways include among others, focal adhesion, integrin signalling, TJ, and actin cytoskeleton regulation, all of the above being linked with miR-183-5p [87, 88]. Bioinformatics databases pointed to a putative binding site of miR-183-5p in the 3′-UTR of integrin 1β. Integrin β1 is a member of the integrin family, which is composed of the major cell surface receptors that mediate adhesion to the extracellular matrix. We validated the negative modulatory role of miR-183-5p in endothelial cell adhesion in the in vitro system, where RBE4 cell transfection was followed by an adhesion assay. We found a significant correlation between miR-183-5p and integrin β1 expression in the brain homogenate samples from TAA rats. Next, we demonstrated that miR-183-5p modulates integrin β1 expression at both the mRNA and protein levels in vitro. Similarly, Dambal et al., found that cell adhesion is the main pathway downregulated in the human prostatic epithelial cell line overexpressing the full miR-183 cluster comprised of miR-96, miR-182, and miR-183-5p [89].

Growing evidence demonstrates that miR-183-5p plays a crucial role in multiple processes of cancer progression by affecting tumor cell interactions [90–92]. These were documented in situ in cervical cancer cell lines transfected with miR-183-5p [93] and human embryonic kidney cells [94]. In this experiment, overexpression of integrin 1β observed in cervical carcinoma samples was negatively correlated with miR-183 level [93]. Another study reported that transfection of HeLa cells with miR-183 decreases cell invasion, but not cell adhesion by down-regulation of integrin 1β [94]. The role of miR-183 in the maintenance of cell integrity in epithelial cells under changing physiological conditions is poorly understood. An increase of miR-183-5p was recently described in mice with intracerebral hemorrhage (ICH) [95], a pathology assessed inter alia with vasogenic edema and BBB breakdown [96]. Administration of miR-183-5p agomir or antagomir into the lateral ventricles reduced neurologic deficits, BBB permeability, brain injury volume, and oxidative damage after ICH [95].

The miR-183-5p was upregulated in BDL-induced liver fibrosis and activated human hepatic stellate cells (LX-2 cell line) [97]. Accordingly, miR-183-5p inhibition alleviated liver fibrosis and downregulated the expression of related fibrotic biomarkers [97]. Additionally, miR-183-5p inhibition reduced LX-2 cell proliferation and promoted apoptosis. The results showed that miR-183-5p might act as a key regulator of liver fibrosis, and miR-183-5p could promote cholestatic liver fibrosis through the TGFβ signaling pathway [97]. Supportively, another study demonstrated upregulation of the miR-183 family in diethylamino ethylamine-induced hepatic fibrosis, suggesting a role in the progression severity of liver fibrosis [98].

In summary, we found that (i) miR-122-5p and miR-185-5p were upregulated in the rat systemic circulation, and that concurrently, occludin and integrin β1, their downstream target genes, were reduced in the endothelium in rat brain homogenate and brain microvessels isolated from TAA treated rats, and that (ii) the above in vivo effects were faithfully reproduced in vitro, in endothelial cells treated with ammonia/TNFα. Whereas miR-122-5p targeting occludin probably does not critically contribute to the BBB permeability increase, the effect of miR-185-5p through integrin β1 decline, presents disturbed integrin β1-mediated interaction within cellular BBB components and the extracellular matrix elements [25], thus limits the ability of BBB to execute proper biological phenotype. Through this study, the molecular mechanism of miR-183-5p as an inhibitory factor affecting endothelial cells at points critical for their BBB has been partially elucidated. The present work indicates that changes in miR, which have straightforward consequences for the expression of endothelial TJ proteins, may be potential indicators of BBB disturbances associated with ALF. As such the changes could be exploited in translational studies to prevent BBB dysfunction occurring due to impaired liver function. The results appear valuable for unraveling further the molecular mechanism of BBB remodeling, likely to be linked to other liver impairment disorders. In terms of scientific perspective, the detection of changes in miR patterns has become a major focus of diagnostic, prognostic, and disease

progression, as well as therapy-response markers using a great variety of detection systems in the future.

Abbreviations

ALF	Acute liver failure
ALT	Alanine aminotransferase
AST	Aspartate aminotransferase
BBB	Blood–brain barrier
HE	Hepatic encephalopathy
ip.	Intraperitoneal
NGS	Next Generation Sequencing
OA	Ammonium acetate/here used to refer to a rat model of hyperammonemia
PBMEC	Primary rat brain microvascular endothelial cells
RBE4	Rat brain endothelial cell line 4
TAA	Thioacetamide//here used to refer to a rat model of ALF
TEER	Transendothelial Electrical Resistance
TEM	Transmission electron microscopy

Supplementary Information

The online version contains supplementary material available at https://doi.org/10.1186/s12987-023-00484-7.

Additional file 1: Table S1. Results of next-generation sequencing of the OA rat plasma. **Table S2.** Results of next-generation sequencing of the TAA rat plasma. **Table S3.** Results of miRs target research in the TAA rat group. **Table S4.** Results of miRs target research in OA rat group. **Figure S1.** miRs tissue specificity, human TissueAtlas miR-183-5p. **Figure S2.** miRs tissue specificity, human TissueAtlas miR-122-5p. **Figure S3.** Immunocytochemical staining of rat brain microvascular endothelial cells with endothelial cell marker. **Figure S4.** Immunocytochemical staining of RBE4 cells with endothelial cell markers.

Author contributions

KOG: methodology, investigation, software, formal analysis, writing—original draft. KM: methodology, investigation, formal analysis, writing—original draft. MZ: conceptualization, resources, writing original draft—review and editing. All authors contributed to writing the protocol. All authors read and approved the final manuscript.

Funding

This work was supported by the National Science Centre of Poland [No. 2015/19/B/NZ4/01902], ESF [POWR.03.02.00-00-I028/17-00] and the MMRI internal funding source [FBW031].

Data availability

The datasets used and/or analysed during this study are available from the corresponding author upon reasonable request.

Declarations

Ethics approval

Animal experiments were performed at Mossakowski Medical Research Institute, Polish Academy of Sciences Warsaw conformed to the legislations for animal protection and care in the European Community Council Directive (2010/63/EU) and were approved by the 4th Local Ethics Committee for Animal Experimentation, Warsaw, Poland (Approval No. 57/2015).

Consent for publication

Not applicable.

Competing interests

The authors declare no competing interests.

Consent to participate

Not applicable.

Author details

[1]Department of Neurotoxicology, Mossakowski Medical Research Institute, Polish Academy of Sciences, Pawińskiego St. 5, 02-106 Warsaw, Poland. [2]Laboratory of Cellular Metabolism, Nencki Institute of Experimental Biology, Polish Academy of Sciences, Pasteura St. 3, 02-093 Warsaw, Poland.

Received: 21 July 2023 Accepted: 30 October 2023
Published online: 08 December 2023

References

1. Ridola L, Faccioli J, Nardelli S, Gioia SO. Riggio, hepatic encephalopathy: diagnosis and management. J Transl Intern Med. 2020;8(4):210–9. https://doi.org/10.2478/jtim-2020-0034.
2. Rudler M, Weiss N, Bouzbib CD. Thabut, diagnosis and management of hepatic encephalopathy. Clin Liver Dis. 2021;25(2):393–417. https://doi.org/10.1016/j.cld.2021.01.008.
3. Weissenborn K. Hepatic encephalopathy: definition, clinical grading and diagnostic principles. Drugs. 2019;79(S1):5–9. https://doi.org/10.1007/s40265-018-1018-z.
4. Coltart I, Tranah TH, Shawcross DL. Inflammation and hepatic encephalopathy. Arch Biochem Biophys. 2013;536(2):189–96. https://doi.org/10.1016/j.abb.2013.03.016.
5. Butterworth RF. The liver–brain axis in liver failure: neuroinflammation and encephalopathy. Nat Rev Gastroenterol Hepatol. 2013;10(9):522–8. https://doi.org/10.1038/nrgastro.2013.99.
6. Nguyen JH. Blood–brain barrier in acute liver failure. Neurochem Int. 2012;60(7):676–83. https://doi.org/10.1016/j.neuint.2011.10.012.
7. Goldbecker A. Blood–brain barrier permeability for ammonia in patients with different grades of liver fibrosis is not different from healthy controls. J Cereb Blood Flow Metab. 2010;30(7):1384–93. https://doi.org/10.1038/jcbfm.2010.22.
8. Kato M, Hughes RD, Keays RT, Williams R. Electron microscopic study of brain capillaries in cerebral edema from fulminant hepatic failure. Hepatology. 1992;15(6):1060–6. https://doi.org/10.1002/hep.1840150615.
9. Ahl B. Regional differences in cerebral blood flow and cerebral ammonia metabolism in patients with cirrhosis. Hepatology. 2004;40(1):73–9. https://doi.org/10.1002/hep.20290.
10. Habash NW, Sehrawat TS, Shah VH, Cao S. Epigenetics of alcohol-related liver diseases. JHEP Rep. 2022;4(5): 100466. https://doi.org/10.1016/j.jhepr.2022.100466.
11. Orzeł-Gajowik K, Milewski K, Zielińska M. Insight into microRNAs-mediated communication between liver and brain: a possible approach for understanding acute liver failure? Int J Mol Sci. 2021;23(1):224. https://doi.org/10.3390/ijms23010224.
12. Lopez-Ramirez MA. MicroRNA-155 negatively affects blood–brain barrier function during neuroinflammation. FASEB J. 2014;28(6):2551–65. https://doi.org/10.1096/fj.13-248880.
13. Reijerkerk A. MicroRNAs regulate human brain endothelial cell-barrier function in inflammation: implications for multiple sclerosis. J Neurosci. 2013;33(16):6857–63. https://doi.org/10.1523/JNEUROSCI.3965-12.2013.
14. Rom S, Dykstra H, Zuluaga-Ramirez V, Reichenbach NL, Persidsky Y. miR-98 and let-7g* protect the blood–brain barrier under neuroinflammatory conditions. J Cereb Blood Flow Metab. 2015;35(12):1957–65. https://doi.org/10.1038/jcbfm.2015.154.
15. Grant S. Direct comparison of the thioacetamide and azoxymethane models of type A hepatic encephalopathy in mice. Gene Expr. 2018;18(3):171–85. https://doi.org/10.3727/105221618X15287315176503.
16. Mladenović D. Behavioral and electroencephalographic manifestations of thioacetamide-induced encephalopathy in rats. Can J Physiol Pharmacol. 2012;90:1219–27. https://doi.org/10.1139/y2012-088.
17. Ruck T, Bittner S, Epping L, Herrmann AM, Meuth SG. Isolation of primary murine brain microvascular endothelial cells. J Vis Exp. 2014;14(93):52204. https://doi.org/10.3791/52204.
18. Lajkó E. Kynurenic acid and its derivatives are able to modulate the adhesion and locomotion of brain endothelial cells. J Neural Transm. 2018;125(6):899–912. https://doi.org/10.1007/s00702-018-1839-7.
19. Butterworth RF. Experimental models of hepatic encephalopathy: ISHEN guidelines. Liver Int. 2009;29(6):783–8. https://doi.org/10.1111/j.1478-3231.2009.02034.x.

20. DeMorrow S, Cudalbu C, Davies N, Jayakumar AR, Rose CF. 2021 ISHEN guidelines on animal models of hepatic encephalopathy. Liver Int. 2021;41(7):1474–88. https://doi.org/10.1111/liv.14911.
21. Li Y. Acute liver failure impairs function and expression of breast cancer-resistant protein (BCRP) at rat blood–brain barrier partly via ammonia-ROS-ERK1/2 activation. J Neurochem. 2016;138(2):282–282. https://doi.org/10.1111/jnc.13666.
22. Jayakumar AR, Norenberg MD. Hyperammonemia in hepatic encephalopathy. J Clin Exp Hepatol. 2018;8(3):272–80. https://doi.org/10.1016/j.jceh.2018.06.007.
23. Koblihová E, Mrázová I, Vernerová Z, Ryska M. Acute liver failure induced by thioacetamide: selection of optimal dosage in Wistar and Lewis rats. Physiol Res. 2014;63:491–503. https://doi.org/10.33549/physiolres.932690.
24. Hawkins BT, Davis TP. The blood–brain barrier/neurovascular unit in health and disease. Pharmacol Rev. 2005;57(2):173–85. https://doi.org/10.1124/pr.57.2.4.
25. Engelhardt B. β1-Integrin/matrix interactions support blood–brain barrier integrity. J Cereb Blood Flow Metab. 2011;31(10):1969–71. https://doi.org/10.1038/jcbfm.2011.98.
26. Claeys W. The neurogliovascular unit in hepatic encephalopathy. JHEP Rep. 2021;3(5): 100352. https://doi.org/10.1016/j.jhepr.2021.100352.
27. Cudalbu C, Taylor-Robinson SD. Brain edema in chronic hepatic encephalopathy. J Clin Exp Hepatol. 2019;9(3):362–82. https://doi.org/10.1016/j.jceh.2019.02.003.
28. Chaganti J. Novel magnetic resonance KTRANS measurement of blood–brain barrier permeability correlated with covert HE. Hepatol Commun. 2023;7(4):e0079. https://doi.org/10.1097/HC9.0000000000000079.
29. Lv S. Tumour necrosis factor-α affects blood–brain barrier permeability and tight junction-associated occludin in acute liver failure: blood–brain barrier in liver failure. Liver Int. 2010;30(8):1198–210. https://doi.org/10.1111/j.1478-3231.2010.02211.x.
30. Vairappan B, Sundhar M, Srinivas BH. Resveratrol restores neuronal tight junction proteins through correction of ammonia and inflammation in CCl4-induced cirrhotic mice. Mol Neurobiol. 2019;56(7):4718–29. https://doi.org/10.1007/s12035-018-1389-x.
31. Shaik IH, Miah MK, Bickel U, Mehvar R. Effects of short-term portacaval anastomosis on the peripheral and brain disposition of the blood–brain barrier permeability marker sodium fluorescein in rats. Brain Res. 2013;1531:84–93. https://doi.org/10.1016/j.brainres.2013.07.040.
32. Quinn M, McMillin M, Galindo C, Frampton G, Pae HY, DeMorrow S. Bile acids permeabilize the blood brain barrier after bile duct ligation in rats via Rac1-dependent mechanisms. Dig Liver Dis. 2014;46(6):527–34. https://doi.org/10.1016/j.dld.2014.01.159.
33. Ahishali B, Kaya M. Evaluation of blood–brain barrier integrity using vascular permeability markers: evans blue, sodium fluorescein, albumin-alexa fluor conjugates, and horseradish peroxidase. In: Turksen K, editor. Permeability barrier, vol. 2367. Methods in molecular biology. New York: Springer; 2020. p. 87–103. https://doi.org/10.1007/7651_2020_316.
34. Duchini A, Govindarajan S, Santucci M, Zampi G, Hofman FM. Effects of tumor necrosis factor-alpha and interleukin-6 on fluid-phase permeability and ammonia diffusion in CNS-derived endothelial cells. J Investig Med Off Publ Am Fed Clin Res. 1996;44(8):474–82.
35. Chastre A, Jiang W, Desjardins P, Butterworth IRF. Ammonia and proinflammatory cytokines modify expression of genes coding for astrocytic proteins implicated in brain edema in acute liver failure. Metab Brain Dis. 2010;25(1):17–21. https://doi.org/10.1007/s11011-010-9185-y.
36. Balzano T. Chronic hyperammonemia induces peripheral inflammation that leads to cognitive impairment in rats: reversed by anti-TNF-α treatment. J Hepatol. 2020;73(3):582–92. https://doi.org/10.1016/j.jhep.2019.01.008.
37. Hernández-Rabaza V. Hyperammonemia induces glial activation, neuroinflammation and alters neurotransmitter receptors in hippocampus, impairing spatial learning: reversal by sulforaphane. J Neuroinflamm. 2016;13(1):41. https://doi.org/10.1186/s12974-016-0505-y.
38. De Boer AG, Gaillard PJ. Blood–brain barrier dysfunction and recovery. J Neural Transm. 2006;113(4):455–62. https://doi.org/10.1007/s00702-005-0375-4.
39. Lockwood AH, Yap EWH, Wong W-H. Cerebral ammonia metabolism in patients with severe liver disease and minimal hepatic encephalopathy. J Cereb Blood Flow Metab. 1991;11(2):337–41. https://doi.org/10.1038/jcbfm.1991.67.
40. Schaefer A. A systemic mechanism of increased transendothelial migration of leukocytes through the blood–brain barrier in hepatic encephalopathy. Clin Res Hepatol Gastroenterol. 2022;46(3):101801. https://doi.org/10.1016/j.clinre.2021.101801.
41. Chastre A, Bélanger M, Beauchesne E, Nguyen BN, Desjardins P, Butterworth RF. Inflammatory cascades driven by tumor necrosis factor-alpha play a major role in the progression of acute liver failure and its neurological complications. PLoS ONE. 2012;7(11): e49670. https://doi.org/10.1371/journal.pone.0049670.
42. Rosenberg GA. Neurological diseases in relation to the blood–brain barrier. J Cereb Blood Flow Metab. 2012;32(7):1139–51. https://doi.org/10.1038/jcbfm.2011.197.
43. Gomides LF. Murine model to study brain, behavior and immunity during hepatic encephalopathy. World J Hepatol. 2014;6(4):243. https://doi.org/10.4254/wjh.v6.i4.243.
44. Dhanda S, Sandhir R. Blood–brain barrier permeability is exacerbated in experimental model of hepatic encephalopathy via MMP-9 activation and downregulation of tight junction proteins. Mol Neurobiol. 2017. https://doi.org/10.1007/s12035-017-0521-7.
45. Wang W, Lv S, Zhou Y, Fu J, Li C, Liu P. Tumor necrosis factor-α affects blood–brain barrier permeability in acetaminophen-induced acute liver failure. Eur J Gastroenterol Hepatol. 2011;23(7):552–8. https://doi.org/10.1097/MEG.0b013e3283470212.
46. Tsao N, Hsu HP, Wu CM, Liu CC, Lei HY. Tumour necrosis factor-α causes an increase in blood–brain barrier permeability during sepsis. J Med Microbiol. 2001;50(9):812–21. https://doi.org/10.1099/0022-1317-50-9-812.
47. Barabási B. Role of interleukin-6 and interleukin-10 in morphological and functional changes of the blood–brain barrier in hypertriglyceridemia. Fluids Barriers CNS. 2023;20(1):15. https://doi.org/10.1186/s12987-023-00418-3.
48. Yang D. MicroRNA-125b-5p mimic inhibits acute liver failure. Nat Commun. 2016. https://doi.org/10.1038/ncomms11916.
49. Ward J. Circulating microRNA profiles in human patients with acetaminophen hepatotoxicity or ischemic hepatitis. Proc Natl Acad Sci. 2014;111(33):12169–74. https://doi.org/10.1073/pnas.1412608111.
50. Salehi S. Serum microRNA signatures in recovery from acute and chronic liver injury and selection for liver transplantation. Liver Transpl. 2020;26(6):811–22. https://doi.org/10.1002/lt.25781.
51. Tavabie OD. A novel microRNA-based prognostic model outperforms standard prognostic models in patients with acetaminophen-induced acute liver failure. J Hepatol. 2021;75(2):424–34. https://doi.org/10.1016/j.jhep.2021.03.013.
52. Kagawa T, Shirai Y, Oda S, Yokoi T. Identification of specific microRNA biomarkers in early stages of hepatocellular injury, cholestasis, and steatosis in rats. Toxicol Sci. 2018;166(1):228–39. https://doi.org/10.1093/toxsci/kfy200.
53. Vemuganti R, Silva VR, Mehta SL, Hazell AS. Acute liver failure-induced hepatic encephalopathy is associated with changes in microRNA expression profiles in cerebral cortex of the rat. Metab Brain Dis. 2014;29(4):891–9. https://doi.org/10.1007/s11011-014-9545-0.
54. Chowdhary V. miRNA-122 protects mice and human hepatocytes from acetaminophen toxicity by regulating cytochrome P450 family 1 subfamily a member 2 and family 2 subfamily E member 1 expression. Am J Pathol. 2017;187(12):2758–74. https://doi.org/10.1016/j.ajpath.2017.08.026.
55. An F. miR-15b and miR-16 regulate TNF mediated hepatocyte apoptosis via BCL2 in acute liver failure. Apoptosis. 2012;17(7):702–16. https://doi.org/10.1007/s10495-012-0704-7.
56. Roy S. miR-1224 inhibits cell proliferation in acute liver failure by targeting the antiapoptotic gene Nfib. J Hepatol. 2017;67(5):966–78. https://doi.org/10.1016/j.jhep.2017.06.007.
57. Krauskopf J. Application of high-throughput sequencing to circulating microRNAs reveals novel biomarkers for drug-induced liver injury. Toxicol Sci. 2015;143(2):268–76. https://doi.org/10.1093/toxsci/kfu232.
58. Trehanpati N. miRNA signatures can predict acute liver failure in hepatitis E infected pregnant females. Heliyon. 2017;3(4): e00287. https://doi.org/10.1016/j.heliyon.2017.e00287.
59. Rose CF. Hepatic encephalopathy: novel insights into classification, pathophysiology and therapy. J Hepatol. 2020;73(6):1526–47. https://doi.org/10.1016/j.jhep.2020.07.013.

60. Kroupina K, Bémeur C, Rose CF. Amino acids, ammonia, and hepatic encephalopathy. Anal Biochem. 2022;649: 114696. https://doi.org/10.1016/j.ab.2022.114696.
61. Ong JP. Correlation between ammonia levels and the severity of hepatic encephalopathy. Am J Med. 2003;114(3):188–93. https://doi.org/10.1016/S0002-9343(02)01477-8.
62. Shawcross DL. Infection and systemic inflammation, not ammonia, are associated with grade 3/4 hepatic encephalopathy, but not mortality in cirrhosis. J Hepatol. 2011;54(4):640–9. https://doi.org/10.1016/j.jhep.2010.07.045.
63. Niranjan-Azadi AM. Ammonia level and mortality in acute liver failure: a single-center experience. Ann Transplant. 2016;21:479–83. https://doi.org/10.12659/AOT.898901.
64. Antoine DJ. Mechanistic biomarkers provide early and sensitive detection of acetaminophen-induced acute liver injury at first presentation to hospital. Hepatology. 2013;58(2):777–87. https://doi.org/10.1002/hep.26294.
65. Krauskopf J. The microRNA-based liquid biopsy improves early assessment of lethal acetaminophen poisoning: a case report. Am J Case Rep. 2020. https://doi.org/10.12659/AJCR.919289.
66. Papageorgiou I, Freytsis M, Court MH. Transcriptome association analysis identifies miR-375 as a major determinant of variable acetaminophen glucuronidation by human liver. Biochem Pharmacol. 2016;117(78–87):78–87. https://doi.org/10.1016/j.bcp.2016.08.014.
67. Vliegenthart ADB. Comprehensive microRNA profiling in acetaminophen toxicity identifies novel circulating biomarkers for human liver and kidney injury. Sci Rep. 2015;5(1):15501. https://doi.org/10.1038/srep15501.
68. Yu D. Multiple microRNAs function as self-protective modules in acetaminophen-induced hepatotoxicity in humans. Arch Toxicol. 2018;92(2):845–58. https://doi.org/10.1007/s00204-017-2090-y.
69. Deutsch-Link S, Moon AM, Jiang Y, Barritt AS, Tapper EB. Serum ammonia in cirrhosis: clinical impact of hyperammonemia, utility of testing, and national testing trends. Clin Ther. 2022;44(3):e45–57. https://doi.org/10.1016/j.clinthera.2022.01.008.
70. Tranah TH. Plasma ammonia levels predict hospitalisation with liver-related complications and mortality in clinically stable outpatients with cirrhosis. J Hepatol. 2022;77(6):1554–63. https://doi.org/10.1016/j.jhep.2022.07.014.
71. Khan A, Ayub M, Khan WM. Hyperammonemia is associated with increasing severity of both liver cirrhosis and hepatic encephalopathy. Int J Hepatol. 2016;1–5:2016. https://doi.org/10.1155/2016/6741754.
72. Chen L, Heikkinen L, Wang C, Yang Y, Sun H, Wong G. Trends in the development of miRNA bioinformatics tools. Brief Bioinform. 2019;20(5):1836–52. https://doi.org/10.1093/bib/bby054.
73. Seenprachawong K, Nuchnoi P, Nantasenamat C, Prachayasittikul V, Supokawej A. Computational identification of miRNAs that modulate the differentiation of mesenchymal stem cells to osteoblasts. PeerJ. 2016;4:e1976. https://doi.org/10.7717/peerj.1976.
74. Wong N, Wang X. miRDB: an online resource for microRNA target prediction and functional annotations. Nucleic Acids Res. 2015;43(D1):D146–52. https://doi.org/10.1093/nar/gku1104.
75. Quillet A. Improving bioinformatics prediction of microRNA targets by ranks aggregation. Front Genet. 2020;10:1330. https://doi.org/10.3389/fgene.2019.01330.
76. Saliminejad K, Khorram Khorshid HR, Soleymani Fard S, Ghaffari SH. An overview of microRNAs: biology, functions, therapeutics, and analysis methods. J Cell Physiol. 2019;234(5):5451–65. https://doi.org/10.1002/jcp.27486.
77. Obermeier B, Daneman R, Ransohoff RM. Development, maintenance and disruption of the blood–brain barrier. Nat Med. 2013;19(12):1584–96. https://doi.org/10.1038/nm.3407.
78. Balbuena P, Li W, Ehrich M. Assessments of tight junction proteins occludin, claudin 5 and scaffold proteins ZO1 and ZO2 in endothelial cells of the rat blood–brain barrier: cellular responses to neurotoxicants malathion and lead acetate. NeuroToxicology. 2011;32(1):58–67. https://doi.org/10.1016/j.neuro.2010.10.004.
79. Correale J, Villa A. Cellular elements of the blood–brain barrier. Neurochem Res. 2009;34(12):2067–77. https://doi.org/10.1007/s11064-009-0081-y.
80. Zhang L, Feng T, Spicer LJ. The role of tight junction proteins in ovarian follicular development and ovarian cancer. Reproduction. 2018;155(4):R183–98. https://doi.org/10.1530/REP-17-0503.
81. Cong X, Kong W. Endothelial tight junctions and their regulatory signaling pathways in vascular homeostasis and disease. Cell Signal. 2020;66:109485. https://doi.org/10.1016/j.cellsig.2019.109485.
82. McCaffrey G. Occludin oligomeric assemblies at tight junctions of the blood–brain barrier are altered by hypoxia and reoxygenation stress. J Neurochem. 2009;110(1):58–71. https://doi.org/10.1111/j.1471-4159.2009.06113.x.
83. Teksoy O, Sahinturk V, Cengiz M, İnal B, Ayhancı A. The protective effects of silymarin on thioacetamide-induced liver damage: measurement of miR-122, miR-192, and miR-194 levels. Appl Biochem Biotechnol. 2020;191(2):528–39. https://doi.org/10.1007/s12010-019-03177-w.
84. Lardizábal MN, Rodríguez RE, Nocito AL, Daniele SM, Palatnik JF, Veggi LM. Alteration of the microRNA-122 regulatory network in rat models of hepatotoxicity. Environ Toxicol Pharmacol. 2014;37(1):354–64. https://doi.org/10.1016/j.etap.2013.12.008.
85. Chang J. miR-122, a mammalian liver-specific microRNA, is processed from hcr mRNA and MayDownregulate the high affinity cationic amino acid transporter CAT-1. RNA Biol. 2004;1(2):106–13. https://doi.org/10.4161/rna.1.2.1066.
86. Zhang H-G. The circulating level of miR-122 is a potential risk factor for endothelial dysfunction in young patients with essential hypertension. Hypertens Res. 2020;43(6):511–7. https://doi.org/10.1038/s41440-020-0405-5.
87. Oliveira-Rizzo C. Hsa-miR-183-5p modulates cell adhesion by repression of ITGB1 expression in prostate cancer. Non-Coding RNA. 2022;8(1):11. https://doi.org/10.3390/ncrna8010011.
88. Weeraratne SD. Pleiotropic effects of miR-183–96–182 converge to regulate cell survival, proliferation and migration in medulloblastoma. Acta Neuropathol. 2012;123(4):539–52. https://doi.org/10.1007/s00401-012-0969-5.
89. Dambal S, Shah M, Mihelich B, Nonn L. The microRNA-183 cluster: the family that plays together stays together. Nucleic Acids Res. 2015;43(15):7173–88. https://doi.org/10.1093/nar/gkv703.
90. Zhang Y-Y, Feng H-M. MEG3 suppresses human pancreatic neuroendocrine tumor cells growth and metastasis by down-regulation of Mir-183. Cell Physiol Biochem. 2017;44(1):345–56. https://doi.org/10.1159/000484906.
91. Yang X, Wang L, Wang Q, Li L, Fu Y, Sun J. MiR-183 inhibits osteosarcoma cell growth and invasion by regulating LRP6-Wnt/β-catenin signaling pathway. Biochem Biophys Res Commun. 2018;496(4):1197–203. https://doi.org/10.1016/j.bbrc.2018.01.170.
92. Chen Y, Song W. Wnt/catenin β1/microRNA 183 predicts recurrence and prognosis of patients with colorectal cancer. Oncol Lett. 2018. https://doi.org/10.3892/ol.2018.7886.
93. Zhang W, Zhang M, Liu L, Jin D, Wang P, Hu J. MicroRNA-183-5p inhibits aggressiveness of cervical cancer cells by targeting integrin subunit beta 1 (ITGB1). Med Sci Monit. 2018;24:7137–45. https://doi.org/10.12659/MSM.910295.
94. Li G, Luna C, Qiu J, Epstein DL, Gonzalez P. Targeting of integrin β1 and kinesin 2α by microRNA 183. J Biol Chem. 2010;285(8):5461–71. https://doi.org/10.1074/jbc.M109.037127.
95. Wang Y. miR-183-5p alleviates early injury after intracerebral hemorrhage by inhibiting heme oxygenase-1 expression. Aging. 2020;12(13):12869–95. https://doi.org/10.18632/aging.103343.
96. Yang J. Multimodality MRI assessment of grey and white matter injury and blood–brain barrier disruption after intracerebral haemorrhage in mice. Sci Rep. 2017;7(1):40358. https://doi.org/10.1038/srep40358.
97. Wang Y. Effect of miR-183-5p on cholestatic liver fibrosis by regulating fork head box protein O1 expression. Front Physiol. 2021;12: 737313. https://doi.org/10.3389/fphys.2021.737313.
98. Chandel R, Saxena R, Das A, Kaur J. Association of rno-miR-183-96-182 cluster with diethyinitrosamine induced liver fibrosis in Wistar rats. J Cell Biochem. 2018;119(5):4072–84. https://doi.org/10.1002/jcb.26583.

Publisher's Note

Publikacja 2

Neurochemical Research (2024) 49:1489–1504
https://doi.org/10.1007/s11064-022-03698-7

ORIGINAL PAPER

Mitochondrial Changes in Rat Brain Endothelial Cells Associated with Hepatic Encephalopathy: Relation to the Blood–Brain Barrier Dysfunction

Krzysztof Milewski[1] · Karolina Orzeł-Gajowik[1] · Magdalena Zielińska[1]

Received: 31 August 2021 / Revised: 17 February 2022 / Accepted: 14 July 2022 / Published online: 2 August 2022

Abstract
The mechanisms underlying cerebral vascular dysfunction and edema during hepatic encephalopathy (HE) are unclear. Blood–brain barrier (BBB) impairment, resulting from increased vascular permeability, has been reported in acute and chronic HE. Mitochondrial dysfunction is a well-documented result of HE mainly affecting astrocytes, but much less so in the BBB-forming endothelial cells. Here we review literature reports and own experimental data obtained in HE models emphasizing alterations in mitochondrial dynamics and function as a possible contributor to the status of brain endothelial cell mitochondria in HE. Own studies on the expression of the mitochondrial fusion-fission controlling genes rendered HE animal model-dependent effects: increase of mitochondrial fusion controlling genes *opa1*, *mfn1* in cerebral vessels in ammonium acetate-induced hyperammonemia, but a decrease of the two former genes and increase of *fis1* in vessels in thioacetamide-induced HE. In endothelial cell line (RBE4) after 24 h ammonia and/or TNFα treatment, conditions mimicking crucial aspects of HE in vivo, we observed altered expression of mitochondrial fission/fusion genes: a decrease of *opa1*, *mfn1*, and, increase of the fission related *fis1* gene. The effect in vitro was paralleled by the generation of reactive oxygen species, decreased total antioxidant capacity, decreased mitochondrial membrane potential, as well as increased permeability of RBE4 cell monolayer to fluorescein isothiocyanate dextran. Electron microscopy documented enlarged mitochondria in the brain endothelial cells of rats in both in vivo models. Collectively, the here observed alterations of cerebral endothelial mitochondria are indicative of their fission, and decreased potential of endothelial mitochondria are likely to contribute to BBB dysfunction in HE.

Keywords Hepatic encephalopathy · Endothelial cell · Blood–brain barrier · Mitochondria · Oxidative stress

Abbreviations

ALF	Acute liver failure
BBB	Blood–brain barrier
BDL	Bile duct ligation
BH4	Tetrahydrobiopterin
DCFH-DA	2′,7′-Dichlorodihydrofluorescein diacetate
HE	Hepatic encephalopathy
MMP	Mitochondrial membrane potential
MMP9	Matrix metalloproteinase 9
mPTP	Mitochondrial permeability transition pore
NO	Nitric oxide
OA	Ammonium acetate/here used to refer to a rat model of hyperammonaemia
ROS	Reactive oxygen species
TAA	Thioacetamide
TAC	Total antioxidant capacity
TJs	Tight junctions
VE- Cadherin	Vascular endothelial-cadherin
ZO	Zonula occludens

✉ Krzysztof Milewski
kmilewski@imdik.pan.pl

✉ Magdalena Zielińska
mzielinska@imdik.pan.pl

[1] Department of Neurotoxicology, Mossakowski Medical Research Institute, Polish Academy of Sciences, Pawińskiego St. 5, 02-106 Warsaw, Poland

Hepatic Encephalopathy: A Brief Overview of Clinical Characteristics and Pathogenesis

Hepatic encephalopathy (HE) is a complex neuropsychiatric disorder that results from impaired liver function. As a consequence, insufficient clearance of toxins from blood, mainly ammonia, results in their accumulation in the brain. Impaired liver function, associated with acute, chronic liver failure or cirrhosis, often results in a wide range of neurological alterations, including cognitive and motor disturbances [1].

The cellular and molecular mechanisms underlying HE are complex and have not yet been fully deciphered. However, there is a consensus that ammonia, as a major neurotoxin, interferes with various aspects of brain metabolism and neural transmission, and impairs cerebral water-ion homeostasis [2, 3]. The above-listed abnormalities contribute to brain edema, the key pathologic manifestation of acute HE [4, 5]. The important role of inflammation in the pathogenesis of HE is being more and more emphasized [6–8].

In acute HE, brain edema leads to the patients' death in more than 50% of cases, which is a consequence of increased intracranial pressure and herniation [4, 9]. While by analogy to other brain pathologies, brain edema associated with HE is likely elicited by a combination of cytotoxic and vasogenic factors their relative roles have long remained a matter of debate [4, 10].

The well-established view is that in brain astrocytes detoxify ammonia by an enzymatic reaction catalyzed by glutamine synthase [11]. The subsequent accumulation of glutamine most likely results in cellular edema formation, despite potential compensatory mechanisms. In agreement with the long-held view that HE is a primarily gliopathy [11, 12]. The development of brain edema in HE is believed to be primarily due to pathological cell swelling referred as cytotoxic edema. Cytotoxic component of brain edema in HE is thought to primarily reflect swelling of astrocytes by mechanisms related to intracellular metabolic and ion imbalance and the ensuing intracellular accumulation of water [13]. The molecular mechanisms underlying HE-induced cytotoxic edema have been relatively well delineated. Both clinical and animal model studies favor the direct role of ammonia in inducing cytotoxic components of brain edema. The current view proposes that ammonia induced astrocytic swelling by a complex interplay of (i) oxidative/nitrosative stress (ONS) (ii) impairment of import and export of osmotically active substances leading to intracellular osmotic imbalance, (iii) mitochondrial dysfunction related to excessive accumulation of ammonia-derived glutamine and successive intra-mitochondrial release of neurotoxic concentrations of ammonia [12, 14]. Some details warrant to be the highlight here.

In the astrocytic mitochondria, ammonia induces ONS by the formation of free radicals that in turn lead to the pathological condition called mitochondrial permeability transition pore (mPTP) [15]. The mPTP is characterized by a rapid loss of inner membrane potential and collapsed mitochondrial ATP-synthesis. Additionally, high intracellular Ca^{2+} concentration is considered to mediate mPTP and altered mitochondrial redox-state and pH [16]. Although mPTP has been extensively investigated due to its involvement in apoptosis in different diseases (e.g., traumatic brain injury, neurodegenerative diseases, and ischemia–reperfusion) the pore complex in the mitochondrial inner membrane responsible for the increase in permeability has not been structurally identified [17]. The occurrence of mPTP in ammonia-treated cultured astrocytes has been associated with cell volume increase suggesting its role in astrocyte swelling [18]. Furthermore, cultured astrocytes treated with ammonia and different cytokines: TNF-α, interleukin-1β, interleukin-6, and interferon-γ, presented the induction of the mPTP in a time-dependent and additive manner [19]. Studies on patients with HE have shown metabolic disturbances in the brain indicating a compromised oxidative metabolism most likely due to mitochondrial dysfunction, that were correlated with elevated levels of glutamine [20].

Experimental evidence underscores the contribution of the inflammatory component (peripheral or intracerebral) to cytotoxic brain edema [21, 22]. In turn, the term vasogenic brain edema reflects water accumulation in the extracellular space, and is related to its uncontrolled flux across a selective blood–brain barrier (BBB), in association with peripheral osmotically active substances. In contrast to cytotoxic edema, the role of the vasogenic component in the induction of brain edema in HE has been disputed [23]. The evidence is still contradictory and the underlying mechanisms remain obscure.

Below we discuss BBB alterations in HE pathology, and the discussion is preceded by a characterization of the composition and cytoarchitecture of BBB. Next, we discuss and present data regarding HE-related impairment in processes that contribute to endothelial dysfunction and culminate in increased BBB dysfunctionality, which is understood as a consequence of the disruption in mitochondrial quality control processes.

Blood–Brain Barrier

The histological structure of the BBB is organized by the basement membrane, endothelial cells, pericytes, and astrocyte end-feet. The penetrability of this highly selective fastener between blood and CNS is controlled by two checkpoints: (1) the endothelial cells, whose cohesive properties and physical resistance of, supported by the inter-endothelial

tight junction (TJ) proteins: zonula occludens-1 (ZO-1), claudin-5, occludin, junctional adhesion molecules (JAM); and, the adherents complexes, E-cadherin; and (2) the basal lamina. Both the endothelial cell permeability barrier and the basal lamina matrix derive from the cooperation between the endothelium and astrocytes and together constitute the BBB [24]. The endothelial cell barrier properties are only partly attributable to TJs proteins [25]; an important role is played by the stability of the endothelial cell–astrocyte assembly, which requires matrix adhesion. This view is supported by (i) high expression of integrins and dystroglycan at the BBB; (ii) correlation of alterations in the expression of integrins and dystroglycan with the degree of BBB permeability, and subsequent glial activation and neuronal injury; (iii) breakdown of the cerebral vasculature in transgenic mice in which specific integrins are absent [26]. The above considerations have collectively implicated that BBB consists of an array of different components, including TJs and the inter-endothelial adherens complexes (ACs), matrix adhesion complexes formed between adhesion receptors integrins on both endothelial cells and astrocytes, dystroglycan, a single heterodimeric transmembrane receptor, distinct from integrins that forms a physical link between the intracellular cytoskeleton and the extracellular matrix and anchors astrocytes (for reviews and references see del Zoppo and Milner [27]). Of note, vertical adhesion could be a central determinant of the endothelial portion of the intact BBB. This statement is supported by data indicating disturbed BBB permeability and decreased occludin-5 expression in mice after functional blocking of 1β-integrin [28].

Pericytes are important constituents of BBB regulating its functional aspects. While pericytes do not per se induce BBB-specific gene expression in endothelial cells, they inhibit the expression of molecules that increase vascular permeability and CNS immune cell infiltration [29]. Only recently, a link between pericytes' loss and symptoms associated with neurologic diseases has begun to be elucidated [30, 31]. Uniquely positioned within the neurovascular unit between endothelial cells of brain capillaries, astrocytes, and neurons, pericytes regulate BBB formation and maintenance, vesicle trafficking in endothelial cells, vascular stability, capillary blood flow, and clearance of toxic cellular by-products necessary for normal functioning of the CNS [32]. Whether pericytes' impairment contributes to BBB dysfunction in HE has not been addressed.

Alteration of the BBB Function and Structure in HE

Fundamental ultrastructural analysis of the cerebral cortex of patients diagnosed with ALF reported by Kato et al., documented swelling of astrocytes end-feet and increased number of vacuoles and vesicles in endothelial cells and pericytes. The study also documented that the basement membrane were enlarged, with generalized rarefaction and vacuolization, while TJs of endothelial cells were intact [33]. The above findings were indicative of BBB disruption in ALF. Otherwise, the contribution of BBB impairment to HE has been a matter of contradictory reports. Rats with severe, acute HE induced by ip. injection of galactosamine and azoxymethane, have presented brain extravasation to Evans Blue and alpha-aminoisobutyric acid, the classical markers of BBB leakage and altered transport, respectively [34, 35]. The reduction in the expression of TJs proteins (occludin, claudin-5, ZO-1, -2) contributing to a reduction in the integrity of the BBB have become evident in brains from this rat models [36, 37]. On the other hand, in galactosamine-induced acute HE in the rabbit, capillary endothelial cells appeared normal, and no evidence of brain extravasation to horseradish peroxidase was observed [38]. Discrepant results have been obtained in animal models of acute HE based on hepatic devascularization [39, 40].

Reported inconsistencies in the observed BBB impairment may be due to differences in the use of animal species and/or acuteness vs chronicity of HE (etiology; toxins/surgical procedures). In a rat model of chronic HE induced by bile duct ligation (BDL), an electron microscopy study revealed anatomically intact BBB structure [41] and decomposition of ZO proteins expression [42]. Furthermore, in the same model, no brain extravasation of Evans blue or sodium fluorescein was found [9], nor any changes in the expression of the TJs proteins were detected. No breakdown of the BBB was likewise demonstrated in a rat model of chronic HE induced by portocaval anastomosis [43]. It is unknown, whether HE may lead to alterations in the matrix elements, matrix adhesion receptor expression by both endothelial cells and astrocytes, factors affecting vascular permeability. Concluding, alternations of the BBB resulting in permeability increase were reported in most of reproducible and well-characterized animal models of HE (Table 1).

In the above mentioned studies chronic HE produced minimal HE and, therefore, it remains to be determined whether BBB breakdown is associated with overt HE. Interestingly, a magnetic resonance imaging study in cirrhotic patients demonstrated the co-existence of both cytotoxic and vasogenic brain edema [64]. Early works indicates a significant increase in the BBB permeability for ammonia [65], but subsequent studies have not substantiated alternations of the permeability-surface area of the BBB for ammonia in HE [66, 67]. Collectively, the role of increased permeability of the BBB in brain edema development and/or progression deserves more complex and detailed investigation (for discussion see Scott et al. [21]).

Importantly, some studies underscore the contribution of inflammatory factors to the vasogenic component of brain

Table 1 BBB related alternations observed in animal models of HE

Animal models of HE			Spec	BBB permeability	Findings	Genes or proteins level	Refs.
Acute	Toxin- induced models	Azoxymethane	Mice	↑		Claudin-5 ↓; MMP9 ↑ mRNA and protein level	[44–46]
		Acetaminophen	Mice	↑	Perivascular astrocytes swelling, extracellular space shrinkage	Occludin ↓protein level	[47]
		Carbon tetrachloride	Rat/mice	↑		ZO-1; VE-cadherin↓ protein level	[48]
		Galactosamine	Rat	Unaltered			[49]
			Rat	↑ In caudate-putamen, cerebellum, motor cortex, and globus pallidus, unchanged in frontal cortex or hippocampus	Vasogenic or cytotoxic edema		[34]
			Rat	Unaltered			[50]
			Rat	↑	Cerebral edema, perivascular astrocytes swelling		[51]
			Mice	↑	Tight junction disruption, extracellular space shrinkage, increased number of vesicles and vacuoles	Occludin ↓ protein level	[37]
			Rabbit	↑			[52]
		Thioacetamide	Mice	Unaltered			[53]
			Mice	↑			[45]
		Hepatic devascularization	Rat	↑	Vacuolization and swelling of perivascular astrocyte processes in cerebral cortex		[54]
	Surgical models	Hepatectomy	Rat	Unaltered			[55]
			Rat	↑	Amino acids active transport increase		[56]
Chronic	Toxin- induced models	Carbon tetrachloride	Mice	↑	Brain edema	Claudin-5; ZO-1; occludin↓ protein level MMP9 ↑ mRNA level	[57, 58]
	Surgical models	Portacaval anastomosis	Rat	↑	Plasma membrane folding of perivascular astrocytes, astrocytes swelling		[59]
			Rat	↑	Perivascular astrocytes swelling, increased number of vesicles in endothelial cells; HRP-devoid endothelial intercellular space		[60]
		Congenital portacaval shunts	Rat	Unaltered			[43]
			Dog	↑			[61]
		Graded portal vein stenosis	Rat	↑			[62]
		Bile duct ligation	Rat	↑	Microvessel integrity loss	Occludin, ZO-1, ZO-2 ↓ immunofluorescence	[63]

edema under HE. Inflammatory mediators in peripheral blood are not able to cross the BBB due to their molecular size. However, different types of cytokines can modulate endothelial TJs and thus unlock the BBB [68], or initiate endothelial inflammatory processes that involve downstream cyclooxygenase (COX), prostanoids, and NO signaling, allowing the direct interaction with astrocytes. Increased brain levels of TNFα, IL-1β, and IL6 and activation of microglia as a source for intracerebral cytokine production were reported in experimental models of ALF [69]. Upon systemic inflammation, microglial cells and astrocytes have been shown to release proinflammatory cytokines, which were suggested to contribute to enhanced neuropsychological impairment induced by hyperammonemia [11, 70, 71]. The study by Lv et al. suggested that deleterious effects of systemic inflammation for the brain are linked with the observed alterations in the BBB [37]. Mentioned study documented the crucial role of TNF-α in the development of BBB abnormalities and corroborated well with the observation of increased TNF-α in patients with ALF [37]. In acetaminophen-induced ALF mice, it was found that increases in BBB permeability positively correlated with elevated serum TNF-α levels, which could be prevented by administering anti-TNFα-IgG [47]. Similarly, TNF-α or TNF-α-R1 antibodies increased the expression of TJs proteins occludin and ZO-1, which result in decreased leakage of Evans Blue in brains of ALF mice induced by D-galactosamine and lipopolysaccharide [72]. Additionally, a possible mutual relation between neuroinflammation, cerebral blood flow, and intracranial hypertension have been suggested [73, 74].

Because cerebral endothelial dysfunction is often associated with compromised BBB, understanding the endothelial factors that regulate vessel function to maintain BBB role and prevent vascular permeability may provide insights into disease prevention and treatment.

Mitochondrial-Derived Reactive Oxygen Species (ROS) in the Endothelial Cells: Implication to Cerebral Dysfunction Observed in HE

Endothelium relies predominantly on anaerobic glycolysis for ATP turnover and mitochondria make up 2–5% of the cytoplasmic volume of endothelial cells in most vascular units [75]. Besides its metabolic role mitochondria integrate signals from the environment, perceive cellular stresses, control cell death signaling to list a key function. Since mitochondria as a major source of oxidative stress contribute to the pathogenesis of HE, its role as a potential trigger of the brain endothelial dysfunction upon HE should be uncovered.

Mitochondrial ROS generation in the endothelial cells is considered as one of the primary cell signaling pathways. Endothelial cells produce different types of ROS, including superoxide (O_2^-), hydrogen peroxide (H_2O_2), peroxynitrite ($ONOO^-$), hydroxyl radicals ($OH^·$), and other reactive oxygen and nitrogen species [76, 77].

However, oxidative stress that results from increased oxidant production, reduced antioxidant capacity or both, leads to endothelial dysfunction by reducing nitric oxide (NO) bioavailability [78, 79]. Importantly, other sources of ROS in the vessels include NADPH oxidase (NOX) and xanthine oxidase [77].

Ammonia was found to cause the increased generation of ROS in rat brain endothelial cell line (RBE4) [80] and primary cultures of brain ECs [81]. In RBE4 cells, treatment with ammonia increased permeability of endothelial cells monolayer to fluorescein isothiocyanate (FITC)-dextran (40 kDa). This effect was ameliorated by co-treatment with a matrix metalloproteinase inhibitor, or an antioxidant, glutathione diethyl ester [80]. The matrix metalloproteinase 9 (MMP9) was also increased in the brain of BDL rats which accompanied an increase in permeability to sodium fluorescein, Evans blue, and FITC-dextran along with an increase in brain water content [82].

Increased levels of hydroxyl radicals were observed in rat brain vessels isolated from thioacetamide-induced HE [83]. An increase of hydroxyl radicals ($OH^·$) was observed in rat brains in vivo after direct infusion of ammonium chloride to the striatum through a microdialysis probe [84]. Increased levels of nitrites and nitrates (markers of NO production) were also frequently detected in the brains of animals with experimentally induced HE [85–87]. Additionally, hyperammonemia in vivo was associated with increased expression and activity of heme oxygenase-1 (HO-1), a ubiquitous marker of oxidative stress [88, 89].

It has been shown that exogenously added L-glutamine reduces NO generation in the brain by inhibiting L-arginine transport via y+LAT2 exchanger. This effect was additionally potentiated after a direct infusion of ammonia to the brain via microdialysis probe [87], or when L-glutamine accumulated in there during HE [86]. Tentatively, the mechanism may also operate in the cerebral capillary endothelial cells forming the BBB, where enhanced glutamine level also would modulate L-arginine transport. Of note, increased expression of y+LAT2 was observed in RBE4 cells upon ammonia exposure [80], and in rat brains upon hyperammonemia in situ [86]. However, the outcome of carrier operation would depend on L-glutamine cell membrane gradient. The importance of this mechanism comes to light when confronted with the previous observation that L-glutamine infusion in the absence of hyperammonemia impairs cerebrovascular CO_2 reactivity, most likely by reducing L-arginine availability and NO synthesis [90]. A recent study from our laboratory demonstrated strong differences in the reactivity of the middle cerebral arteries and in their response to

extravascular L-arginine application between vessels isolated from rats with TAA-induced HE and control animals, implicating that impaired vascular tone of cerebral arteries, which may involve, among other factors, their persistent exposure to high L-glutamine [91].

Excess of ROS reduces NO bioavailability through mechanisms including NO scavenging that occurs when O_2^- reacts with NO to form $ONOO^-$, which broadly contributes to cellular ONS and uncoupling of endothelial nitric oxide synthase (eNOS) [92]. Moreover, dissociation of eNOS monomers in the uncoupled eNOS is associated with a higher ratio of eNOS monomer-to-eNOS dimers [83, 93]. In addition, O_2^- can oxidize the essential eNOS cofactor BH4 to BH2, which subsequently leads to eNOS uncoupling whereby eNOS produces more O_2^- and less NO and lead to inactivation of proteins through the nitration of tyrosine residues. Such proteins include the antioxidant enzyme MnSOD [94, 95].

In our very recent study, a decrease of eNOS content and its uncoupling concurred with and was likely causally related to, both increased brain content of ROS and decreased cerebral cortical blood flow (CBF) in the thioacetamide-induced animal model of acute HE [83].

The specific mechanisms by which mitochondria in the endothelium release ROS and uncouple eNOS involve mitochondrial ATP-dependent potassium channel ($MitoK^+ATP$) activation and subsequent induction of mPTP. $MitoK^+ATP$ activity is regulated by falling ATP and rising ADP levels, thus linking cellular metabolism with membrane excitability [96].

It was recently reported, that the $MitoK^+ATP$ channel is involved in Parkinson's disease (PD) mainly via the regulation of mitochondrial biogenesis and fission/fusion [97]. At the molecular level, the authors using in vivo and in vitro rotenone models of PD documented that the pore subunit of Kir6.1, the major component of the $MitoK^+ATP$ channel was the key contributor in its interaction with mitochondrial dynamics.

It is important to underline that mitochondria are both the source and a target of excess ROS. Excessive generation of ROS, particularly of $ONOO^-$ can result in oxidative damage to the mitochondrial respiratory complexes [98]. Cytoplasmic ROS may elicit mitochondria depolarization, at least in part through the opening of $MitoK^+ATP$ channels, which results in mitochondrial ROS release by respiratory complexes and the mPTP. The release of mitochondrial ROS may further activate NADPH oxidase via protein kinase C, resulting in increased cytoplasmic O^{-2} production and reduced NO bioavailability [99]. On the other hand, hyperammonemia was also found to be associated with a decreased activity of antioxidant enzymes (glutathione peroxidase, superoxide dismutase, and catalase) in the brain, both in the cytosolic and mitochondrial fractions [100]. In line, glutathione accumulation in the extracellular space of rat prefrontal cortex upon ammonia infusion was previously documented [101]. Of note, manipulations resulting in the recovery of the enzyme activities of the GSH metabolism ameliorated HE symptoms both in experimental animals [102] and in human patients [103]. Moreover, excess $ONOO^-$ can also lead to inactivation of the endogenous proteins, antioxidant mechanisms (i.e., mitochondrial SOD2) through nitration. Changes in nitrated proteins content supporting this scenario were observed in brain homogenates obtained from rats with TAA-induced acute HE [83]. The above data support the concept that ONS contribute to the alterations in BBB permeability and thus to the vasogenic component of cerebral edema associated with HE.

Aberrant Mitochondrial Quality Control Linked to Endothelial Dysfunction

The role of mitochondria in brain endothelial cells has previously been underestimated since vascular endothelial cells are located in juxtaposition to types of cells, that heavily rely on oxidative phosphorylation. Such cells, which in the periphery are represented by skeletal muscle cells and cardiomyocytes, predominantly rely on anaerobic glycolysis for ATP turnover, and mitochondria make up 2–5% of their cytoplasmic volume [104].

The location of the mitochondria within the endothelial cell of different organs and locations differs, largely depending on the signaling required. For instance, in pulmonary artery endothelial cells where oxygen sensing is relevant, mitochondria are localized near the nucleus, ensuring hypoxia-induced transcriptional regulation [105]. In turn in coronary arterioles, endothelial mitochondria are anchored to the cytoskeleton, initiating vasodilation in response to shear stress [79].

Cellular mitochondrial content is tightly regulated and is determined by the balance between mitochondrial biogenesis and degradation through the process called mitophagy, the form of autophagy in mitochondria (removal of damaged organelles). Mitochondrial organization, which is fundamental in determining their function, is determined by the balance between fusion and fission that determines the mitochondrial number, morphology, and size (Fig. 1) [106]. The cytoskeletal organization, which has a relevant role in maintaining mitochondrial network and function [107]. Mitochondrial quality control is required for optimal mitochondrial function, therefore dysregulation of these processes due to disease-related alterations initiate mitochondria-mediated cell senescence and apoptosis [78, 108]. In the brain, pathological state-associated disturbances in mitochondria quality control purportedly leading to cerebral endothelial dysfunction,

and BBB impairment have gained attention only lastly [109]. In more general terms, the imbalance between controlling processes was documented and discussed in various disorders such as cancer, neurodegenerative and cardiovascular diseases [110–112].

Decreased mitochondrial biogenesis, one of the deregulatory events in the endothelium, is related to the regulator's peroxisome proliferator-activated receptor-γ coactivator-1α (PGC-1α) and mitochondrial transcription factor A (TFAM) [113]. Further, dysregulation of mitochondrial dynamics is caused by an imbalance between proteins involved in fission [dynamin-related protein 1 (DRP1) and fission 1 (FIS1)] and fusion (transmembrane GTPases mitofusin 1 (MFN1) and 2 (MFN2) and the optic atrophy protein 1 (OPA1)). Mitochondrial fusion allows the transfer of gene products between mitochondria for proper functioning in normal conditions and specifically during metabolic and oxidative stress. In turn, mitochondrial fission is crucial for mitochondrial division and quality control. The role of mitochondrial failure was often described as associated with dysfunctional BBB in different neurologic disorders, including stroke, Alzheimer's disease, Parkinson's disease, Huntington's disease, and epilepsy [114–119]. In so far, the role of altered mitochondrial dynamics involving fission, fusion, and mitophagy processes, has not been adequately explored in the context of BBB dysfunction upon HE.

Effects of HE-Key Factors: Ammonia and TNFα on the Mitochondrial Membrane Potential, the Expression of Genes Involved in Mitochondrial Fusion and Fission, and Morphology of Mitochondria in Cerebral Endothelial Cell

We analyzed mitochondrial membrane potential and the expression of genes involved in mitochondrial fusion and fission in the rat brain endothelial cells (RBE4 cell line) treated with 5 mM ammonium chloride "ammonia" and 50 ng/ml of rat recombinant TNFα (Sigma-Aldrich, St, Louis, MO, USA). Both compounds were added into the cell culture medium for 24 h. We haven't noticed any cell culture density changes or morphological alterations under inverted microscope (Fig. 2A). The expression analysis of genes coding mitochondrial fusion/fission proteins: *opa1*, *mfn1*, *fis1*, and *mff* (mitochondrial fission factor; MFF) revealed a decrease of *opa1*, *mfn1*, and, evident, but to be confirmed tendency to increase of the fission related *fis1* gene indicating disturbed fission process in the mitochondria of RBE4 cells upon treatments with both factors (Fig. 2B). Besides Fis1 participation in the mitochondrial fission via interactions with the Drp1, or by prevention of mitochondrial fusion through the inhibition of Mfn2/Opa1, Fis1 participates in mitophagy through recruitment of TBC1D15/17 and Syntaxin17 to mitochondria [120]. Fis1 is also proposed to interact with BAP31,

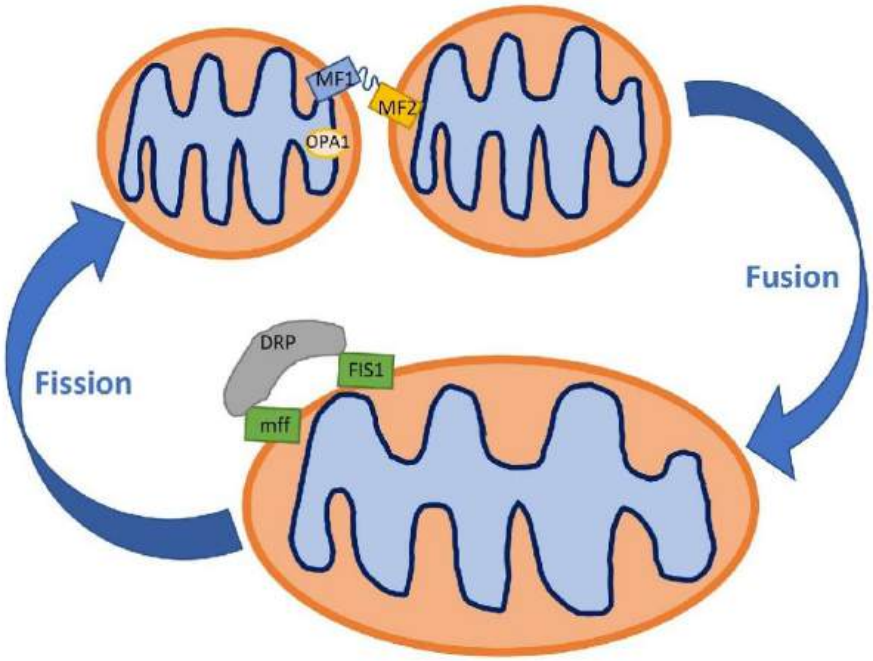

Fig. 1 Schema of fusion/fission processes in the mitochondria. Mitofusin 1/2 and OPA1 are major proteins that control mitochondrial fusion. Mfn1 and Mfn2 locate in the outer mitochondrial membrane with their GTPase site facing the cytosol to coordinate the fusion process with the outer membrane of opposing mitochondria. OPA1 protein, localized in the intermembrane side, controls the fusion of the inner mitochondria membrane. DRP1, Mff, and Fis1 proteins regulated mitochondrial fission. DRP1 is localized in the cytosol and recruited to the outer mitochondrial membrane during fission. Fis1 and Mff are located in the outer mitochondrial membrane and work as the adaptor for DRP1

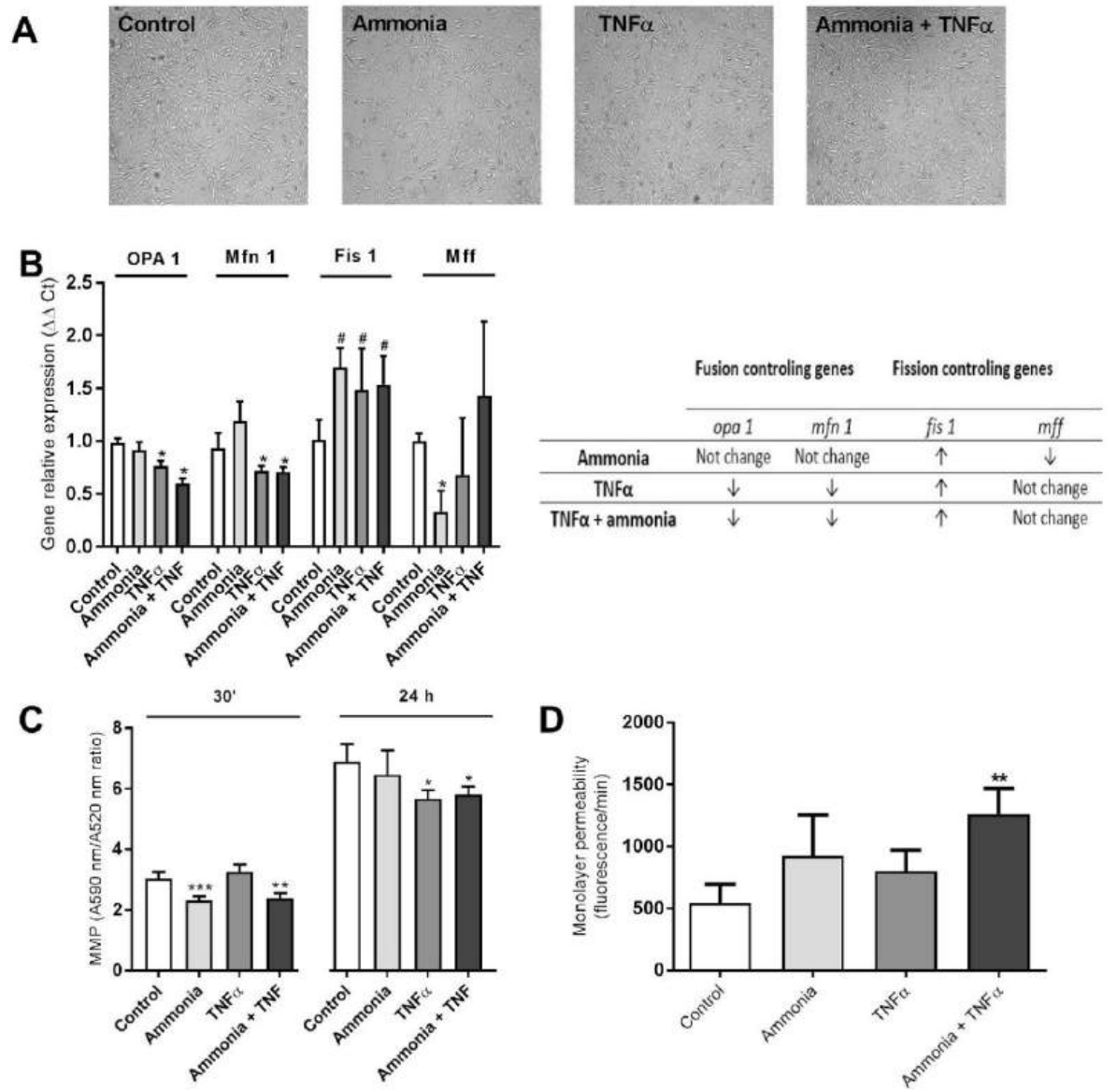

	Fusion controling genes		Fission controling genes	
	opa 1	*mfn 1*	*fis 1*	*mff*
Ammonia	Not change	Not change	↑	↓
TNFα	↓	↓	↑	Not change
TNFα + ammonia	↓	↓	↑	Not change

Fig. 2 The effect of ammonia and/or TNFα treatment (5 mM ammonium chloride; 50 ng/ml TNFα; 24 h; Sigma-Aldrich; St. Louis, MO, USA) on RBE4 cell culture morphology and growth (**A**), mitochondrial gene expression (**B**), mitochondrial membrane potential (MMP) (**C**), monolayer permeability for fluorescein isothiocyanate (FITC) dextran 40 kDa (**D**). Relative gene expression was analyzed using the real-time PCR method followed by ΔΔCt quantification analysis in relation to beta actin gene expression. Probes for *opa1*(#Rn00592200_m1), *mf1* (#Rn00594496_m1), *fis1*(#Rn01480911_m1), *mff* (#Rn01400790_m1) and *actb* (Rn 0066789_m1) were purchased from Applied Biosystems, Waltham, USA. MMP was established using a Mitochondrial Membrane Potential kit, based on a JC-10 fluorescence probe, according to the manufacturer's protocol (cat# MAK159, Sigma-Aldrich, Saint Louis, USA). Cells monolayer permeability for FITC-dextran (30 min exposition) was measured fluorometrically at 485/520 nm. Results are mean ± SD (n = 4); Two-way ANOVA test with Dunnett's multiple comparisons test was performed using Graph Pad Software *$p < 0.05$ vs control; **$p < 0.01$ vs control; # $0.05 < p < 0.1$ (tend toward significance) (panel **B**). One-way ANOVA test with Dunnett post-hoc test was performed using Graph Pad Software *$p < 0.05$ vs control; **$p < 0.01$ vs control; **$p < 0.001$ vs control (panel **C** and **D**)

inciting apoptosis [121]. Thus, Fis1 may act an important role in mitochondrial alternations during HE.

The measurement of mitochondrial membrane potential (MMP) revealed engrossing observation. MMP was decreased in both ammonia-treated groups after a short 30' exposition. In turn, MMP was not significantly affected by ammonia but reduced in both TNFα- treated groups after 24 h (Fig. 2C). The short exposition of ammonia exerts probably toxic effects mainly by disturbing the pH balance. Ammonia in solution is present as NH_3 or NH_4^+. NH_3 is a weak base in gaseous form, since NH_4^+ is a weak acid. Because ammonia pKa is relatively high (approximately 9.2) most of total ammonia at physiologic pH is NH_4^+ [122, 123]. Ammonia toxicity results from disruption of the H^+ gradient across the inner membranes of mitochondria. Due to relative alkalinity of the mitochondrial pH as compared to the cytoplasmic pH ammonia exits the mitochondrial matrix along this gradient and binds to H^+ in the inter-membrane space, thereby eliminating the H^+ gradient necessary for ATP synthesis [124]. In addition, NH_4^+ could compete with K^+ ions at the K^+ binding site of K^+-channels and affect excitability and membrane potential in neurons [125]. Whether the same applies to endothelial mitochondria is not clear. In turn, the effects of TNFα may be linked with TNFα receptor activation and further signals transducing. In the endothelium, TNFα induces inflammatory responses by enhancing adhesion molecule expression and cytokine secretion [126, 127].

To verify if ammonia/TNFα treatment and observed mitochondrial impairment disturb endothelium function we measured cell monolayer permeability to isothiocyanate FITC-dextran. Simultaneous ammonia/TNFα administration caused a significant increase in permeability indicative of a disturbed barrier function of the endothelial cells (Fig. 2D). Experiments demonstrated an almost fourfold increase in ROS content in all treated cells with an accompanying decrease of total antioxidant capacity (TAC) especially, after simultaneous ammonia and TNFα treatment (Fig. 3).

We verified the morphology of mitochondria in cerebral vessels isolated from rats with hyperammonemia (OA) and thioacetamide (TAA)—induced acute liver failure. Both models were performed on male Sprague–Dawley rats (Tac: Cmd: SD, weight 200–220 g) supplied by the Animal House of Mossakowski Medical Research Centre, Warsaw, Poland (Approval no. 57/2015 (14 May 2015 from the 4th Local Ethics Committee for Animal Experimentation, Warsaw, Poland, as compliant with Polish Law). Briefly, hyperammonemia (OA) was induced by ip. injections of ammonium

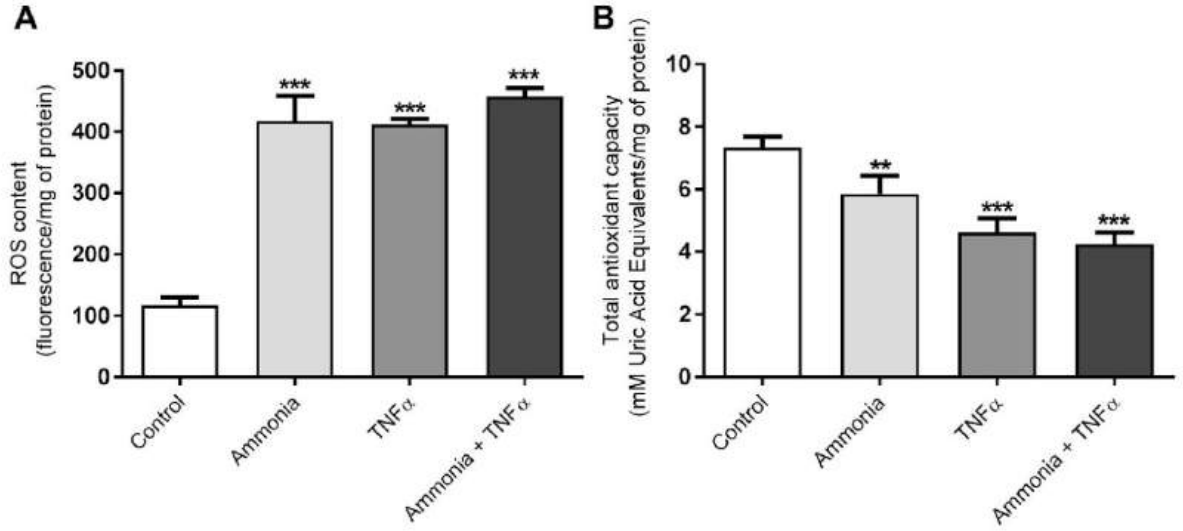

Fig. 3 The effect of ammonia and/or TNFα treatment (5 mM ammonium chloride; 50 ng/ml TNFα; 24 h; Sigma-Aldrich; St. Louis, MO, USA) on the content of reactive oxygen species (ROS) (**A**) and total antioxidant capacity (TAC) (**B**). ROS levels were measured using the fluorescent probe 2',7'-dichlorofluorescein diacetate (DCF-DA) 5 μM for 30 min at 37 °C. The fluorescence of cells was detected using Fluorescence Microplate Reader FLUOstar OMEGA (BMG Labtech, Ortenberg, Germany) with an excitation wavelength of 485/20 nm and emission wavelength of 528/20 nm. TAC was measured using the TAC Assay kit (cat# MAK187, Sigma-Aldrich, Saint Louise, USA) according to the manufacturer's instructions by the estimation of the capacity of the total antioxidants in the sample to convert Cu^{2+} in its reduced form, Cu^+ which chelates with a colorimetric probe, giving a broad absorbance peak at ~570 nm. Results are mean ± SD (n = 4); One-way ANOVA test with Dunnett post-hoc test was performed using Graph Pad Software $^{**}p < 0.01$ vs control; $^{***}p < 0.001$ vs control

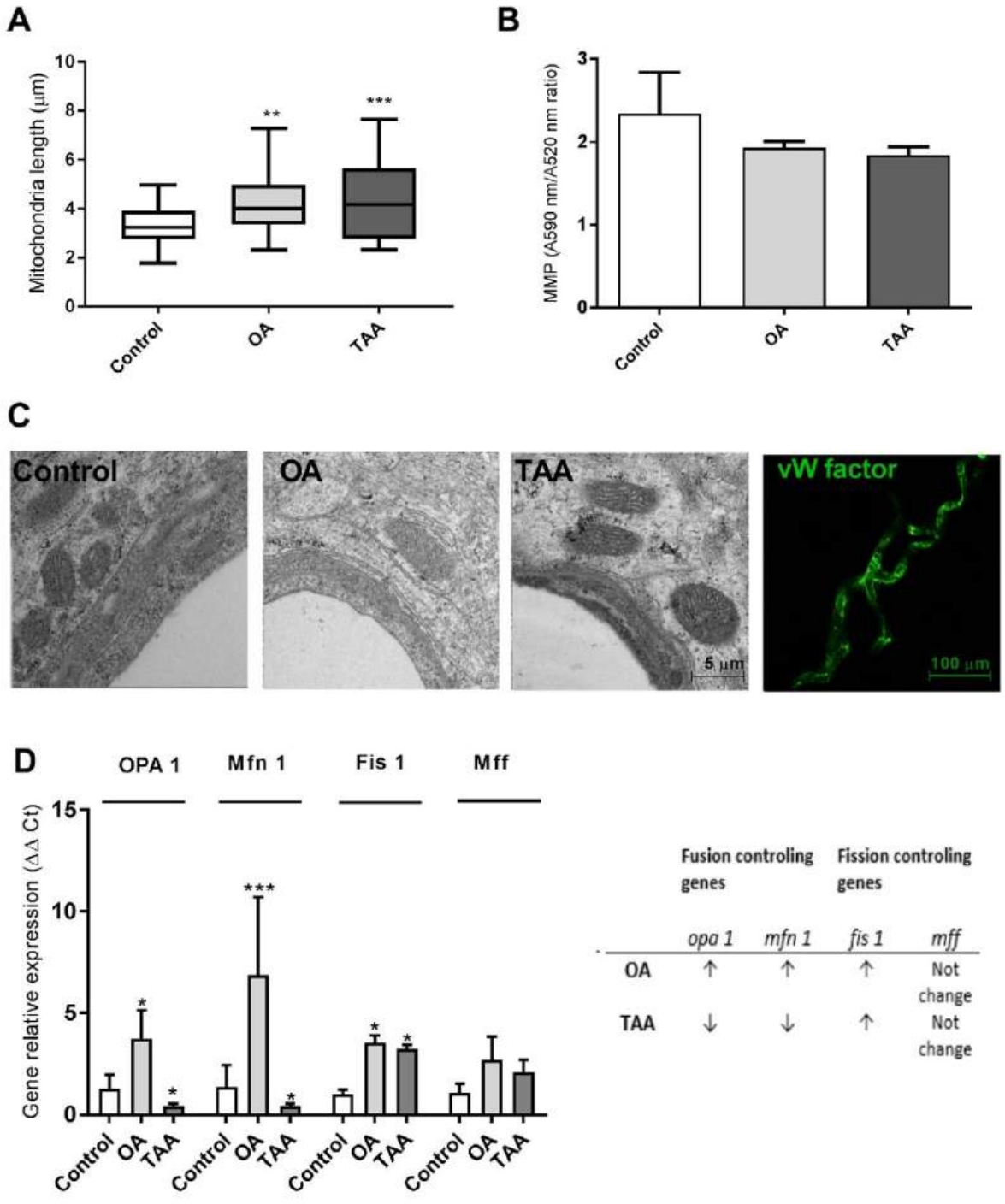

	Fusion controling genes		Fission controling genes	
	opa 1	*mfn 1*	*fis 1*	*mff*
OA	↑	↑	↑	Not change
TAA	↓	↓	↑	Not change

◂**Fig. 4** Mitochondria of cerebral vessels isolated from the brains of rats with hyperammonemia (OA) and thioacetamide (TAA)-induced acute liver failure. The length of the mitochondria in the brain vessels endothelium in the electron microscopy images was determined by quantitative evaluation using Digimizer Image Analysis Software (MedCalc Software Ltd, Ostend, Belgium) (**A**). Mitochondrial membrane potential (MMP) in cerebral vessels mitochondria of control, (OA), and (TAA)-administered rats was determined using Mitochondrial Membrane Potential kit (cat# MAK159, Sigma-Aldrich, Saint Louis, USA) (**B**). Representative electron microscopy images of cerebral vessel mitochondria and confocal microscopic image of vessels with von Willebrand factor immunostaining (**C**). Relative mitochondrial gene expression was measured using the real-time PCR method followed by ΔΔCt quantification analysis to beta-actin gene expression. Details of probes used are listed in the legend to Fig. 3 (**D**). All results are mean ± SD (n = 4); Two-way ANOVA test with Dunnett's multiple comparisons test was performed using Graph Pad Software *p < 0.05 vs control; **p < 0.01 vs control (panel **B**). One-way ANOVA test with Dunnett post-hoc test was performed using Graph Pad Software *p < 0.05; **p < 0.01; ***p < 0.001 (panel **C** and **D**)

acetate (600 mg per kg) at 12 h intervals for three days. Acute liver failure was induced by thioacetamide (TAA) ip. administration (300 mg per kg at 24 intervals for three days). The control (sham) group received 0.3 mL of 0.9% NaCl (ip. for 3 days). Brain cortex microvessels were isolated on saccharose gradient as described earlier [63].

Electron microscopy documented enlarged mitochondria in the brain endothelial cells of OA and TAA rats suggesting mitochondrial swelling that occurs in both models (Fig. 4A), however, the mitochondria aspect ratio (width/length) evaluated using Digimizer Software (MedCalc Software Ltd., Ostend, Belgium) was unchanged. The mitochondrial membrane potential measurement in rat brain microvessels revealed a tendency toward a decrease in both experimental models which implies mitochondrial dysfunction leading to brain vessels energy depletion (Fig. 4B). The expression analysis of genes coding key fusion/fission proteins: *opa1*, *mfn*, *fis1*, and *mff* indicated possible increased fission of OA cerebral mitochondria and a decreased fusion of cerebral mitochondria from TAA rats, but further experiments are needed to prove this phenomenon (Fig. 4D), since gene expression changes are not necessarily reflected at the protein level.

Roles of Mitochondrial Membrane Potential (Δψ) and Calcium for ROS Generation by the Mitochondria

The issues circumscribed by the title of this section have not been elaborated in our laboratory, but, definitely deserve comment. The role of mitochondrial membrane potential (Δψ) in ROS production is ambiguous. The complexity of the issue is underscored by findings variably associating ROS production with hyperpolarization and depolarization, likely depending on pharmacologically active agents and substrates being used, and the respiratory and cytoplasmic redox potential of the mitochondria. Selective MitoK^+ATP openers that decrease Δψ in the cerebrovasculature do not increase ROS production [128].

The role of mitochondrial Δψ and ROS production in vascular dysfunction derives from data demonstrating that compared to healthy controls, arterioles and circulating mononuclear cells from patients with obesity and type 2 diabetes are characterized by mitochondrial membrane hyperpolarization (more negative Δψ), reduced mitochondrial mass, and greater ROS production [129–131]. Importantly, differences in mitochondrial membrane potential were observed as well. Mitochondrial alterations including membrane hyperpolarization reduced NO bioavailability and affected vascular function [103, 104]. In the former study, mitochondrial ROS production in monocytes was negatively correlated with artery flow-mediated dilation [129], a marker of endothelial function in humans.

Intracellular Ca^{2+} is essential for maintaining endothelium integrity and function [132]. In particular, the interaction of mitochondria with the endoplasmic reticulum is central in regulating intracellular Ca^{2+} levels, and this process directly involves mitochondrial Ca^{2+} uptake and cycling [133]. In addition to intracellular Ca^{2+} homeostasis control, mitochondrial Ca^{2+} levels play obvious roles in mitochondrial metabolism, cell signaling, biogenesis, and morphology [134], processes pertinent to optimal vascular function. In endothelial cells, increases in intracellular Ca^{2+} lead to eNOS activation and subsequent NO production [132]. As previously documented by our group, high levels of ammonia evoked a durable decrease of the basal intracellular Ca^{2+} level in RBE4 cells [135], which may contribute to cerebral vascular endothelial dysfunction associated with hyperammonemia and/or HE. The presence of ammonia-sensitive intracellular Ca^{2+} reservoirs has been previously described in bovine aortic endothelial cells [136]. However, the details of the evolution of Ca^{2+} to BBB dysfunction associated with HE have not been unraveled in those studies. Of note, increased Ca^{2+} efflux from brain mitochondria was observed in rats injected with ammonia [137].

Whether and how Ca^{2+} fluxes or other intermediary events occurring at the molecular or cellular level affect the function of cerebral blood vessels are translated into their functioning are intriguing questions worth further investigation.

Conclusions

Investigations carried out to date revealed numerous potential links between various aspects of mitochondrial dynamics in rat brain endothelial cells and BBB dysfunction and its role in the pathogenesis of HE. However, the picture is far from being complete and the roads to the goal are filled with methodological obstacles. In terms of mitochondrial dynamics itself, the evidence regarding responses of its executors is still in a very preliminary stage. In terms of its link to BBB disruption, the status is obscured by a great model-to-model variability, which makes it difficult to translate the experimental results to clinical observations. Undoubtedly, an extension of the present knowledge on endothelial ammonia metabolism and how it affects the endothelial mitochondria is needed. Issues such as the role of glutamine metabolism and transport, operation of the glutamate/glutamine cycle, very well described in astrocytes, remain almost unaddressed concerning brain endothelial cells. Raising the level of knowledge of the above aspects of metabolism in HE-affected endothelial mitochondria to that already acquired about astrocytic mitochondria should help to unravel the secrets of BBB disruption and brain edema in HE.

Acknowledgements The authors thank Professor Jan Albrecht for his critical reading of the manuscript.

Author Contributions MZ and KM conceived and designed the experiments; KM and KO-G performed the experiments and analyzed the data; MZ and KM wrote the paper.

Funding This study was supported by the National Science Centre of the Republic of Poland (NCN) Grant number: 2015/19/B/NZ4/01902 and the statutory MMRI funds No.13.

Data Availability The data generated or analyzed during this study are available from the corresponding author upon reasonable request.

Declarations

Conflict of interest The authors declare no conflict of interest.

References

1. Prakash R, Mullen KD (2010) Mechanisms, diagnosis and management of hepatic encephalopathy. Nat Rev Gastroenterol Hepatol 7:515–525
2. Albrecht J, Jones EA (1999) Hepatic encephalopathy: molecular mechanisms underlying the clinical syndrome. J Neurol Sci 170:138–146
3. Felipo V, Butterworth RF (2002) Neurobiology of ammonia. Prog Neurobiol 67:259–279
4. Blei AT (2008) Brain edema in acute liver failure. Crit Care Clin 24(99–114):ix
5. Liotta EM, Kimberly WT (2020) Cerebral edema and liver disease: Classic perspectives and contemporary hypotheses on mechanism. Neurosci Lett 721:134818
6. Shawcross DL, Sharifi Y, Canavan JB, Yeoman AD, Abeles RD, Taylor NJ, Auzinger G, Bernal W, Wendon JA (2011) Infection and systemic inflammation, not ammonia, are associated with Grade 3/4 hepatic encephalopathy, but not mortality in cirrhosis. J Hepatol 54:640–649
7. Milewski K, Oria M (2016) What we know: the inflammatory basis of hepatic encephalopathy. Metab Brain Dis 31(6):1239–1247
8. Cabrera-Pastor A, Llansola M, Montoliu C, Malaguarnera M, Balzano T, Taoro-Gonzalez L, Garcia-Garcia R, Mangas-Losada A, Izquierdo-Altarejos P, Arenas YM, Leone P, Felipo V (2019) Peripheral inflammation induces neuroinflammation that alters neurotransmission and cognitive and motor function in hepatic encephalopathy: underlying mechanisms and therapeutic implications. Acta Physiol 226:e13270
9. Bosoi CR, Rose CF (2013) Brain edema in acute liver failure and chronic liver disease: similarities and differences. Neurochem Int 62:446–457
10. Chavarria L, Cordoba J (2014) Magnetic resonance of the brain in chronic and acute liver failure. Metab Brain Dis 29:937–944
11. Norenberg MD (1987) The role of astrocytes in hepatic encephalopathy. Neurochem Pathol 6:13–33
12. Albrecht J, Zielinska M, Norenberg MD (2010) Glutamine as a mediator of ammonia neurotoxicity: a critical appraisal. Biochem Pharmacol 80:1303–1308
13. Haussinger D, Schliess F (2008) Pathogenetic mechanisms of hepatic encephalopathy. Gut 57:1156–1165
14. Albrecht J, Norenberg MD (2006) Glutamine: a Trojan horse in ammonia neurotoxicity. Hepatology 44:788–794
15. Rama Rao KV, Jayakumar AR, Norenberg MD (2005) Role of oxidative stress in the ammonia-induced mitochondrial permeability transition in cultured astrocytes. Neurochem Int 47:31–38
16. Zhang J, Wang X, Vikash V, Ye Q, Wu D, Liu Y, Dong W (2016) ROS and ROS-mediated cellular signaling. Oxid Med Cell Longev 2016:4350965
17. Tsujimoto Y, Shimizu S (2007) Role of the mitochondrial membrane permeability transition in cell death. Apoptosis 12:835–840
18. Rama Rao KV, Jayakumar AR, Norenberg MD (2003) Induction of the mitochondrial permeability transition in cultured astrocytes by glutamine. Neurochem Int 43:517–523
19. Alvarez VM, Rama Rao KV, Brahmbhatt M, Norenberg MD (2011) Interaction between cytokines and ammonia in the mitochondrial permeability transition in cultured astrocytes. J Neurosci Res 89:2028–2040

20. Bjerring PN, Hauerberg J, Frederiksen HJ, Jorgensen L, Hansen BA, Tofteng F, Larsen FS (2008) Cerebral glutamine concentration and lactate-pyruvate ratio in patients with acute liver failure. Neurocrit Care 9:3–7
21. Scott TR, Kronsten VT, Hughes RD, Shawcross DL (2013) Pathophysiology of cerebral oedema in acute liver failure. World J Gastroenterol 19:9240–9255
22. Jayakumar AR, Rama Rao KV, Norenberg MD (2015) Neuroinflammation in hepatic encephalopathy: mechanistic aspects. J Clin Exp Hepatol 5:S21-28
23. Hadjihambi A, Arias N, Sheikh M, Jalan R (2018) Hepatic encephalopathy: a critical current review. Hep Intl 12:135–147
24. Risau W, Wolburg H (1990) Development of the blood-brain barrier. Trends Neurosci 13:174–178
25. Langen UH, Ayloo S, Gu C (2019) Development and cell biology of the Blood-Brain Barrier. Annu Rev Cell Dev Biol 35:591–613
26. Almutairi MM, Gong C, Xu YG, Chang Y, Shi H (2016) Factors controlling permeability of the blood-brain barrier. Cell Mol Life Sci 73:57–77
27. del Zoppo GJ, Milner R (2006) Integrin-matrix interactions in the cerebral microvasculature. Arterioscler Thromb Vasc Biol 26:1966–1975
28. Osada T, Gu YH, Kanazawa M, Tsubota Y, Hawkins BT, Spatz M, Milner R, del Zoppo GJ (2011) Interendothelial claudin-5 expression depends on cerebral endothelial cell-matrix adhesion by beta(1)-integrins. J Cereb Blood Flow Metab 31:1972–1985
29. Daneman R, Zhou L, Kebede AA, Barres BA (2010) Pericytes are required for blood-brain barrier integrity during embryogenesis. Nature 468:562–566
30. Armulik A, Genove G, Betsholtz C (2011) Pericytes: developmental, physiological, and pathological perspectives, problems, and promises. Dev Cell 21:193–215
31. Castro V, Skowronska M, Lombardi J, He J, Seth N, Velichkovska M, Toborek M (2018) Occludin regulates glucose uptake and ATP production in pericytes by influencing AMP-activated protein kinase activity. J Cereb Blood Flow Metab 38:317–332
32. Grubb S, Lauritzen M, Aalkjaer C (2021) Brain capillary pericytes and neurovascular coupling. Comp Biochem Physiol A 254:110893
33. Kato M, Hughes RD, Keays RT, Williams R (1992) Electron microscopic study of brain capillaries in cerebral edema from fulminant hepatic failure. Hepatology 15:1060–1066
34. Cauli O, Lopez-Larrubia P, Rodrigo R, Agusti A, Boix J, Nieto-Charques L, Cerdan S, Felipo V (2011) Brain region-selective mechanisms contribute to the progression of cerebral alterations in acute liver failure in rats. Gastroenterology 140:638–645
35. Yamamoto S, Nguyen JH (2006) TIMP-1/MMP-9 imbalance in brain edema in rats with fulminant hepatic failure. J Surg Res 134:307–314
36. Chen F, Ohashi N, Li W, Eckman C, Nguyen JH (2009) Disruptions of occludin and claudin-5 in brain endothelial cells in vitro and in brains of mice with acute liver failure. Hepatology 50:1914–1923
37. Lv S, Song HL, Zhou Y, Li LX, Cui W, Wang W, Liu P (2010) Tumour necrosis factor-alpha affects blood-brain barrier permeability and tight junction-associated occludin in acute liver failure. Liver Int 30:1198–1210
38. Traber PG, Dal Canto M, Ganger DR, Blei AT (1987) Electron microscopic evaluation of brain edema in rabbits with galactosamine-induced fulminant hepatic failure: ultrastructure and integrity of the blood-brain barrier. Hepatology 7:1272–1277
39. Potvin M, Finlayson MH, Hinchey EJ, Lough JO, Goresky CA (1984) Cerebral abnormalities in hepatectomized rats with acute hepatic coma. Lab Investig 50:560–564
40. Kristiansen RG, Lindal S, Myreng K, Revhaug A, Ytrebo LM, Rose CF (2010) Neuropathological changes in the brain of pigs with acute liver failure. Scand J Gastroenterol 45:935–943
41. Wright G, Davies NA, Shawcross DL, Hodges SJ, Zwingmann C, Brooks HF, Mani AR, Harry D, Stadlbauer V, Zou Z, Williams R, Davies C, Moore KP, Jalan R (2007) Endotoxemia produces coma and brain swelling in bile duct ligated rats. Hepatology 45:1517–1526
42. Maly IP, Landmann L (2008) Bile duct ligation in the rat causes upregulation of ZO-2 and decreased colocalization of claudins with ZO-1 and occludin. Histochem Cell Biol 129:289–299
43. Alexander B, Li X, Benjamin IS, Segal MB, Sherwood R, Preston JE (2000) A quantitative evaluation of the permeability of the blood brain barrier of portacaval shunted rats. Metab Brain Dis 15:93–103
44. McMillin MA, Frampton GA, Seiwell AP, Patel NS, Jacobs AN, DeMorrow S (2015) TGFbeta1 exacerbates blood-brain barrier permeability in a mouse model of hepatic encephalopathy via upregulation of MMP9 and downregulation of claudin-5. Lab Investig 95:903–913
45. Grant S, McMillin M, Frampton G, Petrescu AD, Williams E, Jaeger V, Kain J, DeMorrow S (2018) Direct comparison of the thioacetamide and azoxymethane models of Type A hepatic encephalopathy in mice. Gene Expr 18:171–185
46. Obara-Michlewska M, Ding F, Popek M, Verkhratsky A, Nedergaard M, Zielinska M, Albrecht J (2018) Interstitial ion homeostasis and acid-base balance are maintained in oedematous brain of mice with acute toxic liver failure. Neurochem Int 118:286–291
47. Wang W, Lv S, Zhou Y, Fu J, Li C, Liu P (2011) Tumor necrosis factor-alpha affects blood-brain barrier permeability in acetaminophen-induced acute liver failure. Eur J Gastroenterol Hepatol 23:552–558
48. Estevao C, Bowers CE, Luo D, Sarker M, Hoeh AE, Frudd K, Turowski P, Greenwood J (2021) CCL4 induces inflammatory signalling and barrier disruption in the neurovascular endothelium. Brain Behav Immunity Health 18:100370
49. Knudsen GM, Poulsen HE, Paulson OB (1988) Blood-brain barrier permeability in galactosamine-induced hepatic encephalopathy. No evidence for increased GABA-transport. J Hepatol 6:187–192
50. Lo WD, Ennis SR, Goldstein GW, McNeely DL, Betz AL (1987) The effects of galactosamine-induced hepatic failure upon blood-brain barrier permeability. Hepatology 7:452–456
51. Dixit V, Chang TM (1990) Brain edema and the blood brain barrier in galactosamine-induced fulminant hepatic failure rats. An animal model for evaluation of liver support systems. ASAIO Trans 36:21–27
52. Horowitz ME, Schafer DF, Molnar P, Jones EA, Blasberg RG, Patlak CS, Waggoner J, Fenstermacher JD (1983) Increased blood-brain transfer in a rabbit model of acute liver failure. Gastroenterology 84:1003–1011
53. Liu L, Miao M, Chen Y, Wang Z, Sun B, Liu X (2018) Altered function and expression of ABC Transporters at the Blood-Brain barrier and increased brain distribution of phenobarbital in acute liver failure mice. Front Pharmacol 9:190
54. Traber P, DalCanto M, Ganger D, Blei AT (1989) Effect of body temperature on brain edema and encephalopathy in the rat after hepatic devascularization. Gastroenterology 96:885–891
55. Miah MK, Shaik IH, Bickel U, Mehvar R (2015) Effects of Pringle maneuver and partial hepatectomy on the pharmacokinetics and blood-brain barrier permeability of sodium fluorescein in rats. Brain Res 1618:249–260
56. Zaki AE, Ede RJ, Davis M, Williams R (1984) Experimental studies of blood brain barrier permeability in acute hepatic failure. Hepatology 4:359–363

57. Vairappan B, Sundhar M, Srinivas BH (2019) Resveratrol restores neuronal tight junction proteins through correction of ammonia and inflammation in CCl4-induced cirrhotic mice. Mol Neurobiol 56:4718–4729
58. Baek SY, Lee EH, Oh TW, Do HJ, Kim KY, Park KI, Kim YW (2020) Network pharmacology-based approaches of rheum undulatum linne and glycyrriza uralensis fischer imply their regulation of liver failure with hepatic encephalopathy in Mice. Biomolecules 10:437
59. Shaik IH, Miah MK, Bickel U, Mehvar R (2013) Effects of short-term portacaval anastomosis on the peripheral and brain disposition of the blood-brain barrier permeability marker sodium fluorescein in rats. Brain Res 1531:84–93
60. Laursen H, Schroder H, Westergaard E (1975) The effect of portocaval anastomosis on the permeability to horseradish peroxidase of cerebral vessels of the rat. Acta Pathol Microbiol Scand Sect A 83:266–268
61. Or M, Devriendt N, Kitshoff AM, Peremans K, Vandermeulen E, Paepe D, Polis I, Martle V, de Rooster H (2017) Ammonia concentrations in arterial blood, venous blood, and cerebrospinal fluid of dogs with and without congenital extrahepatic portosystemic shunts. Am J Vet Res 78:1313–1318
62. Eizayaga F, Scorticati C, Prestifilippo JP, Romay S, Fernandez MA, Castro JL, Lemberg A, Perazzo JC (2006) Altered blood-brain barrier permeability in rats with prehepatic portal hypertension turns to normal when portal pressure is lowered. World J Gastroenterol 12:1367–1372
63. Quinn M, McMillin M, Galindo C, Frampton G, Pae HY, DeMorrow S (2014) Bile acids permeabilize the blood brain barrier after bile duct ligation in rats via Rac1-dependent mechanisms. Diges Liver Dis 46:527–534
64. Chavarria L, Alonso J, Rovira A, Cordoba J (2011) Neuroimaging in acute liver failure. Neurochem Int 59:1175–1180
65. Lockwood AH, Yap EW, Wong WH (1991) Cerebral ammonia metabolism in patients with severe liver disease and minimal hepatic encephalopathy. J Cereb Blood Flow Metab 11:337–341
66. Keiding S, Sorensen M, Bender D, Munk OL, Ott P, Vilstrup H (2006) Brain metabolism of 13N-ammonia during acute hepatic encephalopathy in cirrhosis measured by positron emission tomography. Hepatology 43:42–50
67. Goldbecker A, Buchert R, Berding G, Bokemeyer M, Lichtinghagen R, Wilke F, Ahl B, Weissenborn K (2010) Blood-brain barrier permeability for ammonia in patients with different grades of liver fibrosis is not different from healthy controls. J Cereb Blood Flow Metab 30:1384–1393
68. de Boer AG, Gaillard PJ (2006) Blood-brain barrier dysfunction and recovery. J Neural Transm 113:455–462
69. Jiang W, Desjardins P, Butterworth RF (2009) Direct evidence for central proinflammatory mechanisms in rats with experimental acute liver failure: protective effect of hypothermia. J Cereb Blood Flow Metab 29:944–952
70. Balzano T, Dadsetan S, Forteza J, Cabrera-Pastor A, Taoro-Gonzalez L, Malaguarnera M, Gil-Perotin S, Cubas-Nunez L, Casanova B, Castro-Quintas A, Ponce-Mora A, Arenas YM, Leone P, Erceg S, Llansola M, Felipo V (2020) Chronic hyperammonemia induces peripheral inflammation that leads to cognitive impairment in rats: reversed by anti-TNF-alpha treatment. J Hepatol 73:582–592
71. Butterworth RF (2019) Hepatic encephalopathy in cirrhosis: pathology and pathophysiology. Drugs 79:17–21
72. Tsao N, Hsu HP, Wu CM, Liu CC, Lei HY (2001) Tumour necrosis factor-alpha causes an increase in blood-brain barrier permeability during sepsis. J Med Microbiol 50:812–821
73. Wright G, Shawcross D, Olde Damink SW, Jalan R (2007) Brain cytokine flux in acute liver failure and its relationship with intracranial hypertension. Metab Brain Dis 22:375–388
74. Jalan R, Olde Damink SW, Hayes PC, Deutz NE, Lee A (2004) Pathogenesis of intracranial hypertension in acute liver failure: inflammation, ammonia and cerebral blood flow. J Hepatol 41:613–620
75. Culic O, Gruwel ML, Schrader J (1997) Energy turnover of vascular endothelial cells. Am J Physiol 273:C205-213
76. Freed JK, Gutterman DD (2013) Mitochondrial reactive oxygen species and vascular function: less is more. Arterioscler Thromb Vasc Biol 33:673–675
77. Zhang DX, Gutterman DD (2007) Mitochondrial reactive oxygen species-mediated signaling in endothelial cells. Am J Physiol Heart Circ Physiol 292:H2023-2031
78. Kluge MA, Fetterman JL, Vita JA (2013) Mitochondria and endothelial function. Circ Res 112:1171–1188
79. Quintero M, Colombo SL, Godfrey A, Moncada S (2006) Mitochondria as signaling organelles in the vascular endothelium. Proc Natl Acad Sci USA 103:5379–5384
80. Skowrońska M, Zielińska M, Wójcik-Stanaszek L, Ruszkiewicz J, Milatovic D, Aschner M, Albrecht J (2012) Ammonia increases paracellular permeability of rat brain endothelial cells by a mechanism encompassing oxidative/nitrosative stress and activation of matrix metalloproteinases. J Neurochem 121:125–134
81. Jayakumar AR, Tong XY, Ospel J, Norenberg MD (2012) Role of cerebral endothelial cells in the astrocyte swelling and brain edema associated with acute hepatic encephalopathy. Neuroscience 218:305–316
82. Dhanda S, Sandhir R (2018) Blood-Brain Barrier permeability is exacerbated in experimental model of hepatic encephalopathy via MMP-9 activation and downregulation of tight junction proteins. Mol Neurobiol 55:3642–3659
83. Milewski K, Czarnecka AM, Albrecht J, Zielinska M (2021) Decreased expression and uncoupling of endothelial nitric oxide synthase in the cerebral cortex of rats with thioacetamide-induced acute liver failure. Int J Mol Sci 22:6662
84. Hilgier W, Anderzhanova E, Oja SS, Saransaari P, Albrecht J (2003) Taurine reduces ammonia- and N-methyl-D-aspartate-induced accumulation of cyclic GMP and hydroxyl radicals in microdialysates of the rat striatum. Eur J Pharmacol 468:21–25
85. Genesca J, Gonzalez A, Segura R, Catalan R, Marti R, Varela E, Cadelina G, Martinez M, Lopez-Talavera JC, Esteban R, Groszmann RJ, Guardia J (1999) Interleukin-6, nitric oxide, and the clinical and hemodynamic alterations of patients with liver cirrhosis. Am J Gastroenterol 94:169–177
86. Zielińska M, Ruszkiewicz J, Hilgier W, Fresko I, Albrecht J (2011) Hyperammonemia increases the expression and activity of the glutamine/arginine transporter y+ LAT2 in rat cerebral cortex: implications for the nitric oxide/cGMP pathway. Neurochem Int 58:190–195
87. Hilgier W, Fresko I, Klemenska E, Beresewicz A, Oja SS, Saransaari P, Albrecht J, Zielinska M (2009) Glutamine inhibits ammonia-induced accumulation of cGMP in rat striatum limiting arginine supply for NO synthesis. Neurobiol Dis 35:75–81
88. Rama Rao KV, Reddy PV, Tong X, Norenberg MD (2010) Brain edema in acute liver failure: inhibition by L-histidine. Am J Pathol 176:1400–1408
89. Gorg B, Karababa A, Schutz E, Paluschinski M, Schrimpf A, Shafigullina A, Castoldi M, Bidmon HJ, Haussinger D (2019) O-GlcNAcylation-dependent upregulation of HO1 triggers ammonia-induced oxidative stress and senescence in hepatic encephalopathy. J Hepatol 71:930–941
90. Okada T, Watanabe Y, Brusilow SW, Traystman RJ, Koehler RC (2000) Interaction of glutamine and arginine on cerebrovascular

reactivity to hypercapnia. Am J Physiol Heart Circ Physiol 278:H1577-1584
91. Czarnecka A, Aleksandrowicz M, Jasinski K, Jazwiec R, Kalita K, Hilgier W, Zielinska M (2018) Cerebrovascular reactivity and cerebral perfusion of rats with acute liver failure: role of L-glutamine and asymmetric dimethylarginine in L-arginine-induced response. J Neurochem 147:692–704
92. Cassuto J, Dou H, Czikora I, Szabo A, Patel VS, Kamath V, Belin de Chantemele E, Feher A, Romero MJ, Bagi Z (2014) Peroxynitrite disrupts endothelial caveolae leading to eNOS uncoupling and diminished flow-mediated dilation in coronary arterioles of diabetic patients. Diabetes 63:1381–1393
93. Katakam PV, Snipes JA, Steed MM, Busija DW (2012) Insulin-induced generation of reactive oxygen species and uncoupling of nitric oxide synthase underlie the cerebrovascular insulin resistance in obese rats. J Cereb Blood Flow Metab 32:792–804
94. Forstermann U, Munzel T (2006) Endothelial nitric oxide synthase in vascular disease: from marvel to menace. Circulation 113:1708–1714
95. Werner ER, Blau N, Thony B (2011) Tetrahydrobiopterin: biochemistry and pathophysiology. Biochem J 438:397–414
96. Tinker A, Aziz Q, Thomas A (2014) The role of ATP-sensitive potassium channels in cellular function and protection in the cardiovascular system. Br J Pharmacol 171:12–23
97. Peng K, Hu J, Xiao J, Dan G, Yang L, Ye F, Zou Z, Cao J, Sai Y (2018) Mitochondrial ATP-sensitive potassium channel regulates mitochondrial dynamics to participate in neurodegeneration of Parkinson's disease. Biochim Biophys Acta 1864:1086–1103
98. Daiber A (2010) Redox signaling (cross-talk) from and to mitochondria involves mitochondrial pores and reactive oxygen species. Biochem Biophys Acta 1797:897–906
99. Reinehr R, Gorg B, Becker S, Qvartskhava N, Bidmon HJ, Selbach O, Haas HL, Schliess F, Haussinger D (2007) Hypoosmotic swelling and ammonia increase oxidative stress by NADPH oxidase in cultured astrocytes and vital brain slices. Glia 55:758–771
100. Kosenko E, Kaminsky Y, Kaminsky A, Valencia M, Lee L, Hermenegildo C, Felipo V (1997) Superoxide production and antioxidant enzymes in ammonia intoxication in rats. Free Radic Res 27:637–644
101. Hilgier W, Wegrzynowicz M, Ruszkiewicz J, Oja SS, Saransaari P, Albrecht J (2010) Direct exposure to ammonia and hyperammonemia increase the extracellular accumulation and degradation of astroglia-derived glutathione in the rat prefrontal cortex. Toxicol Sci 117:163–168
102. Jiang W, Desjardins P, Butterworth RF (2009) Minocycline attenuates oxidative/nitrosative stress and cerebral complications of acute liver failure in rats. Neurochem Int 55:601–605
103. Sushma S, Dasarathy S, Tandon RK, Jain S, Gupta S, Bhist MS (1992) Sodium benzoate in the treatment of acute hepatic encephalopathy: a double-blind randomized trial. Hepatology 16:138–144
104. Oldendorf WH, Cornford ME, Brown WJ (1977) The large apparent work capability of the blood-brain barrier: a study of the mitochondrial content of capillary endothelial cells in brain and other tissues of the rat. Ann Neurol 1:409–417
105. Al-Mehdi AB, Pastukh VM, Swiger BM, Reed DJ, Patel MR, Bardwell GC, Pastukh VV, Alexeyev MF, Gillespie MN (2012) Perinuclear mitochondrial clustering creates an oxidant-rich nuclear domain required for hypoxia-induced transcription. Sci Signaling 5:ra47
106. Murphy E (2015) Solving mitochondrial mysteries. J Mol Cell Cardiol 78:1–2
107. Moore AS, Holzbaur ELF (2018) Mitochondrial-cytoskeletal interactions: dynamic associations that facilitate network function and remodeling. Curr Opin Physiol 3:94–100
108. Srinivasan S, Guha M, Kashina A, Avadhani NG (2017) Mitochondrial dysfunction and mitochondrial dynamics—the cancer connection. Biochim Biophys Acta 1858:602–614
109. Busija DW, Rutkai I, Dutta S, Katakam PV (2016) Role of mitochondria in cerebral vascular function: energy production, cellular protection, and regulation of vascular tone. Compr Physiol 6:1529–1548
110. Ordys BB, Launay S, Deighton RF, McCulloch J, Whittle IR (2010) The role of mitochondria in glioma pathophysiology. Mol Neurobiol 42:64–75
111. Chakravorty A, Jetto CT, Manjithaya R (2019) Dysfunctional mitochondria and mitophagy as drivers of Alzheimer's disease pathogenesis. Front Aging Neurosci 11:311
112. Bhatti JS, Bhatti GK, Reddy PH (2017) Mitochondrial dysfunction and oxidative stress in metabolic disorders—a step towards mitochondria based therapeutic strategies. Biochim Biophys Acta 1863:1066–1077
113. Ungvari Z, Labinskyy N, Gupte S, Chander PN, Edwards JG, Csiszar A (2008) Dysregulation of mitochondrial biogenesis in vascular endothelial and smooth muscle cells of aged rats. Am J Physiol Heart Circ Physiol 294:H2121-2128
114. Kovac S, Dinkova Kostova AT, Herrmann AM, Melzer N, Meuth SG, Gorji A (2017) Metabolic and homeostatic changes in seizures and acquired epilepsy-mitochondria, calcium dynamics and reactive oxygen species. Int J Mol Sci 18:1935
115. Doll DN, Hu H, Sun J, Lewis SE, Simpkins JW, Ren X (2015) Mitochondrial crisis in cerebrovascular endothelial cells opens the blood-brain barrier. Stroke 46:1681–1689
116. Drouin-Ouellet J, Sawiak SJ, Cisbani G, Lagace M, Kuan WL, Saint-Pierre M, Dury RJ, Alata W, St-Amour I, Mason SL, Calon F, Lacroix S, Gowland PA, Francis ST, Barker RA, Cicchetti F (2015) Cerebrovascular and blood-brain barrier impairments in Huntington's disease: potential implications for its pathophysiology. Ann Neurol 78:160–177
117. Gray MT, Woulfe JM (2015) Striatal blood-brain barrier permeability in Parkinson's disease. J Cereb Blood Flow Metab 35:747–750
118. Kirk J, Plumb J, Mirakhur M, McQuaid S (2003) Tight junctional abnormality in multiple sclerosis white matter affects all calibres of vessel and is associated with blood-brain barrier leakage and active demyelination. J Pathol 201:319–327
119. Sweeney MD, Sagare AP, Zlokovic BV (2018) Blood-brain barrier breakdown in Alzheimer disease and other neurodegenerative disorders. Nat Rev Neurol 14:133–150
120. Ihenacho UK, Meacham KA, Harwig MC, Widlansky ME, Hill RB (2021) Mitochondrial fission protein 1: emerging roles in organellar form and function in health and disease. Front Endocrinol 12:660095
121. Iwasawa R, Mahul-Mellier AL, Datler C, Pazarentzos E, Grimm S (2011) Fis1 and Bap31 bridge the mitochondria-ER interface to establish a platform for apoptosis induction. EMBO J 30:556–568
122. Bosoi CR, Rose CF (2009) Identifying the direct effects of ammonia on the brain. Metab Brain Dis 24:95–102
123. Hamm LL, Nakhoul N, Hering-Smith KS (2015) Acid-base homeostasis. Clin J Am Soc Nephrol 10:2232–2242
124. Cooper AJ, Plum F (1987) Biochemistry and physiology of brain ammonia. Physiol Rev 67:440–519
125. Hertz L, Song D, Peng L, Chen Y (2017) Multifactorial effects on different types of brain cells contribute to ammonia toxicity. Neurochem Res 42:721–736
126. Li M, van Esch B, Henricks PAJ, Garssen J, Folkerts G (2018) Time and concentration dependent effects of short chain fatty acids on lipopolysaccharide- or tumor necrosis factor alpha-induced endothelial activation. Front Pharmacol 9:233

127. Xia P, Gamble JR, Rye KA, Wang L, Hii CS, Cockerill P, Khew-Goodall Y, Bert AG, Barter PJ, Vadas MA (1998) Tumor necrosis factor-alpha induces adhesion molecule expression through the sphingosine kinase pathway. Proc Natl Acad Sci USA 95:14196–14201
128. Katakam PV, Wappler EA, Katz PS, Rutkai I, Institoris A, Domoki F, Gaspar T, Grovenburg SM, Snipes JA, Busija DW (2013) Depolarization of mitochondria in endothelial cells promotes cerebral artery vasodilation by activation of nitric oxide synthase. Arterioscler Thromb Vasc Biol 33:752–759
129. Kizhakekuttu TJ, Wang J, Dharmashankar K, Ying R, Gutterman DD, Vita JA, Widlansky ME (2012) Adverse alterations in mitochondrial function contribute to type 2 diabetes mellitus-related endothelial dysfunction in humans. Arterioscler Thromb Vasc Biol 32:2531–2539
130. Shenouda SM, Widlansky ME, Chen K, Xu G, Holbrook M, Tabit CE, Hamburg NM, Frame AA, Caiano TL, Kluge MA, Duess MA, Levit A, Kim B, Hartman ML, Joseph L, Shirihai OS, Vita JA (2011) Altered mitochondrial dynamics contributes to endothelial dysfunction in diabetes mellitus. Circulation 124:444–453
131. Widlansky ME, Wang J, Shenouda SM, Hagen TM, Smith AR, Kizhakekuttu TJ, Kluge MA, Weihrauch D, Gutterman DD, Vita JA (2010) Altered mitochondrial membrane potential, mass, and morphology in the mononuclear cells of humans with type 2 diabetes. Transl Res 156:15–25
132. Zhao Y, Vanhoutte PM, Leung SW (2015) Vascular nitric oxide: Beyond eNOS. J Pharmacol Sci 129:83–94
133. Kannurpatti SS (2017) Mitochondrial calcium homeostasis: Implications for neurovascular and neurometabolic coupling. J Cereb Blood Flow Metab 37:381–395
134. Szabadkai G, Duchen MR (2008) Mitochondria: the hub of cellular Ca2+ signaling. Physiology 23:84–94
135. Konopacka A, Zielinska M, Albrecht J (2008) Ammonia inhibits the C-type natriuretic peptide-dependent cyclic GMP synthesis and calcium accumulation in a rat brain endothelial cell line. Neurochem Int 52:1160–1166
136. Danthuluri NR, Kim D, Brock TA (1990) Intracellular alkalinization leads to Ca2+ mobilization from agonist-sensitive pools in bovine aortic endothelial cells. J Biol Chem 265:19071–19076
137. Kosenko E, Kaminsky Y, Stavroskaya IG, Felipo V (2000) Alteration of mitochondrial calcium homeostasis by ammonia-induced activation of NMDA receptors in rat brain in vivo. Brain Res 880:139–146

Publikacja 3

Sensors & Actuators: B. Chemical 404 (2024) 135192

Contents lists available at ScienceDirect

Sensors and Actuators: B. Chemical

journal homepage: www.elsevier.com/locate/snb

The Ohm-azing custom-made Transendothelial Electrical Resistance measuring device (and why is it a current sensation?)

Karolina Orzeł- Gajowik [a,*], Tomasz Gajowik [b], Łukasz Rówienicz [c], Magdalena Zielińska [a,*]

[a] Department of Neurotoxicology, Mossakowski Medical Research Institute, Polish Academy of Sciences, Pawińskiego St. 5, Warsaw 02-106, Poland
[b] Institute of Control and Power Electronics, Warsaw University of Technology, Koszykowa 75, Warsaw 00-662, Poland
[c] Faculty of Power and Aeronautical Engineering, Warsaw University of Technology, Nowowiejska 24, Warsaw 00-665, Poland

ARTICLE INFO

Keywords:
Transendothelial Electrical Resistance
Barrier
Cell Monolayer Resistance

ABSTRACT

The endothelial and epithelial cells form biological barriers, the unique anatomical structures that control substance movement between circulation and i.e., organs. Measuring trans-endothelial electrical resistance (TEER) is a standard method that enables the evaluation of barrier integrity. The capability of a novel measuring system (MS) that combines innovative components, customized electrodes, and user-friendly software tailored to provide accurate and adjustable measurements of endothelial barrier integrity. We demonstrated MS usage in TEER measurement of rat brain microvascular endothelial cell line (RBE-4), primary rat brain microvascular endothelial cells (PBMEC), rat brain microvascular endothelial cells (BMEC), and human intestinal epithelial cell line (HIEC-6). The MS was successfully applied to measure the TEER of cultured cell monolayers, finding that i) the device records stable values; ii) cells treated with ammonium chloride had lower TEER values compared to untreated cells, which was verified with permeability measurements with fluorescein dye and confocal microscopy. In conclusion, we invented a low-cost MS capable of accurate TEER measures in relevant biological ranges. The MS instrument facilitates long-time, real-time monitoring of the cellular barriers, giving vital insights into cell barrier stability, permeability, and the effects of pharmacological substances. The customized measurement duration and electrode configuration meet a broad range of experimental designs.

1. Introduction

The biological barriers are formed by endothelial and epithelial cells throughout the body. The tight junctions (TJ) composed of different proteins are critical for the maintenance of body homeostasis by controlling the permeability of substances across the cellular barriers separating the luminal and ab-luminal sides [1]. Therefore, the permeability of endothelial/epithelial cell monolayers forming a particular barrier has been widely studied in pharmaceutical research [2–4], and is well recognized in biology, medicine and pharmacology. The trans-endothelial electrical resistance (TEER) measurement technique is employed to quantify the barrier function and integrity of endothelial cell monolayers. This assessment is of utmost importance in comprehending various physiological processes and the transport of drugs across biological barriers. Additionally, TEER measurements are used to assess the impact of drugs, drug candidates, and therapeutic interventions on cell barriers, a critical feature in studies of drug safety and efficacy. With time, a multitude of technologies and methodologies have been created with the purpose of precise value quantification. TEER is a quantitative assessment of the electrical resistance presented by a cellular monolayer, consisting of endothelial cells, that is cultured on a permeable membrane [5]. The main factor contributing to electrical resistance is the ion-selective characteristics of the cell membrane and the TJ composed of different proteins between neighboring cells [6]. The essential idea underlying TEER measurement entails the application of a minute electric current across the cellular monolayer, followed by the measurement of the resultant voltage drop [7] Ohm's law, denoted by the equation $V = IR$, is commonly employed in the computation of TEER. In this context, V represents the voltage, I denotes the current, and R signifies the resistance. This technique is commonly measured in units of Ohm·cm^2 and serves as an indicator of barrier integrity [8,9]. Higher TEER values are indicative of tighter cell

Abbreviations: BBB, Blood-brain barrier; BMEC, rat Brain Microvascular Endothelial Cells; HIEC-6, Human Intestinal Epithelial Cell line 6; PBMEC, Primary rat Brain Microvascular Endothelial Cells; RBE-4, Rat Brain Endothelial Cell line 4; TEER, Trans-Endothelial Electrical Resistance.

* Corresponding authors.
E-mail addresses: mzielinska@imdik.pan.pl (K. Orzeł- Gajowik), korzel@imdik.pan.pl (M. Zielińska).

https://doi.org/10.1016/j.snb.2023.135192
Received 31 October 2023; Accepted 18 December 2023
Available online 27 December 2023

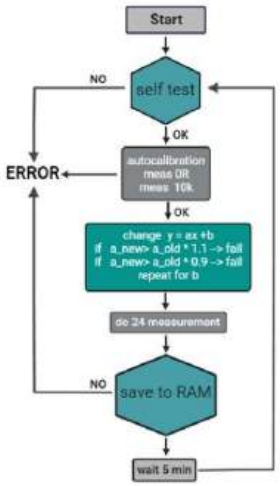

Scheme 1. Measuring system (MS) state machine.

junctions and proper barrier function [10]. There have been notable improvements in the development of TEER measurement devices during evolution. Usually, the measurement of TEER is conducted using ordinary voltmeters and electrodes, resulting in restricted precision and necessitating manual computations. Nevertheless, with the growing demands of research, there is a need for the development of increasingly advanced instruments.

Since TEER technique limitations are related to measured signal stability due to setup difficulties and the accuracy of the results, here we report a custom-made TEER measurement system (MS) that can be tailored to specific experimental setups, improving accuracy and reproducibility. The MS provided precise and consistent measurements, allowing for monitoring of time-dependent changes progression with the elimination of the effects of pH, temperature, and potential drug treatments in a controlled environment. The capability of the MS was demonstrated by using a confluent rat brain microvascular endothelial cell line (RBE-4), primary rat brain microvascular endothelial cells (PBMEC), and human intestinal epithelial cell line (HIEC-6). The recordings were verified with cultured cells monolayer permeability measurements and microscopy analysis with immunofluorescence staining towards TJ protein, zonula occludens 1 (ZO-1), and nucleus, conducted to observe the morphology of the cells. In addition, compared with measurement with Millicell ® ERS-2 Voltohmmeter- derived values (EVOM).

The advantages of simple design and the low cost make the technology translational to other laboratories to facilitate TEER research. Customizable MS for TEER measurements can aid in the development of drug delivery systems, such as nanoparticles or liposomes, by assessing their ability to cross or bypass cell barriers. The MS is designed to meet specific needs, providing higher precision and control over experimental conditions that can lead to more standardized and reproducible results across different laboratories.

2. Materials and methods

2.1. Electrode fabrication

Silver round rod with 1 mm in diameter was machined to achieve 20 mm long, smooth electrodes. Those small rods were soldered to PCB, keeping perpendicularity to PCB surface and length equality [9].

2.2. Measuring system programming

Automatic systems require a CPU for operation. C2000 family (TMS32369D) from Texas Instruments was used in MS. The system contains many components governed by the main CPU. Implemented software takes care of the proper sequence of the control state algorithm. After powering up, a self-test is conducted. CPU checks communication and supply levels. Next autocalibration takes place. Autocalibration is also performed before each measurement series to ensure that environmental changes (temperature, humidity) are not ignored in the final results. Calibration checks the resistance of wires and compensates the a and b components of the a function $y = ax + b$. Two test resistance values were chosen: 0 Ω and 10 kΩ, which are mounted on the headboard. Some deviations are minimized by the use of high-precision reference resistors. Scheme 1.

2.3. Electromagnetic compatibility test according to EN IEC 55016-1-1:2019 standard

The test of MS was conducted in a controlled environment, including an anechoic chamber to minimize external electromagnetic interference. A radiated emission test was conducted after positioning the device in the test chamber according to the standard's requirements. Appropriate antennas and measurement equipment to record emissions at various frequency ranges were used. An emission test was carried out after connecting the appropriate test setup with the necessary probes. The emissions over a range of frequencies and amplitudes were measured. An immunity test was performed by applying electromagnetic fields to the device at specified levels and frequencies. Data tests were recorded, including emissions levels, test parameters, and any observed anomalies or failures. Data were analyzed with the EMC requirements specified in the EN 55016 standard.

2.4. Cell culture and treatment

RBE-4 (a kind gift from prof. Michael Aschner, Albert Einstein College of Medicine) and rat Brain Microvascular Endothelial Cells (BMEC, ScienCell, Cat. No. #R1000) were cultured on the 100 mm dishes (Corning, NY, USA) coated with collagen type I with Minimum Essential Media (MEM)/Gibco Ham's F-10 Nutrient Mixture (Thermo Fisher Scientific, Waltham, MA, USA) with the addition of 10% Fetal Bovine Serum (FBS), Basic Fibroblast Growth Factor (bFGF) and Gentamicin (Thermo Fisher Scientific, Waltham, MA, USA). After 14–21 days when most cells displayed an endothelial phenotype and covered a minimum of 90% of the surface cells were used for further experiments.

Primary Brain Microvascular Endothelial Cells (PBMEC) were isolated from the brain cortex of 14-day-old Sprague-Dawley male rats from the animal colony of Mossakowski Medical Research Institute, Polish Academy of Sciences directly according to the protocol [11]. Cells were seeded on a 6-well plate coated with collagen I (Corning, NY, USA) and cultured in Dulbecco's Modified Eagle's Medium (DMEM) containing 20% FBS and supplemented with basic fibroblast growth factor (bFGF) and heparin. In the first two days, puromycin was added to the culture medium to inhibit neuron and astrocyte growth.

Human intestinal epithelial cell line (HIEC-6, ATCC, Manassas, VA) was cultured in OptiMEM 1 Reduced Serum Medium (Gibco), containing 4% FBS, 20 mM HEPES, 10 mM GlutaMAX (Gibco) and 10 ng/mL Epidermal Growth Factor. Subsequently, cells were incubated in a humidified atmosphere of 5% CO_2 at 37 °C. Cells were seeded at a density of 6×10^5, cultured in 0.4-mm polycarbonate filter transwell chambers, previously coated with collagen I (Corning Costar, Corning, NY, United States) at 37 °C in a humidified atmosphere of 95% air and 5% CO_2.

Cells were treated with 5 mM ammonium chloride ("Ammonia") or methylammonium chloride (MA), serving as a control of pH influence of TEER values, and incubated for 24 h. TEER values of cell cultures were measured and expressed in $\Omega.cm^2$, calculated by subtracting the

resistance of control without cells and a transwell with cells.

2.5. Resistance measurements

Chopsticks of the Millicell ® EVOM system were first submerged in the 1X PBS. The electrode was placed into the buffer solution, and after 30 s, the instrument displayed a stable resistance value, which served as a baseline. Each trans-well with cell monolayer was oriented correctly, the liquid in the 24-well plate contacted the culture medium in the trans-well. The electrode was inserted into the medium in a trans-well, avoiding cell contact or any air bubbles. After measurements cells were returned to the incubator for further experiments. The electrode was cleaned according to the manufacturer's instructions and kept in an incubator at 37 °C. Measurements were repeated in 6-hour intervals for 72 h. Each well of trans-well was measured 4 times with two devices in random order.

The experiment carried out with MS was followed by 24-electrode array disinfection by 70% and sterilized in UV light for 30 min. Electrodes were placed into the cell culture medium upon the surface of the cell monolayer. Electrodes were plugged into the measuring system and measurement started by pressing the "Single" button. The resistance values were displayed in every 24 wells and recorded on a memory card. Also, by using the "Record" button the resistance of each 24-transwell was continuously measured every five minutes for 72 h. During this time device with a cell culture plate was placed in the incubator.

2.6. Resistance measurements in variable culture medium pH and temperature

Three different cell culture media were adjusted to the desired temperature (37 °C, 35 °C, and 32 °C) as well as pH levels (6.8, 7.8, and 8.8) using a pH meter and appropriate pH-adjusting chemical. For accurate results, measurements were maintained 1 h after reaching the desired pH and temperature culture medium and repeated 4-times in each cell culture transwell.

2.7. Permeability assay and protein measurement

The experiments were carried out immediately after the resistance measurements. Monolayer permeability was measured using 40 kDa fluorescein-5-isothiocyanate (FITC)-labeled Dextran (Sigma Aldrich, St. Louis, MO, USA) at a concentration of 1 mg/mL. After 40 min incubation, 100 μL of samples were taken from the lower compartment, fluorescence was measured (in triplicates) in a FLUOstar Omega (BMG LABTECH, Offenburg, Germany) at excitation/emission wavelength of 485 nm/520 nm. The intensity of (FITC)-labeled Dextran fluorescence was expressed in arbitrary units (a.u.).

2.8. Immunocytochemical and immunofluorescent staining

Cells were seeded onto collagen I-coated coverslips at a density of 3×10^2 cells/well and cultured for 5–7 days. Cells were fixed with 4% paraformaldehyde/PBS and permeabilized with 0.25% Triton X-100/PBS. Secondly, were incubated with antibodies against ZO-1 (1:400, 33–9100, Thermo Fisher Scientific, Waltham, MA, USA,) overnight at 4°C and then exposed to secondary antibody Alexa Fluor 488 goat anti-rabbit IgG (H+L) (1:1000, Thermo Fisher Scientific, Waltham, MA, USA, Cat. No. A11008). The nuclei were labeled with Hoechst 33258 (Thermo Fisher Scientific, Waltham, MA, USA, Cat. No.: H1398). Images were acquired in a confocal laser scanning microscope LSM780 (Zeiss, Jena, Germany) and processed using the ZEN 2012 (Zeiss, Jena, Germany).

2.9. Statistical analysis

Data were analyzed and visualized using Prism 7 (GraphPad Software Inc., La Jolla, USA). Results were presented as mean ± SD. The statistical significance between various groups or treatments was measured by unpaired t-test or one-way ANOVA with Dunnett's post hoc test. In all experiments, p-value < 0.05 was considered to be statistically significant, **** $p < 0.0001$, ** $p < 0.01$, * $p < 0.05$, without asterisks means no significance.

3. Results

3.1. MS construction

The cellular integrity measuring transducer consists of a base frame plate constructed from laminate material, including both an upper and bottom surface. The cranial area is distinguished by the presence of a structural plate on which at least one pair of measuring electrodes is attached. The electrodes have been purposefully designed for insertion into the transwell, which is strategically located inside the cell culture plate. The measuring electrodes consist of a peripheral electrode and a central measurement electrode, both of which are aligned in a parallel configuration. Moreover, electrodes are attached to the bottom surface in a perpendicular configuration and their design is characterized by elongated and thin cylindrical shapes. The top surface of the frame plate is comprised of a copper layer, to provide electromagnetic shielding. The measuring electrodes are attached to a connecting point using a multi-wire ribbon. Within the framework of the MS setting, the electrodes are arranged in the form of cylindrical rods, which are placed vertically starting from the topmost section, namely from the head. The choice of this specific design is chosen to reduce the influence of the probe's form on the precision of the measurements. The technology adopted successfully reduces the impact to a level substantially lower than the accuracy shown by the analog-to-digital converters (ADCs) used in actual applications. In addition, the use of vertically aligned electrodes serves to efficiently mitigate the potential occurrence of measurement errors arising from transwell membrane displacement. The phenomenon of membrane bending is concomitant with a concurrent modification in the separation between the membrane and the probes, resulting in alterations to the resistance and impedance of the system. Furthermore, it is important to acknowledge that the length of the measurement is limited to a certain time frame of 1- milliseconds. Subsequently, this is followed by a 5-minute delay during which no excitation signal is present. The deliberate absence of stimulation leads to a significant decrease in the invasive effects of the measuring approach on the cell culture, exhibiting a reduction of 30,000 times in comparison to measurements conducted using a continuous signal. Furthermore, the device guarantees the preservation of uniform measurement parameters, hence assuring the reliability and consistency of the collected data. The geometric repeatability of the mutual arrangement of the wells concerning the probes is ensured by the proper design of the head and probes. This procedure ensures the systematic gathering and uniformization of measurements acquired from each culture well. The item has many notable characteristics that set it apart from other items in its specific category. Initially, the system operates at a heightened speed due to its use of a parallel measuring approach, as opposed to sequential measurements. Moreover, it ensures the reliability of measurements by the implementation of auto-calibration before each set of measurements. Moreover, the gadget has outstanding characteristics, including an extended scope of measurements and improved accuracy. Lastly, it is crucial to note that the gadget is priced in a comparatively competitive way concerning other existing alternatives. Furthermore, the distinctive arrangement of the head facilitates the effective use of conveniently accessible plates that house culture wells. Battery-operated gadgets can be situated inside a hermetically sealed incubator close to the culture. The use of MS technology ensures a consistent and reliable setting, hence eliminating the need to address the inconvenience associated with installing power cords inside the sterile incubator. When faced with the presence of sizable, immobile machinery, it becomes crucial to extract the culture plate from the incubator, thereby exposing it to external

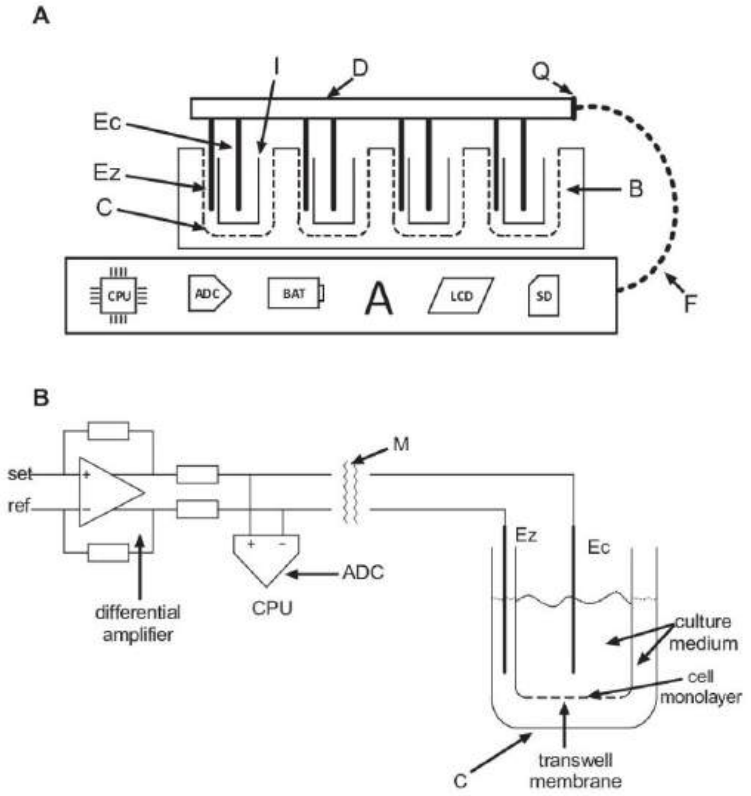

Fig. 1. General device construction **A.** Lateral representation of the instrument with measuring head **B.** MS scheme including a single culture well. A- device cover, B- culture plate, C- culture well, D- measuring head, F- detachable multi-wire ribbon, I- transwell, Q- connector, ADC- analog-to-digital converter, CPU- signaling processor Ec- central electrode, Ez- external electrode, LCD- display, SD- memory card.

variables that might result in contamination. The apparatus can perform automatic measurements while consistently remaining inside the incubator. Furthermore, MS is equipped with batteries that provide uninterrupted operation for a continuous period of two consecutive days. Furthermore, it is feasible to extend the duration of maintenance-free operation to a span of four days. Following the completion of a four-day duration, it is possible to detach the depleted power bank and substitute it with a fully charged alternative, facilitating an extra period of functionality lasting two days. The device shown in Fig. 1 comprises a housing (A) onto which a culture plate (B) is positioned. The culture plate consists of culture wells (C) and culture transwell (I). The measuring device, known as the measuring head (D), is situated above the culture plate and comprises two measurement probes: a center probe (Ec) and an outside probe (Ez). The measuring head is connected to the housing (A) by a detachable multi-wire ribbon cable (F) which is secured through a connector (Q). The housing encompasses all essential components required for the functioning of the gadget. The aforementioned components refer to electronic systems that are responsible for controlling device operations and processing measurement data. The housing of the system comprises many integral components necessary for its operational efficacy. The system is composed of many essential elements, including a signal processor, an analog-to-digital converter, a power supply system powered by a current source, a control panel that may have a touch display or analog panel, and a memory card. The housing serves as the primary mechanical component of the gadget as a whole. The device's construction has a designated area for the positioning of a culture plate (B).

The culture plate (B), culture wells (C), and transwell (I) are commonly used and standardized components employed for conducting cell cultures. These elements exhibit consistent size and structure and are offered in a range of cultural well shapes, including 3×3, 3×4, 4×6, 6×8, and 8×12. The frame board (L) of the measuring head (D) functions as a structural base for the measuring electrodes (Ec and Ez) and enables the transmission of measurement signals from the electrodes (Ec and Ez) through the connection (Q) and the multi-wire ribbon (F) to the housing (A) apparatus. The measuring electrodes, labeled Ec and Ez, are elongated, slender cylindrical objects that are affixed perpendicularly to the frame board (L) of the measuring head (D) through soldering. The positioning of the electrodes is designed so that the central electrode (Ec) is located within the culture transwell (I), while the outer electrode (Ez) is situated between the transwell (I) and the cell culture well (C). The precise separation between these electrodes does not have substantial importance in this particular scenario. It is crucial to locate one electrode within the transwell, whereas the second electrode should be placed outside. It is recommended that electrodes be constructed using physiologically inert elements that exhibit superior electrical conductivity, such as silver, gold, titanium, platinum, and CrNiMo alloys. Silver is a substance that is easily obtainable and affordable, making it the primary material selected for probes. The laminate (L) is outfitted with measurement electrodes (Ec and Ez) that are placed in a grid-like formation of columns and rows, resembling the typical configuration often observed in the wells of culture plates. It is imperative to thoroughly evaluate the dimensions of the measuring electrodes (Ec, Ez) to prevent a significant rise in fluid level within the

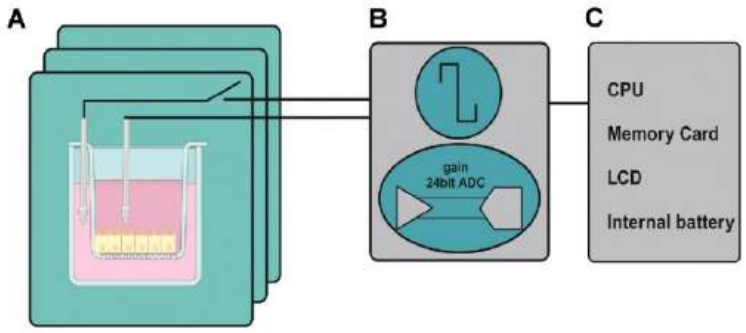

Fig. 2. Schematic diagram of the measurement system. **A.** Transwell with measurement electrodes. **B.** Signal conditioning and multiplexing. **C.** Microprocessor (CPU) and auxiliary circuits.

Fig. 3. Construction of MS with culture plate guide; **A.** head with electrodes. **B.** lowering lever. **C.** cell culture plate, **D.** position adjustment of cell culture plate, **E.** LCD, **F.** memory card input.

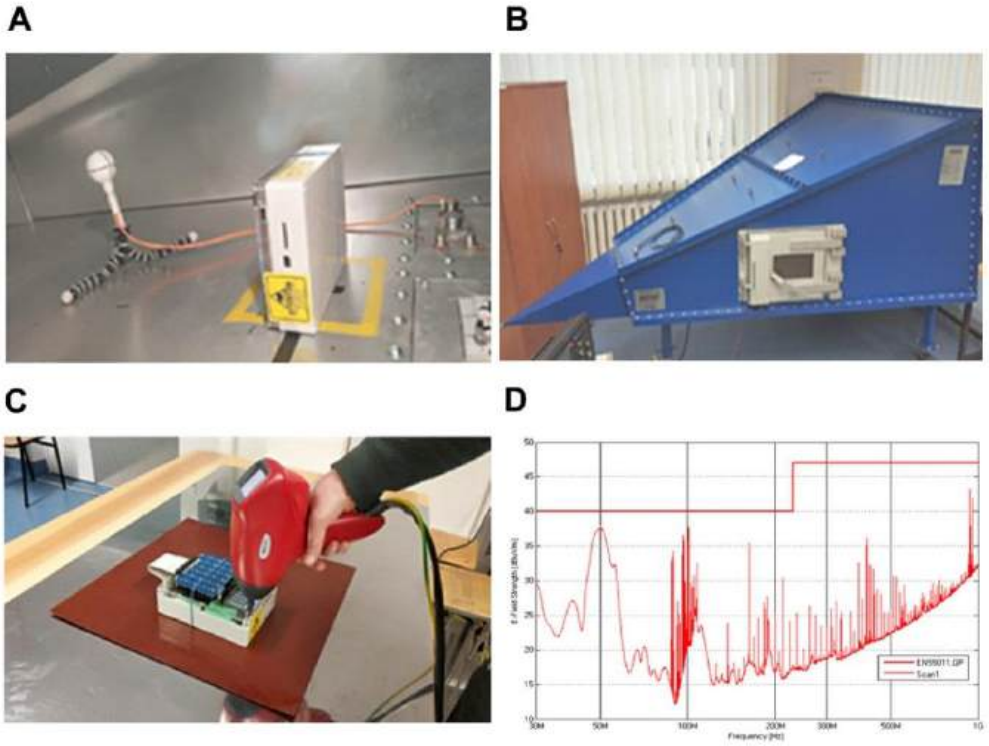

Fig. 4. The verification of measurements compliance with EU standards. **A.** Electromagnetic compatibility testing following the EN55016 standard. **B.** External field immunity test **C.** Electrostatic discharge immunity **D.** Compatibility emission test.

trans-well (I) when attaching the head (D). Simultaneously, the electrodes must exhibit adequate mechanical resilience to endure the washing procedure. As a result, a silver wire with a diameter of 1 mm that was easily obtainable was utilized. The determination of the length of the probes, employed as measuring electrodes, is contingent upon the depth of the trans-well's bottom, which measures 15 mm. The entire electrical diagram of the device is depicted in Fig. 2. The pseudo-current source, represented by the symbol Z, is responsible for producing an excitation pulse. The process of choosing the electrode pair (Ez/Ec) in the measurement well (C) is achieved by the utilization of an analog multiplexer (M). The quantification of resistance is followed by the transfer of the analog multiplexer (M) to the subsequent wells. The schematic diagram in Fig. 2 illustrates the intricate electrical configuration of the instrument. The flow of electric current through the circuit leads to the generation of a voltage difference across the resistance of the analyzed cell culture in a specified well (C). The dip noted before is later processed using a specialized and precise analog-to-digital converter (ADC).

The measuring head (D) depicted in Fig. 3 performs three essential functions. The skeleton plate is composed of a fiberglass laminate (L) that is securely attached to electrodes (Ec and Ez). The electrodes (Ec and Ez) produce electrical signals which are then conveyed to the multi-wire ribbon (F) through the connector (Q). Furthermore, the utilization of an electromagnetic screen (P) serves the purpose of safeguarding the signals that originate from the electrodes (Ec and Ez). The frame board (L) of the measuring head is composed of a glass fiber-reinforced epoxy laminate and incorporates a printed circuit board (PCB) with both upper and bottom surfaces. The lower surface of the board, referred to as L, is covered with discrete copper tracks that are specifically allocated to each particular electrode, namely Ec and Ez. The paths stated above enable the transfer of signals to the connection (Q), which then pass through the busbar (F) and ultimately reach the signal processing and analysis circuitry contained within the device (A). The upper surface of the board (L) is comprised of a uniform layer of copper, which functions as a protective barrier to mitigate the impact of electromagnetic interference on the signals transmitted by the electrodes. Polychlorinated biphenyls (PCBs) are extensively employed as a conventional substance within the realm of electronics. The construction utilized is also regarded as standard and widely acknowledged within the discipline. The structure comprises two copper layers, each having a thickness of 35 micrometers, which are segregated by a fiberglass laminate core with a thickness of 1.6 millimeters. The laminate (L) displays a contour that accurately corresponds to the size and proportions of the culture plate (B), thus assuming its geometric properties. After placing the culture plate (B), it is noted that the lower surface of the plate (L) is aligned parallel to the upper plane of the culture plate (B). The head plate (L) exhibits a robust adhesion to the culture plate (B), hence mitigating the incidence of undesired evaporation of the culture medium. The systematic positioning of electrode mounting points (Ec and Ez) concerning the culture wells (C) allows for the establishment of consistent measurement conditions throughout all wells of the culture plate (B). The measuring electrodes (Ec, Ez) are arranged in a grid-like configuration on the skeleton board (L), featuring both columns and rows. The arrangement of the measurement electrodes in this experimental setup aligns with the spatial distribution of the culture wells on the culture plate. However, the current iteration of the embodiment does not place any limitations on the dimensions of the head (D) to the designated size of the culture plate.

3.2. *Electromagnetic compatibility test according to EN55016 standard*

Next, we examined the impact of external electromagnetic fields on

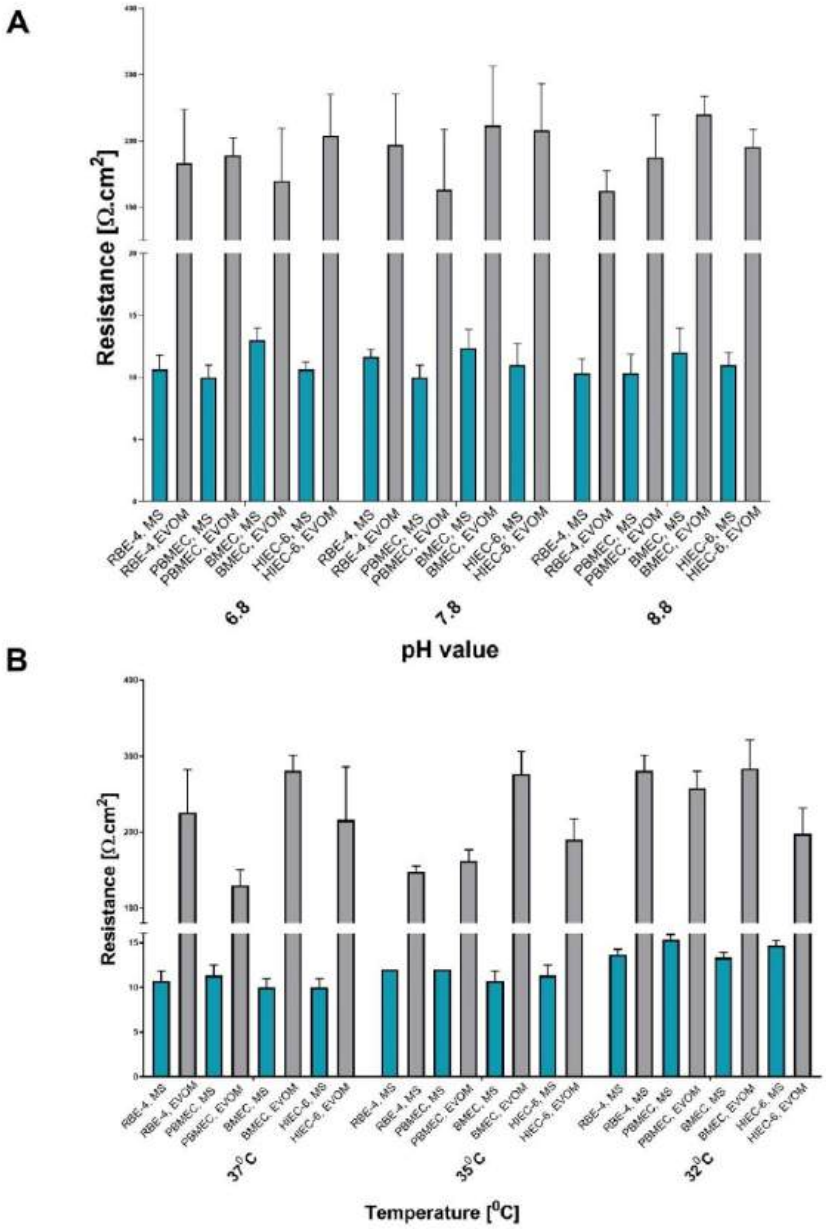

Fig. 5. The influence of temperature **A.** and pH **B.** on resistance of particular cell culture medium measured with MS and EVOM, n = 4.

the accuracy of measurement recordings. Fig. 4 displays a course of studies depicting the installation of MS within the chamber (A, B). In the case of touch discharge, there was no discernible interference with the functionality (C). The measuring system demonstrated compliance with the specified requirements, as evidenced by its uninterrupted functionality in 96 out of 100 instances (D). The measurements document compliance with EU standards, confirming the possibility of being approved for use in a laboratory environment; additionally, they guarantee the safe operation of other electrical devices.

3.3. *The effect of variable pH and temperature on resistance measurement with both devices used*

We carried out the pH and temperature fluctuation test demonstrating the influence on measured resistance values (Fig. 5A). Average resistance in all cells type culture medium, measured with EVOM oscillated at 37°C 197.73 ± 56.54 Ω.cm^2, decreased at 35°C to 191.46 ± 8.02 Ω.cm^2 and finally reached 239.4 ± 20.07 Ω.cm^2 in 32°C. Observed TEER reduction in 32°C is a consequence of kinetic energy loss leading to a reduction in ion mobility and the possibility of elevated TEER values.

Table 1
Measurements of cell culture resistance with MS in the 0th, 6th, 24th, and 72th hour of the experiment. Cells treated with 5 mM ammonium chloride (Ammonia, middle column) or 5 mM methylammonium chloride (MA, right column) for 24 h Results are mean ± SD, n = 4 **** p < 0.000 and * p < 0.01 vs. control, one-way ANOVA, Dunnett's post hoc test.

	0 h			6 h			24 h			72 h		
	Control	Ammonia	MA	Control	Ammonia	MA	Control	Ammonia	MA	Control	Ammonia	MA
RBE-4	206.6 ± 2.46	218.18 ± 0.15	184.72 ± 1.45	225.42 ± 2.28	215.98 ± 9.9 ****	185.85 ± 0.05	269.70 ± 4.09	214.70 ± 3.19 ****	196.07 ± 0.05	362.67 ± 29.24	163.5 ± 9.9 ****	286.57 ± 29.51
PBMEC	219.264 ± 0.35	223.54 ± 5.58	220.93 ± 1.5	228.83 ± 4.36	222.83 ± 0.5 ***	225.6 ± 2.34	244.85 ± 6.21	215.85 ± 3.64 ****	235.13 ± 0.41	257.11 ± 2.87	201.91 ± 1.58 ****	252.75 ± 8.49
BMEC	227.07 ± 0.12	230.65 ± 4.72	184.97 ± 0.81	234.92 ± 0.05	233.33 ± 9.67 *	186.47 ± 1.01	255.02 ± 0.12	196.42 ± 1.62 ****	197.02 ± 1.02	329.32 ± 2.2	191.44 ± 2.31 ****	235.6 ± 5.00
HIEC-6	184.25 ± 1.7	151.5 ± 0.57	184.45 ± 0.63	202.75 ± 18.2	178.5 ± 3.0 *	185.95 ± 0.07	208.62 ± 13.86	201.75 ± 1.5	197.35 ± 1.48	255.275 ± 20.34	237.93 ± 0.49	233.05 ± 0.07

Table 2
Measurements of cell cultures resistance with EVOM device in 0th, 6th, 24th, and 72th hour of experiment. Cells treated with 5 mM ammonium chloride (Ammonia, middle column) or 5 mM methylammonium chloride (MA, right column) for 24 h. Results are mean ± SD, n = 4.

	0 h			6 h			24 h			72 h		
	Control	Ammonia	MA	Control	Ammonia	MA	Control	Ammonia	MA	Control	Ammonia	MA
RBE-4	238.5 ± 68.96	153 ± 69.96	242.75 ± 100.1	253.75 ± 46.07	377.75 ± 108.44	242.75 ± 140.54	340.25 ± 125.54	320.75 ± 62.62	269 ± 46.02	386 ± 351.1	412 ± 127.77	259 ± 113.1
PBMEC	732 ± 756.22	206.25 ± 110.56	405.5 ± 296.36	317.5 ± 90.23	349 ± 194.21	288 ± 77.36	154 ± 109.41	206.75 ± 116.82	171.75 ± 80.69	243.5 ± 34.79	213.75 ± 10.71	254.25 ± 37.44
BMEC	257.5 ± 23.35	153 ± 69.18	242.75 ± 100.1	253.75 ± 46.07	377.75 ± 108.44	263.75 ± 56.96	340.25 ± 125.54	320.75 ± 162.62	269 ± 46.02	386 ± 351.1	412 ± 127.77	259 ± 113.1
HIEC-6	200 ± 113.13	296 ± 62.22	304.5 ± 16.26	254 ± 114.55	223.5 ± 7.77	178.5 ± 62.93	530 ± 98.98	200 ± 33.94	248.5 ± 4.94	418 ± 339.41	193 ± 5.65	193 ± 22.62

Equally to EVOM results, an increase of resistance maintained with MS, at lower temperatures was also observed (Fig. 5B). The initial resistance of 8.77 ± 0.55 Ω.cm^2 in 37°C was raised to 9.44 ± 0.66 Ω.cm^2 in 35°C, finally leading to 11.83 ± 0.8 Ω.cm^2 in 32°C suggesting variability of resistance in response to changes in temperature, due to the temperature-dependent characteristics of ion mobility and membrane properties. Worth noting is that high basal resistance in EVOM devices may cover minor changes in resistance in cells subjected to additional factors, which is crucial to obtaining reliable and reproducible results. Culture medium resistance alignment by EVOM in three different pH conditions showed values: 155.9375 ± 56.43 Ω.cm^2, 180.375 ± 75.98 Ω.cm^2 and 161 ± 54.25 Ω.cm^2 in pH= 6.8, 7.8 and 8.8 respectively. In contrast, values obtained with MS in pH= 6.8, 11 ± 1.44 Ω.cm^2, pH= 7.8, 11.33 ± 1.422 Ω.cm^2 and pH= 8.8 10.8 ± 1.44 Ω.cm^2 did not show association of resistance values with pH variability.

3.4. The employment of resistance measurements with MS and EVOM Millicell ®, combined with cell monolayer permeability and ZO-1 immunofluorescence verification

The initial TEER values at 0 h fluctuated from 161.73 ± 1.14 Ω.cm^2 to 230.66 ± 4.72 Ω.cm^2 for MS and 153 ± 69.18 Ω.cm^2 to 732 ± 756.26 Ω.cm^2 for EVOM device. The average standard deviation of resistance for the custom-made device was 12.2 and 113.27 for EVOM Millicell ® [Table 1].

The transepithelial electrical resistance gained with MS of cells maintained in ammonia showed a significant decline within 72 h. The statistical analysis revealed that 72-hour data points obtained a p-value of < 0.0001. This indicates that ammonia had a substantial effect on reducing the TEER and endothelial barrier integrity, which aligns with previous findings in the literature [12]. As depicted in Table 1 TEER values of the samples subjected to ammonia chloride conditions didn't exhibit a significant reduction. Table 2.

TEER measurement determines cell monolayer resistance, and is a measure of cell barrier functionality. To additionally assess the permeability of the cell monolayers – forming barriers, we used 40 kDa fluorescein isothiocyanate (FITC) dextran tracer and quantify fluorescence intensity in the medium. Cells exposed to ammonia for 24 h presented an increased permeability of RBE-4, PBMEC, and BMEC cells monolayer by ~44%, ~58%, and 43%, respectively. A lack of differences was observed between HIEC-6 control cells and cells treated with ammonia. The increase in ammonia-evoked permeability of cell monolayer correlated well with TEER values gathered with MS in studied cells. We also evaluated the studied in vitro models by immunocytochemistry analysis of ZO-1 junctional protein expression. The intensity reduction of ZO-1 stainnng was noted, in ammonia-treated RBE-4, PBMEC, and BMEC cells. The obtained results confirm the applicability of our device usage. We documented that reduced TEER values gathered with MS device can functionally support the observed cell monolayer permeability changes in line with ZO-1 expression decrease. Fig. 6.

4. Discussion

The TEER measurement is a technique that allows to control and functionally characterize cell monolayer tightness and is used in research and medical applications. Recently, there has been a notable emergence of custom TEER measurement devices, which hold great promise for researchers in their pursuit of more precise, effective, and adaptable tools for conducting studies. Although specialized TEER measurement devices offer a multitude of advantages, they also pose certain challenges, particularly in experimental protocol and process standardization, hence necessitating the establishment of protocols for data reporting and device calibration.

In this study, we focus on the new specialized TEER measurement device and its prospective use. We investigate the working feasibility of the custom-made system for TEER measurements in different cell lines known to form tight junctions (TJs) [13–17]. Additionally, to add credence to the correctness of our measures, we parallely and independently analyze TEER values with commercially available devices. We documented the recordings' stability and our measurement insensitivity on medium pH and temperature changes. The cell barrier integrity was also verified with zonula occludens (ZO-1) immunostaining analysis, and measurement of cell monolayer permeability of

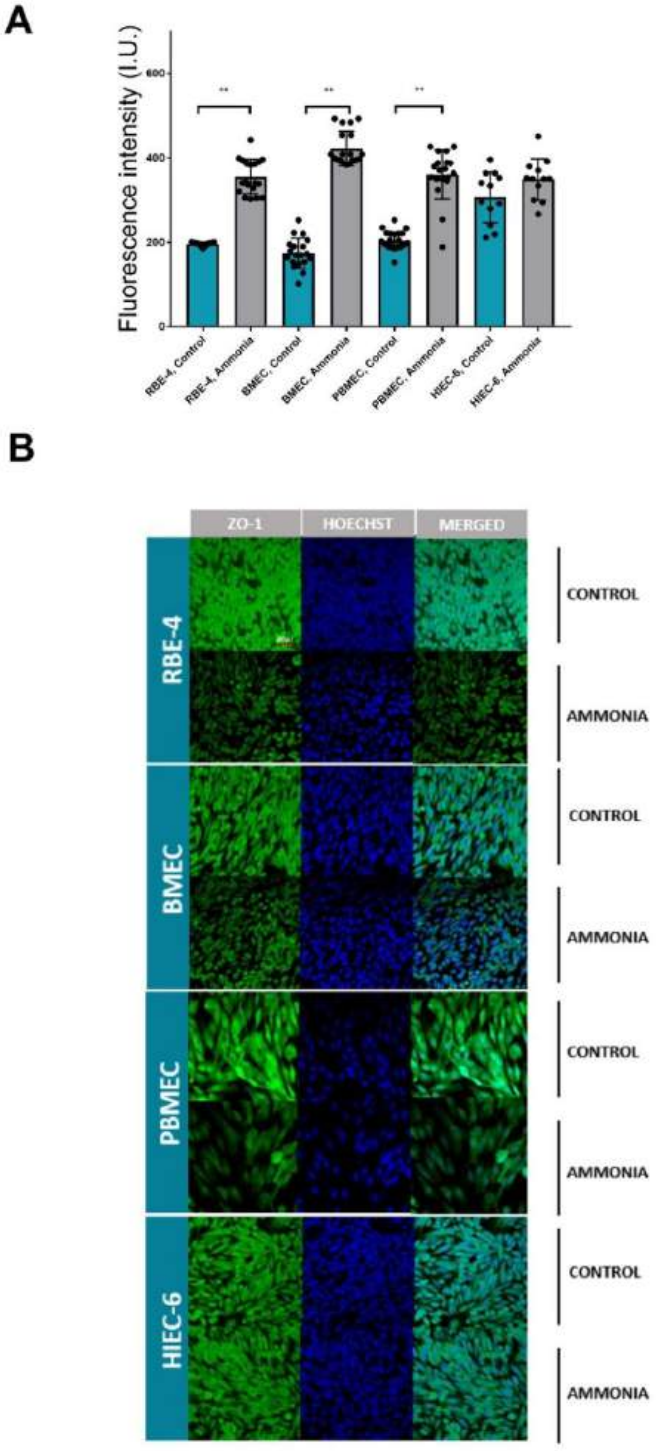

Fig. 6. Examination of resistance results based on cell monolayer permeability and immunocytochemical staining. **A.** Permeability of cell monolayer treated or not (Control, upper panels) with 5 mM ammonium chloride (Ammonia, bottom panels) for 24 h. **B.** Immunofluorescence for TJ protein, ZO-1 (green fluorescence) and nucleus (blue, Hoechst). Results are mean ± SD, n = 4, ** $p < 0.01$ vs. control, one-way ANOVA, Dunnett's post hoc test.

medium size (40 kDa) molecules. Of note, the family of ZO proteins (ZO-1, ZO-2, and ZO-3), cingulin, and several other proteins are essential for TJs functioning as they form the cytoplasmic bridge connecting the TJs to the cell cytoskeleton, and provide structural support to the endothelial cells [18,19]. With the abovementioned analysis of three selected cell types, we proved the validity and usefulness of our MS system in endothelial and epithelial cell barrier integrity evaluation.

The TEER system, designed for this study exhibited remarkable precision in quantifying TEER values, exhibiting minor discrepancies among repeated measurements. The data consistently displayed low standard deviation, suggesting a high level of repeatability in the particular measurements. The EVOM Millicell ® system demonstrates good precision, albeit with somewhat much greater variability in measurements when compared to the bespoke device. The custom device shows high sensitivity in detecting subtle changes in TEER, making it suitable for applications requiring precise measurements, such as drug permeability studies or barrier function assessments. In turn market available system, while sensitive, exhibited a slightly lower sensitivity when compared to the custom device.

The development of custom systems necessitates a high level of proficiency in electronics, software programming, and, engineering since data acquisition holds significant importance in comprehending pathological conditions, conducting drug permeability investigations, and facilitating development in tissue engineering. The MS integrates sophisticated sensors and data-gathering systems specifically designed for the experimental configuration, resulting in heightened measurement accuracy and diminished data variability.

The electrodes of MS might be modified by researchers to support several cell culture formats, rendering them appropriate for a broad spectrum of applications. What is more, the validation of measuring systems which is crucial in ensuring the dependability and precision of custom devices, necessitates thorough validation procedures and comparisons with proven commercial systems. The MS calibration is automatically repeated before each usage and on demand.

Commercially available systems offer standard measurement features but may not adequately fulfill the distinct demands of diverse research goals. The limitation is overcome by the utilization of a custom TEER measuring device, which provides researchers with the ability to customize the instrumentation according to their requirements.

The described measurement device is user-friendly since requires minimal training for researchers to obtain accurate measurements allowed by easy setup and operation. In turn, EVOM Millicell ® requires meticulous, long initial setup and calibration, which might be less intuitive for novice users. Both systems provide data output in a format suitable for analysis. Data processing software associated with the custom device is user-friendly and allows for real-time analysis, while the EVOM Millicell ® has its software for data interpretation. Finally, our MS is cost-effective, as it was assembled using readily available components, and maintenance costs are relatively low. Our custom MS has the potential to yield long-term cost savings by mitigating the necessity for regular system upgrades and replacements.

The presented made-to-order MS could be customized and adapted for specific experimental needs, making it versatile for various research applications. MS offers an excellent alternative to the commercially available TEER measuring systems, with the potential for higher precision, sensitivity, and cost-effectiveness. The future of biomedical and pharmaceutical research is expected to be significantly influenced by the utilization of tailored devices, as research continues to advance. The MS device represents a significant step forward in the field of vascular biology, offering researchers a powerful tool to unravel the complexities of endothelial barrier regulation.

Additional information

Fig. 1 The trans-endothelial electrical resistance measurement with MS of RBE-4 (**A.**), PBMEC (**B.**), BMEC (**C.**), and HIEC-6 (**D.**).

Authors' contributions

K.O-G., T.G., T.R.: Methodology, Investigation, Software, Formal Analysis, Writing-original draft. M.Z.: Methodology, Investigation, Formal Analysis, Writing-original draft. K.O-G., M.Z.: Conceptualization, Resources, Writing original draft-Review & Editing. All authors contributed to writing the protocol. All authors read and approved the final manuscript.

Consent for publication

Not applicable.

Funding

This work was supported by the National Science Centre of Poland [No. 2015/19/B/NZ4/01902], ESF (POWR.03.02.00–00-I028/17–00) and the MMRI internal funding source (FBW031).

Declaration of Competing Interest

The authors declare that they have no known competing financial interests or personal relationships that could have appeared to influence the work reported in this paper.

Data Availability

The datasets used and/or analysed during this study are available from the corresponding author upon reasonable request.

References

[1] W.M. Pardridge, Blood-brain barrier biology and methodology, J. Neurovirol. 5 (1999) 556–569, https://doi.org/10.3109/13550289909021285.
[2] T.S. Frost, L. Jiang, R.M. Lynch, Y. Zohar, Permeability of epithelial/endothelial barriers in transwells and microfluidic bilayer devices, Micromachines 10 (2019) 533, https://doi.org/10.3390/mi10080533.
[3] D.-P. Wang, K. Kang, J. Sun, Q. Lin, Q.-L. Lv, J. Hai, URB597 and andrographolide improve brain microvascular endothelial cell permeability and apoptosis by reducing oxidative stress and inflammation associated with activation of Nrf2 signaling in oxygen-glucose deprivation, Oxid. Med. Cell. Longev. 2022 (2022) 1–23, https://doi.org/10.1155/2022/4139330.
[4] H. Liu, S. Xu, Z. Xu, S. Cheng, M. Du, Absorption characteristics and the effect on vascular endothelial cell permeability of an anticoagulant peptide, Food Res. Int. 173 (2023) 113405, https://doi.org/10.1016/j.foodres.2023.113405.
[5] J.P. Vigh, A. Kincses, B. Ozgür, F.R. Walter, A.R. Santa-Maria, S. Valkai, M. Vastag, W. Neuhaus, B. Brodin, A. Dér, et al., Transendothelial electrical resistance measurement across the blood–brain barrier: a critical review of methods, Micromachines 12 (2021) 685, https://doi.org/10.3390/mi12060685.
[6] Chaing, Y.-Y.; Tu, K.-H. In Vitro Microfluidics-Based Blood–Brain Barrier Model. In Proceedings of the 2019 IEEE 14th International Conference on Nano/Micro Engineered and Molecular Systems (NEMS); IEEE: Bangkok, Thailand, April 2019; pp. 351–354.
[7] C. Crone, S.P. Olesen, Electrical resistance of brain microvascular endothelium, Brain Res. 241 (1982) 49–55, https://doi.org/10.1016/0006-8993(82)91227-6.
[8] J. Haorah, K. Schall, S.H. Ramirez, Y. Persidsky, Activation of protein tyrosine kinases and matrix metalloproteinases causes blood-brain barrier injury: novel mechanism for neurodegeneration associated with alcohol abuse, Glia 56 (2008) 78–88, https://doi.org/10.1002/glia.20596.
[9] R. Booth, H. Kim, Characterization of a microfluidic in vitro model of the blood-brain barrier (μBBB), Lab Chip 12 (2012) 1784, https://doi.org/10.1039/c2lc40094d.
[10] B. Srinivasan, A.R. Kolli, M.B. Esch, H.E. Abaci, M.L. Shuler, J.J. Hickman, TEER measurement techniques for in vitro barrier model systems, SLAS Technol. 20 (2015) 107–126, https://doi.org/10.1177/2211068214561025.
[11] T. Ruck, S. Bittner, L. Epping, A.M. Herrmann, S.G. Meuth, Isolation of primary murine brain microvascular endothelial cells, JoVE (2014) 52204, https://doi.org/10.3791/52204.
[12] M. Skowrońska, M. Zielińska, L. Wójcik-Stanaszek, J. Ruszkiewicz, D. Milatovic, M. Aschner, J. Albrecht, Ammonia increases paracellular permeability of rat brain endothelial cells by a mechanism encompassing oxidative/nitrosative stress and activation of matrix metalloproteinases: ammonia-induced brain endothelium damage, J. Neurochem. 121 (2012) 125–134, https://doi.org/10.1111/j.1471-4159.2012.07669.x.

[13] X. Cong, W. Kong, Endothelial tight junctions and their regulatory signaling pathways in vascular homeostasis and disease, Cell. Signal. 66 (2020) 109485, https://doi.org/10.1016/j.cellsig.2019.109485.
[14] E. Sasson, S. Anzi, B. Bell, O. Yakovian, M. Zorsky, U. Deutsch, B. Engelhardt, E. Sherman, G. Vatine, R. Dzikowski, et al., Nano-scale architecture of blood-brain barrier tight-junctions, eLife 10 (2021) e63253, https://doi.org/10.7554/eLife.63253.
[15] S. Tietz, B. Engelhardt, Brain barriers: crosstalk between complex tight junctions and adherens junctions, J. Cell Biol. 209 (2015) 493–506, https://doi.org/10.1083/jcb.201412147.
[16] T. Paradis, H. Bègue, L. Basmaciyan, F. Dalle, F. Bon, Tight junctions as a key for pathogens invasion in intestinal epithelial cells, IJMS 22 (2021) 2506, https://doi.org/10.3390/ijms22052506.
[17] T. Suzuki, Regulation of the intestinal barrier by nutrients: the role of tight junctions, Anim. Sci. J. 91 (2020) e13357, https://doi.org/10.1111/asj.13357.
[18] H. Kadry, B. Noorani, L. Cucullo, A blood–brain barrier overview on structure, function, impairment, and biomarkers of integrity, Fluids Barriers CNS 17 (2020) 69, https://doi.org/10.1186/s12987-020-00230-3.
[19] A. Reinhold, H. Rittner, Barrier function in the peripheral and central nervous system—a review, Pflug. Arch. Eur. J. Physiol. 469 (2017) 123–134, https://doi.org/10.1007/s00424-016-1920-8.

Publikacja 4

International Journal of
Molecular Sciences

MDPI

Review

Insight into microRNAs-Mediated Communication between Liver and Brain: A Possible Approach for Understanding Acute Liver Failure?

Karolina Orzeł-Gajowik, Krzysztof Milewski and Magdalena Zielińska *

Department of Neurotoxicology, Mossakowski Medical Research Institute, Polish Academy of Sciences, 5 Pawińskiego Str., 02-106 Warsaw, Poland; korzel@imdik.pan.pl (K.O.-G.); kmilewski@imdik.pan.pl (K.M.)
* Correspondence: mzielinska@imdik.pan.pl; Tel.: +48-22-608-6470

Abstract: Acute liver failure (ALF) is a life-threatening consequence of hepatic function rapid loss without preexisting liver disease. ALF may result in a spectrum of neuropsychiatric symptoms that encompasses cognitive impairment, coma, and often death, collectively defined as acute hepatic encephalopathy. Micro RNAs are small non-coding RNAs that modulate gene expression and are extensively verified as biomarker candidates in various diseases. Our systematic literature review based on the last decade's reports involving a total of 852 ALF patients, determined 205 altered circulating miRNAs, of which 25 miRNAs were altered in the blood, regardless of study design and methodology. Selected 25 miRNAs, emerging predominantly from the analyses of samples obtained from acetaminophen overdosed patients, represent the most promising biomarker candidates for a diagnostic panel for symptomatic ALF. We discussed the role of selected miRNAs in the context of tissue-specific origin and its possible regulatory role for molecular pathways involved in blood–brain barrier function. The defined several common pathways for 15 differently altered miRNAs were relevant to cellular community processes, indicating loss of intercellular, structural, and functional components, which may result in blood-brain barrier impairment and brain dysfunction. However, a causational relationship between circulating miRNAs differential expression, and particular clinical features of ALF, has to be demonstrated in a further study.

Keywords: acute liver failure; acetaminophen toxicity; circulating microRNA; hepatic encephalopathy; viral hepatitis

Citation: Orzel-Gajowik, K.; Milewski, K.; Zielińska, M. Insight into microRNAs-Mediated Communication between Liver and Brain: A Possible Approach for Understanding Acute Liver Failure? *Int. J. Mol. Sci.* **2022**, 23, 224. https://doi.org/10.3390/ijms23010224

Academic Editor: Barbara Mroczko

Received: 22 November 2021
Accepted: 21 December 2021
Published: 25 December 2021

1. Background

1.1. Liver Disease a Global Burden

Liver disease does not usually cause unequivocally symptoms until it is advanced, and the liver is seriously damaged and dysfunctional. The liver comes in close contact with harmful substances and defends itself in two ways. First, it can regenerate by repairing or replacing injured tissue. Second, as it is composed of units with similar functions, thus, if one area is injured, other cells will perform the work of the injured section indefinitely or until the damage is repaired. Despite the existing, albeit, in theory, self-repairing and regenerative abilities, liver disease is an increasing global problem.

The burden of liver disease worldwide continues to grow. Each year, the liver disease accounts for about 2 million deaths, i.e., 1 million due to cirrhosis and 1 million due to viral hepatitis and hepatocellular carcinoma (HCC) [1,2]. Liver diseases account for a significant burden in terms of health and costs worldwide. This group of diseases encompasses epidemiologically diverse alcohol-related liver disease, non-alcoholic fatty liver disease, hepatitis caused by a viral infection, or exposure to drugs, hemochromatosis, an inherited disorder with a gradual build-up of iron usually around the liver, primary biliary cirrhosis, and liver tumors.

Epidemiological studies of liver disease limit caveats, such as heterogeneous population under study, incomplete ascertainment, lack of unified disease definitions, and method of assessment (laboratory tests, biopsy, non-invasive markers, imaging). The aforementioned caveats suggest that the global burden of both acute and chronic liver diseases is prevalent worldwide and expected to increase, causing significant mortality [3,4].

1.2. Acute Liver Failure

Acute liver failure (ALF), originally defined by Trey and Davidson in 1970 as fulminant liver failure, refers to a specific syndrome, characterized by loss of liver function that occurs rapidly—in hours or days, and by abnormality of liver blood tests, usually in a person who has no preexisting history of liver disease [5]. After two decades, the syndrome was redefined to take into account, i.e., etiology and prognosis [6]. Despite being less common than chronic liver disease, ALF is associated with a high mortality grade and approximately half of the cases progress and require liver transplantation so immediate diagnosis and management of that syndrome need to be applied [7,8]. A wide range of insults can create a clinical picture of ALF (Table 1). The most common causes of ALF are drugs overdose and hepatitis virus infection, causing about 70% of cases [9]. Moreover, prognosis suggests that many drug-induced ALF cases will grow and dominate as a major cause of ALF in the future decades.

Table 1. Etiology of ALF.

Cause	Causative Factor	Therapy	Frequencyin Adults *
Intoxication	Acetaminophen Isoniazid Other drug-driven liver damage Mushrooms poisoning	N-acetyl cysteine Hydration Penicillin	58%
Viral	Hepatitis B/C/A/E/ **	Antiviral therapy	10%
Metabolic	Wilson disease Autoimmune hepatitis Acute fatty liver of pregnancy	Copper chelation Steroids Delivery of the fetus	7%
Other	Budd-Chiari syndrome Ischemic/sepsis shock Heat stroke	Surgery Hemodynamic stabilization Hydration	5%
Unknown	Undetermined etiology		14%

* According to Rajaram et al., 2018; ** Ordered by frequency of occurrence.

Drug-induced liver injuries are clinically challenging due to their idiosyncratic (unpredictable) character arising from the enormous amount of commercially available drugs, herbs, and dietary supplements with hepatotoxic potential. Acetaminophen is the most common drug that indicates ALF. It is responsible for approximately 50% of cases of ALF in Western Europe and the United States, [10–12], while traditional complementary and dietary supplements dominate as the main causative factor of ALF in Asia [13]. A variety of clinical and pathological phenotypes with the current lack of specific biomarkers increases the uncertainty of liver disease diagnosis and output and requires highly careful exclusion of alternative diagnosis.

The second most frequent etiological cause of ALF is viral hepatitis infections affecting individuals in all geographic regions, but mostly in low and middle-income countries. In 2010, deaths from viral hepatitis accounted for 0.3 million per year, an increase of about 50% from 1990. There are five main types of hepatitis viruses, including type A, B, C, D, and E, of which, type B and C remain prevalent globally, albeit differ in the geographical distribution of disease prevalence.

In 2019, ~1.5 million (1.1–2.6 million) people newly infected with hepatitis B virus, and ~1.5 million (1.3–1.8 million) newly infected with hepatitis C virus [14], account for ~1.1 million cases of patient deaths per year globally. Viral hepatitis-related number of deaths is higher than the mortality caused by HIV (~680,000 deaths in 2020) or malaria (~400,000 deaths in 2020), not much less than deaths number caused by tuberculosis (~1.4 million in 2020), additionally exaggerated with the unprecedented COVID-19 pandemic, which disrupted health care globally [15,16]. ALF may also develop due to infec-

tions by other rare viruses, including herpes simplex virus, cytomegalovirus, Epstein–Barr virus [11], and parvoviruses. It is estimated that 10% of acute HBV infection progresses to chronic disease [17].

Other pathological conditions referred to as ALF causes are relatively rare but require mentioning as potentially life-threatened. Autoimmune hepatitis (AIH) accounts for 4 to 5% of ALF; it is typically presented in the third to sixth decades of life, more often in women than in men as a growing loss of tolerance to hepatocyte-specific autoantigens results in intensified autoimmune reaction [18]. Metabolic diseases, such as Wilson's disease or acute fatty liver of pregnancy, besides their specific symptoms, may be accompanied by overwhelming infection (sepsis), which impairs blood flow to the liver, inducing ALF episodes. Additionally, a heatstroke combined with excessive physical activity can trigger ALF [19,20]. It is worth mentioning that despite extensive evaluation of patients' medical history, blood tests, radiological studies, and liver biopsy, up to 20% of ALF cases remain indeterminate.

The frequent consequence of ALF is acute hepatic encephalopathy (A type of HE), a spectrum of neuropsychiatric symptoms ranging from subtle cognitive impairment to coma [21]. ALF-evoked HE develops as a result of accumulating toxic doses of liver metabolites, that may eventually pass from the circulation to the brain. Importantly, HE is often accompanied by massive systemic inflammation and severe intracranial hemodynamic alterations [22,23]. Cerebral edema defined as a pathological increase in total brain water leading to elevation of brain volume and intracranial pressure is one of the most serious complications of ALF, accompanied by impaired cerebral blood flow or even life-threatening herniation.

The scale of HE is often graded following the West Haven criteria (WHC) grade, the I–IV diagnostic scale range from minimal cognitive disturbances, sleep-wake cycle impairments, apathy, ataxia, up to coma and death [24]. Rapid cerebral edema diagnosis is essential to prevent irreversible brain damage. Unfortunately, diagnosis and scale determination of cerebral edema is difficult, despite patients displaying symptoms such as hypertension, a slow heart rate, abnormal reflexes, and loss of the reaction of the pupils to light. In addition, a head CT scan may reveal changes in the junction between gray and white brain matter, compression of the fluid-filled spaces, and loss of the brain surface folds (sulci). However, CT imaging and WHC evaluation of ALF patients are not a routine part of the liver disease diagnostic panel, especially in smaller health centers and in undeveloped countries.

Pathogenesis of HE is multifactorial, with several key factors that determine clinical manifestation, of which the dominant role of ammonia was repeatedly reported. However, lack of correlation between clinical picture and ammonia level is relatively frequent [25–28]. This clinically relevant fact often results from divergent factors affecting ammonia measurement, such as the lack of a unified methodology (venous or arterial blood for ammonia measurement, sample storage, temperature, pH- changes), and clinical determinants, including disease stage, renal function, sarcopenia, diet, etc. [28–30].

Significant but poorly explored is the blood–brain barrier (BBB) impairment during ALF. The BBB is a selective structure that, in normal conditions, guards the passage of neurotoxic substances into the brain. The BBB composes the basement membrane, endothelial monolayer, pericytes, astrocytes end-feet, and at molecular level, many specialized proteins comprising tight, adherens junctions, and intracellular matrix. Alternation in each of these components can disrupt BBB integrity [31]. Ultrastructural analysis of the ALF patients' cerebral cortex tissue confirmed structural BBB abnormalities [32], pointing to its potential role in the liver–brain crosstalk that may occur in ALF. However, details of BBB impairment, visible at both cellular and molecular levels, underlying this process are complex and are of continuous interest.

There is a need to identify more specific factors of ALF development to reduce patient death or the requirement for liver transplantation. The lack of ALF prognostic biomarkers makes the diagnostic appraisal of suspected cases strongly dependent on the interpretation of serum biochemistry and other routine laboratory tests and imaging evaluation to

carefully rule out alternative causative factors of ALF. The liver enzymes activity panel: ALT, AST, GGT, ALP assisted with total bilirubin, and creatine is the standard laboratory screening procedure to define liver damage and liver dysfunction using blood samples. Of note, in this context, the AST measurement can be a reliable substitute for ALT in determining the injury when the latter is unavailable, whereas GGT is considered a less reliable ALP substitute [33,34].

1.3. Micro RNA

Micro RNAs (miRNAs) are small, approximately 18–23 nucleotides long, members of small non-coding RNAs which can negatively regulate gene expression at the mRNA level [35,36]. The first human miRNA was described in 2000 [37], and up to date, approximately 2700 human miRNAs have been described [open-source miRNA database "miRbase", https://www.mirbase.org/, accessed on 22 November 2021]. It is estimated that approximately 50% of miRNAs are expressed from "non-coding" transcripts since the rest are located in the introns of protein-coding genes and are generally cotranscribed with their host genes and expressed separately [36].

In a general view, most miRNAs are transcribed by RNA polymerase II and then processed into a shorter hairpin-shaped precursor miRNA (pre-miRNA) by the class 2 nuclear RNase III Drosha complexed with DGCR8 [38]. Pre-miRNA is then exported from the nucleus into the cytoplasm by exportin 5 protein (Exp-5) [39]. Here, the pre-miRNAs proceed into 18–23 nucleotides long duplexes by RNase III enzyme Dicer-1. Finally, mature miRNAs (single-stranded) are incorporated into a stable multi-component protein complex called RISC which "guides" miRNAs into 3′ UTR sequence of the target mRNA [35]. The 3′ UTR blockage by partial base pairing with miRNA interrupts further translation. An alternative mechanism of action assumes that binding of miRNA leads to faster deadenylation of mRNA thereby decreasing mRNA stability and inducing their degradation [40].

miRNAs can act as negative regulators of gene expression at the posttranscriptional level by interacting with the 3′-untranslated region (3′-UTR) of the target mRNA sequence. Partial paring disturbs translation since complete pairing results in miRNA-mRNA complex degradation by nucleases [36]. In addition, miRNAs also exert their regulatory effects through some non-canonical ways: pri-miRNAs, the precursors of miRNAs, encode short peptides with regulatory functions; miRNAs are involved in the activation of Toll-like Receptors (TLRs); miRNAs upregulate the expression of specific proteins, and so forth [41]. Due to the complexity of these regulatory mechanisms, it is not surprising that miRNAs have been confirmed to be crucial players in many molecular pathways. The discovery of cell-free miRNAs in various body fluids, such as plasma, serum, saliva, urine, cerebrospinal fluid, bronchial lavage, suggests that miRNAs might act as signaling molecules outside the cell and may serve as suitable biomarkers that may support diagnosis and monitoring of treatment response for a variety of diseases [42–44]. MiRNAs expression profiles in body fluids present by definition a specific pattern that may exclude passive release from the injured cells and suggest its more selective release [45,46]. Furthermore, there is growing evidence that miRNAs can act as potential biomarkers that may be sensitive and specific for early diagnosis, prognosis, and therapeutic interventions, especially through their stability and easy detection in plasma or serum.

2. Study Concept and Data Analysis Strategy

The study concept was based on the assumption that the molecular signature of the ALF in the blood may include molecules originating from peripheral organs, including the liver and the brain. First, we performed a systematic search in the electronic database MEDLINE via Pubmed access [www.ncbi.nlm.nih.gov/pubmed, accessed on 22 November 2021] and Elsevier Scopus [www.scopus.com, accessed on 22 November 2021] for original publications published from 1 January 2011 up to 1 July 2021 focusing on ALF patients and miRNA expression studies using subjectively selected keywords based on literature

revision and medical subject heading. The summary of searching steps underlying our systematic review is presented in Figure 1. Two authors of the review (K.O.G. and K.M.) independently extracted data using eligibility criteria and removed duplicates. To unify the data based on full-text screening, we excluded studies on patients with unclear ALF diagnosis (e.g., relation to chronic liver disease, multifactorial disease problems interfering with ALF, such as alcohol history, liver transplantation, or pregnancy (Figure 1)).

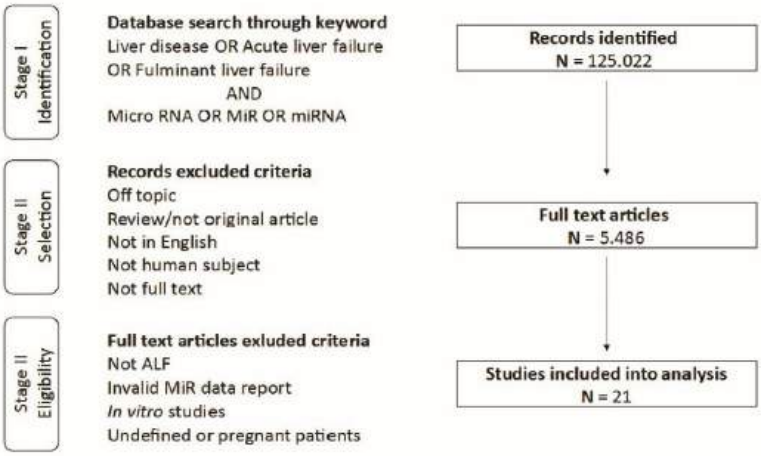

Figure 1. Flow chart of database searching and selection process.

After identification of repeatedly reported differential blood-based miRNAs, in the next step, we revised reports of the differential miRNA profiles in the liver and urine with a search for the overlap between the miRNA alterations in these specimens. Thus, we verified the number of up and down-regulated miRNAs in serum and plasma samples and the number of miRNAs reported to be both up and down-regulated. Finally, we addressed the questions of ALF specificity and miRNAs functional implications in the pathogenesis of the disease. To this end, we performed a computational prediction of genes and pathways regulated by the selected miRNAs.

MiRNAs target genes and biological pathways analysis were performed using freeware tools available on DIANA website (http://diana.imis.athena-innovation.gr, accessed on 22 November 2021). Micro-T tool based on the miRBase database was used to identify potential miRNA target genes and pathways. TargetScan was used to study the prediction of the potential target genes and demonstrate relationships between them. The MiRPath v3.0 pathways analysis was performed to verify the involvement of selected genes in biological pathways according to the Kyoto Encyclopedia of Genes and Genomes (KEGG, http://www.genome.ad.jp/kegg, accessed on 22 November 2021), [47]. MiRPath was also used to visualize the clustering of the selected miRNAs based on their influence on molecular pathways. The Diana tool enables clustering miRNAs dependent on the subset which targets regulated pathways and the significance level of the interaction. Heatmaps used for visualization and other graphs were performed using licensed Prism 5 software by GraphPad, San Diego, CA, USA.

3. Research Summary

Database search resulted in 5486 full-text references. After removing duplicates, not-related, not-human, or the in vitro studies, articles were screened for eligibility (Figure 1). As a result, 21 publications covering data collected from a total number of 852 patients from seven different countries were included in our analysis (Table 2). As mentioned in the introduction, the etiology of the ALF is much varied. The causes of ALF are summarized in Figure 2 panel A.

Table 2. Summary of the included studies.

Ref.	Year	Disease	Specimen	Region	N **	Analysis Method	Changed miRNAs	Notes
[48]	2013	Acetaminophen overdose	Plasma	UK	129	RT-qPCR	1	
[49]	2017	ALF *	Plasma/liver	USA	9/4	RT-qPCR	1	
[50]	2015	HBV	Liver	Italy	4/10	RT-qPCR	17	
[51]	2014	ALF *	Serum	USA	35/12	RT-qPCR	1	
[52]	2014	ALF *	Serum	Germany	63/15	RT-qPCR	3	
[53]	2015	Acetaminophen overdose	Serum	Netherlands	6/6	RT-qPCR, HiSeq 2000	3	
[54]	2017	Acetaminophen/HBV	Serum	USA	16/22	Illumina HiSeq 2000	132	
[55]	2020	Acetaminophen overdose	Serum	Netherlands	1	RT-qPCR, NGS	57	Case Study
[56]	2019	HBV	Liver	China	4/10	Microarray	38	
[57]	2017	ALF *	Serum/liver	USA	39/5	RT-qPCR	1	
[38]	2017	Drug induced ALF	Serum	USA	78/40	GeneChip® 3.0 miRNA microarrays	1	
[58]	2020	Acetaminophen overdose	Serum	UK	18/undefined	RT-qPCR	7	HE grade diagnosed
[59]	2011	Acetaminophen overdose	Serum	UK	53/25	RT-qPCR	2	Controlled Clinical Trial/HE grade
[60]	2018	HBV	Liver	India	30/6	Microarray	1	
[61]	2021	Acetaminophen overdose	Serum	USA	194	RT-qPCR	7	HE grade diagnosed
[62]	2014	Acetaminophen overdose	Serum/plasma	USA	42/12	RT-qPCR	3	
[63]	2018	HBV	Serum	China	55	RT-qPCR	3	
[64]	2015	Acetaminophen overdose	Serum	UK	68	RT-qPCR (miScript System)	6	
[65]	2015	Acetaminophen overdose	Serum/urine	USA	8/10	Whole genome PCR array	12	
[66]	2016	Acetaminophen overdose	Serum/liver	Germany	9/4	RT-qPCR	1	same cohort as Chowdhary et al., 2017 [49]
[67]	2018	Acetaminophen overdose	Serum	USA	8/10	RT-qPCR	4	same cohort as Yang X et al., 2015 [65]

* Cases characteristics Chowdhary et al. [49], non-acetaminophen ALF (8 unknown, 1 mushroom); Dubin et al. [51], 20 acetaminophen, 6 autoimmune hepatitis, 4 drug-induced, 2 hepatitis A virus, 1 hepatitis B virus, 1 Epstein Barr virus; John et al. [52], viral hepatitis (NSR, n 5 4; SR, n 5 5), toxic liver injury (NSR, n 5 11; SR, n 5 12), Budd–Chiari syndrome (NSR, n 5 5; SR, n 5 0), Wilson's disease (NSR, n 5 1; SR, n 5 0), autoimmune hepatitis (NSR, n 5 2; SR, n 5 2), and indeterminate etiology (NSR, n 5 19; SR, n 5 2); Roy et al. [57], 15 drug-induced toxicity, 3 Budd–Chiari Syndrome, 7 viral hepatitis, 3 autoimmune hepatitis, 11 unknown, and 10 livers biopsies from ALF patients. ** Number of patients/ number of healthy controls.

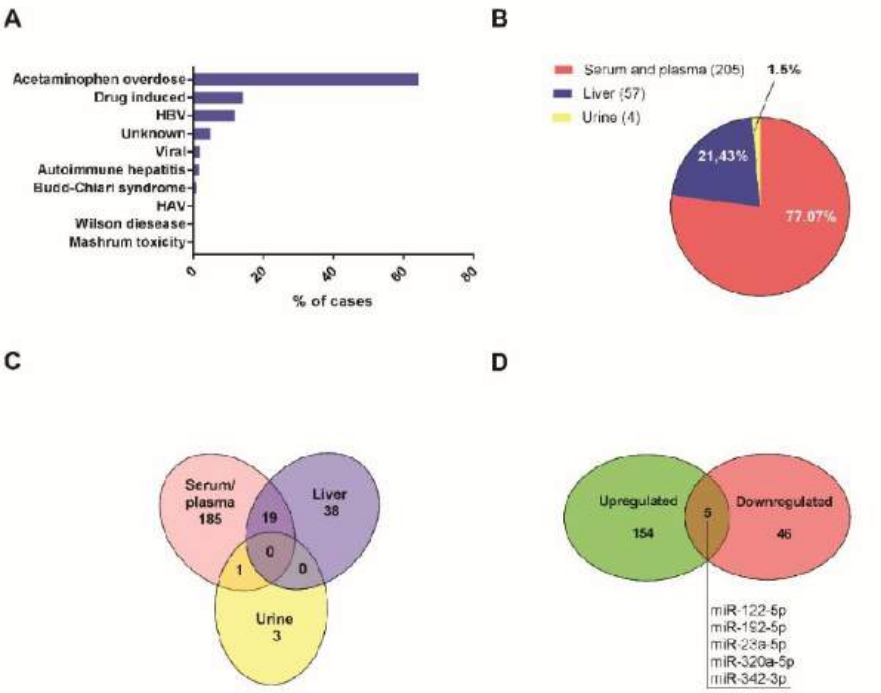

Figure 2. Characteristics of the last decade's studies on differential miRNAs in ALF. Etiology of ALF (panel (**A**)). Pie chart presenting the number of differently expressed miRNAs in the referred specimens (panel (**B**)). Venn diagram showing overlapping of differently expressed miRNAs (panel (**C**)). The number of up and down-regulated miRNAs in serum and plasma samples. Overlapped miRNAs were regulated both up and down as was based on selected publications (panel (**D**)).

The etiological distribution of ALF cases delivered from our study search corresponds well to clinical data described in the literature [68,69]. In total, 78% of patients suffered from drug-induced ALF, the vast majority were acetaminophen overdose cases (548 patients). Various viral infections were a direct cause of 14% of ALF, whereas only 7% of ALF causes were due to other conditions that included almost 5% of undetermined causes. The rarest single reports cases were Hepatitis A, Wilson disease, and mushroom *Amanita phalloides* poisoning.

MiRNAs expression data were mostly derived from blood samples (serum or plasma) of ALF patients. Five studies described miRNAs detected in ALF liver biopsies predominantly taken from HBV patients due to their significant diagnostic value in hepatitis management [70]. A single study evaluated miRNAs levels in the urine of ALF patients in relation to serum [65], (Table 2 and Figure 2, panel B).

In total, 246 differentially expressed miRNAs were reported in selected publications. The number of 217 miRNAs, were identified in a single study. Seven of the studies detected single miRNAs, while 4 of the studies used microarray or quantitative real-time polymerase chain reaction (qPCR) to recognize the large patch of miRNAs sequences (Table 2). Studies by Krauskopf et al., 2017 [54], 2020 [55] used the next-generation sequencing (NGS) technique to interrogate global miRNA signature. The advantage of NGS technology is its ability to detect the whole miRNome, including structural modifications of miRNAs, also called iso-miRNAs [54,55]. Due to the variety of techniques used in the referred studies, a quantitative single miRNA expression meta-analysis was not able to be performed. Data presenting all differently expressed miRNAs reported in patients with ALF, including information about the direction of observed miRNA level change (Up or

Down), miRNA family membership, ALF cause, and respective reference, are shown in Supplementary Tables S1 and S2. It is noteworthy that the descriptions of some miRNAs used in the publications do not match the current nomenclature requirement due to the lack of a descriptor tag indicating from which double-stranded RNA the sequence comes from (3p/5p) or miRNA identity was uncertain. This fact, unfortunately, disallows the input of such data into the online database. These miRNAs are included in Supplementary Tables S1 and S2 and marked with a star.

The Venn diagram demonstrates the distribution of miRNAs in evaluated specimens (Figure 2, panel C). From 205 miRNAs differently expressed in ALF serum/plasma, only 19 overlap with 57 miRNAs detected in liver biopsies. In turn, from four miRNAs (miR-9-3p; miR-320a; miR-375, and miR-940) described in the urine of ALF patients, only miR 320a was also found upregulated in the serum. From miRNAs differently expressed in ALF patients serum/plasma 75% were upregulated since for five different miRNAs direction of change was inconsistent throw-out analyzed publications (Figure 2, panel D).

Despite the evident progress in current methodologies, diagnosis of ALF still has several limitations and relies on verification of liver enzymes in the patients' blood. As an effort to better integrate miRNAs data into a full clinical picture, we established relations between miRNAs (represented in Table 3) and serum biochemical parameters. In our study, serum biochemical data were available from 16 publications covering 740 patients with ALF. Three of the studies also confirmed HE using the WHC scale [58,59,61]. We analyzed the clinical parameters of ALF patients and correlated the two most consistently evaluated parameters: ALT and AST plasma levels, to differently expressed miRNAs observed in each study (Figure 3).

This comparison revealed wide dispersion in measured enzyme activity between patients inside the group and matched side to side cohorts. This is not surprising taking into account a divergent etiology, clinical appearance of ALF, and variable analytical methods and instruments used. More importantly, approximately 95% of evaluated ALF patients presented much higher ALT/AST activity in the blood than is considered as norm range by American College of Gastroenterology guidelines [71]. Regarding evaluated miRNAs, only miR-122-5p has been explored in most of the studies, and, importantly in all cases, upregulation of miR-122-5p accompanied the ALT/AST activity increase. This clearly indicates its potential as a biomarker in human ALF.

Understanding and analysis of miRNAs data gathered by various techniques and, without row data available, are quite problematic. In subsequent steps, we decided to exclude miRNAs that were reported ones or sequences not precisely defined. We focused on serum and plasma samples due to the majority of available data and the potent diagnostic role of circulating miRNAs. Thus, we selected a set of altered 25 miRNAs repetitively reported in ALF patients' blood in a minimum of two independent reports (Table 3). Of selected 25 miRNAs, miR-122-5p was referred in 14 publications, whereas 15 miRNAs were reported in only two publications.

Across miRNAs assessed in this study, notable trends in the genomic spread of dysregulated miRNA genes were observed. Firstly, the dysregulated miRNAs were seen across multiple chromosomes. No defined chromosomes were showing a higher proportion of their miRNAs becoming dysregulated during ALF. Selected miRNAs were distributed on 17 different chromosomes including chromosome X (Table 3). Analysis of ALF-related miRNAs revealed seven miRNAs that have cluster organization (cluster members are shown in Table 3). Furthermore, miR-23b and miR-24-1 localized on chromosome 9 belong to the same cluster thus are probably expressed in an interdependent manner. We also checked Supplementary Table S1 for the occurrence of miRNA cluster members listed in Table 3. Indeed, four more cluster members were elevated in ALF patients: miR-103b, miR-301b, miR-194, and miR-27b suggesting the possibility of common upregulation of the whole miRNAs clusters.

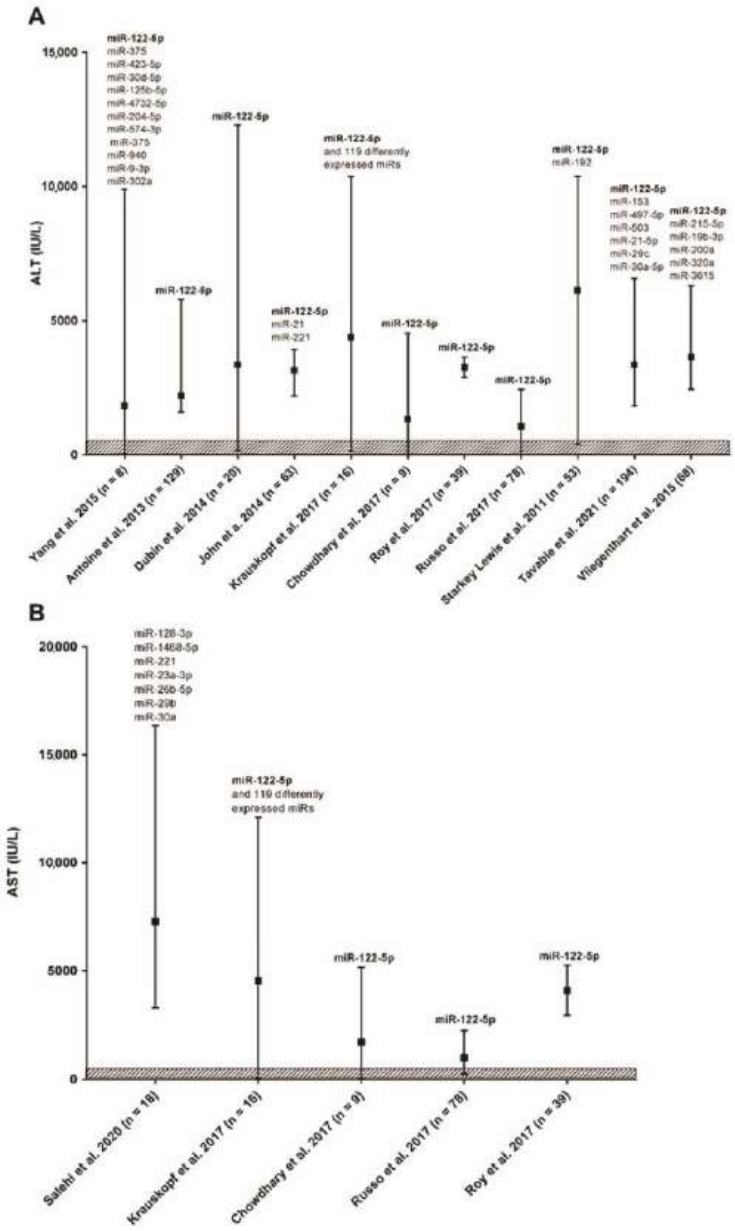

Figure 3. ALT (panel (**A**)) and AST (panel (**B**)) activity in serum of ALF patients with upregulated miRNAs. Black squares represent medians, bars range of measured ALT activity. Above the bars are listed differently expressed miRNAs reported in each cohort. The norm value for ALT/AST activity in blood for people without risk factors for liver disease in international units per liter (IU/L), according to the American College of Gastroenterology, is indicated as a patterned box.

Table 3. Characteristics of miRNAs reported in at least two independent publications carried on ALF patients.

Family	MiRNA	Localization	Cluster Members	References
miR-10	miR-99a-5p	chr21		[54,55]
miR-10	miR-100-5p	chr11		[54,55]
miR-10	miR-125b-5p	chr11		[54,55,65,72]
miR-103	miR-103a-3p	chr20	miR-103b-2	[54,55]
miR-103	miR-107	chr10		[54,55]
miR0122	miR-122-5p	chr18	miR-122b	[49,53,54,65]
miR-1224	miR-1224-5p	chr3		[38,48,51,52,59,61–64]
miR-1247	miR-1247-5p	chr14		[54,55]
miR-1307	miR-1307-5p	chr10		[54,55]
miR-130	miR-130b-3p	chr22	miR-301b	[54,55]
miR-148	miR-148a-3p	chr7		[54,55]
miRR-192	miR-192-5p	chr11	miR-194-2; miR-6750; miR-6749	[54,55,64]
miR-194	miR-194-5p	chr1	miR-215	[54,55]
miR-21	miR-21-5p	chr17		[54,61,62]
miR-221	miR-221-3p	chrX		[52,54]
miR-23	miR-23b-3p	chr9	miR-27b; miR-3074; miR-24-1	[54,55]
miR-24	miR-24-3p	chr9	miR-27b; miR-3074; miR-23b	[54,55]
miR-30	miR-30a-5p	chr6		[54,61]
miR-30	miR-30d-5p	chr8		[55,65]
miR-320	miR-320a	chr8		[54,64,67]
miR-320	miR-320b	chr1		[54,67]
miR-320	miR-320c	chr18		[54,67]
miR-320	miR-320d	chr13		[54,67]
miR-375	miR-375	chr2		[55,65]
miR-188	miR-660-5p	chrX		[54,55]

Considering that the spectrum of ALF symptoms includes both liver and brain alterations, we checked the tissues' distribution pattern of selected miRNAs using Human miRNATissueAtlas [https://ccb-web.cs.uni-saarland.de/tissueatlas/patterns, accessed on 22 November 2021]. Among the selected 25 miRNAs elevating in the ALF patients' blood, miR-122-5p, miR-21-5p, miR-320c, and miR-148 represented highly specific liver expression. In turn, miR-125b-5p, miR-103a-3p, miR-107, miR-99a-5p, and miR-100-5p were more abundant in human brain tissue compared to the liver (Figure 4). The normalized expression of ALF-induced miR-125b-5p was two-fold higher than the miR-122-5p expression level indicated in the liver, a well-proven example of a high tissue-specific miRNA sequence [73,74]. Other miRNAs presented relatively low and comparable expression patterns in both organs. We have also verified selected miRNAs regarding their plasma and serum expression levels. Worth noting here, in normal conditions, highly specific for the liver or the brain miRNA: miR-122-5p and miR-125b-5p are in the plasma at a relatively low level. The significant increase in miRNAs expression level observed in ALF patients might suggest tissue impairment. Of note, in this context, the role of circulating miR-122-5p as a marker of liver damage was previously widely discussed [73,75,76]. However, to our knowledge, there are no data documenting alterations of circulating miRNAome and CNS impairments observed as a result of liver failure.

Equalized enrichment of liver and brain-origin miRNAs in the blood samples of ALF patients, prompted us to formulate the hypothesis of the miRNAs-dependent axis between liver and brain. Moreover, ALF-caused alterations in CNS and/or impaired BBB integrity may induce the release of brain-specific miRNAs into the circulatory system reflecting CNS status and ALF molecular signature.

The most significant pathways prediction for twenty-five differentially expressed miRNAs in serum of ALF patients was performed and visualized as a single color scale heatmap (Figure 5). The biological pathways were predicted with mirPath v3.0., after setting up the target prediction threshold on a 0.8. As a result, 94 significant KEGG pathways were found (Figure 5).

miR name	Brain	Liver	Serum
hsa-miR-99a-5p	837.52	56.37	2.07
hsa-miR-100-5p	698.46	21.93	2.31
hsa-miR-125b-5p	8215.40	253.46	1.72
hsa-miR-103a-3p	1063.85	69.60	4.91
hsa-miR-107	1003.37	90.73	6.81
hsa-miR-122-5p	10.03	4468.00	3.64
hsa-miR-1224-5p	288.55	444.34	5.13
hsa-miR-1247-5p	4.58	10.02	1.83
hsa-miR-1307-5p	15.33	21.80	0.00
hsa-miR-130b-3p	25.92	69.71	4.50
hsa-miR-148a-3p	163.26	1322.83	4.16
hsa-miR-192-5p	29.82	289.44	3.40
hsa-miR-194-5p	25.93	745.91	1.97
hsa-miR-21-5p	1166.68	4616.64	8.02
hsa-miR-221-3p	253.18	14.65	3.66
hsa-miR-23b-3p	1149.08	387.48	3.05
hsa-miR-24-3p	601.61	447.55	6.00
hsa-miR-30a-5p	530.83	363.59	2.76
hsa-miR-30d-5p	346.74	511.73	5.84
hsa-miR-320a	585.76	330.97	6.79
hsa-miR-320b	294.93	163.49	6.94
hsa-miR-320c	539.97	2007.10	10.09
hsa-miR-320d	221.56	141.61	7.65
hsa-miR-375	215.65	4.43	1.35
hsa-miR-660-5p	25.69	14.90	3.56

Figure 4. Normalized miRNA expression level in the normal human brain, liver, and serum analyzed by Human miRNATissueAtlas of miRNAs expression. MiRNAs with distinctive high expression are highlighted.

KEGG pathways cover a large number of genes reflecting a diversity of biological processes. However, the expression of genes within particular pathways provides a way to estimate the activity of certain biological processes.

Worth noting, five of the identified pathways associated with 15 of the analyzed miRNAs belongs to the same KEGG pathway functional group called "Cellular community" containing: Focal adhesion (hsa04520); Adherens junction (hsa04530); Tight junction (hsa04540); and Gap junction (hsa04550) (Figure 6).

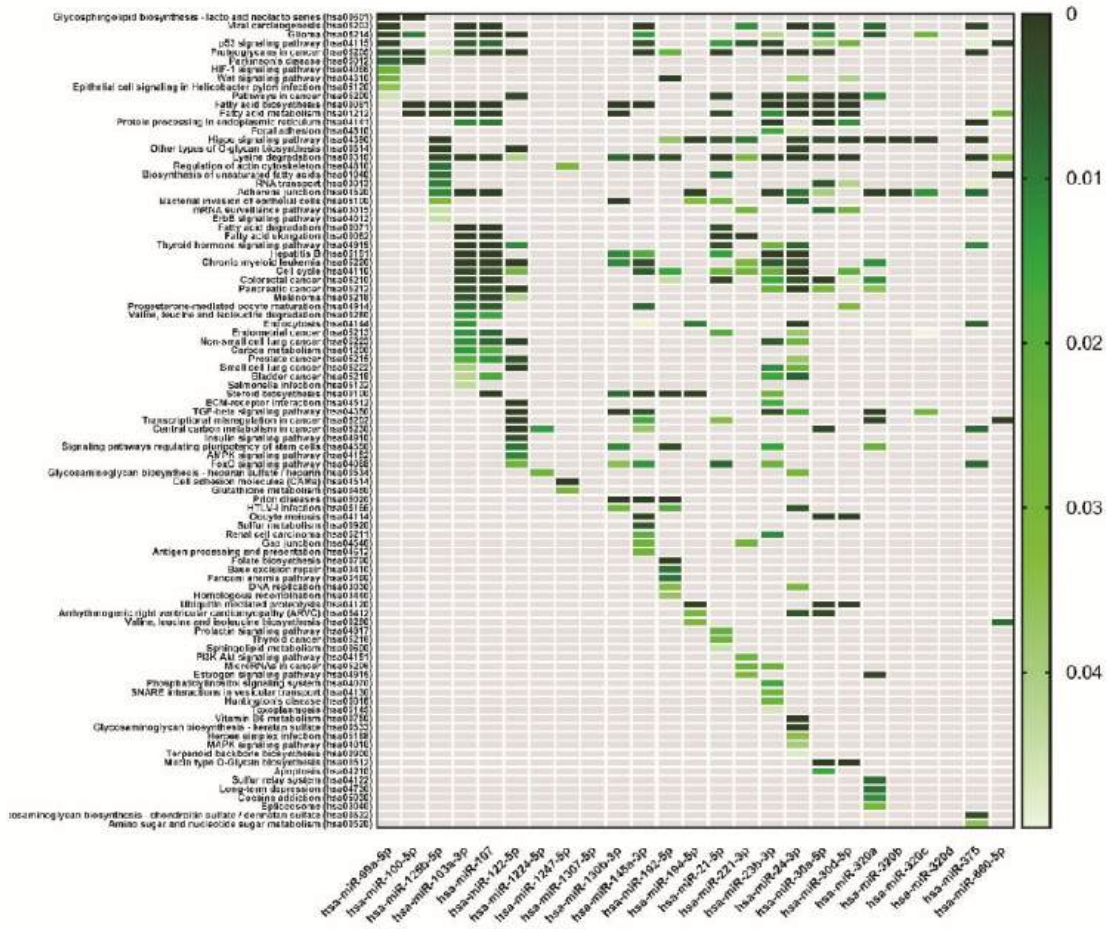

Figure 5. Heatmap of significant pathways predicted by DIANA-miRPath (v.3.0) for twenty-seven differentially expressed miRNAs in serum of ALF patients. KEGG pathways classification analysis of differentially expressed miRNAs is presented on the y-axis and miRNAs on the x-axis. The color intensity represents the p-value with dark green as the most significant predicted miRNA-pathway interactions ($p < 0.05$ in Fisher's Exact Test).

We designed a dendrogram grouping miRNAs related to Cellular community pathways according to their biological function regarding miRNAs family membership (Figure 6). The branch lengths represent a difference between miRNAs and show variability in miRNAs' abundances in their regulation of specific pathways. A dendrogram revealed strong relation between miR-103a-3p and miR-107 in controlling the adherens junction pathway. On the other hand, it displayed a distinct CAMs pathway regulating miR-1247 from the other evaluated miRNAs.

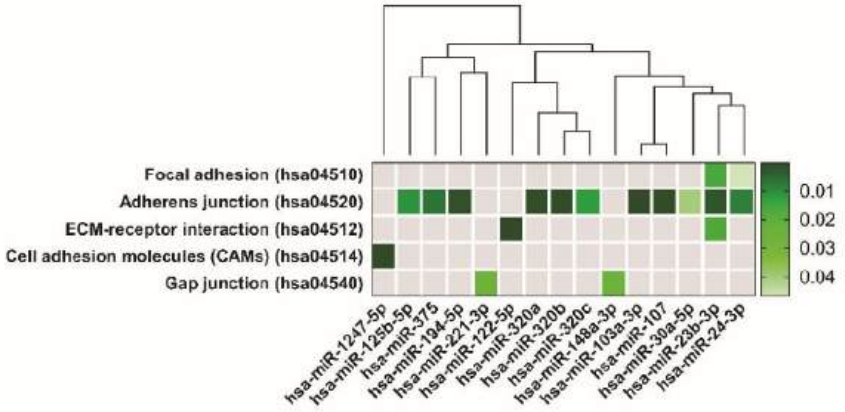

Figure 6. Heatmap of selected pathways predicted by DIANA-miRPath miRNA with hierarchical cluster dendrogram achieved by the linkage clustering method via TarBase. KEGG pathways classification analysis of differentially expressed miRNAs is presented on the y-axis and miRNAs on the x-axis. The color intensity represents the p-value with dark green as the most significant predicted miRNA-pathway interactions ($p < 0.05$ in Fisher's Exact Test).

The only member of the cellular community pathways group not predicted in DIANA-miRPath analysis was a "Tight junction". However, this pathway covers the inter-alia tight junction protein 1 (*TJP1*) gene, which is also a significant part of the Adherens junction pathway and a predicted target of miR-23b-3p and miR-320a (Table 4). Tight junction KEGG pathway contains also Cingulin/RhoA/Rock signaling path regulating Zonula occludens-1 barrier formation in endothelial tight junctions [77]. Genes of those three signaling proteins are potentially controlled by miRNAs included in our analysis (miR-125-3p for Cingulin; miR-122-5p, miR-375 for RhoA, and miR-148a for Rock) [78–81]. Moreover, a significant amount of scientific reports convincingly point out the role of miR-122-5p in the regulation of occludin expression, one of the most prominent tight junction proteins [82–84]. Those merely points to the need for a deeper discussion of the results obtained using a bioinformatics algorithm.

Table 4. ALF-related miRNAs comprising cellular community KEGG pathways and its predicted gene targets.

KEGG Pathways	miRNA Name	Gene Name	*p*-Value
Focal adhesion	miR-125b-2-3p	*BRAF, GSK3B, ITGB1, LAMB1, THBS1, PAK2, VCL, RHOA, PAK3, FYN, PPP1R12A, JUN, DIAPH1, VEGFC, PTEN, BIRC2*	4.7×10^{-2}
	miR-23b-3p	*TLN2, PRKCA, ACTN2, MYLK4, MET, ITGB1, FLNC, CRKL, THBS1, MYL12B, PAK2, TNXB, PP1CC, BCL2, EGFR, FYN, COL6A1, AKT2, ARHGAP35, PPP1R12A, MAPK9, PIK3R3, CCND1, CTNNB1, COL4A2, PAK6, PRKCB, LAMC1, PDK', LAMC2, ITGA6, VEGFA, PTEN, MAPK1, KDR, MYL12A, XIAP, COL4A1, PPP1CB*	1.5×10^{-2}
	miR-24-3p	*ACTB, GSK3B, ITGB1, ITGB8, FLNC, LAMA5, PIK3CB, CAV1, PXN, RAF1, BCAR1, EGFR, MYLK2, CAV2, ITGB5, ARHGAP35, PTK2, ITGA11, JUN, PIK3R3, CTNNB1, DIAPH1, FLNB, FLT1, FLNA, RAC1, LAMC1, VASP, FN1, TNC, BIRC3, PDPK1, VEGFA, TLN1, KDR, LAMA4*	4.6×10^{-2}

Table 4. *Cont.*

KEGG Pathways	miRNA Name	Gene Name	*p*-Value
Adherens junction	miR-125b-5p	*ERBB2, ACTG1, IQGAP1, MLLT4, CTNNB1, CTNNA1, WASF2, INSR, FGFR1*	10^{-2}
	miR-103a-3p	*ACTB, CTNND1, ACTG1, IQGAP1, IGF1R, MLLT4, SMAD4, CTNNB1, CTNNA1, ACTN1, WASF2, CSNK2A1, FARP2, PTPRJ, CDC42, PTPRB, MAP3K7, CREBBP, TGFBR2, PVRL1*	1.2×10^{-3}
	miR-107	*ACTB1, CTNND1, ACTG1, IQGAP1, IGF1R, PTPRF, MLLT4, DMAD4, CTNNB1, CTNNA1, ACTN1, WASF2, CSNK2A1, FARP2, PTPRJ, MAPK3, CDC42, PVRL3, PTPRB, MAP3K7, CREBBP, TGFBR2, PVRL1*	3×10^{-4}
	miR-194-5p	*TGFBR1, WASL, ACTG1, LMO7, IGF1R, PVRL4, RAC1*	9.6×10^{-4}
	miR-23b-3p	*ACTN2, CSNK2A2, MET, CTNND1, LMO7, IQGAP1, SMAD3, EGFR, TJP1, FYN, SMAD4, CTNNB1, WASF2, CSNK2A1, FARP2, PTPRJ, YES1, MAPK1, TGFBR2*	1.9×10^{-3}
	miR-24-3p	*ACTB, CSNK2A2, SMAD2, PVRL2, SMAD3, EGFR, PTPRF, NLK, CTNNB1, CTNNA1, WASF2, RAC1, EP300, YES1, CREBBP, TGFBR2, PVRL1*	8.4×10^{-3}
	miR-30a-5p	*CSNK2A2, MET, WASL, CTNND1, SMAD2, PTPN1, IGFR1, EGFR, NLK, RAC1, PVRL3, MAPK1, MAP3K7, TGFBR2*	3.9×10^{-2}
	miR-320a	*SMAD2, SMAD3, IGF1R, VCL, TJP1, CDH1, CTNNB1, RAC1, INSR, SSX2IP, MAPK1, TGFBR2*	5.2×10^{-4}
	miR-320b	*SMAD3, TJP1, CDH1, CTNNB1, RAC1, INSR, SSX2IP, MAPK1*	4×10^{-4}
	miR-320c	*SMAD3, TJP1, CDH1, CTNNB1, INSR, SSX2IP, MAPK1*	1.2×10^{-3}
	miR-375	*ERBB2, IQGAP1, PTPN1, IGF1R, PTPRF, RHOA, CTNNA1, WASF2, CDC42, PARD3*	6.9×10^{-4}
ECM-receptor interaction	miR-122-5p	*ITGB1, ITGB8, LAMB1, LAMA5, COL27A1, AGRN, LAMC3, COL4A2, COL5A1, COL4A3, CD44*	8.3×10^{-8}
	miR-23b-3p	*ITGB1, THBS1, TNXB, COL6A1, COL4A2, LAMC1, LAMC2, ITGA6, HMMR, COL4A1*	1.6×10^{-2}
Cell adhesion molecules	miR-1247-5p	*CDH2*	9.6×10^{-7}
Gap junction	miR-148a-3p	*ADCY1, ADCY8, GNAS, MAP2K5, RAF1, TUBB, TUBB6, CDK1, KRAS, TUBA8, GNA11, TUBB2B, SOS1, GNAI2, HTR2C, TUBB4B, MAPK1, GRB2, GNAI1*	2.4×10^{-2}
	miR-221-3p	*RAF1, CDK1, PDGFD, GNAI2, GJA1*	2.6×10^{-2}

The link between gene pathways related to intercellular communication and ALF-induced miRNAs may indicate its involvement in the pathomechanism of ALF. Indeed, hepatic decomposition referred to as a loss of intercellular integrity, easily recognized during histological evaluation, is one of the marks of acetaminophen toxicity [85–87].

The "Cellular community" pathways encompass genes coding proteins strongly associated with the BBB structure and function [31]. Considering KEGG pathways obtained from our analysis, the adherens junction pathway (hsa:04514), is related to most selected miRNAs (Figure 6). In the context of BBB function and structure maintaining, the adherens junction pathway (hsa:045020), with cell adhesion molecules pathway (hsa:04514), including *CDH2* gene coding for cadherin 2 involved in the regulation of protein localization to adherens junction, is critically involved. Adherens junction is a cell–cell junction composed of the epithelial cadherin–catenin complex at which the cytoplasmic face of the plasma membrane is attached to actin filaments. The adherens junction pathway genes control vascular permeability [88] and brain vascular homeostasis [89]. In our study hsa:045020

pathway constitutes the majority (more than 40 defined genes; Table 4). Among them, genes: *ACTG1*, *ACTB*, *ACTB1*, and *ACTN1* encoding different isoforms of actin (β and γ actin) [90], are critical for actin cytoskeleton changes linked with the functioning of several cellular processes (cell shape maintenance, chemotaxis, cell movement, adhesion, and other). Other genes: *CTNNB1*, *CTNNA1*, *CTNND1* coding isoforms of catenin proteins, form a complex that constitute adherens junctions and are necessary for the maintenance of epithelial cell layers by regulating cell growth and adhesion. The catenin proteins also anchor the actin cytoskeleton. The adhesion molecules of nectin family genes: *PVRL4*, *PVRL1*, *PVRL3* are involved in the formation of cell–cell junctions, including adherens junctions and synapses. The cytoskeletal proteins vinculin and tight junction protein 1, coded by *VIN* and *TJP1*, respectively, regulate adherens junctions, are associated with cell–cell and cell–matrix junctions, and are involved in anchoring F-actin to the membrane. Tight junctions regulate the movement of ions and macromolecules between endothelial and epithelial cells. The large groups of genes are engaged in signaling processes that include genes coding different types of receptors of tyrosine phosphatase (*PTPRJ*, *PTPRB*, *PTPRF*, *PTPN1*), tyrosine kinase 2 (*ERBB2*), mitogen-activated protein kinases (*MAP3K7*, *MAPK3*, *MAPK1*), and genes associated with transforming growth factor-β signaling pathway (*SMAD2*, *SMAD3*, *SMAD4*, *TGFBR1*, *TGFBR2*), one of the most important and complex signaling pathways in vascular development and homeostasis of the brain vessel. The TGF-β signaling pathway dysfunction has been repeatedly linked to various cerebrovascular diseases [91–93] and implicated in BBB formation and permeability control by regulating tight and adherens junctions [94–96].

The loss of intercellular structural components is linked with the cytoplasmic side of focal adhesions molecules (hsa:04520) pathway comprising genes coding proteins forming large molecular complexes linking transmembrane receptors (e.g., integrins). One of a hallmark of focal adhesions is the clustering of integrins to the actin cytoskeleton and mediating intercellular signaling. These heterogeneous complexes are highly dynamic structures and are targeted by regulatory signals of proteins *GSK3B*, *PI3K*, *PTEN*, *JUN*, *RHOA*, *PAK2*, and *PAK3*. At the brain vasculature level, direct signal-transducing regulates cerebrovascular morphogenesis and endothelial barrier integrity. Recent reports have shown that focal adhesion kinase (*PTK2*) colocalizes with the tight junction proteins occludin and Zonula occludens-1 (*ZO-1*) [97]. The protein coded by the *PTK2* gene is also one of the key molecules that negatively regulate RhoA activity, an important regulator of BBB integrity [98]. In this context, studies have demonstrated that increased RhoA activity leads to disassembly of the complexes within cell-cell junctions and subsequent barrier disruption [96,97]. The proteins coded by *VEGFA*, *-B*, *-C* genes are members of the vascular endothelial growth factor family, best known as key regulators of angiogenesis. VEGFs play a role in blood and lymph vessel development and homeostasis. Particularly, *VEGFA* is involved in angiogenesis and vasculogenesis, and *VEGFC* mediates mostly lymphangiogenesis but also has angiogenic activity [99]. No less importantly, the gene coding for vasodilator-stimulated phosphoprotein (*VASP*) is associated with filamentous actin formation, and likely plays a widespread role in cell adhesion and motility. *VASP*, which function is regulated by the cyclic nucleotide-dependent kinases PKA and PKG may also be involved in the intracellular signaling pathways that regulate integrin–ECM interactions [100].

Consequently, the extracellular matrix (ECM)-receptor interaction (hsa:04512) pathway was highlighted in our analysis (Figure 6). The pathway is relevant for neural tissue, in particular by composing a cellular architecture, synapse arrangement, and stabilization. In addition, the hsa:04512 pathway may be of importance in the regulation of neuroplasticity and memory formation [101]. In total, 18 different reported genes were annotated in our study into this pathway (Table 4). They include 3 member genes of integrin heterodimeric transmembrane receptors composed of alpha and a beta subunit: *ITGB1*, *ITGB8*, *ITGA6*, all of which are involved in cell adhesion and signaling. Next, collagenous (6 members of collagen family: *COL4A1*, *COL4A2*, *COL5A1*, *COL4A3*, *COL6A1*, *COL27A1*) and non-

collagenous, the extracellular matrix glycoproteins (5 members of laminin family: *LAMC1*, *LAMC2*, *LAMC3*, *LAMB1*, *LAMA5*), constituents of the basement membranes with TNXB gene coding tenascin-X controlling production and assembly of collagen. Collagen isoforms *COL4A1* and *COL4A2*, defined in a GWAS analysis of cerebral small vessel disease as mainly expressed in the brain endothelial cells [93]. Collagens and laminins, implicated in a wide variety of biological processes, regulate cell adhesion, signaling, neurite outgrowth, differentiation, migration, and metastasis. The abnormal expression of laminin family genes is associated with clinical outcomes of, for example, hepatocellular carcinoma [102].

Since, the ECM features are high concentrations of proteoglycans and glycosaminoglycans, of particular relevance are changes of heparan sulfate proteoglycans (HSPGs), a family of glycoproteins with a small heparan sulfate side chain. HSPGs, attached directly to the ECM, are secreted into the extracellular space, or on secreted vesicles [103]. HSPGs that are present throughout the neural ECM are potentially secreted by activated glial cells and seem to be associated with neurodegenerative diseases [104]. Interestingly, HSPGs are likewise involved in BBB organization [105] and control monocytes' crossing the BBB. Agrin, encoded by the gene *AGRN*, is a large HSPG essential for neuromuscular synapse formation [106]. Finally, the *CD44* gene, coding for multifunctional cell surface adhesion receptor for hyaluronan or hyaluronic acid and several other ligands, including osteopontin, collagens, and matrix metalloproteinases [107], was indicated in our analysis. In line with the above, hyaluronan-mediated motility receptor (*HMMR* gene) was likewise defined. Another matricellular protein with multiple effects due to interacting with structural components of the ECM is thrombospondin 1 coded by the *THBS1* gene [108].

Within the Gap junction pathway (hsa04550), including the intercellular membrane channels facilitating the direct cytoplasmic exchange of small molecules between adjacent cells, apart from the *GJA1* gene encoding one of the most important connexin proteins, connexin-43 (Cx43), most of the genes constitute a family of genes encoding tubulins: *TUBB*, *TUBB6*, *TUBA8*, *TUBB2B*, *TUBB4B*. Tubulins compose microtubules, key cytoskeletal fibers, which regulate the shape, polarity, migration, and survival of the endothelial cells [109]. Tubulins posttranslational modifications, including acetylation, play an important role in the control of microtubule structure and microtubule-based cellular functions [110]. The family of genes encoding different subunits of G protein-coupled receptors (*GPRC*, *GNAS*, *GNA11*, *GNAI2*) is the largest family of cell surface receptors involved in signal transduction. The GPRC proteins, characterized by a 7-transmembrane domain structure with an extracellular N-terminus and an intracellular C-terminus, play roles in a variety of physiological processes, including immune responses, neurotransmission, cardiac function, and sensory functions and their aberrant activity or expression contributes to some of the most prevalent human diseases [111]. The GPRC proteins via RhoA activation induce cytoskeletal changes, important for cell migration. Another gene in the hsa04550 pathway, *GRB2*, coding for Growth Factor Receptor Bound Protein 2, is associated with Hepatitis C and Hepatitis E. In turn, Calmodulin-activated adenylate cyclases (*ADCY1* and *ADCY8* genes) generate cAMP. Collectively, despite indicated genes pathways that are important for BBB maintenance, a causational relationship between differential miRNA expression identified in body fluids and these features of BBB alterations needs to be established in future studies.

The current knowledge, based mostly on clinical imaging (MRI) and experimental studies, indicates persistent BBB dysfunction with increased paracellular barrier permeability in ALF patients [112]. The previous postmortem studies on the human brain revealed signs of both the cytotoxic and vasogenic components of ALF-induced edema [32]. BBB increased permeability in the subacute and chronic HE stages is significantly less visible than changes observed in acute HE when there can be uncontrolled extravasation of plasma proteins, leukocytes, and vasogenic edema formation [113]. Additionally, the signs of systemic or neuroinflammation during ALF or as a result of associated bacterial infection can disturb the integrity of the BBB. In line with a few studies referring to BBB alterations in ALF patients, more pieces of evidence were supplied from studies of animal models which

documented BBB permeability changes upon ALF [113–115]. How BBB alterations and recovery occur in ALF is unclear. One hypothesized scenario suggests fast sealing of the barrier due to compensatory overexpression of BBB-composing proteins, the presence of which can be found along blood vessels in ALF-injured tissue. In addition to protein expression changes, BBB functioning is controlled by protein-protein interactions and signaling. Since the recovery of the BBB is a complex process, the final effect is dependent on the expression pattern of functional proteins, and involves the *de novo* organization of junction proteins. BBB components disorganization leads to increased para-cellular permeability. Whose duration, and intensity may override any effect described as increased transcellular permeability [114].

4. Concluding Remarks

The increase in the concentrations of liver metabolites reaching the CNS dominates in ALF pathology thus ALF alters the homeostasis of the liver-brain axis by a mechanism encompassing the expression changes of hundreds of genes responsible, i.e., for the antioxidant system, neurotransmitter biogenesis, inflammatory processes, to list a few. MiRNAs acting as modulators of gene expression seems to play a crucial but still not well-established role in this control. Therefore, a more detailed analysis of selected miRNAs in the context of signaling mediators and/or biomarker candidates for ALF offering new safety biomarkers that outperform current markers in terms of their sensitivity, specificity, and clinical predictivity is highly desirable.

The systematic analysis of 21 reports from the last decade, involving a total of 852 participants, determined 205 circulating miRNAs to be altered in the blood of ALF patients regardless of the study design and methodology. From this set, 25 miRNAs were repetitively altered in independent reports. We selected 25 miRNAs, emerging predominantly from the analyses of blood samples obtained from the acetaminophen-overdose group of patients, that represented the most promising biomarker candidates for a diagnostic panel for symptomatic ALF. A new miRNAs identification is the most promising alternatives for classic liver tests. In addition, the small RNAs are also attractive therapeutic targets due to their size, and relative availability of chemically designed active substances, in a safe manner used in targeting and inhibiting miRNAs.

Since acetaminophen-induced liver injury results in oncotic necrosis, hepatocyte-specific miRNAs elevate in the plasma within hours, such as miR-122-5p or miR-192-5p, proposed so far as a potential biomarker tool. The diagnostic potential of miR-122-5p to predict the subsequent onset of early liver injury was documented experimentally before the increase in ALT [115,116]. In preclinical studies, both miR-122-5p and miR-192-5p were enriched in liver tissue and presented dose- and exposure-dependent changes in plasma, paralleled with serum ALT/AST levels and the liver histology [115,116]. Although our systematic search revealed considerable coincidence of miR-122-5p elevation and ALT/AST increase in plasma of ALF patients throughout the studies, no other miRNAs seem to serve as a diagnostic tool.

The results of our analysis offer a selected group of miRNAs to assess whether pathognomonic "signatures" of circulating miRs could serve as a diagnostic tool. The defined common pathways targeted by selected miRNAs are highly relevant to cellular community processes and suggest that loss of intercellular structural and functional components may result in brain dysfunction with BBB impairment. However, a causational relationship between differential miRNAs expression identified in the circulation and clinical features observed in ALF patients has to be demonstrated in further study.

The difference between the criteria of scientific research and clinical application is quite obvious. Therefore, imperfect verification of potential miRNA biomarkers candidates may limit the study impact. An applicable biomarker must not only be significantly differentially expressed, but also be capable of defining the correlation with the outcome of patients. It is important to underline that the analyzed studies were differently designed and several cohort comparisons were made in each study. In general, the limited sample

size or not an equal group of patients was the limitation of this study, thus a larger sample size cohort is needed for further assessment implementation. Moreover, miRNA detection could also be affected by measurement principle, method, instrument, and the researcher operation. Thus the sample size may be a critical point to guarantee the accuracy for detection. In addition, the absolute quantitative detection protocol may be crucial, as well as a correction of the circulating biomarker to healthy volunteers. In clinical application, the level of circulating biomarkers is under the influence of multiple individual classifications, including age, gender, lifestyle, and so on. Unfortunately, only very few reports performed validation experiments and used greater cohorts, which might be the reason for the limited reproducibility of the reported data.

In terms of the conceptual design, around 61.9% of the studies employed a candidate approach, 23.8% used high throughput technologies, and 9.5% combined these two strategies. miRNA profiles were determined usually by RT-qPCR. However, other methodologies, including NGS, or microarray were also used. Importantly, the methods used differ in terms of sensibility and accuracy, especially at single-base resolution.

For RNA extracted from biofluids, the source of microRNAs and the extraction method that may influence recovery and the outcome is substantial. RNA isolation kits were preferentially used over the manual methods. The normalization of the signal is another limitation since a normalizer choice is critical and challenging. In analyzed studies, the internal normalization controls for relative quantification in RT-qPCR were not identical. The universal endogenous control is unlikely to be discovered and a suitable reference should be assessed every time considering the different biological conditions of the samples.

The complete understanding of both positive and negative roles of miRNAs in the pathomechanism of ALF might be a problem. Highly specific to the brain tissue miRNAs may impair cell function, exacerbate brain injury-causing oxidative stress, neurotransmission, metabolism, neuroinflammation, attendant cell morphology, and cell composition, contributing to increased brain dysfunction. The literature revealed that, for example, increased miR-125b expression has been observed in the cerebellum, hippocampus, medial frontal gyrus [117], temporal lobe neocortex [118,119], and frontal cortex [120] in AD patients. Thus, observed in ALF upregulation of brain-specific miRNAs in the serum might reflect neuronal status. Additionally, released miRNAs may dependently or independently on the disease status affect microcirculation, endothelial activation, and lead to the BBB disturbance. Alternatively, after the BBB cross, miRNAs may initiate a cascade of neurological processes alterations mediated by oxidative stress, brain signaling, neuroinflammation, etc., to list a major. These concepts open an exciting new chapter on disease mechanisms and strategies for developing non-invasive tools to monitor the proneness and progression of the disease. It is noteworthy that miRNA identification may in the future contribute to elucidating the ALF pathogenesis via the liver-brain axis since the miRNAs signature of ALF clinical features (e.g., edema) is still missing. Among the newly available techniques, circulating miRNAs have an irrefutable potential for new biomarkers and expand our understanding of ALF pathophysiology. It is crucial in the future to elucidate the mechanisms governing the biogenesis, sorting, release, and uptake of secreted miRNAs. Other questions remaining to be addressed in the future are whether miRNAs convey physiologically important information for specific cells and whether secretion is a selective process. Determination of sufficient amounts of secreted miRNAs required for cell-to-cell signaling is essential to understanding the role of secreted miRNAs in the pathological processes regulation. Next, the secretion and incorporation of miRNAs are generally conserved phenomena that remain unexplored. Nevertheless, the miRNA-mediated form of inter-organ communication presents an open field for the understanding of signal and molecule transfer between cells. The elucidation of this information transfer system will be important in understanding many biological processes.

Supplementary Materials: The following are available online at https://www.mdpi.com/article/10.3390/ijms23010224/s1.

Author Contributions: K.O.-G., K.M. and M.Z.; conceptualization and methodology, K.O.-G. and K.M.; literature investigation, K.O.-G. and K.M.; writing—original draft preparation, M.Z.; writing—review and editing, M.Z.; funding acquisition. All authors have read and agreed to the published version of the manuscript.

Funding: This research was funded by the National Science Centre of the Republic of Poland (NCN), grant number 2015/19/B/NZ4/01902.

Institutional Review Board Statement: Not applicable.

Informed Consent Statement: Not applicable.

Data Availability Statement: Not applicable.

Conflicts of Interest: The authors declare no conflict of interest.

References

1. Mokdad, A.A.; Lopez, A.D.; Shahraz, S.; Lozano, R.; Mokdad, A.H.; Stanaway, J.; Murray, C.J.L.; Naghavi, M. Liver cirrhosis mortality in 187 countries between 1980 and 2010: A systematic analysis. *BMC Med.* **2014**, *12*, 145. [CrossRef] [PubMed]
2. Asrani, S.K.; Devarbhavi, H.; Eaton, J.; Kamath, P.S. Burden of liver diseases in the world. *J. Hepatol.* **2019**, *70*, 151–171. [CrossRef]
3. Beste, L.A.; Leipertz, S.L.; Green, P.K.; Dominitz, J.A.; Ross, D.; Ioannou, G.N. Trends in Burden of Cirrhosis and Hepatocellular Carcinoma by Underlying Liver Disease in US Veterans, 2001–2013. *Gastroenterology* **2015**, *149*, 1471–1482.e5. [CrossRef] [PubMed]
4. *WHO Global Health Estimates 2015: Deaths by Cause, Age, Sex, by Country and by Region, 2000–2015*; World Health Organization: Geneva, Switzerland, 2016.
5. Trey, C.; Davidson, C.S. The management of fulminant hepatic failure. *Prog. Liver Dis.* **1970**, *3*, 282–298.
6. Williams, R.; Schalm, S.W.; O'Grady, J.G. Acute liver failure: Redefining the syndromes. *Lancet* **1993**, *342*, 273–275. [CrossRef]
7. Kandiah, P.A.; Olson, J.C.; Subramanian, R.M. Emerging strategies for the treatment of patients with acute hepatic failure. *Curr. Opin. Crit. Care* **2016**, *22*, 142–151. [CrossRef]
8. Bernal, W.; Auzinger, G.; Sizer, E.; Wendon, J. Intensive care management of acute liver failure. *Semin. Liver Dis.* **2008**, *28*, 188–200. [CrossRef] [PubMed]
9. Fontana, R.J. Acute liver failure. *Curr. Opin. Gastroenterol.* **1999**, *15*, 270–277. [CrossRef] [PubMed]
10. Pimpin, L.; Cortez-Pinto, H.; Negro, F.; Corbould, E.; Lazarus, J.V.; Webber, L.; Sheron, N. Burden of liver disease in Europe: Epidemiology and analysis of risk factors to identify prevention policies. *J. Hepatol.* **2018**, *69*, 718–735. [CrossRef] [PubMed]
11. Bernal, W.; Wendon, J. Acute liver failure. *N. Engl. J. Med.* **2013**, *369*, 2525–2534. [CrossRef]
12. Andrade, R.J.; Aithal, G.P.; Björnsson, E.S.; Kaplowitz, N.; Kullak-Ublick, G.A.; Larrey, D.; Karlsen, T.H. EASL Clinical Practice Guidelines: Drug-induced liver injury. *J. Hepatol.* **2019**, *70*, 1222–1261. [CrossRef] [PubMed]
13. Wai, C.T.; Tan, B.H.; Chan, C.L.; Sutedja, D.S.; Lee, Y.M.; Khor, C.; Lim, S.G. Drug-induced liver injury at an Asian center: A prospective study. *Liver Int.* **2007**, *27*, 465–474. [CrossRef]
14. WHO. *Recommendations and Guidance on Hepatitis C Virus Self-Testing*; WHO: Geneva, Switzerland, 2021; ISBN 9789240031128.
15. OMS, (Organização Mundial da Saúde). *Global Progress Report on HIV, Viral Hepatitis and Sexually Transmitted Infections, 2021*; WHO: Geneva, Switzerland, 2021; Volume 53, ISBN 9788578110796.
16. Zumla, A.; Chakaya, J.; Khan, M.; Fatima, R.; Wejse, C.; Al-Abri, S.; Fox, G.J.; Nachega, J.; Kapata, N.; Knipper, M.; et al. World Tuberculosis Day 2021 Theme—'The Clock is Ticking'—And the world is running out of time to deliver the United Nations General Assembly commitments to End TB due to the COVID-19 pandemic. *Int. J. Infect. Dis.* **2021**, *113* (Suppl. S1), S1–S6. [CrossRef]
17. McKeating, C.; Cadden, I.; McDougall, N.; Jessop, L.; Quah, S.; Lavelle, M.; Griffths, A.; McCaughey, C. Progression from acute to chronic hepatitis B is more common in older adults. *Ulster Med. J.* **2018**, *87*, 177–180. [PubMed]
18. Sahebjam, F.; Vierling, J.M. Autoimmune hepatitis. *Front. Med.* **2015**, *9*, 187–219. [CrossRef]
19. Dong, V.; Nanchal, R.; Karvellas, C.J. Pathophysiology of Acute Liver Failure. *Nutr. Clin. Pract.* **2020**, *35*, 24–29. [CrossRef] [PubMed]
20. Aquilina, A.; Pirotta, T.; Aquilina, A. Acute liver failure and hepatic encephalopathy in exertional heat stroke. *BMJ Case Rep.* **2018**, *2018*, bcr-2018-224808. [CrossRef] [PubMed]
21. Vilstrup, H.; Amodio, P.; Bajaj, J.; Cordoba, J.; Ferenci, P.; Mullen, K.D.; Weissenborn, K.; Wong, P. Hepatic encephalopathy in chronic liver disease: 2014 Practice Guideline by the American Association for the Study Of Liver Diseases and the European Association for the Study of the Liver. *Hepatology* **2014**, *60*, 715–735. [CrossRef] [PubMed]
22. Bjerring, P.N.; Eefsen, M.; Hansen, B.A.; Larsen, F.S. The brain in acute liver failure. A tortuous path from hyperammonemia to cerebral edema. *Metab. Brain Dis.* **2009**, *24*, 5–14. [CrossRef]
23. Wendon, J.; Cordoba, J.; Dhawan, A.; Larsen, F.S.; Manns, M.; Nevens, F.; Samuel, D.; Simpson, K.J.; Yaron, I.; Bernardi, M.; et al. EASL Clinical Practical Guidelines on the management of acute (fulminant) liver failure. *J. Hepatol.* **2017**, *66*, 1047–1081. [CrossRef]
24. Weissenborn, K. Hepatic Encephalopathy: Definition, Clinical Grading and Diagnostic Principles. *Drugs* **2019**, *79*, 5–9. [CrossRef]

25. Haj, M.; Rockey, D.C. Ammonia levels do not guide clinical management of patients with hepatic encephalopathy caused by cirrhosis. *Am. J. Gastroenterol.* **2020**, *115*, 723–728. [CrossRef] [PubMed]
26. Sheasgreen, C.; Lu, L.; Patel, A. Pathophysiology, diagnosis, and management of hepatic encephalopathy. *Inflammopharmacology* **2014**, *22*, 319–326. [CrossRef]
27. Gonzalez, J.J.; Tapper, E.B. A Prospective, Blinded Assessment of Ammonia Testing Demonstrates Low Utility Among Front-Line Clinicians. *Clin. Gastroenterol. Hepatol.* **2021**, 1–2. [CrossRef] [PubMed]
28. Shalimar; Sheikh, M.F.; Mookerjee, R.P.; Agarwal, B.; Acharya, S.K.; Jalan, R. Prognostic Role of Ammonia in Patients With Cirrhosis. *Hepatology* **2019**, *70*, 982–994. [CrossRef] [PubMed]
29. Amodio, P.; Montagnese, S. Lights and shadows in hepatic encephalopathy diagnosis. *J. Clin. Med.* **2021**, *10*, 341. [CrossRef]
30. Rahimi, R.S.; Rockey, D.C. Hepatic Encephalopathy: Pharmacological Therapies Targeting Ammonia. *Semin. Liver Dis.* **2016**, *36*, 48–55. [CrossRef]
31. Abbott, N.J.; Patabendige, A.A.K.; Dolman, D.E.M.; Yusof, S.R.; Begley, D.J. Structure and function of the blood-brain barrier. *Neurobiol. Dis.* **2010**, *37*, 13–25. [CrossRef]
32. Kato, M.; Hughes, R.D.; Keays, R.T.; Williams, R. Electron microscopic study of brain capillaries in cerebral edema from fulminant hepatic failure. *Hepatology* **1992**, *15*, 1060–1066. [CrossRef]
33. Kong, L.Z.; Chandimali, N.; Han, Y.H.; Lee, D.H.; Kim, J.S.; Kim, S.U.; Kim, T.D.; Jeong, D.K.; Sun, H.N.; Lee, D.S.; et al. Pathogenesis, early diagnosis, and therapeutic management of alcoholic liver disease. *Int. J. Mol. Sci.* **2019**, *20*, 2712. [CrossRef]
34. Torbenson, M.; Washington, K. Pathology of liver disease: Advances in the last 50 years. *Hum. Pathol.* **2020**, *95*, 78–98. [CrossRef]
35. Ha, M.; Kim, V.N. Regulation of microRNA biogenesis. *Nat. Rev. Mol. Cell Biol.* **2014**, *15*, 509–524. [CrossRef] [PubMed]
36. Wang, H.; Wang, H.; Duan, X.; Liu, C.; Li, Z. Digital quantitative analysis of microRNA in single cell based on ligation-depended polymerase colony (Polony). *Biosens. Bioelectron.* **2017**, *95*, 146–151. [CrossRef]
37. Pasquinelli, A.E.; Reinhart, B.J.; Slack, F.; Martindale, M.Q.; Kuroda, M.I.; Maller, B.; Hayward, D.C.; Ball, E.E.; Degnan, B.; Müller, P.; et al. Conservation of the sequence and temporal expression of let-7 heterochronic regulatory RNA. *Nature* **2000**, *408*, 86–89. [CrossRef] [PubMed]
38. Russo, M.W.; Steuerwald, N.; Norton, H.J.; Anderson, W.E.; Foureau, D.; Chalasani, N.; Fontana, R.J.; Watkins, P.B.; Serrano, J.; Bonkovsky, H.L. Profiles of miRNAs in serum in severe acute drug induced liver injury and their prognostic significance. *Liver Int.* **2017**, *37*, 757–764. [CrossRef] [PubMed]
39. Lund, E.; Güttinger, S.; Calado, A.; Dahlberg, J.E.; Kutay, U. Nuclear Export of MicroRNA Precursors. *Science* **2004**, *303*, 95–98. [CrossRef]
40. Wu, L.; Fan, J.; Belasco, J.G. MicroRNAs direct rapid deadenylation of mRNA. *Proc. Natl. Acad. Sci. USA* **2006**, *103*, 4034–4039. [CrossRef]
41. Dragomir, M.P.; Knutsen, E.; Calin, G.A. SnapShot: Unconventional miRNA Functions. *Cell* **2018**, *174*, 1038. [CrossRef]
42. Witwer, K.W. Circulating MicroRNA biomarker studies: Pitfalls and potential solutions. *Clin. Chem.* **2015**, *61*, 56–63. [CrossRef]
43. Turchinovich, A.; Weiz, L.; Langheinz, A.; Burwinkel, B. Characterization of extracellular circulating microRNA. *Nucleic Acids Res.* **2011**, *39*, 7223–7233. [CrossRef]
44. McDonald, J.S.; Milosevic, D.; Reddi, H.V.; Grebe, S.K.; Algeciras-Schimnich, A. Analysis of circulating microRNA: Preanalytical and analytical challenges. *Clin. Chem.* **2011**, *57*, 833–840. [CrossRef]
45. Mar-Aguilar, F.; Mendoza-Ramírez, J.A.; Malagón-Santiago, I.; Espino-Silva, P.K.; Santuario-Facio, S.K.; Ruiz-Flores, P.; Rodríguez-Padilla, C.; Reséndez-Pérez, D. Serum circulating microRNA profiling for identification of potential breast cancer biomarkers. *Dis. Markers* **2013**, *34*, 163–169. [CrossRef] [PubMed]
46. Noferesti, S.S.; Sohel, M.M.H.; Hoelker, M.; Salilew-Wondim, D.; Tholen, E.; Looft, C.; Rings, F.; Neuhoff, C.; Schellander, K.; Tesfaye, D. Controlled ovarian hyperstimulation induced changes in the expression of circulatory miRNA in bovine follicular fluid and blood plasma. *J. Ovarian Res.* **2015**, *8*, 81. [CrossRef]
47. Kanehisa, M.; Sato, Y.; Kawashima, M.; Furumichi, M.; Tanabe, M. KEGG as a reference resource for gene and protein annotation. *Nucleic Acids Res.* **2016**, *44*, D457–D462. [CrossRef] [PubMed]
48. Antoine, D.J.; Dear, J.W.; Lewis, P.S.; Platt, V.; Coyle, J.; Masson, M.; Thanacoody, R.H.; Gray, A.J.; Webb, D.J.; Moggs, J.G.; et al. Mechanistic biomarkers provide early and sensitive detection of acetaminophen-induced acute liver injury at first presentation to hospital. *Hepatology* **2013**, *58*, 777–787. [CrossRef] [PubMed]
49. Chowdhary, V.; Teng, K.Y.; Thakral, S.; Zhang, B.; Lin, C.H.; Wani, N.; Bruschweiler-Li, L.; Zhang, X.; James, L.; Yang, D.; et al. miRNA-122 Protects Mice and Human Hepatocytes from Acetaminophen Toxicity by Regulating Cytochrome P450 Family 1 Subfamily A Member 2 and Family 2 Subfamily E Member 1 Expression. *Am. J. Pathol.* **2017**, *187*, 2758–2774. [CrossRef] [PubMed]
50. Diaz, G.; Zamboni, F.; Tice, A.; Farci, P. Integrated ordination of miRNA and mRNA expression profiles. *BMC Genom.* **2015**, *16*, 767. [CrossRef]
51. Dubin, P.H.; Yuan, H.; Devine, R.K.; Hynan, L.S.; Jain, M.K.; Lee, W.M.; Larson, A.M.; Liou, I.; Davern, T.; Fix, O.; et al. Micro-RNA-122 levels in acute liver failure and chronic hepatitis C. *J. Med. Virol.* **2014**, *86*, 1507–1514. [CrossRef]
52. John, K.; Hadem, J.; Krech, T.; Wahl, K.; Manns, M.P.; Dooley, S.; Batkai, S.; Thum, T.; Schulze-Osthoff, K.; Bantel, H. MicroRNAs play a role in spontaneous recovery from acute liver failure. *Hepatology* **2014**, *60*, 1346–1355. [CrossRef]

53. Krauskopf, J.; Caiment, F.; Claessen, S.M.; Johnson, K.J.; Warner, R.L.; Schomaker, S.J.; Burt, D.A.; Aubrecht, J.; Kleinjans, J.C. Application of high-throughput sequencing to circulating microRNAs reveals novel biomarkers for drug-induced liver injury. *Toxicol. Sci.* **2015**, *143*, 268–276. [CrossRef]
54. Krauskopf, J.; De Kok, T.M.; Schomaker, S.J.; Gosink, M.; Burt, D.A.; Chandler, P.; Warner, R.L.; Johnson, K.J.; Caiment, F.; Kleinjans, J.C.; et al. Serum microRNA signatures as "liquid biopsies" for interrogating hepatotoxic mechanisms and liver pathogenesis in human. *PLoS ONE* **2017**, *12*, e0177928. [CrossRef]
55. Krauskopf, J.; Gosink, M.M.; Schomaker, S.; Caiment, F.; Warner, R.; Johnson, K.; Kleinjans, J.; Aubrecht, J. The microrna-based liquid biopsy improves early assessment of lethal acetaminophen poisoning: A case report. *Am. J. Case Rep.* **2020**, *21*, e919289. [CrossRef]
56. Pan, K.; Wang, Y.; Pan, P.; Xu, G.; Mo, L.; Cao, L.; Wu, C.; Shen, X. The regulatory role of microRNA-mRNA co-expression in hepatitis B virus-associated acute liver failure. *Ann. Hepatol.* **2019**, *18*, 883–892. [CrossRef]
57. Roy, S.; Bantel, H.; Wandrer, F.; Schneider, A.T.; Gautheron, J.; Vucur, M.; Tacke, F.; Trautwein, C.; Luedde, T.; Roderburg, C. miR-1224 inhibits cell proliferation in acute liver failure by targeting the antiapoptotic gene Nfib. *J. Hepatol.* **2017**, *67*, 966–978. [CrossRef] [PubMed]
58. Salehi, S.; Tavabie, O.D.; Verma, S.; McPhail, M.J.W.; Farzaneh, F.; Bernal, W.; Menon, K.; Agarwal, K.; Aluvihare, V.R. Serum MicroRNA Signatures in Recovery From Acute and Chronic Liver Injury and Selection for Liver Transplantation. *Liver Transplant.* **2020**, *26*, 811–822. [CrossRef] [PubMed]
59. Starkey Lewis, P.J.; Dear, J.; Platt, V.; Simpson, K.J.; Craig, D.G.N.; Antoine, D.J.; French, N.S.; Dhaun, N.; Webb, D.J.; Costello, E.M.; et al. Circulating microRNAs as potential markers of human drug-induced liver injury. *Hepatology* **2011**, *54*, 1767–1776. [CrossRef] [PubMed]
60. Singh, A.K.; Rooge, S.B.; Varshney, A.; Vasudevan, M.; Bhardwaj, A.; Venugopal, S.K.; Trehanpati, N.; Kumar, M.; Geffers, R.; Kumar, V.; et al. Global microRNA expression profiling in the liver biopsies of hepatitis B virus–infected patients suggests specific microRNA signatures for viral persistence and hepatocellular injury. *Hepatology* **2018**, *67*, 1695–1709. [CrossRef]
61. Tavabie, O.D.; Karvellas, C.J.; Salehi, S.; Speiser, J.L.; Rose, C.F.; Menon, K.; Prachalias, A.; Heneghan, M.A.; Agarwal, K.; Lee, W.M.; et al. A novel microRNA-based prognostic model outperforms standard prognostic models in patients with acetaminophen-induced acute liver failure. *J. Hepatol.* **2021**, *75*, 424–434. [CrossRef]
62. Ward, J.; Kanchagar, C.; Veksler-Lublinsky, I.; Lee, R.C.; McGill, M.R.; Jaeschke, H.; Curry, S.C.; Ambros, V.R. Circulating microRNA profiles in human patients with acetaminophen hepatotoxicity or ischemic hepatitis. *Proc. Natl. Acad. Sci. USA* **2014**, *111*, 12169–12174. [CrossRef]
63. Wen, Y.; Peng, S.F.; Fu, L.; Fu, X.Y.; Wu, D.X.; Liu, B.J.; Tan, D.M.; Ouyang, Y. Serum levels of miRNA in patients with hepatitis B virus-associated acute-on-chronic liver failure. *Hepatobiliary Pancreat. Dis. Int.* **2018**, *17*, 126–132. [CrossRef]
64. Vliegenthart, A.D.B.; Shaffer, J.M.; Clarke, J.I.; Peeters, L.E.J.; Caporali, A.; Bateman, D.N.; Wood, D.M.; Dargan, P.I.; Craig, D.G.; Moore, J.K.; et al. Comprehensive microRNA profiling in acetaminophen toxicity identifies novel circulating biomarkers for human liver and kidney injury. *Sci. Rep.* **2015**, *5*, 15501. [CrossRef] [PubMed]
65. Yang, X.; Salminen, W.F.; Shi, Q.; Greenhaw, J.; Gill, P.S.; Bhattacharyya, S.; Beger, R.D.; Mendrick, D.L.; Mattes, W.B.; James, L.P. Potential of extracellular microRNAs as biomarkers of acetaminophen toxicity in children. *Toxicol. Appl. Pharmacol.* **2015**, *284*, 180–187. [CrossRef] [PubMed]
66. Zhao, H.; Zhang, X.; Dai, Z.; Feng, Y.; Li, Q.; Zhang, J.H.; Liu, X.; Chen, Y.; Feng, H. P2X7 Receptor Suppression Preserves Blood-Brain Barrier through Inhibiting RhoA Activation after Experimental Intracerebral Hemorrhage in Rats. *Sci. Rep.* **2016**, *6*, 23286. [CrossRef] [PubMed]
67. Yu, D.; Wu, L.; Gill, P.; Tolleson, W.H.; Chen, S.; Sun, J.; Knox, B.; Jin, Y.; Xiao, W.; Hong, H.; et al. Multiple microRNAs function as self-protective modules in acetaminophen-induced hepatotoxicity in humans. *Arch. Toxicol.* **2018**, *92*, 845–858. [CrossRef]
68. Stravitz, R.T.; Lee, W.M. Acute liver failure. *Lancet* **2019**, *394*, 869–881. [CrossRef]
69. Rovegno, M.; Vera, M.; Ruiz, A.; Benítez, C. Current concepts in acute liver failure. *Ann. Hepatol.* **2019**, *18*, 543–552. [CrossRef]
70. Jeong, S.H.; Lee, H.S. Hepatitis a: Clinical manifestations and management. *Intervirology* **2010**, *53*, 15–19. [CrossRef]
71. Kwo, P.Y.; Cohen, S.M.; Lim, J.K. ACG Clinical Guideline: Evaluation of Abnormal Liver Chemistries. *Am. J. Gastroenterol.* **2017**, *112*, 18–35. [CrossRef] [PubMed]
72. Yang, D.; Yuan, Q.; Balakrishnan, A.; Bantel, H.; Klusmann, J.H.; Manns, M.P.; Ott, M.; Cantz, T.; Sharma, A.D. MicroRNA-125b-5p mimic inhibits acute liver failure. *Nat. Commun.* **2016**, *7*, 11916. [CrossRef]
73. Bandiera, S.; Pfeffer, S.; Baumert, T.F.; Zeisel, M.B. MiR-122—A key factor and therapeutic target in liver disease. *J. Hepatol.* **2015**, *62*, 448–457. [CrossRef]
74. Jopling, C.L. Liver-specific microRNA-122: Biogenesis and function. *RNA Biol.* **2012**, *9*, 137–142. [CrossRef] [PubMed]
75. Howell, L.S.; Ireland, L.; Park, B.K.; Goldring, C.E. MiR-122 and other microRNAs as potential circulating biomarkers of drug-induced liver injury. *Expert Rev. Mol. Diagn.* **2018**, *18*, 47–54. [CrossRef]
76. Fu, S.; Wu, D.; Jiang, W.; Li, J.; Long, J.; Jia, C.; Zhou, T. Molecular biomarkers in drug-induced liver injury: Challenges and future perspectives. *Front. Pharmacol.* **2020**, *10*, 1667. [CrossRef]
77. Tornavaca, O.; Chia, M.; Dufton, N.; Almagro, L.O.; Conway, D.E.; Randi, A.M.; Schwartz, M.A.; Matter, K.; Balda, M.S. ZO-1 controls endothelial adherens junctions, cell-cell tension, angiogenesis, and barrier formation. *J. Cell Biol.* **2015**, *208*, 821–838. [CrossRef]

78. Martínez, C.; Rodinõ-Janeiro, B.K.; Lobo, B.; Stanifer, M.L.; Klaus, B.; Granzow, M.; González-Castro, A.M.; Salvo-Romero, E.; Alonso-Cotoner, C.; Pigrau, M.; et al. MiR-16 and miR-125b are involved in barrier function dysregulation through the modulation of claudin-2 and cingulin expression in the jejunum in IBS with diarrhoea. *Gut* **2017**, *66*, 1597–1610. [CrossRef]
79. Wang, S.C.; Lin, X.L.; Li, J.; Zhang, T.T.; Wang, H.Y.; Shi, J.W.; Yang, S.; Zhao, W.T.; Xie, R.Y.; Wei, F.; et al. MicroRNA-122 triggers mesenchymal-epithelial transition and suppresses hepatocellular carcinoma cell motility and invasion by targeting RhoA. *PLoS ONE* **2014**, *9*, e101330. [CrossRef] [PubMed]
80. Osmak, G.; Kiselev, I.; Baulina, N.; Favorova, O. From mirna target gene network to mirna function: mir-375 might regulate apoptosis and actin dynamics in the heart muscle via rho-gtpases-dependent pathways. *Int. J. Mol. Sci.* **2020**, *21*, 9670. [CrossRef]
81. Zhang, J.; Ying, Z.Z.; Tang, Z.L.; Long, L.Q.; Li, K. MicroRNA-148a promotes myogenic differentiation by targeting the ROCK1 gene. *J. Biol. Chem.* **2012**, *287*, 21093–21101. [CrossRef] [PubMed]
82. Jingushi, K.; Kashiwagi, Y.; Ueda, Y.; Kitae, K.; Hase, H.; Nakata, W.; Fujita, K.; Uemura, M.; Nonomura, N.; Tsujikawa, K. High miR-122 expression promotes malignant phenotypes in ccRCC by targeting occludin. *Int. J. Oncol.* **2017**, *51*, 289–297. [CrossRef]
83. Yang, W.; Xu, H.W.; Lu, X.R.; Xu, Q.F.; Tao, M.H.; Dai, Y.M. Overexpression of miR-122 Impairs Intestinal Barrier Function and Aggravates Acute Pancreatitis by Downregulating Occludin Expression. *Biochem. Genet.* **2021**. [CrossRef]
84. Liu, L.; Zhu, M.; Liu, X.; Fei, L.; Shen, J.; Chen, D. miR-122-5p regulates the tight junction of the blood-testis barrier of mice via occludin: miR-122-5p can regulate the tight junction. *Basic Clin. Androl.* **2021**, *31*, 7. [CrossRef]
85. Shojaie, L.; Iorga, A.; Dara, L. Cell death in liver diseases: A review. *Int. J. Mol. Sci.* **2020**, *21*, 9682. [CrossRef] [PubMed]
86. Yan, M.; Huo, Y.; Yin, S.; Hu, H. Mechanisms of acetaminophen-induced liver injury and its implications for therapeutic interventions. *Redox Biol.* **2018**, *17*, 274–283. [CrossRef]
87. Iwarson, S.; Lundin, P.; Hermodsson, S. Liver morphology in acute viral hepatitis related to the hepatitis B antigen. *J. Clin. Pathol.* **1972**, *25*, 850–855. [CrossRef]
88. Sanphui, P.; Biswas, S.C. FoxO3a is activated and executes neuron death via Bim in response to β-amyloid. *Cell Death Dis.* **2013**, *4*, e625. [CrossRef] [PubMed]
89. Winkler, E.A.; Bell, R.D.; Zlokovic, B.V. Central nervous system pericytes in health and disease. *Nat. Neurosci.* **2011**, *14*, 1398–1405. [CrossRef]
90. Malek, N.; Mrówczyńska, E.; Michrowska, A.; Mazurkiewicz, E.; Pavlyk, I.; Mazur, A.J. Knockout of ACTB and ACTG1 with CRISPR/Cas9(D10A) technique shows that non-muscle β and γ actin are not equal in relation to human melanoma cells' motility and focal adhesion formation. *Int. J. Mol. Sci.* **2020**, *21*, 2746. [CrossRef]
91. Von Bernhardi, R.; Cornejo, F.; Parada, G.E.; Eugenín, J. Role of TGFβ signaling in the pathogenesis of Alzheimer's disease. *Front. Cell. Neurosci.* **2015**, *9*, 426. [CrossRef] [PubMed]
92. Wang, K.; Zhao, S.; Liu, B.; Zhang, Q.; Li, Y.; Liu, J.; Shen, Y.; Ding, X.; Lin, J.; Wu, Y.; et al. Perturbations of BMP/TGF-β and VEGF/VEGFR signalling pathways in non-syndromic sporadic brain arteriovenous malformations (BAVM). *J. Med. Genet.* **2018**, *55*, 675–684. [CrossRef]
93. Chung, J.; Marini, S.; Pera, J.; Norrving, B.; Jimenez-Conde, J.; Roquer, J.; Fernandez-Cadenas, I.; Tirschwell, D.L.; Selim, M.; Brown, D.L.; et al. Genome-wide association study of cerebral small vessel disease reveals established and novel loci. *Brain* **2019**, *142*, 3176–3189. [CrossRef]
94. Zhang, Y.; Yang, X. The Roles of TGF-β Signaling in Cerebrovascular Diseases. *Front. Cell Dev. Biol.* **2020**, *8*, 567682. [CrossRef] [PubMed]
95. Armulik, A.; Genové, G.; Mäe, M.; Nisancioglu, M.H.; Wallgard, E.; Niaudet, C.; He, L.; Norlin, J.; Lindblom, P.; Strittmatter, K.; et al. Pericytes regulate the blood-brain barrier. *Nature* **2010**, *468*, 557–561. [CrossRef]
96. Bell, R.D.; Winkler, E.A.; Sagare, A.P.; Singh, I.; LaRue, B.; Deane, R.; Zlokovic, B.V. Pericytes Control Key Neurovascular Functions and Neuronal Phenotype in the Adult Brain and during Brain Aging. *Neuron* **2010**, *68*, 409–427. [CrossRef]
97. Siu, E.R.; Wong, E.W.P.; Mruk, D.D.; Sze, K.L.; Porto, C.S.; Cheng, C.Y. An occludin-focal adhesion kinase protein complex at the blood-testis barrier: A study using the cadmium model. *Endocrinology* **2009**, *150*, 3336–3344. [CrossRef] [PubMed]
98. Stamatovic, S.M.; Dimitrijevic, O.B.; Keep, R.F.; Andjelkovic, A.V. Protein kinase Cα-RhoA cross-talk in CCL2-induced alterations in brain endothelial permeability. *J. Biol. Chem.* **2006**, *281*, 8379–8388. [CrossRef]
99. Mushimiyimana, I.; Tomas Bosch, V.; Niskanen, H.; Downes, N.L.; Moreau, P.R.; Hartigan, K.; Ylä-Herttuala, S.; Laham-Karam, N.; Kaikkonen, M.U. Genomic Landscapes of Noncoding RNAs Regulating VEGFA and VEGFC Expression in Endothelial Cells. *Mol. Cell. Biol.* **2021**, *41*, MCB-00594. [CrossRef]
100. Gui, P.; Wu, X.; Ling, S.; Stotz, S.C.; Winkfein, R.J.; Wilson, E.; Davis, G.E.; Braun, A.P.; Zamponi, G.W.; Davis, M.J. Integrin receptor activation triggers converging regulation of Cav1.2 calcium channels by c-Src and protein kinase A pathways. *J. Biol. Chem.* **2006**, *281*, 14015–14025. [CrossRef]
101. Morawski, M.; Filippov, M.; Tzinia, A.; Tsilibary, E.; Vargova, L. *ECM in Brain Aging and Dementia*, 1st ed.; Elsevier B.V.: Amsterdam, The Netherlands, 2014; Volume 214, ISBN 9780444634863.
102. Jhunjhunwala, S.; Jiang, Z.; Stawiski, E.W.; Gnad, F.; Liu, J.; Mayba, O.; Du, P.; Diao, J.; Johnson, S.; Wong, K.F.; et al. Diverse modes of genomic alteration in hepatocellular carcinoma. *Genome Biol.* **2014**, *15*, 436. [CrossRef]
103. Sarrazin, S.; Lamanna, W.C.; Esko, J.D. Heparan sulfate proteoglycans. *Cold Spring Harb. Perspect. Biol.* **2011**, *3*, 1–33. [CrossRef] [PubMed]

104. Bonneh-Barkay, D.; Wiley, C.A. Brain extracellular matrix in neurodegeneration. *Brain Pathol.* **2009**, *19*, 573–585. [CrossRef] [PubMed]
105. Van Horssen, J.; Dijkstra, C.D.; De Vries, H.E. The extracellular matrix in multiple sclerosis pathology. *J. Neurochem.* **2007**, *103*, 1293–1301. [CrossRef] [PubMed]
106. Bamaga, A.; Al-Lozi, M.; Weihl, C. A novel mutation in AGRN gene causing congenital myasthenic syndrome with distal myopathy. *Neuromuscul. Disord.* **2017**, *27*, S222. [CrossRef]
107. Senbanjo, L.T.; Chellaiah, M.A. CD44: A multifunctional cell surface adhesion receptor is a regulator of progression and metastasis of cancer cells. *Front. Cell Dev. Biol.* **2017**, *5*, 18. [CrossRef]
108. Zhang, K.; Li, M.; Yin, L.; Fu, G.; Liu, Z. Role of thrombospondin–1 and thrombospondin–2 in cardiovascular diseases (Review). *Int. J. Mol. Med.* **2020**, *45*, 1275–1293. [CrossRef]
109. Hammond, J.W.; Cai, D.; Verhey, K.J. Tubulin modifications and their cellular functions. *Curr. Opin. Cell Biol.* **2008**, *20*, 71–76. [CrossRef] [PubMed]
110. Hashimoto-Komatsu, A.; Hirase, T.; Asaka, M.; Node, K. Angiotensin II induces microtubule reorganization mediated by a deacetylase SIRT2 in endothelial cells. *Hypertens. Res.* **2011**, *34*, 949–956. [CrossRef]
111. Pierce, K.L.; Premont, R.T.; Lefkowitz, R.J.; Hughes, T.H. Seven-transmembrane receptors. *Nat. Rev. Mol. Cell Biol.* **2002**, *3*, 639–650. [CrossRef]
112. Rai, V.; Nath, K.; Saraswat, V.A.; Purwar, A.; Rathore, R.K.S.; Gupta, R.K. Measurement of cytotoxic and interstitial components of cerebral edema in acute hepatic failure by diffusion tensor imaging. *J. Magn. Reson. Imaging* **2008**, *28*, 334–341. [CrossRef]
113. Kale, R.A.; Gupta, R.K.; Saraswat, V.A.; Hasan, K.M.; Trivedi, R.; Mishra, A.M.; Ranjan, P.; Pandey, C.M.; Narayana, P.A. Demonstration of interstitial cerebral edema with diffusion tensor MR imaging in type C hepatic encephalopathy. *Hepatology* **2006**, *43*, 698–706. [CrossRef]
114. Cui, W.; Sun, C.; Liu, P. Alterations of Blood-Brain Barrier and Associated Factors in Acute Liver Failure. *Gastroenterol. Res. Pract.* **2013**, *2013*, 841707. [CrossRef] [PubMed]
115. Baker, L.A.; Lee, K.C.L.; Jimenez, C.P.; Alibhai, H.; Chang, Y.; Leckie, P.J.; Mookerjee, R.P.; Davies, N.A.; Andreola, F.; Jalan, R. Circulating microRNAs reveal time course of organ injury in a porcine model of acetaminophen-induced acute liver failure. *PLoS ONE* **2015**, *10*, e0128076. [CrossRef]
116. Wang, K.; Zhang, S.; Marzolf, B.; Troisch, P.; Brightman, A.; Hu, Z.; Hood, L.E.; Galas, D.J. Circulating microRNAs, potential biomarkers for drug-induced liver injury. *Proc. Natl. Acad. Sci. USA* **2009**, *106*, 4402–4407. [CrossRef]
117. Cogswell, J.; Ward, J.; Taylor, I.; Waters, M.; Shi, Y.; Cannon, B.; Kelnar, K.; Kemppainen, J.; Brown, D.; Chen, C.; et al. Identification of miRNA Changes in Alzheimer's.pdf. *J. Alzheimer's Dis.* **2008**, *14*, 27–41. [CrossRef] [PubMed]
118. Lukiw, W.J.; Alexandrov, P.N.; Zhao, Y.; Hill, J.M.; Bhattacharjee, S. Spreading of Alzheimer's disease inflammatory signaling through soluble micro-RNA. *Neuroreport* **2012**, *23*, 621–626. [CrossRef]
119. Sethi, P.; Lukiw, W.J. Micro-RNA abundance and stability in human brain: Specific alterations in Alzheimer's disease temporal lobe neocortex. *Neurosci. Lett.* **2009**, *459*, 100–104. [CrossRef] [PubMed]
120. Banzhaf-Strathmann, J.; Benito, E.; May, S.; Arzberger, T.; Tahirovic, S.; Kretzschmar, H.; Fischer, A.; Edbauer, D. Micro RNA -125b induces tau hyperphosphorylation and cognitive deficits in Alzheimer's disease. *EMBO J.* **2014**, *33*, 1667–1680. [CrossRef] [PubMed]

Manuskryptu wysłanego do recenzji

Free Radical Biology and Medicine

Unraveling Hyperammonemia-Induced Brain Saga: The Role of miRNA-183-5p in the Endothelial Senescence and Cerebrovascular Density Decline

--Manuscript Draft--

Manuscript Number:	FRBM-D-24-01297
Article Type:	Original article
Section/Category:	Research Paper
Keywords:	ammonia; endothelium; miRNA; Senescence; in vitro
Corresponding Author:	Magdalena Zielińska Mossakowski Medical Research Institute Polish Academy of Sciences POLAND
First Author:	Karolina Orzeł-Gajowik
Order of Authors:	Karolina Orzeł-Gajowik
	Krzysztof Milewski
	Marta Obara-Michlewska
	Aleksandra Ellert-Miklaszewska
	Aneta Karpińska
	Karina Kwapiszewska
	Magdalena Zielińska
Abstract:	Peripherally, high circulating neurotoxic ammonium ions, defined as hyperammonemia, occur in different brain pathologies. However, hyperammonemia effects on cerebrovascularity and underlying mechanisms, are far from clear. Here, we verified the senescence in brain endothelium upon hyperammonemia and the role of non-coding miRNA-183-5p. Reduction of cerebrovascular density in rats with induced hyperammonemia (ip. ammonium acetate (OA) at 600 mg/kg bw for three days), evaluated by fluorescence intensity of von Willebrand marker, resembles density reduction of 12-month rats. The in silico analysis of Next Generation Sequencing miRNA profiles of OA brain cortex and plasma allows the selection of miRNA-183-5p, as endothelial senescence inducer. The miRNA-183-5p increase was detected in ammonia-treated rat brain endothelial cell line 4 (RBE4) and media-derived exosomes. Experiments in vitro on RBE4 and primary rat brain endothelial cells (PBMEC) treated with ammonia (5 mmol/L, 24h) document cell senescent phenotype characterized by: i) increased β-galactosidase staining/ fluorescence intensity; ii) increased p16 mRNA and p21mRNA expression level and p53 fluorescence intensity increase iii) changes in senescence-associated secretory phenotype (SASP) factors and iv) RBE4 cells proliferation decrease. Accordingly, analysis of i) SASP factors; ii) β-galactosidase and p53 fluorescence intensity increase in RBE4 cells at 21 DIV and PBMEC from elderly, 12-month rats. Transfection of RBE4 cells with mimic miRNA183-5p resembles senescent features: i) p53 fluorescence and ii) SASP factors. The study documents the ammonia-induced effect on brain endothelial cells towards senescence induction, which involves miR-183-5p. It thus may contribute to reduced cerebrovasculature density, a factor of cerebral dysfunction observed in hyperammonemia.
Suggested Reviewers:	Irena Ciećko-Michalska i.ciecko-michalska@uj.edu.pl
	Adam Krzystyniak a.krzystyniak@nencki.edu.pl
	Małgorzata Burek Burek_M@ukw.de
	Hassan Rashidi h.rashidi@ucl.ac.uk

Cover Letter

Mossakowski
Medical Research Institute
Polish Academy of Sciences

Department of Neurotoxicology, Head
Professor Magdalena Zielińska

phone: 48 22 608 64 70
e-mail: mzielinska@imdik.pan.pl

Warsaw, June 10, 2024

Editor-in-Chief: *Professor Kelvin J. A. Davies, PhD, DSc*

Dear Prof. *Davies*:

I am pleased to submit an original research article entitled "*Unraveling Hyperammonemia-Induced Brain Saga: The Role of miRNA-183-5p in the Endothelial Senescence and Cerebrovascular Density Decline*" by Karolina Orzeł-Gajowik1, Krzysztof Milewski, Marta Obara-Michlewska, Aleksandra Ellert-Miklaszewska, Aneta Karpińska, Karina Kwapiszewska, Magdalena Zielińska which we intend to publish in *Free Radical Biology & Medicine*. The manuscript contains 27 pages of text, five Figures, and supplement materials. This manuscript follows the Authorship statement of ethical standards for manuscripts submitted to *Free Radical Biology and Medicine*. We confirm that this work is original and is not under consideration for publication elsewhere.

In the study, we linked a hyperammonemia-induced reduction of cerebromicrovascularity in rats with selected, upon *in silico* analysis mir-183-5p. The study documents an ammonia-induced effect on rat brain endothelial cells towards the senescence process, likely to involve non-coding miRNA-183-5p as demonstrated in the in vitro study.

We hope our work will attract the attention of scientists studying brain endothelium alterations by enhancing communication between workers in the field. Since *Free Radical Biology and Medicine* enjoys an excellent reputation as a high-quality journal for publishing articles on pre-clinical and clinical research, we hope that, upon consideration, you will find our article interesting and suitable for publication in this journal.

Thank you for your consideration of this manuscript.

Yours Sincerely,

Magdalena Zielińska, Ph.D.

Highlights

- Hyperammonemia reduces cerebrovasculature density in rats
- Hyperammonemia alters brain and serum microRNA profiles
- Hyperammonemia results in senescent phenotype of brain endothelial cells *in vitro*
- Mimic miR-183-5p induces senescent phenotype in brain endothelial cells *in vitro*

Graphical abstract

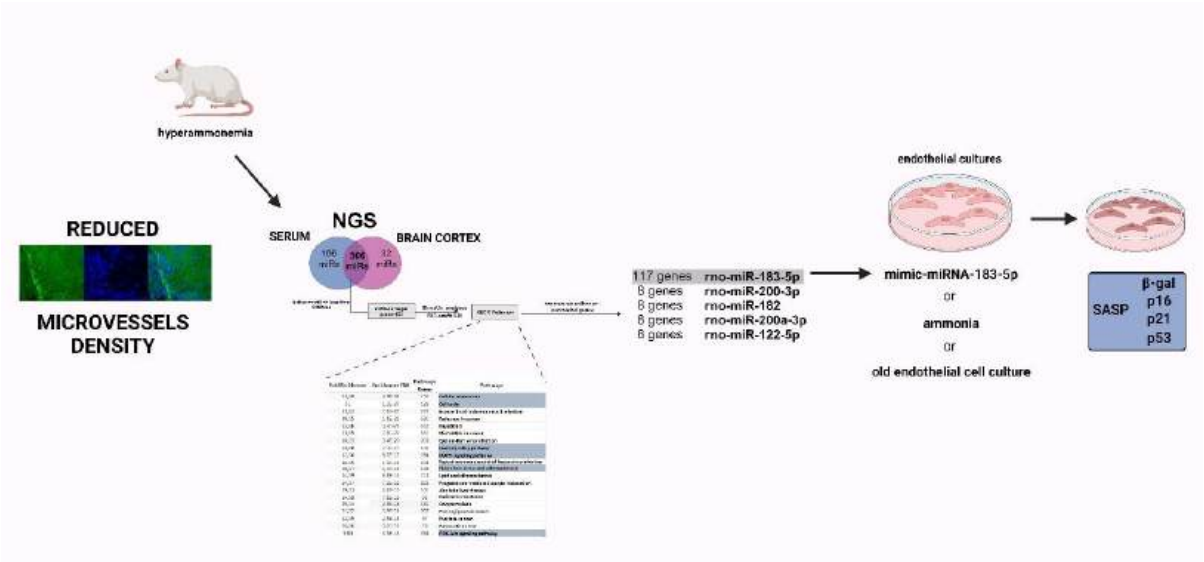

Unraveling Hyperammonemia-Induced Brain Saga: The Role of miRNA-183-5p in the Endothelial Senescence and Cerebrovascular Density Decline

Karolina Orzeł-Gajowik[1*], Krzysztof Milewski[2], Marta Obara-Michlewska[1], Aleksandra Ellert-Miklaszewska[3], Aneta Karpińska[4], Karina Kwapiszewska[4], Magdalena Zielińska[1*]

[1]Department of Neurotoxicology, Mossakowski Medical Research Institute, Polish Academy of Sciences, Pawińskiego St. 5, 02-106 Warsaw, Poland
[2]Laboratory of Cellular Metabolism, Nencki Institute of Experimental Biology, Pasteur St. 3, 02-093 Warsaw, Poland
[3]Laboratory of Molecular Neurobiology, Nencki Institute of Experimental Biology, Pasteur St. 3, 02-093 Warsaw, Poland
[4]Department of Soft Condensed Matter, Institute of Physical Chemistry PAS, Kasprzaka St. 44/52, 01-224 Warsaw, Poland
*Corresponding authors: Magdalena Zielińska (mzielinska@imdik.pan.pl), Karolina Orzeł-Gajowik (korzel@imdik.pan.pl)

Abstract

Peripherally, high circulating neurotoxic ammonium ions, defined as hyperammonemia, occur in different brain pathologies. However, hyperammonemia effects on cerebrovascularity and underlying mechanisms, are far from clear. Here, we verified the senescence in brain endothelium upon hyperammonemia and the role of non-coding miRNA-183-5p. Reduction of cerebrovascular density in rats with induced hyperammonemia (ip. ammonium acetate (OA) at 600 mg/kg bw for three days), evaluated by fluorescence intensity of von Willebrand marker, resembles density reduction of 12-month rats. The *in silico* analysis of Next Generation Sequencing miRNA profiles of OA brain cortex and plasma allows the selection of miRNA-183-5p, as endothelial senescence inducer. The miRNA-183-5p increase was detected in ammonia-treated rat brain endothelial cell line 4 (RBE4) and media-derived exosomes. Experiments *in vitro* on RBE4 and primary rat brain endothelial cells (PBMEC) treated with ammonia (5 mmol/L, 24h) document cell senescent phenotype characterized by: i) increased β-galactosidase staining/ fluorescence intensity; ii) increased p16 mRNA and p21mRNA expression level and p53 fluorescence intensity increase iii) changes in senescence-associated secretory phenotype (SASP) factors and iv) RBE4 cells proliferation decrease. Accordingly, analysis of i) SASP factors; ii) β-galactosidase and p53 fluorescence intensity increase in RBE4 cells at 21 DIV and PBMEC from elderly, 12-month rats. Transfection of RBE4 cells with mimic miRNA183-5p resembles senescent features: i) p53 fluorescence and ii) SASP factors. The study documents the ammonia-induced effect on brain endothelial cells towards senescence induction, which involves miR-183-5p. It thus may contribute to reduced cerebrovasculature density, a factor of cerebral dysfunction observed in hyperammonemia.

Introduction

Hyperammonemia co-occurs in neurological disorders with toxic, metabolic, and neurodegenerative etiology e.g., hepatic disorders, including non-alcoholic fatty liver disease, neurodegenerative diseases (e.g., Alzheimer's diseases), postoperative cognitive dysfunction,

metabolic syndrome or aging [1–6]. Clinically, the most frequent cause of hyperammonemia results from liver impairment resulting in insufficient clearance of circulating ammonia, which, with a synergic role of systemic inflammation, induces a multi-complex neuropsychiatric syndrome, named hepatic encephalopathy (HE) [7,8]. Circulating ammonia enters the CNS and affects various aspects of brain homeostasis, exerting mild-to-severe alterations leading to brain functioning decline [9–12]. Developing cerebral edema involves ammonia-triggering self-amplifying mechanisms linked to osmotic- and oxidative/nitrosative stress, exaggerated with disruption of the blood-brain barrier (BBB), and fatally complicates HE [13]. Changes in ECs-composed cerebromicrovasculature accompany the dysregulation of cerebral blood flow, further promoting brain dysfunction [14–17].

In recent years, endothelial cell senescence has emerged as a mechanism involved in vascular pathologies. In contrast to the extensive studies of the process in the periphery, limited studies documented the senescent ECs in the brain [18–20]. In the context of hyperammonemia-related disorders, senescent-like features of the brain endothelium, escape verification. Importantly, ammonia-induced markers of asthenic, senescent-like astrocytes *in vitro* and brains of HE animal models, and, albeit indirectly, in the *post-mortem* brain tissue samples of HE patients with cirrhosis, were demonstrated [10,21–24]. We decided to verify the neurotoxic effect of ammonia on the induction of senescent phenotype in brain ECs in an attempt to decipher the molecular mechanism of this process, not been studied directly as yet.

First, we checked whether induced systemic hyperammonemia in rats evokes changes in the cerebrovasculature density, and confronted our findings with changes observed during normative age-related alterations. Then, based on miRNAs' profiles resulting from NGS analysis of hyperammonemia rat brain cortex tissue and serum, followed by *in silico* analysis and results of subsequent verification of miRNA in RBE4 cells treated with ammonia and cultured medium-derived exosomes, we evaluated the potential of mimic-miRNA-183-5p towards to induction of cellular endothelial senescence process. We indicate that hyperammonemia affects the cellular senescence of brain endothelium via miRNA-183-5p and thus disturbs the function of brain endothelium.

Methods

Animal models

Ninety-five 8-10th- week- old and nine 48 to 53rd week- old male Sprague Dawley rats, from the outbred animal colony re-supplied by the Animal House of Mossakowski Medical Research Institute, Warsaw, Poland (Approval no. 57/2015; 473/2017 and 462/2017 of Local Ethics Committee for Animal Experimentation, Warsaw, Poland, as compliant with Polish Law) were randomized to the experimental groups. All efforts have been made to reduce the number of animals and minimize their suffering. The study complies with the ARRIVE (Animal Research: Reporting In Vivo Experiments) guidelines (study design, experimental procedures, housing and husbandry, statistical methods) for reporting animal research. Animals were given free access to water and standard rodent chow and housed in constant temperature, humidity, and 12 h light-dark cycling.

Hyperammonemia was induced by ip. administration of ammonium acetate (OA) in a dose of 600 mg per kg for three days. Rats were sacrificed by decapitation and the brains were quickly removed, and the cerebral cortex and blood serum [25] were isolated.

RNA extraction and Next Generation Sequencing

Total RNA was extracted from 200 µL rat plasma using the miRNeasy Serum/Plasma Advanced Kit (Qiagen, Hilden, Germany) and 20 mg of brain cortex using Invitrogen™ *mir*Vana™ miRNA Isolation Kit (Thermo Fisher Scientific, Waltham, USA).

Plasma samples were thawed on ice and centrifuged at 12,000 x g for 5 min to remove cellular debris. For each sample, 200 µL of plasma was mixed with 1 mL of Qiazol followed by extraction steps directly according to the manufacturer's instructions. Finally, RNA was eluted in 10 µL of nuclease-free water and stored at −80 °C for further analysis.

Brain tissue samples were dispensed in 2 mL of Lysis/Binding Buffer in a homogenization vessel placed on ice. Next, an amount of Acid-Phenol: Chloroform equal in volume to the homogenate volume was added and vortexed for 60 seconds to mix; after centrifugation for 5 minutes at the highest speed (10,000 x g) at room temperature, the water phase was carefully removed, and RNA was eluted in 100 µL nuclease-free and stored at −80°C to for further analysis.

Total RNA quantification was made spectrophotometrically with a NanoDrop 2000 (Thermo Fisher Scientific, Waltham, USA) and 1 µg of total RNA was used for library preparation.

The Serum NGS was performed using the DNBSEQ G400 (MGI2000) system in SE50 mode (BGI Company, Shenzen, China). A minimum of 20 million paired-end reads were generated per sample and, quantification includes the raw read count and normalized expression level as CPM values (counts per million reads mapped) to account for the variability in the library size. Next, miRDeep2 Quantifier analysis based miRbase2.0 library was used to identify miR sequences. The Quantifier script of the miRDeep2 tool applying the default parameters was used to quantify the miR expression level.

Brain cortex NGS was conducted on a NextSeq 500 sequencing instrument. The average number of reads was 10 million reads per sample; next, RNA was converted into microRNA NGS libraries. Library preparation QC was performed using either Bioanalyzer 2100 (Agilent) or TapeStation 4200 (Agilent). Based on the quality of the inserts and the concentration measurements, the libraries were pooled in equimolar ratios. NGS raw data was de-multiplexed and FASTQ files for each sample were generated using the bcl2fastq software (Illumina Inc.).

Bioinformatic analysis

To establish the subsequent procedures brain cortex and serum NGS data were analyzed. A total of 306 identified serum and brain cortex miRNAs were taken for further analysis (Fig. 2). The miRNAs were analyzed, using miRNA-target prediction databases (TarBase, miRDB, TargetScan) to forecast the potential target genes regulated by selected miRNAs. ShinyGO analysis was conducted on the predicted target genes list with their biological functions and participation in different pathways. The statistical significance was maintained by an FDR cut-off of 0.05 following database recommendations. The analysis yielded fold enrichment scores, enrichment scores, FDR values, and gene counts, which serve as robustness indicators and statistical significance of the relationship between the miRNAs and the identified pathways.

The KEGG pathway analysis revealed miRNAs' target genes, potentially associated with senescence pathways.

Cell culture

Primary brain microvascular endothelial cells (PBMEC) were isolated from the brain cortex of 14-day- or 12-month-old Sprague-Dawley male rats from the animal colony of Mossakowski Medical Research Institute, Polish Academy of Sciences, directly according to the protocol [26]. Briefly, after decapitation, brains were isolated, and cortices were dissected under sterile conditions. After homogenization, tissue was enzymatically and mechanically dissociated with 1 ml of 10 × Trypsin/ and Type IV collagenase solution at 37°C for ~30 min. Pellets followed centrifugation and cleaning steps (800 × g for 5 min, ~20°C; 1,500 × g for 15 min ~20°C; 800 × g for 15 min), then the supernatant was discarded. Cells were seeded on a 6-well plate coated with collagen I (Corning, NY, USA) and cultured in Dulbecco's Modified Eagle's Medium (DMEM) containing 20% FBS and supplemented with 1.0 ng/ml *basic fibroblast growth factor* (bFGF) and 20 µg/ml bovine sodium heparin. In the first two days, puromycin was added to the culture medium to inhibit neuron and astrocyte growth. The medium was changed the next day, and then every 2-3 days.

Rat brain endothelial cell lines (RBE4) were cultured in 24-transwell plates, or 100 mm dishes (Corning, NY, USA) coated with collagen type I. Cells were cultured on the DMEM/Ham's F10 medium with Glutamax (Gibco, Thermo Fisher Scientific, Walthman, USA) with the addition of 10% of heat-inactivated FBS, 1 ng/ml bFGF, and gentamicin (Gibco, Thermo Fisher Scientific, Waltham, USA) at 37 °C in a humidified atmosphere of 95% air and 5% CO_2 and cultured for 5 days when cells displayed endothelial phenotype and reached ~ 90% of the surface confluence.

RBE4 were seeded at the density of 2 x 10^4 for 5 days and reached 90% confluence. RBE4 cultured for 21-day cells served to determine senescence, with the culture media being replaced every 3 days.

Treatment and transfection

The RBE4 cells were treated with 5 mM ammonium chloride ("ammonia") for 24 h. Of note, the extracellular ammonium concentration was 2-3 times lower than the intracellular level in autopsied brain tissue of patients with severe hyperammonemia [25,27].

The transfection was carried out using the HiPerFect transfection reagent (Qiagen, Cat. No. 301704, Hilden, Germany), according to the recommendations provided by the manufacturer. The applied concentration of the mimic was 20 nM for 24 hours. RBE4 cells were seeded at a density of 3.3 × 10^5 and were transfected with the following sequences: 5′-UAUGGCACUGGUAGAAUUCACU-3′ for mimic miR-183-5p (Qiagen; Cat. No. 339173YM00471390-ADA, Hilden, Germany), 5'-UCACCGGGUGUAAAUCAGCUUG-3' for negative control (Qiagen Cat. No. 339173YM00479902-ADA, Hilden, Germany).

Proliferation analysis

The cells were seeded in 6-well plates at a density of 1 x 10^5 cells per well and incubated for 24 hours with ammonia before real-time monitoring. The digital holograms of cells were created using the HoloMonitor M4 Digital Holography Cytometer (Phase Holographic Imaging

PHI AB, Lund, Sweden). Results were computed using Hstudio M4 software, developed by Phase Holographic Imaging PHI AB, located in Lund, Sweden.

SA-β-gal staining

Staining was performed using a beta Galactosidase Staining Kit (ab102534, Abcam, Cambridge, UK). Cells were washed with PBS, fixed for 15 min at room temperature, and washed, and the working solution of β-galactosidase plus X-Gal was incubated overnight at 37°C in a dry incubator (no CO_2). The senescent cells were observed under an optical microscope (Nikon DIAPHOT 300) and counted from three random vision fields.

SASP analysis

TNF-α, ICAM-1, V-CAM, and VEGF were measured using custom preconfigured ProcartaPlex Immunoassays (Cat. No. PX010-10420-901 Thermo Fisher Scientific, Waltham, USA). Cells were treated as mentioned in the Materials and Method section, and cell-free supernatants were collected, vortexed, and, centrifuged at 10,000 × *g* for 7 min and kept at - 80°C. Afterward, 50 µl of cell culture supernatants and standards were added to a custom plate. The analytes concentration was measured using MAGPIX Multiplexing Instrument (Luminex, TX, USA) with XPonent software. Fresh culture media were used as controls for background subtraction.

RNA extraction and Quantitative RT-PCR

To separate total RNA from RBE4 cells and EVs, TRI Reagent (Cat. No. T9424, Sigma-Aldrich, Missouri, USA) was used. Then 1µg of the RNA was reverse transcribed using the high-capacity cDNA reverse transcriptase kit (Cat. No. 10400745, Applied Biosystems, Waltham, MA, USA). Real-time PCR was carried out using TaqMan assays from Applied Biosystems: p21(Rn00589996_m1), p16 (Rn00580664_m1), β-actin (Rn00667869) and TaqMan Universal PCR Master (Cat. No. 43-044-37, Applied Biosystems, Waltham, MA, USA) mix in a total volume of 10 µl, with 1µl cDNA added. Reactions were run for 10 minutes at 95 °C, then 40 cycles of 15 seconds at 95 °C and 1 minute at 60 °C using the ABI 7500 instrument (Applied Biosystems). The results were computed for the actin product and presented using the equation ($2^{-\Delta\Delta Ct}$) as the quantity of target, normalized to an endogenous reference; where the Ct was the target amplification threshold cycle.

To quantify miRNAs, reverse transcription, and cDNA synthesis was performed, using TaqMan Advanced miRNA cDNA Synthesis Kit (Cat. No. A28007, Invitrogen, Walthman, MA, USA) according to the manufacturer's protocol. The levels of miRNAs expression were measured by quantitative RT-PCR with a miRCURY LNA SYBR Green PCR Kit (Cat no. 339345, Qiagen, Hilden, Germany,) with miRCURY LNA miRNA PCR Assay primer: rno-miR-183-5p (Cat no. QG-339306_YP00206030, Qiagen, Hilden, Germany,). The snRNA U6 was used as, a normalization control (Cat no. QG-339306_ YP02119464, Qiagen, Hilden, Germany). The Applied Biosystems 7500 Sequence Detection System (Applied Biosystems, Foster City, CA, USA) according to the manufacturer's instructions was used. The relative expression levels of miRNAs were calculated using the $2^{-\Delta\Delta Ct}$.

Immunohistochemical and immunofluorescent staining

Brain cortex slices were fixed with 4 % paraformaldehyde/PBS and permeabilized with 0.25 % Triton X-100/PBS. Secondly, slices incubated with antibodies against vWF (1:400, Cat. No. ab6994 Abcam, Cambridge, UK) overnight at 4 °C, and then exposed to secondary antibody Alexa Fluor 488 goat anti-rabbit IgG (H+L) (1:1000, Cat. No. A11008, Thermo Fisher Scientific, Waltham, MA, USA). The nuclei were labeled with Hoechst 33258 (Cat. No.: H1398, Thermo Fisher Scientific, Waltham, MA, USA). Images were acquired in a confocal laser scanning microscope LSM780 (Zeiss, Jena, Germany) and processed using the ZEN 2012 (Zeiss, Jena, Germany). Fluorescence intensities were measured using the Image J software (NIH, Bethesda, MD, United States).

RBE4 and PBMEC cells were seeded onto collagen I-coated coverslips at 3 x 10^2 cells/well density, and cultured for 5-7 days. Cells were rinsed with PBS and were fixed, with 4 % paraformaldehyde/PBS and permeabilized with 0.25 % Triton X-100/PBS. Secondly, cells were incubated with antibodies against β-Gal (1:400, Cat. No. ab616, Abcam, Cambridge, UK) or p53 (1:400, Cat. No. ab131442, Abcam, Cambridge, UK), CD-31 (1:400, Cat. No. ab28364, Abcam, Cambridge, UK) and incubated overnight at 4°C and then exposed to secondary antibody Alexa Fluor 488 goat anti-rabbit IgG (H+L) (1:1000, Cat. No. A11008, Thermo Fisher Scientific, Waltham, MA, USA).

Images were acquired in a confocal laser scanning microscope LSM780 (Zeiss, Jena, Germany) and processed using the ZEN 2012 (Zeiss, Jena, Germany).

Extracellular vesicle (EV) isolation and immunocytochemical staining

EVs were isolated from the culture media of RBE4. A total of 10^6 cells were grown on 100 mm^2 cell culture dishes. The supernatants of the cell culture were gathered and subjected to centrifugation at a force of 200 x g for 10 minutes, followed by another centrifugation at a force of 500 x g for 10 minutes at a temperature of 4°C. The resulting samples were divided into smaller portions and stored at a temperature of -70°C for future utilization. Cell culture supernatants were thawed, spun down at 2000 x g for 20 min to remove cellular debris, and then centrifuged at 100.000 x g for 75 min at 4 °C. The pellets were rinsed with deionized phosphate-buffered saline (DPBS) and then underwent additional centrifugation at 100.000 x g for 75 minutes at 4°C. Next, the supernatant was removed, and the pellet was resuspended in 1 ml of DPBS and kept at a temperature of -70°C until it was required.

The isolated EVs were rinsed with PBS, centrifuged for 100.000 x g for 20 minutes, fixed with 4 % paraformaldehyde/PBS, and permeabilized with 0.25 % Triton X-100/PBS. Then EVs were incubated with antibody against CD-9 (1:400, Cat. No. ab223052, Cambridge, UK) and incubated overnight at 4°C and then exposed to secondary antibody Alexa Fluor 488 goat anti-rabbit IgG (H+L) (1:1000, Cat. No. A11008, Thermo Fisher Scientific, Waltham, MA, USA).

Fluorescence correlation spectroscopy (FCS) analysis

FCS measurements of EVs were conducted using a Nikon Eclipse TE2000U confocal microscope coupled with Pico Harp 300 FCS equipment (PicoQuant, Germany). We used a 60x objective (N.A. 1.2) with water immersion. A 561 nm pulsed diode laser was used to excite the fluorescence of labeled exosomes. The fluorescence photons were collected by Single-Photon

Avalanche Diodes (MPD and PerkinElmer). A 594 long-pass filter (Chroma, USA) was positioned in the optical path before the detector. The laser power was equal to 16 μW.
The confocal volume was characterized during calibration using a nanomolar solution of Rhodamine B in PBS. All measurements were conducted at 25 ± 0.5 °C temperature, maintained by a climate chamber (Okolab, Italy). Twenty independent FCS measurements, lasting 120s, were performed for the tested sample.
Obtained FCS data were fitted with one component anomalous diffusion model, using Equation 1.

$$G(\tau) = \frac{1}{N}\left(1 + \frac{\theta_{trip}}{1-\theta_{trip}}\exp\left(-\frac{\tau}{\tau_{trip}}\right)\right)A\frac{1}{1+\left(\frac{\tau}{\tau_D}\right)^{\alpha}}\frac{1}{\sqrt{1+\frac{1}{\kappa^2}\left(\frac{\tau}{\tau_D}\right)^{\alpha}}} \quad (1)$$

where N stands for total exosomes number in confocal volume, θ_{trip} corresponds to the fraction of tested objects in a triplet state, τ_{Di} is the diffusion time of diffusing exosomes, A stands for the amplitude of fluorescent objects, while κ is the aspect ratio of the Gaussian used to approximate the focus. α corresponds to the anomalous exponent. During calibration, the parameter κ was determined and was in the range of 5.5-6.5.
The QiuckFit 3.0 software (DKFZ, Germany) was used to fit the appropriate mathematical model to the FCS curves. The fitted parameter was the diffusion time of exosomes (one component). Based on the value τ_D, we determined the diffusion coefficient given by Equation 2,

$$D = \frac{{\omega_{xy}}^2}{4\tau_D} \quad (2)$$

where ω_{xy} stands for the dimension of a confocal volume determined during calibration.
The hydrodynamic radius of fluorescent exosomes, R_h, was calculated using the Stokes–Sutherland–Einstein equation:

$$R_h = \frac{kT}{6\pi\eta D}$$

where k stands Boltzmann's constant, T is the absolute temperature, η corresponds to the PBS viscosity.

The principle of FCS measurements is presented in Scheme 1. Firstly, the focal volume was positioned within the tested sample. Then, the SymphoTime software (PicoQuant, Germany) captured a fluctuation record of the fluorescence intensity of molecules diffusing through this volume. Using mathematical processing, detected fluctuations were represented as an autocorrelation curve. Finally, we fit the obtained FCS curve by an appropriate mathematical model, describing the process inside the tested sample.

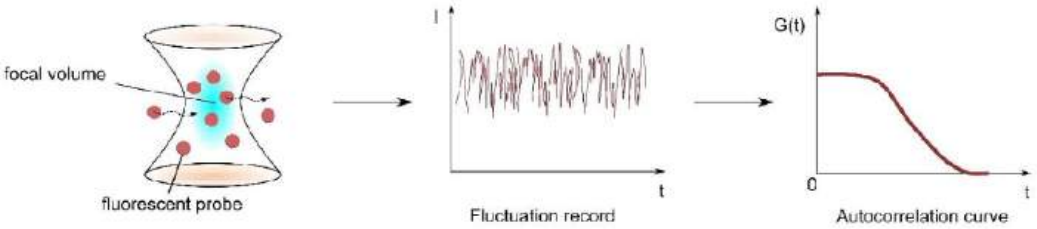

Scheme 1. The scheme of FCS measurements' principle in a buffer.

Statistical analysis

Data were analyzed and visualized using Prism 7 (GraphPad Software Inc., La Jolla, USA). Results were presented as mean ± SD. The statistical significance between various groups or treatments was measured by unpaired t-test or one-way ANOVA with Dunnett's post hoc test. In all experiments, p-value < 0.05 was considered to be statistically significant, **** $p < 0.0001$, *** $p < 0.001$, ** $p < 0.01$, * $p < 0.05$.

Results

Ammonia and aging reduce brain microvascular density

The effects of ammonia or aging on microvascular density were evaluated in the brain cortex of control (2-months-old), middle-aged (12-months-old), and OA rats (Fig. 1). We measured the immunofluorescence intensity vWF, a marker of ECs- composing microvessels. The cortical region of a 12-month rat brain exhibits a significant reduction (~40%) in vWF staining compared to the control. A noticeable (~35%) decrease in vWF intensity, indicating a decline in microvessels fluorescence was observed in the OA group.

Identification of differential miRNAs in both serum and brain cortex of OA rats: pathway enrichment and target genes identification

In total, 306 overlapped, differently altered miRNAs in both, the serum and brain cortex of OA rats were identified (Fig. 2; top; Suppl. 1. Tab. 2). We build the current approach on previously obtained NGS row data from plasma samples, and from the newly received data from the brain samples which were used to identify miRNAs associated with BBB disruption [28]. Raw data from prior work are accessed to the public in the supplemental files (Additional file 1: Table S1) and the present study served for *in silico* analysis. By reusing the NGS row data, we aimed to supplement our current analysis and enhance the robustness of our findings while adhering to 3R rules that advocate for the reduction of animal usage in scientific research. These miRNAs were cross-referenced against three databases (TarBase/miRDB/TargetScan) to define 852 miRNA target genes. To get insight into the shortlisted 306 miRNA pathways, their 852 target genes were assigned to the defined physiological processes using ShinyGO analysis [29]. ShinyGO analysis offers distinctive functionalities, including visual representations of enrichment results and gene characteristics and the ability to access KEGG and STRING through an API to retrieve route diagrams and protein-protein interaction networks. ShinyGO

analysis was carried out to identify the functional enrichment of selected genes using a false discovery rate (FDR) level of 0.05. The pathways, along with their relative fold enrichment and FDR values, indicate the frequency of pathways appearing in the list of miRNA target genes compared to what would be predicted by chance. Indicated pathways include the following biological processes: Cellular senescence, Cell cycle, FoxO signaling pathway, MAPK signaling pathway, Fluid Shear Stress and Atherosclerosis, and Pi3K-AKT signaling pathway. Indicated pathways along with their relative fold enrichment and FDR values, indicate the frequency of pathways appearing in the list of miRNA target genes compared to what would be predicted by chance. Comparing the number of common genes acquired through TarBase/miRDB/TargetScan databases with the senescence-associated ShinyGo analysis pathways, miRNA-183-5p was reported to regulate 117 genes. Since the next on the list, miR-200-3p regulates only 17 genes (see heatmap), miR-183-5p was chosen for further research. The miRNAs listed along the x-axis include rno-miR-182, rno-miR-200a-3p, and rno-miR-122-5p (the most changed miRNAs from NGS analysis). The colour intensity in the heatmap represents the enrichment of each miRNA in these pathways. The colour intensity reflects the number of genes involved in specific KEGG pathways regulated by each miRNA, with green indicating the highest number of genes and red indicating the lowest number of genes. The number of genes from KEGG pathways and their enrichment regulated by the miRNAs are thus visually depicted in this heatmap.

The effect of ammonia on rat brain ECs phenotype

Treatment with 5 mM ammonia for 24h induces changes in the phenotype of RBE4 cells toward the senescent character. First, we observed reduced by ~20% RBE4 cell proliferation, captured by the live cell HoloMonitor recording of cell number. Results corroborate with observation from our laboratory demonstrating ammonia-induced RBE4 cell reduction with an MTT test assessing cell viability [30]. The cell parameters verified with HoloMonitor are presented in Supplementary Figure 1 (Supp. Fig. 1). Ammonia treatment of RBE4 cells induces a 1.7-fold increase in β-galactosidase staining intensity (Fig. 3A) in comparison to the control, the effect also illustrated with fluorescence intensity of β-galactosidase (Fig. 3C; top left). Similarly, the β-galactosidase fluorescence intensity in RBE4 cells cultured for three weeks was observed (Fig. 3C, top right). We determine the mRNA level of two cell cycle regulatory genes, namely p21 and p16 in ammonia-treated RBE4 cells (Fig. 3B). A notable rise in the expression levels of 66% and 44% in the p21 mRNA and p16 mRNA, respectively, was demonstrated in RBE4 cells treated with 5mM ammonia.

Next, we documented an increase in tumor suppressor protein-p53 (p53) fluorescence intensity, indicating DNA damage and/or cellular stress in RBE4 cells treated with ammonia and in RBE4 cells cultured for 3 weeks (Fig. 3C, low).

Finally, we measured concentrations of selected senescence-associated secretory phenotype (SASP) factors (I-CAM, TNF-α, V-CAM, VEGF) of the RBE4 secretome. The RBE4 cells treated with ammonia induced ~8-fold change increase of V-CAM. 3-weeks RBE4 cells reached ~100-fold changes elevation of TNF-α level and ~100-fold change of V-CAM (Fig. 3D).

The activity of β-galactosidase in PBMEC treated with 5mM ammonia for 24 h was increased by ~40% (Fig. 4A), concurrently with visible immunofluorescence intensity of β-galactosidase in both PBMEC cells treated with ammonia and PBMEC cells derived from 12-months rats (Fig. 4B, left). The identity of ECs was marked with CD-31 immunofluorescence. The p53 fluorescence intensity was observed in PBMEC culture from 12-month rats (Fig. 4B, right panel). No significant changes were observed in the p16 and p21 mRNA expression levels (data not shown).

The changes of SASP factor levels in PBMEC were divergent (Fig. 4C). ICAM-1 level was significantly reduced (~0,7-fold change) in the ammonia and 12-month-old cultures (~1.2-fold change). TNF-α level was increased by ~900-fold change in ammonia-exposed cells and to ~1300-fold in cells cultured from 12-month rats. The V-CAM level was elevated by ~ 1000-fold in ammonia and ~800-fold change augmentation was noted in the PBMEC cultured from 12-month rats. The VEGF concentration was unaltered.

The involvement of miR-183-5p in the ammonia-induced phenotype of brain ECs

We then verified whether ammonia directly affects the expression level of miR-183-5p in the RBE4 cell line. The qRT-PCR analysis of miR-183-5p expression level in RBE4 cells (Fig. 5A; left) indicates a ~ 1.5-fold increase compared to the respective control.

The correctness of EV isolation was verified before conducting qRT-PCR analysis. FCS measurements were employed to analyze exosome size, distribution, and diffusion properties. The quantitation was performed on isolated and fluorescently stained exosomes, confirming the presence of objects with an average hydrodynamic radius of 11.6 nm in the sample. The fluorescence signals from the exosomes was significantly higher than the background signal (see Suppl. 1, Fig. 2). The FCS autocorrelation curves were fitted with a one-component anomalous diffusion model due to the non-uniform size of the measured particles. An example of an FCS autocorrelation curve is shown in Suppl. 1, Fig. 2B. In the sample, molecules with hydrodynamic radii of 22.5 nm and 7.6 nm with a median of 11.1 nm were present. Importantly, no mobile fluorescent molecules other than exosomes were identified in the sample according to the one-component fit model. The values of all parameters obtained from FCS analysis are summarized in Supp., Table 1.

We further evaluated the miR-183-5p levels in EVs isolated from media of ammonia-treated RBE4 cells (Fig. 5A; right). The effect of ammonia results in a significant increase in miR-183-5p expression level (~2.8-fold), suggesting that miR-183-5p may contribute to ECs response to ammonia.

We analyzed mRNA expression levels of the cell cycle regulators p16 and p21 mRNA and β-galactosidase, and p53 fluorescence intensity in RBE4 cells transfected with mimic miR-183-5p. The p16 mRNA level increased by ~ 70% and unchanged p21 mRNA was observed (Fig. 5B). The degree of complementarity between the miRNA sequence and the p16 and p21 mRNA genes was utilized with TargetScan bioinformatics software. The alignment identified putative binding locations of miR-183-5p and both mRNA interaction (Suppl. 1, Fig. 3). Consequently, β-galactosidase and p53 immunofluorescence intensity of RBE4 cells transfected with mimic-

miR-183-5p confirmed the impact of miR-183-5p to induce features of senescent phenotype in the ECs.

SASP factors (ICAM-1, TNF-α, V-CAM, and VEGF) upon transfection of RBE4 and PBMEC with mimic-miR-183-5p depict divergent responses. The concentrations of ICAM-1 in both the transfected and control groups were similar. TNF-α level was significantly increased in both RBE4 and PBMEC cells (Fig. 5D), and ~four times higher, compared to the respective control. The transfection with mimic-miR-183-5p presents a significant rise 400-fold change in VEGF level in both RBE4 and PBMEC cell types.

Discussion

Cerebrovascularity guarantees proper brain functioning with an active guided role of the BBB. BBB disturbances accompany to a varying degree many neurological diseases, including disorders with hyperammonemia-related components [31,32]. The present study demonstrates a new aspect of ammonia neurotoxicity related to cerebrovascular dysfunction associated with EC senescence. We analyzed hyperammonemia-induced circulating miRNA vs cerebral miRNA profile in OA rats and identified the potential miRNA candidate that might contribute to endothelial senescence.

We documented hyperammonemia-induced reduction of rat brain cerebrovascular density and compared the observation with decreased cerebrovasculature measured in 12-month-old rats. Further, we verified the impact of identified miRNA-183-5p toward senescent phenotype changes and implicate not yet described alterations in ECs evoked by hyperammonemia. Reduction in endothelial marker vWF staining observed in older rats is consistent with the age-dependent drop in microvascular density associated with endothelial dysfunction and/or cellular senescence [33,34]. Such changes are often accompanied by cerebral blood flow reduction, affecting hemodynamic response and vascular reactivity detected during physiological aging-to-mild cognitive impairment [35]. Such alterations were detected in patients with acute liver failure, congenital hyperammonemia, and neurological disorders, including neurodegenerative diseases. Experimentally, acute liver failure in rats induces decreased cerebral perfusion [36] Impaired tight junction (TJ) organization within senescent ECs was shown in progeroid mice [37] and in brain tissue of mice models of Alzheimer's disease [38]. The BBB leakage with substantial disruption in TJ proteins within the ECs [39–41] also occurs mostly at the late stages and severe onset of hyperammonemia encephalopathies [42–46] where changes develop progressively [47–51].

Cellular senescence contributes to physiological aging and numerous age-related pathologies [52]. Senescence, the irreversible cell growth arrest induces signaling cascades of p53/p21 and p16 pathways [53,54]. The process can be triggered by a variety of stressors that include replicative and oxidative stress, oncogenic activation [55], telomere attrition [15] DNA damage [56], and mitochondrial dysfunction [57]. The mitochondrial dysfunction was documented in senescent ECs and was characterized by mitochondria mass decline and decreased electron transport chain activity, resulting in oxidative stress induction [15,58]. Recently, our group reported that high ammonia concentrations induced the reduction of mitochondria number, and altered mitochondria morphology in EC-composing BBB in two animal models of acute hepatic encephalopathy [59]. The observations were associated with ECs mitochondrial membrane

potential drop and monolayer permeability changes studied *in vitro* [28]. In this context, the earlier study by Jayakumar et al. [60] also demonstrated alterations in ammonia-affected ECs *in vitro* and monolayer permeability increase. Hyperammonemia affects the activity of endothelial nitric oxide synthase (eNOS) by reducing nitric oxide (NO) availability and thus contributes to endothelial dysfunction [13]. In the cerebral cortex tissue of rats with acute liver failure, reduced eNOS activity and protein level expression co-occurred with eNOS uncoupling [61].

Brain-composing cells undergo senescence [62–67], however senescent ECs have not been frequently identified in the brain tissue of patients with neurodegenerative diseases [68]. In turn, *in vitro* studies have shown that oligomeric β-amyloid can induce secretion of SASP from the ECs [69].
In aging human ECs at the periphery it was demonstrated that endothelial NOS failure is crucial to EC senescence [70] and that eNOS decrease contributes to oxidative stress, and inflammation, all contributing to EC death [71]. In addition, eNOS uncoupling adds to the mechanism of ECs' premature aging [72]. While the SASP is heterogeneous and can vary [73–75] endothelial SASP, beyond increased levels of reactive oxygen species and NO levels, is characteristic of endothelial markers ICAM-1, VCAM, and VEGF; of note, ammonia elicits a pro-inflammatory response that aligns to a great degree with SASP [76–78].

MiRNA profiling contributes to inter-organ communication and homeostasis within the liver-brain axis. Dysregulation of specific miRNAs contributes to both liver and cerebral diseases [79] for example, miR212/132 is expressed in the brain and is sensitive to external cues from the liver [80,81]. Circulating miRNAs regulate BBB integrity by targeting TJ proteins, basement membrane components, and inflammatory pathways [82], and several miRNAs such as miR-15a/16-1, miR-501-3p, and miR-210 are acknowledged in these processes [83–86].
We profiled the most significantly changed miRNA in the brain cortex and serum from OA rats and identified 306 miRNAs with predicted target genes using TarBase, miRDB, and TargetScan databases. Using the ShinyGO web-based program, miR-183-5p which controls 117 genes, associated with senescence pathways was selected. Within *in silico* analysis, we revealed possible miR-183-5p targets, pathways of Cellular Senescence, Cell Cycle, FoxO Signaling, and MAPK Signaling, and respective genes, such as p53, p21, p16INK4a, cyclin-dependent kinases, and FoxO [87]. miRNA-183-5p verification implicated its contribution to ammonia-evoked brain endothelium senescence. In this context, our data corroborates with previously published data [28] documenting ~3-fold increase of miR-183-5p in 5mM ammonia-treated primary culture of rat ECs.

MiR-183-5p is a member of the miR-183 cluster situated on chromosome 7q32.2 consisting beyond miRNA-183-5p also miR-96 and miR-182 [88]. miR-183-5p has been linked to apoptosis regulation, cell proliferation, and migration in various cancers [89–93]. Under physiological conditions, miR-183-5p has been detected in neurons, and sensory organs [94,95] and documented to regulate the expression of genes involved in synaptic formation and plasticity [96], metabolism of glucose and lipid balance in ECs [97].
Other data documented the involvement of miR-183-5p in age- and endothelium-specific

related processes. An age-dependent increase of miR-183-5p levels was related to suppression of proliferation and induction of senescent phenotype in bone marrow stromal cells [87]. miR-183-5p was also identified within the panel of 15 miRNAs, overlapping human and mouse miRNA profiles showing altered expression in the aging neurovascular unit [98]. Notably, the miR-183 family members, miR-183 and miR-182 via control of SUMOylation, preserve homeostasis under stress conditions [99].

In our study, transfection of ECs with mimic-miR-183-5p induces secretion of inflammatory response factors characteristic of endothelial dysfunction and inflammation. The accumulation of ICAM-1, transmembrane glycoprotein regulating cell-to-cell interaction signals, characterized late passages of ECs [100]. In line, senescence-associated ICAM-1 overexpression was documented in conditionally immortalized human vascular smooth muscle cells [101]. Also, senescent endothelial progenitor cells benefit from VEGF gene delivery, which enhances angiogenesis [102]. Additionally, senescent fibroblasts secrete VEGF, suggesting VEGF's role in the senescent cell microenvironment maintenance [103]. VEGF increases levels of miR-183-5p [104], suggesting a feedback mechanism thus, VEGF not only promotes angiogenesis but also influences EC senescence through miR-183-5p. The existing regulatory loop emphasizes miR-183-5p's function in facilitating the impact of VEGF [104]. TNF-α promotes ECs senescence through various mechanisms, e.g. upregulation of senescence marker p21 [105] and secretions of SASP factors [106]. TNF-α can induce premature senescence in endothelial progenitor cells [107] and other cell types [108] through PI3K/Akt signaling pathway activation [108]. The upregulation of VCAM-1 adhesion molecule is also notable in senescent ECs [109]. The improvement of endothelial function was associated with the reverse action of senescence-related changes, which includes VCAM-1 and ICAM-1 molecules [110,111].

Recently, single-cell RNASeq analysis allowed the detection of a higher prevalence of senescent brain ECs in aged mice. The senescent brain ECs expressed a unique SASP profile [19] and were characterized by increased levels of genes related to leukocyte trans-endothelial migration (Cxcl12 and Ctnnb1), suggesting a mechanism associated with inflammation, cell-cell adhesion (Ctnnb1), or tissue plasminogen activator (Plat) [112]. Population-based studies have shown a positive correlation between DNA damage and p53 in the endothelium in human brain samples of AD and may occur independently of disease pathology [68].

In brief, the study indicates that hyperammonemia *in vivo* alters cerebrovasculature density possibly via a mechanism reflecting endothelial senescence, involving miR-183-5p. Endothelial senescence, beyond the contribution to brain aging, may exacerbate cerebrovasculature dysfunction at the level of the neurovascular unit in patients with hyperammonemia. The results offer a perspective for therapeutic intervention directed at mitigating endothelium senescence, an accompanying component of cerebral dysfunction.

Abbreviations

BBB: Blood-brain barrier
EV: Extracellular vesicle
FCS: Fluorescence Correlation Spectroscopy
ip.: Intraperitoneal
NGS: Next Generation Sequencing
OA: Ammonium acetate/here used to refer to a rat model of hyperammonemia
PBMEC: Primary Brain Microvascular Endothelial Cells
RBE4: Rat Brain Endothelial Cell Line 4
SASP: Senescence-Associated Secretory Phenotype

Authors' contributions

K.O.-G., and M.Z. conceptualization; K.O.-G., K.M., M.O.-M., A.E.-M., A.K., K.K. data acquisition and methodology; K.O.-G. data analysis; K.O.-G. and M.Z. writing and original draft preparation; M.Z. writing, review, and editing; M.Z.; funding acquisition. All authors have read and agreed to the published version of the manuscript.

Data availability

The datasets used and analyzed during this study are available from the corresponding author upon reasonable request.

Funding

This work was supported by the National Science Centre of Poland [No. 2015/19/B/NZ4/01902 and ESF [POWR.03.02.00-00-I028/17-00].

Declarations

Ethics approval

Animal experiments were performed at Mossakowski Medical Research Institute, Polish Academy of Sciences Warsaw conformed to the legislations for animal protection and care in the European Community Council Directive (2010/63/EU), and were approved by the 4th Local Ethics Committee for Animal Experimentation, Warsaw, Poland (Approval no. 57/2015).

Consent for publication

Not applicable.

Competing interests

The authors declare no competing interests.

Supplementary information

Supplementary File 1:
Fig. 1-3
Table 1-3

Legends to figures

Fig. 1. Brain capillary microvessels density in control, 12-month-old, and OA rats. The results are the mean ± SD. n=5; **p <0.001 vs. control, one-way ANOVA, and Dunnett's' post hoc.

Fig. 2. Bioinformatics analysis of miRNA profiles in the brain cortex and serum of OA rats, focusing on cellular senescence-associated pathways. A Venn diagram at the top-left with identified 306 miRNAs, was next analyzed using TarBase, miRDB, and TargetScan databases ShinyGO analysis of predicted 852 target genes. The heatmap illustrates the involvement of specific miRNAs in senescence-related pathways with target gene numbers indicated by colour intensity.

Fig. 3. The effect of ammonia on senescent phenotype characteristics of the RBE4 cell line. **A.** β-galactosidase activity in RBE4 cells following 5mM ammonia treatment for 24h. **B.** Cell cycle inhibitors p16 and p21 mRNA relative level in RBE4 cells treated with 5mM ammonia for 24h. **C.** β-galactosidase and p53 fluorescence intensity in RBE4 cells treated with 5mM ammonia for 24h and RBE4 cell cultured for 3 weeks. **D.** Senescence-Associated Secretory Phenotype in 5 mM ammonia-inducing senescence in RBE4 cells and 3-weeks RBE4. The results are the mean ± SD. n=4 *p < 0.05 vs. control, **p < 0.01 vs. control, ***p < 0.001 vs. control, ****p < 0.0001 vs. control, one-way ANOVA, and Dunnett's post hoc test.

Fig. 4. The effect of ammonia treatment and age of rats on senescent phenotype in PBMEC. **A.** Activity of β-galactosidase in PBMEC in response to 5mM ammonia **B.** β-galactosidase and p53 fluorescence intensity in 12-month-old rats PBMEC. **C.** Senescence-Associated Secretory Phenotype (SASP) factors in PBMEC. The results are the mean ± SD. n=4 **p < 0.01 vs. control, ****p < 0.0001 vs control, one-way ANOVA, and Dunnett's post hoc test comprise the results.

Fig. 5. The contribution of miR-183-5p on ammonia-induced brain ECs senescence phenotype **A.** miR-183-5p expression level in RBE4 cells treated with 5mM ammonia (left) and miR-183-5p expression level in extracellular vesicle (EVs) isolated from cultured medium of RBE4 cells following 5mM ammonia treatment (right). **B.** The effect of mimic miR-183-5p transfection on p16 (left) and p21 (right) transcript levels in RBE4 cells **C.** β-galactosidase and p53 fluorescence intensity in RBE4 cells transfected with miR-183-5p mimic. **D.** The effect of miR-183-5p transfection on selected SASP factors of RBE4 cells (left) and PBMEC (right). The results are the mean ± SD. n=4; *p <0.05 vs. control, ***p < 0.001 vs. control, ****p < 0.0001 vs. control one-way ANOVA and Dunnett's' post hoc.

References

1. Piazzolla, V.A.; Mangia, A. Noninvasive Diagnosis of NAFLD and NASH. *Cells* **2020**, *9*, 1005, doi:10.3390/cells9041005.
2. De Chiara, F.; Heebøll, S.; Marrone, G.; Montoliu, C.; Hamilton-Dutoit, S.; Ferrandez, A.; Andreola, F.; Rombouts, K.; Grønbæk, H.; Felipo, V.; et al. Urea Cycle Dysregulation in Non-Alcoholic Fatty Liver Disease. *Journal of Hepatology* **2018**, *69*, 905–915, doi:10.1016/j.jhep.2018.06.023.
3. Shavkuta, G.V.; Shnyukova, T.V.; Kolesnikova, E.S.; Kruchinin, V.V.; Lyutova, A.K.; Timchenko, A.S. Increased Ammonia Levels and Its Association with Visceral Obesity and Insulin Resistance. *jour* **2020**, 75–79, doi:10.31146/1682-8658-ecg-169-9-75-79.
4. Venediktova, N.I.; Kosenko, E.A.; Kaminsky, Yu.G. Studies on Ammocytes: Development, Metabolic Characteristics, and Detoxication of Ammonium. *Bull Exp Biol Med* **2008**, *146*, 730–732, doi:10.1007/s10517-009-0388-3.
5. Kumar, A.; Welch, N.; Mishra, S.; Bellar, A.; Silva, R.N.; Li, L.; Singh, S.S.; Sharkoff, M.; Kerr, A.; Chelluboyina, A.K.; et al. Metabolic Reprogramming during Hyperammonemia Targets Mitochondrial Function and Postmitotic Senescence. *JCI Insight* **2021**, *6*, e154089, doi:10.1172/jci.insight.154089.
6. Department of Psychiatry, Changhua Christian Hospital, Changhua, Taiwan; Huang, S.-S. Hyperammonemia-Associated Delirium Mimics Dementia: A Case Report. *Psychiatry and Clinical Psychopharmacology* **2022**, *32*, 181–183, doi:10.5152/pcp.2022.21108.
7. Upadhyay, R.; Bleck, T.P.; Busl, K.M. Hyperammonemia: What Urea-Lly Need to Know: Case Report of Severe Noncirrhotic Hyperammonemic Encephalopathy and Review of the Literature. *Case Reports in Medicine* **2016**, *2016*, 1–10, doi:10.1155/2016/8512721.
8. Kromas, M.L. Hyperammonemia-Induced Encephalopathy: A Rare Devastating Complication of Bariatric Surgery. *WJH* **2015**, *7*, 1007, doi:10.4254/wjh.v7.i7.1007.
9. Bosoi, C.R.; Rose, C.F. Identifying the Direct Effects of Ammonia on the Brain. *Metab Brain Dis* **2009**, *24*, 95–102, doi:10.1007/s11011-008-9112-7.
10. Bajaj, J.S.; Schubert, C.M.; Heuman, D.M.; Wade, J.B.; Gibson, D.P.; Topaz, A.; Saeian, K.; Hafeezullah, M.; Bell, D.E.; Sterling, R.K.; et al. Persistence of Cognitive Impairment After Resolution of Overt Hepatic Encephalopathy. *Gastroenterology* **2010**, *138*, 2332–2340, doi:10.1053/j.gastro.2010.02.015.
11. Dethloff, T.; Hansen, B.A.; Larsen, F.S. Tacrolimus Ameliorates Cerebral Vasodilatation and Intracranial Hypertension in the Rat with Portacaval Anastomosis and Hyperammonemia. *Liver Transpl* **2004**, *10*, 922–927, doi:10.1002/lt.20141.
12. Reynolds, A.S.; Brush, B.; Schiano, T.D.; Reilly, K.J.; Dangayach, N.S. Neurological Monitoring in Acute Liver Failure. *Hepatology* **2019**, *70*, 1830–1835, doi:10.1002/hep.30760.
13. Jayakumar, A.R.; Tong, X.Y.; Ospel, J.; Norenberg, M.D. Role of Cerebral Endothelial Cells in the Astrocyte Swelling and Brain Edema Associated with Acute Hepatic Encephalopathy. *Neuroscience* **2012**, *218*, 305–316, doi:10.1016/j.neuroscience.2012.05.006.
14. Reitsma, S.; Slaaf, D.W.; Vink, H.; Van Zandvoort, M.A.M.J.; Oude Egbrink, M.G.A. The Endothelial Glycocalyx: Composition, Functions, and Visualization. *Pflugers Arch - Eur J Physiol* **2007**, *454*, 345–359, doi:10.1007/s00424-007-0212-8.
15. Kurz, D.J.; Decary, S.; Hong, Y.; Trivier, E.; Akhmedov, A.; Erusalimsky, J.D. Chronic Oxidative Stress Compromises Telomere Integrity and Accelerates the Onset of Senescence in Human Endothelial Cells. *Journal of Cell Science* **2004**, *117*, 2417–2426, doi:10.1242/jcs.01097.

16. Worzfeld, T.; Schwaninger, M. Apicobasal Polarity of Brain Endothelial Cells. *J Cereb Blood Flow Metab* **2016**, *36*, 340–362, doi:10.1177/0271678X15608644.
17. Loetscher, T. Cognitive Training Interventions for Dementia and Mild Cognitive Impairment in Parkinson's Disease - A Cochrane Review Summary with Commentary. *NRE* **2021**, *48*, 385–387, doi:10.3233/NRE-218001.
18. Sikora, E.; Bielak-Zmijewska, A.; Dudkowska, M.; Krzystyniak, A.; Mosieniak, G.; Wesierska, M.; Wlodarczyk, J. Cellular Senescence in Brain Aging. *Front. Aging Neurosci.* **2021**, *13*, 646924, doi:10.3389/fnagi.2021.646924.
19. Kiss, T.; Nyúl-Tóth, Á.; Balasubramanian, P.; Tarantini, S.; Ahire, C.; DelFavero, J.; Yabluchanskiy, A.; Csipo, T.; Farkas, E.; Wiley, G.; et al. Single-Cell RNA Sequencing Identifies Senescent Cerebromicrovascular Endothelial Cells in the Aged Mouse Brain. *GeroScience* **2020**, *42*, 429–444, doi:10.1007/s11357-020-00177-1.
20. Alavi, P.; Yousef Abdualla, R.; Brown, D.; Mojiri, A.; Nagendran, J.; Lewis, J.; Bourque, S.L.; Jahroudi, N. Aging Is Associated With Organ-Specific Alterations in the Level and Expression Pattern of von Willebrand Factor. *ATVB* **2023**, *43*, 2183–2196, doi:10.1161/ATVBAHA.123.319255.
21. Görg, B.; Karababa, A.; Shafigullina, A.; Bidmon, H.J.; Häussinger, D. Ammonia-Induced Senescence in Cultured Rat Astrocytes and in Human Cerebral Cortex in Hepatic Encephalopathy: Hepatic Encephalopathy and Senescence. *Glia* **2015**, *63*, 37–50, doi:10.1002/glia.22731.
22. Görg, B.; Karababa, A.; Häussinger, D. Hepatic Encephalopathy and Astrocyte Senescence. *Journal of Clinical and Experimental Hepatology* **2018**, *8*, 294–300, doi:10.1016/j.jceh.2018.05.003.
23. Oenarto, J.; Karababa, A.; Castoldi, M.; Bidmon, H.J.; Görg, B.; Häussinger, D. Ammonia-Induced miRNA Expression Changes in Cultured Rat Astrocytes. *Sci Rep* **2016**, *6*, 18493, doi:10.1038/srep18493.
24. Chinta, S.J.; Woods, G.; Rane, A.; Demaria, M.; Campisi, J.; Andersen, J.K. Cellular Senescence and the Aging Brain. *Experimental Gerontology* **2015**, *68*, 3–7, doi:10.1016/j.exger.2014.09.018.
25. Hindfelt, B. The Distribution of Ammonia between Extracellular and Intracellular Compartments of the Rat Brain. *Clinical Science* **1975**, *48*, 33–37, doi:10.1042/cs0480033.
26. Ruck, T.; Bittner, S.; Epping, L.; Herrmann, A.M.; Meuth, S.G. Isolation of Primary Murine Brain Microvascular Endothelial Cells. *JoVE* **2014**, 52204, doi:10.3791/52204.
27. Hindfelt, B. ON MECHANISMS IN HYPERAMMONEMIC COMA—WITH PARTICULAR REFERENCE TO HEPATIC ENCEPHALOPATHY. *Annals of the New York Academy of Sciences* **1975**, *252*, 116–123, doi:10.1111/j.1749-6632.1975.tb19148.x.
28. Orzeł-Gajowik, K.; Milewski, K.; Zielińska, M. miRNA-Ome Plasma Analysis Unveils Changes in Blood–Brain Barrier Integrity Associated with Acute Liver Failure in Rats. *Fluids Barriers CNS* **2023**, *20*, 92, doi:10.1186/s12987-023-00484-7.
29. Ge, S.X.; Jung, D.; Yao, R. ShinyGO: A Graphical Gene-Set Enrichment Tool for Animals and Plants. *Bioinformatics* **2020**, *36*, 2628–2629, doi:10.1093/bioinformatics/btz931.
30. Skowrońska, M.; Zielińska, M.; Wójcik-Stanaszek, L.; Ruszkiewicz, J.; Milatovic, D.; Aschner, M.; Albrecht, J. Ammonia Increases Paracellular Permeability of Rat Brain Endothelial Cells by a Mechanism Encompassing Oxidative/Nitrosative Stress and Activation of Matrix Metalloproteinases: Ammonia-Induced Brain Endothelium Damage. *Journal of Neurochemistry* **2012**, *121*, 125–134, doi:10.1111/j.1471-4159.2012.07669.x.

31. Hernández-Rabaza, V.; Cabrera-Pastor, A.; Taoro-González, L.; Malaguarnera, M.; Agustí, A.; Llansola, M.; Felipo, V. Hyperammonemia Induces Glial Activation, Neuroinflammation and Alters Neurotransmitter Receptors in Hippocampus, Impairing Spatial Learning: Reversal by Sulforaphane. *J Neuroinflammation* **2016**, *13*, 41, doi:10.1186/s12974-016-0505-y.
32. Oja, S.S.; Saransaari, P.; Korpi, E.R. Neurotoxicity of Ammonia. *Neurochem Res* **2017**, *42*, 713–720, doi:10.1007/s11064-016-2014-x.
33. Manwani, B.; Friedler, B.; Verma, R.; Venna, V.R.; McCullough, L.D.; Liu, F. Perfusion of Ischemic Brain in Young and Aged Animals: A Laser Speckle Flowmetry Study. *Stroke* **2014**, *45*, 571–578, doi:10.1161/STROKEAHA.113.002944.
34. Reed, M.J.; Vernon, R.B.; Damodarasamy, M.; Chan, C.K.; Wight, T.N.; Bentov, I.; Banks, W.A. Microvasculature of the Mouse Cerebral Cortex Exhibits Increased Accumulation and Synthesis of Hyaluronan With Aging. *GERONA* **2016**, glw213, doi:10.1093/gerona/glw213.
35. Sweeney, M.D.; Kisler, K.; Montagne, A.; Toga, A.W.; Zlokovic, B.V. The Role of Brain Vasculature in Neurodegenerative Disorders. *Nat Neurosci* **2018**, *21*, 1318–1331, doi:10.1038/s41593-018-0234-x.
36. Czarnecka, A.; Aleksandrowicz, M.; Jasiński, K.; Jaźwiec, R.; Kalita, K.; Hilgier, W.; Zielińska, M. Cerebrovascular Reactivity and Cerebral Perfusion of Rats with Acute Liver Failure: Role of L-glutamine and Asymmetric Dimethylarginine in L-arginine-induced Response. *Journal of Neurochemistry* **2018**, *147*, 692–704, doi:10.1111/jnc.14578.
37. Yamazaki, Y.; Baker, D.J.; Tachibana, M.; Liu, C.-C.; Van Deursen, J.M.; Brott, T.G.; Bu, G.; Kanekiyo, T. Vascular Cell Senescence Contributes to Blood–Brain Barrier Breakdown. *Stroke* **2016**, *47*, 1068–1077, doi:10.1161/STROKEAHA.115.010835.
38. Kook, S.-Y.; Hong, H.S.; Moon, M.; Ha, C.M.; Chang, S.; Mook-Jung, I. A 1-42-RAGE Interaction Disrupts Tight Junctions of the Blood-Brain Barrier Via Ca2+-Calcineurin Signaling. *Journal of Neuroscience* **2012**, *32*, 8845–8854, doi:10.1523/JNEUROSCI.6102-11.2012.
39. Stafford, P.; Mitra, S.; Debot, M.; Lutz, P.; Stem, A.; Hadley, J.; Hom, P.; Schaid, T.R.; Cohen, M.J. Astrocytes and Pericytes Attenuate Severely Injured Patient Plasma Mediated Expression of Tight Junction Proteins in Endothelial Cells. *PLoS ONE* **2022**, *17*, e0270817, doi:10.1371/journal.pone.0270817.
40. Wang, W.; Dentler, W.L.; Borchardt, R.T. VEGF Increases BMEC Monolayer Permeability by Affecting Occludin Expression and Tight Junction Assembly. *American Journal of Physiology-Heart and Circulatory Physiology* **2001**, *280*, H434–H440, doi:10.1152/ajpheart.2001.280.1.H434.
41. Haorah, J.; Knipe, B.; Gorantla, S.; Zheng, J.; Persidsky, Y. Alcohol-induced Blood–Brain Barrier Dysfunction Is Mediated via Inositol 1,4,5-triphosphate Receptor (IP $_3$ R)-gated Intracellular Calcium Release. *Journal of Neurochemistry* **2007**, *100*, 324–336, doi:10.1111/j.1471-4159.2006.04245.x.
42. Pathogenesis of Hepatic Encephalopathy in Acute Liver Failure. *Semin Liver Dis* **2003**, *23*, 259–270, doi:10.1055/s-2003-42644.
43. Reis, E.; Coolen, T.; Lolli, V. MRI Findings in Acute Hyperammonemic Encephalopathy: Three Cases of Different Etiologies. *Journal of the Belgian Society of Radiology* **2020**, *104*, 9, doi:10.5334/jbsr.2017.
44. Chen, F.; Ohashi, N.; Li, W.; Eckman, C.; Nguyen, J.H. Disruptions of Occludin and Claudin-5 in Brain Endothelial Cells in Vitro and in Brains of Mice with Acute Liver Failure. *Hepatology* **2009**, *50*, 1914–1923, doi:10.1002/hep.23203.

45. Nguyen, J.H. Blood–Brain Barrier in Acute Liver Failure. *Neurochemistry International* **2012**, *60*, 676–683, doi:10.1016/j.neuint.2011.10.012.
46. Baek, S.Y.; Lee, E.H.; Oh, T.W.; Do, H.J.; Kim, K.-Y.; Park, K.-I.; Kim, Y.W. Network Pharmacology-Based Approaches of Rheum Undulatum Linne and Glycyrriza Uralensis Fischer Imply Their Regulation of Liver Failure with Hepatic Encephalopathy in Mice. *Biomolecules* **2020**, *10*, 437, doi:10.3390/biom10030437.
47. Bhatt, H.; Rao, G.S. Medical Management of Acute Liver Failure. In *Pediatric Critical Care*; Mastropietro, C.W., Valentine, K.M., Eds.; Springer International Publishing: Cham, 2019; pp. 155–173 ISBN 978-3-319-96498-0.
48. Zhu, Q.M.; Singh, A.K.; Chang, H.-E.R.; Konka, S.A. Hyperammonemic Encephalopathy Induced by Valproic Acid. *BMJ Case Rep* **2024**, *17*, e257144, doi:10.1136/bcr-2023-257144.
49. Savy, N.; Brossier, D.; Brunel-Guitton, C.; Ducharme-Crevier, L.; Du Pont-Thibodeau, G.; Jouvet, P. Acute Pediatric Hyperammonemia: Current Diagnosis and Management Strategies. *HMER* **2018**, *Volume 10*, 105–115, doi:10.2147/HMER.S140711.
50. Häberle, J.; Burlina, A.; Chakrapani, A.; Dixon, M.; Karall, D.; Lindner, M.; Mandel, H.; Martinelli, D.; Pintos-Morell, G.; Santer, R.; et al. Suggested Guidelines for the Diagnosis and Management of Urea Cycle Disorders: First Revision. *J of Inher Metab Disea* **2019**, *42*, 1192–1230, doi:10.1002/jimd.12100.
51. Tantengco, O.A.G.; De Jesus, F.C.C.; Gampoy, E.F.S.; Ornos, E.D.B.; Vidal, M.S.; Abad, C.L.R. Hyperammonemia Syndrome Associated with *Ureaplasma* Spp. Infections in Immunocompromised Patients and Transplant Recipients: A Systematic Review and Meta-analysis. *Clinical Transplantation* **2021**, *35*, e14334, doi:10.1111/ctr.14334.
52. Muñoz-Espín, D.; Serrano, M. Cellular Senescence: From Physiology to Pathology. *Nat Rev Mol Cell Biol* **2014**, *15*, 482–496, doi:10.1038/nrm3823.
53. Barboza, J.A.; Liu, G.; Ju, Z.; El-Naggar, A.K.; Lozano, G. P21 Delays Tumor Onset by Preservation of Chromosomal Stability. *Proc. Natl. Acad. Sci. U.S.A.* **2006**, *103*, 19842–19847, doi:10.1073/pnas.0606343104.
54. Serrano, M.; Lee, H.-W.; Chin, L.; Cordon-Cardo, C.; Beach, D.; DePinho, R.A. Role of the INK4a Locus in Tumor Suppression and Cell Mortality. *Cell* **1996**, *85*, 27–37, doi:10.1016/S0092-8674(00)81079-X.
55. Warboys, C.M.; De Luca, A.; Amini, N.; Luong, L.; Duckles, H.; Hsiao, S.; White, A.; Biswas, S.; Khamis, R.; Chong, C.K.; et al. Disturbed Flow Promotes Endothelial Senescence via a P53-Dependent Pathway. *ATVB* **2014**, *34*, 985–995, doi:10.1161/ATVBAHA.114.303415.
56. Zhan, H.; Suzuki, T.; Aizawa, K.; Miyagawa, K.; Nagai, R. Ataxia Telangiectasia Mutated (ATM)-Mediated DNA Damage Response in Oxidative Stress-Induced Vascular Endothelial Cell Senescence. *Journal of Biological Chemistry* **2010**, *285*, 29662–29670, doi:10.1074/jbc.M110.125138.
57. Dai, D.-F.; Rabinovitch, P.S.; Ungvari, Z. Mitochondria and Cardiovascular Aging. *Circulation Research* **2012**, *110*, 1109–1124, doi:10.1161/CIRCRESAHA.111.246140.
58. Ungvari, Z.; Labinskyy, N.; Gupte, S.; Chander, P.N.; Edwards, J.G.; Csiszar, A. Dysregulation of Mitochondrial Biogenesis in Vascular Endothelial and Smooth Muscle Cells of Aged Rats. *American Journal of Physiology-Heart and Circulatory Physiology* **2008**, *294*, H2121–H2128, doi:10.1152/ajpheart.00012.2008.
59. Milewski, K.; Orzeł-Gajowik, K.; Zielińska, M. Mitochondrial Changes in Rat Brain Endothelial Cells Associated with Hepatic Encephalopathy: Relation to the Blood–Brain Barrier Dysfunction. *Neurochem Res* **2024**, *49*, 1489–1504, doi:10.1007/s11064-022-03698-7.

60. Jayakumar, A.R.; Norenberg, M.D. Endothelial-Astrocytic Interactions in Acute Liver Failure. *Metab Brain Dis* **2013**, *28*, 183–186, doi:10.1007/s11011-012-9344-4.
61. Milewski, K.; Czarnecka, A.M.; Albrecht, J.; Zielińska, M. Decreased Expression and Uncoupling of Endothelial Nitric Oxide Synthase in the Cerebral Cortex of Rats with Thioacetamide-Induced Acute Liver Failure. *IJMS* **2021**, *22*, 6662, doi:10.3390/ijms22136662.
62. Han, X.; Zhang, T.; Liu, H.; Mi, Y.; Gou, X. Astrocyte Senescence and Alzheimer's Disease: A Review. *Front. Aging Neurosci.* **2020**, *12*, 148, doi:10.3389/fnagi.2020.00148.
63. Cohen, J.; Torres, C. Astrocyte Senescence: Evidence and Significance. *Aging Cell* **2019**, *18*, e12937, doi:10.1111/acel.12937.
64. Zhang, P.; Kishimoto, Y.; Grammatikakis, I.; Gottimukkala, K.; Cutler, R.G.; Zhang, S.; Abdelmohsen, K.; Bohr, V.A.; Misra Sen, J.; Gorospe, M.; et al. Senolytic Therapy Alleviates Aβ-Associated Oligodendrocyte Progenitor Cell Senescence and Cognitive Deficits in an Alzheimer's Disease Model. *Nat Neurosci* **2019**, *22*, 719–728, doi:10.1038/s41593-019-0372-9.
65. Knopp, R.C.; Erickson, M.A.; Rhea, E.M.; Reed, M.J.; Banks, W.A. Cellular Senescence and the Blood–Brain Barrier: Implications for Aging and Age-Related Diseases. *Exp Biol Med (Maywood)* **2023**, *248*, 399–411, doi:10.1177/15353702231157917.
66. Guerrero, A.; De Strooper, B.; Arancibia-Cárcamo, I.L. Cellular Senescence at the Crossroads of Inflammation and Alzheimer's Disease. *Trends in Neurosciences* **2021**, *44*, 714–727, doi:10.1016/j.tins.2021.06.007.
67. Cercy, S.P. Pericytes and the Neurovascular Unit: The Critical Nexus of Alzheimer Disease Pathogenesis? *Exploratory Research and Hypothesis in Medicine* **2021**, *000*, 000–000, doi:10.14218/ERHM.2020.00062.
68. Garwood, C.J.; Simpson, J.E.; Al Mashhadi, S.; Axe, C.; Wilson, S.; Heath, P.R.; Shaw, P.J.; Matthews, F.E.; Brayne, C.; Ince, P.G.; et al. DNA Damage Response and Senescence in Endothelial Cells of Human Cerebral Cortex and Relation to A Lzheimer's Neuropathology Progression: A Population-based Study in the M Edical R Esearch C Ouncil C Ognitive F Unction and A Geing S Tudy (MRC - CFAS) Cohort. *Neuropathology Appl Neurobio* **2014**, *40*, 802–814, doi:10.1111/nan.12156.
69. Angom, R.S.; Wang, Y.; Wang, E.; Pal, K.; Bhattacharya, S.; Watzlawik, J.O.; Rosenberry, T.L.; Das, P.; Mukhopadhyay, D. VEGF Receptor-1 Modulates Amyloid β 1–42 Oligomer-induced Senescence in Brain Endothelial Cells. *FASEB j.* **2019**, *33*, 4626–4637, doi:10.1096/fj.201802003R.
70. Matsushita, H.; Chang, E.; Glassford, A.J.; Cooke, J.P.; Chiu, C.-P.; Tsao, P.S. eNOS Activity Is Reduced in Senescent Human Endothelial Cells: Preservation by hTERT Immortalization. *Circulation Research* **2001**, *89*, 793–798, doi:10.1161/hh2101.098443.
71. Rippe, C.; Blimline, M.; Magerko, K.A.; Lawson, B.R.; LaRocca, T.J.; Donato, A.J.; Seals, D.R. MicroRNA Changes in Human Arterial Endothelial Cells with Senescence: Relation to Apoptosis, eNOS and Inflammation. *Experimental Gerontology* **2012**, *47*, 45–51, doi:10.1016/j.exger.2011.10.004.
72. Rajapakse, A.G.; Yepuri, G.; Carvas, J.M.; Stein, S.; Matter, C.M.; Scerri, I.; Ruffieux, J.; Montani, J.-P.; Ming, X.-F.; Yang, Z. Hyperactive S6K1 Mediates Oxidative Stress and Endothelial Dysfunction in Aging: Inhibition by Resveratrol. *PLoS ONE* **2011**, *6*, e19237, doi:10.1371/journal.pone.0019237.

73. Hernandez-Segura, A.; De Jong, T.V.; Melov, S.; Guryev, V.; Campisi, J.; Demaria, M. Unmasking Transcriptional Heterogeneity in Senescent Cells. *Current Biology* **2017**, *27*, 2652-2660.e4, doi:10.1016/j.cub.2017.07.033.
74. Maciel-Barón, L.A.; Morales-Rosales, S.L.; Aquino-Cruz, A.A.; Triana-Martínez, F.; Galván-Arzate, S.; Luna-López, A.; González-Puertos, V.Y.; López-Díazguerrero, N.E.; Torres, C.; Königsberg, M. Senescence Associated Secretory Phenotype Profile from Primary Lung Mice Fibroblasts Depends on the Senescence Induction Stimuli. *AGE* **2016**, *38*, 26, doi:10.1007/s11357-016-9886-1.
75. He, S.; Sharpless, N.E. Senescence in Health and Disease. *Cell* **2017**, *169*, 1000–1011, doi:10.1016/j.cell.2017.05.015.
76. Wang, F.; Zhao, Y.; Chen, S.; Chen, L.; Sun, L.; Cao, M.; Li, C.; Zhou, X. Astragaloside IV Alleviates Ammonia-Induced Apoptosis and Oxidative Stress in Bovine Mammary Epithelial Cells. *IJMS* **2019**, *20*, 600, doi:10.3390/ijms20030600.
77. Zou, Y.; Chen, W.; Xia, B.; Xiang, Y.; Shen, Z.; Han, Y.; Xue, S. Ammonia Toxicity in the Bighead Carp (Aristichthys Nobilis): Hematology, Antioxidation, Immunity, Inflammation and Stress. *Toxics* **2023**, *11*, 243, doi:10.3390/toxics11030243.
78. Williams, E.; Kobs, Z.; Chu, C.; Venter, J.; Petrescu, A.; An, S.; DeMorrow, S. Hyperammonemia-induced DNA-damage Response Leads to the Acquisition of Cellular Senescence in Neurons after Chronic Liver Failure. *The FASEB Journal* **2022**, *36*, fasebj.2022.36.S1.R4234, doi:10.1096/fasebj.2022.36.S1.R4234.
79. Szabo, G.; Bala, S. MicroRNAs in Liver Disease. *Nat Rev Gastroenterol Hepatol* **2013**, *10*, 542–552, doi:10.1038/nrgastro.2013.87.
80. Bala, S.; Szabo, G. MicroRNA Signature in Alcoholic Liver Disease. *International Journal of Hepatology* **2012**, *2012*, 1–6, doi:10.1155/2012/498232.
81. Tognini, P.; Putignano, E.; Coatti, A.; Pizzorusso, T. Experience-Dependent Expression of miR-132 Regulates Ocular Dominance Plasticity. *Nat Neurosci* **2011**, *14*, 1237–1239, doi:10.1038/nn.2920.
82. Wang, J.; Xu, F.; Zhu, X.; Li, X.; Li, Y.; Li, J. Targeting microRNAs to Regulate the Integrity of the Blood–Brain Barrier. *Front. Bioeng. Biotechnol.* **2021**, *9*, 673415, doi:10.3389/fbioe.2021.673415.
83. Toyama, K.; Igase, M.; Spin, J.M.; Abe, Y.; Javkhlant, A.; Okada, Y.; Wagenhäuser, M.U.; Schelzig, H.; Tsao, P.S.; Mogi, M. Exosome miR-501-3p Elevation Contributes to Progression of Vascular Stiffness. *Circ Rep* **2021**, *3*, 170–177, doi:10.1253/circrep.CR-20-0135.
84. Ye, E.-A.; Liu, L.; Steinle, J.J. miR-15a/16 Inhibits TGF-Beta3/VEGF Signaling and Increases Retinal Endothelial Cell Barrier Proteins. *Vision Research* **2017**, *139*, 23–29, doi:10.1016/j.visres.2017.07.007.
85. Burek, M.; König, A.; Lang, M.; Fiedler, J.; Oerter, S.; Roewer, N.; Bohnert, M.; Thal, S.C.; Blecharz-Lang, K.G.; Woitzik, J.; et al. Hypoxia-Induced MicroRNA-212/132 Alter Blood-Brain Barrier Integrity Through Inhibition of Tight Junction-Associated Proteins in Human and Mouse Brain Microvascular Endothelial Cells. *Transl. Stroke Res.* **2019**, *10*, 672–683, doi:10.1007/s12975-018-0683-2.
86. Orzeł-Gajowik, K.; Milewski, K.; Zielińska, M. Insight into microRNAs-Mediated Communication between Liver and Brain: A Possible Approach for Understanding Acute Liver Failure? *IJMS* **2021**, *23*, 224, doi:10.3390/ijms23010224.
87. Davis, C.; Dukes, A.; Drewry, M.; Helwa, I.; Johnson, M.H.; Isales, C.M.; Hill, W.D.; Liu, Y.; Shi, X.; Fulzele, S.; et al. MicroRNA-183-5p Increases with Age in Bone-Derived Extracellular Vesicles, Suppresses Bone Marrow Stromal (Stem) Cell Proliferation, and Induces Stem Cell Senescence. *Tissue Engineering Part A* **2017**, *23*, 1231–1240, doi:10.1089/ten.tea.2016.0525.

88. Nguyen, M.T.; Min, K.-H.; Lee, W. MiR-183-5p Induced by Saturated Fatty Acids Hinders Insulin Signaling by Downregulating IRS-1 in Hepatocytes. *IJMS* **2022**, *23*, 2979, doi:10.3390/ijms23062979.
89. Sarver, A.L.; Li, L.; Subramanian, S. MicroRNA miR-183 Functions as an Oncogene by Targeting the Transcription Factor *EGR1* and Promoting Tumor Cell Migration. *Cancer Research* **2010**, *70*, 9570–9580, doi:10.1158/0008-5472.CAN-10-2074.
90. Zhang, Q.; Ren, W.; Huang, B.; Yi, L.; Zhu, H. MicroRNA-183/182/96 Cooperatively Regulates the Proliferation of Colon Cancer Cells. *Molecular Medicine Reports* **2015**, *12*, 668–674, doi:10.3892/mmr.2015.3376.
91. Huangfu, L.; Liang, H.; Wang, G.; Su, X.; Li, L.; Du, Z.; Hu, M.; Dong, Y.; Bai, X.; Liu, T.; et al. miR-183 Regulates Autophagy and Apoptosis in Colorectal Cancer through Targeting of UVRAG. *Oncotarget* **2016**, *7*, 4735–4745, doi:10.18632/oncotarget.6732.
92. Bi, D.-P.; Yin, C.-H.; Zhang, X.-Y.; Yang, N.-N.; Xu, J.-Y. miR-183 Functions as an Oncogene by Targeting ABCA1 in Colon Cancer. *Oncology Reports* **2016**, *35*, 2873–2879, doi:10.3892/or.2016.4631.
93. Zou, H.; Chen, H.; Liu, S.; Gan, X. Identification of a Novel Circ_0018289/miR-183-5p/TMED5 Regulatory Network in Cervical Cancer Development. *World J Surg Onc* **2021**, *19*, 246, doi:10.1186/s12957-021-02350-y.
94. Pierce, M.L.; Weston, M.D.; Fritzsch, B.; Gabel, H.W.; Ruvkun, G.; Soukup, G.A. MicroRNA-183 Family Conservation and Ciliated Neurosensory Organ Expression. *Evolution and Development* **2008**, *10*, 106–113, doi:10.1111/j.1525-142X.2007.00217.x.
95. Li, H.; Kloosterman, W.; Fekete, D.M. MicroRNA-183 Family Members Regulate Sensorineural Fates in the Inner Ear. *J. Neurosci.* **2010**, *30*, 3254–3263, doi:10.1523/JNEUROSCI.4948-09.2010.
96. Piscopo, P.; Lacorte, E.; Feligioni, M.; Mayer, F.; Crestini, A.; Piccolo, L.; Bacigalupo, I.; Filareti, M.; Ficulle, E.; Confaloni, A.; et al. MicroRNAs and Mild Cognitive Impairment: A Systematic Review. *Ageing Research Reviews* **2019**, *50*, 131–141, doi:10.1016/j.arr.2018.11.005.
97. Wang, H.; Ma, M.; Li, Y.; Liu, J.; Sun, C.; Liu, S.; Ma, Y.; Yan, Y.; Tang, Z.; Shen, S.; et al. miR-183 and miR-96 Orchestrate Both Glucose and Fat Utilization in Skeletal Muscle. *EMBO Reports* **2021**, *22*, e52247, doi:10.15252/embr.202052247.
98. Goodall, E.F.; Leach, V.; Wang, C.; Cooper-Knock, J.; Heath, P.R.; Baker, D.; Drew, D.R.; Saffrey, M.J.; Simpson, J.E.; Romero, I.A.; et al. Age-Associated mRNA and miRNA Expression Changes in the Blood-Brain Barrier. *IJMS* **2019**, *20*, 3097, doi:10.3390/ijms20123097.
99. Bernstock, J.D.; Lee, Y.; Peruzzotti-Jametti, L.; Southall, N.; Johnson, K.R.; Maric, D.; Volpe, G.; Kouznetsova, J.; Zheng, W.; Pluchino, S.; et al. A Novel Quantitative High-Throughput Screen Identifies Drugs That Both Activate SUMO Conjugation via the Inhibition of microRNAs 182 and 183 and Facilitate Neuroprotection in a Model of Oxygen and Glucose Deprivation. *J Cereb Blood Flow Metab* **2016**, *36*, 426–441, doi:10.1177/0271678X15609939.
100. Zhou, X.; Perez, F.; Han, K.; Jurivich, D.A. Clonal Senescence Alters Endothelial ICAM-1 Function. *Mechanisms of Ageing and Development* **2006**, *127*, 779–785, doi:10.1016/j.mad.2006.07.003.
101. Gorgoulis, V.G.; Pratsinis, H.; Zacharatos, P.; Demoliou, C.; Sigala, F.; Asimacopoulos, P.J.; Papavassiliou, A.G.; Kletsas, D. P53-Dependent ICAM-1 Overexpression in Senescent Human Cells Identified in Atherosclerotic Lesions. *Laboratory Investigation* **2005**, *85*, 502–511, doi:10.1038/labinvest.3700241.

102. Lee, Y.-N.; Wu, Y.-J.; Lee, H.-I.; Wang, H.-H.; Chang, C.-Y.; Tien, T.-Y.; Lin, C.-F.; Su, C.-H.; Yeh, H.-I. Ultrasonic Microbubble VEGF Gene Delivery Improves Angiogenesis of Senescent Endothelial Progenitor Cells. *Sci Rep* **2021**, *11*, 13449, doi:10.1038/s41598-021-92754-3.
103. Coppé, J.-P.; Desprez, P.-Y.; Krtolica, A.; Campisi, J. The Senescence-Associated Secretory Phenotype: The Dark Side of Tumor Suppression. *Annu. Rev. Pathol. Mech. Dis.* **2010**, *5*, 99–118, doi:10.1146/annurev-pathol-121808-102144.
104. Zhang, Z.-Z.; Qin, X.-H.; Zhang, J. MicroRNA-183 Inhibition Exerts Suppressive Effects on Diabetic Retinopathy by Inactivating *BTG1* -Mediated PI3K/Akt/VEGF Signaling Pathway. *American Journal of Physiology-Endocrinology and Metabolism* **2019**, *316*, E1050–E1060, doi:10.1152/ajpendo.00444.2018.
105. Wan, Y.; Liu, Z.; Wu, A.; Khan, A.H.; Zhu, Y.; Ding, S.; Li, X.; Zhao, Y.; Dai, X.; Zhou, J.; et al. Hyperglycemia Promotes Endothelial Cell Senescence through AQR/PLAU Signaling Axis. *IJMS* **2022**, *23*, 2879, doi:10.3390/ijms23052879.
106. Nikolajevic, J.; Ariaee, N.; Liew, A.; Abbasnia, S.; Fazeli, B.; Sabovic, M. The Role of MicroRNAs in Endothelial Cell Senescence. *Cells* **2022**, *11*, 1185, doi:10.3390/cells11071185.
107. Zhang, Y.; Herbert, B.; Rajashekhar, G.; Ingram, D.A.; Yoder, M.C.; Clauss, M.; Rehman, J. Premature Senescence of Highly Proliferative Endothelial Progenitor Cells Is Induced by Tumor Necrosis Factor-α *via* the P38 Mitogen-activated Protein Kinase Pathway. *FASEB j.* **2009**, *23*, 1358–1365, doi:10.1096/fj.08-110296.
108. Li, P.; Gan, Y.; Xu, Y.; Song, L.; Wang, L.; Ouyang, B.; Zhang, C.; Zhou, Q. The Inflammatory Cytokine TNF-α Promotes the Premature Senescence of Rat Nucleus Pulposus Cells via the PI3K/Akt Signaling Pathway. *Sci Rep* **2017**, *7*, 42938, doi:10.1038/srep42938.
109. Yepuri, G.; Velagapudi, S.; Xiong, Y.; Rajapakse, A.G.; Montani, J.; Ming, X.; Yang, Z. Positive Crosstalk between arginase-II and S6K1 in Vascular Endothelial Inflammation and Aging. *Aging Cell* **2012**, *11*, 1005–1016, doi:10.1111/acel.12001.
110. Yu, Y.; Ren, Y.; Li, Z.; Li, Y.; Li, Y.; Zhang, Y.; Gui, R.; Cui, Y.; Qian, L.; Xiong, Y. Myo1b Promotes Premature Endothelial Senescence and Dysfunction via Suppressing Autophagy: Implications for Vascular Aging. *Oxidative Medicine and Cellular Longevity* **2023**, *2023*, 1–19, doi:10.1155/2023/4654083.
111. Le, A.-N.; Park, S.-S.; Le, M.-X.; Lee, U.H.; Ko, B.K.; Lim, H.R.; Yu, R.; Choi, S.H.; Lee, B.J.; Ham, S.-Y.; et al. DRG2 Depletion Promotes Endothelial Cell Senescence and Vascular Endothelial Dysfunction. *IJMS* **2022**, *23*, 2877, doi:10.3390/ijms23052877.
112. Mehta, D.; Malik, A.B. Signaling Mechanisms Regulating Endothelial Permeability. *Physiological Reviews* **2006**, *86*, 279–367, doi:10.1152/physrev.00012.2005.

Figure 1.

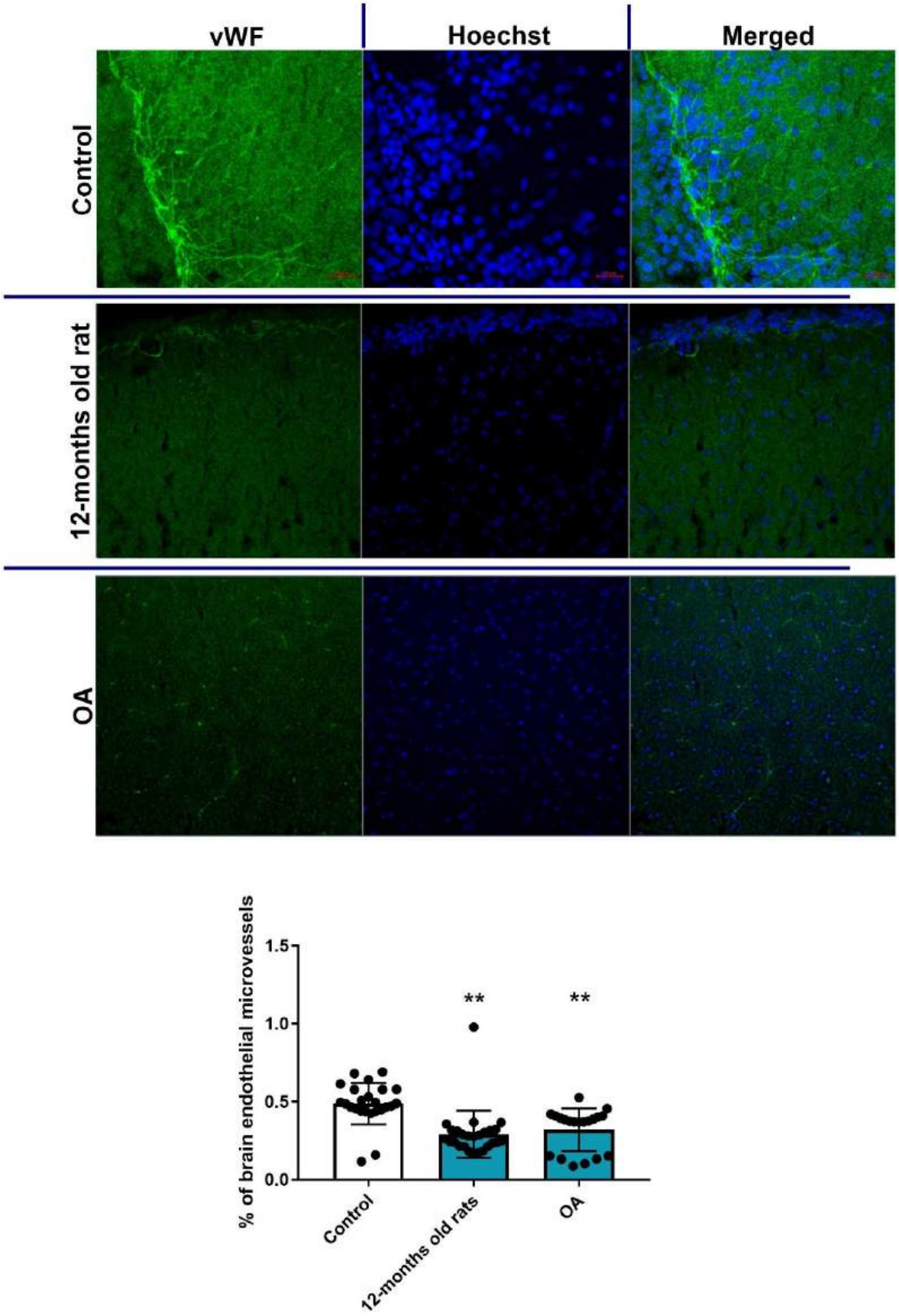

Figure 2.

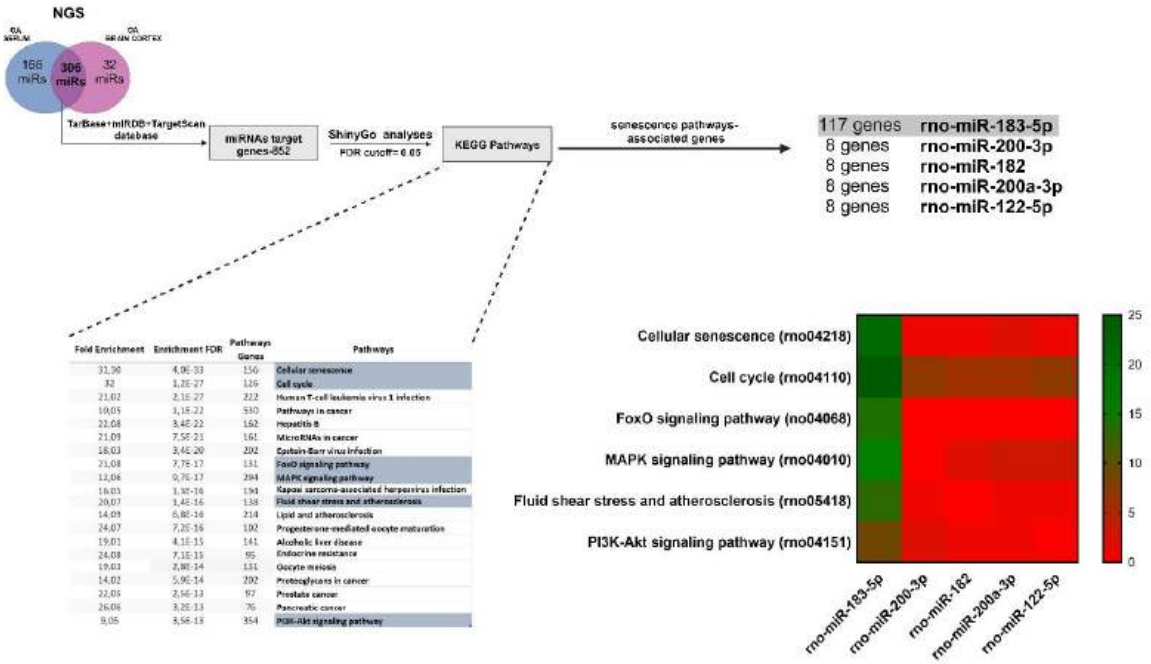

Figure 3.

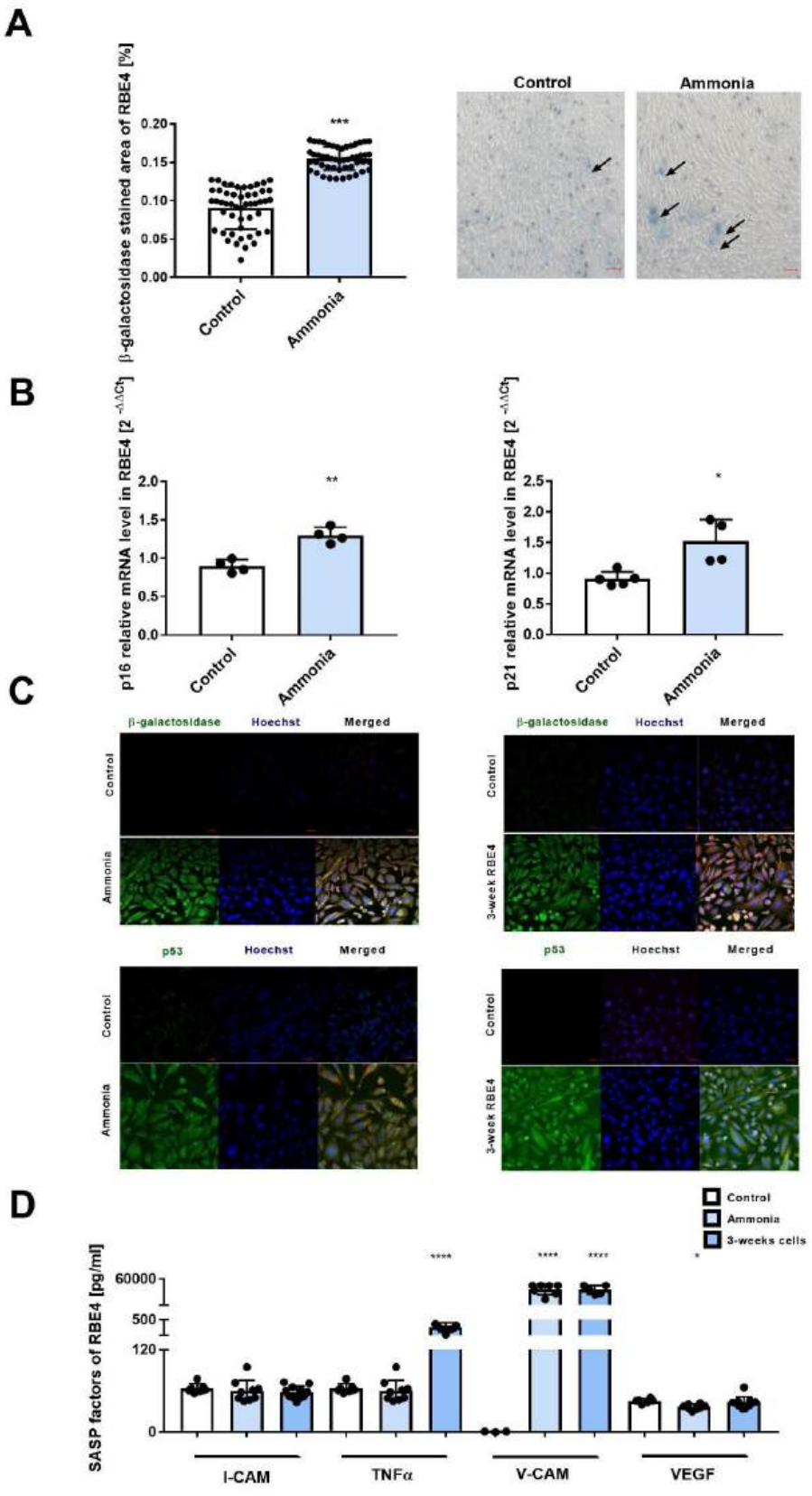

Figure 4.

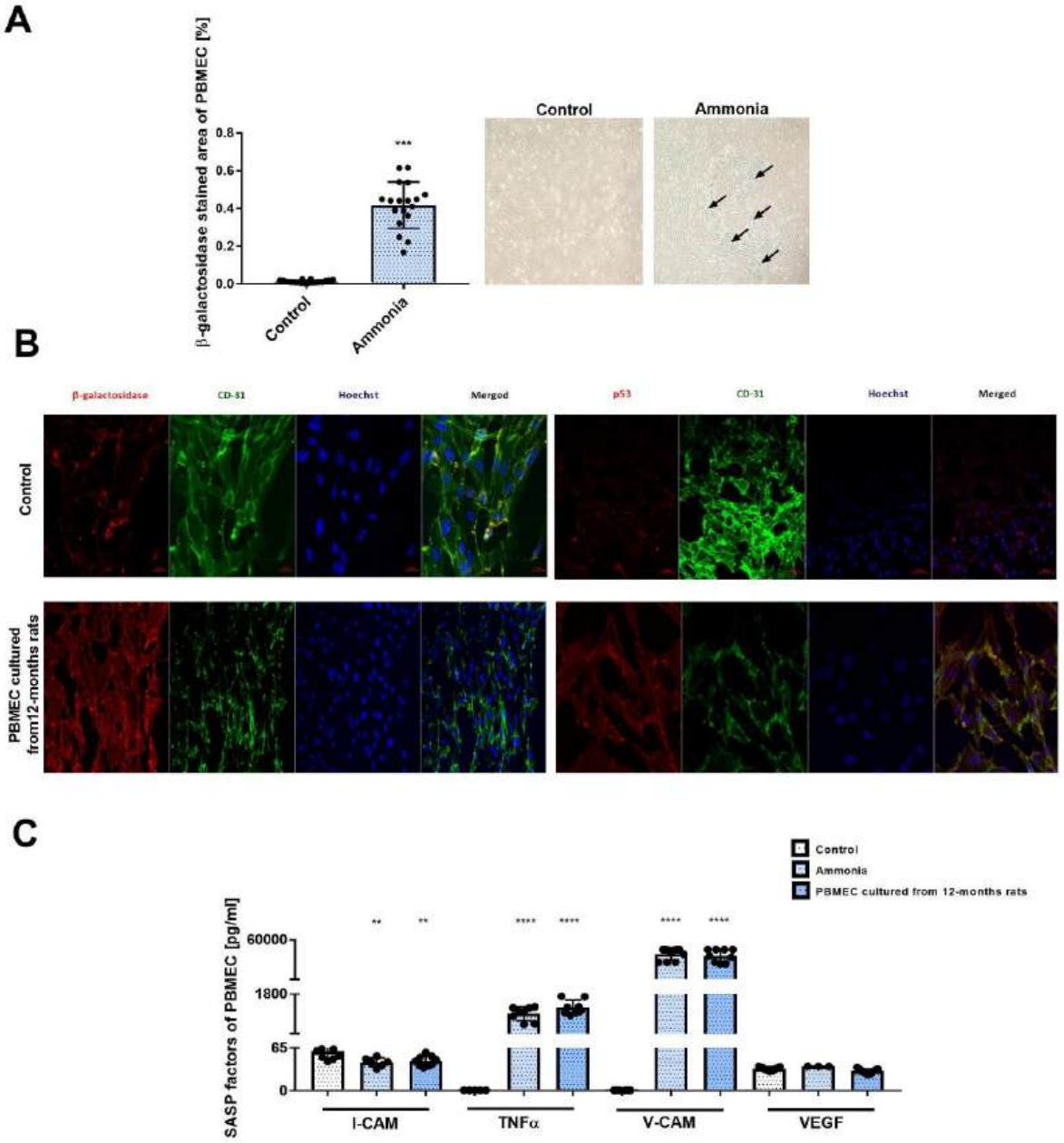

Figure 5

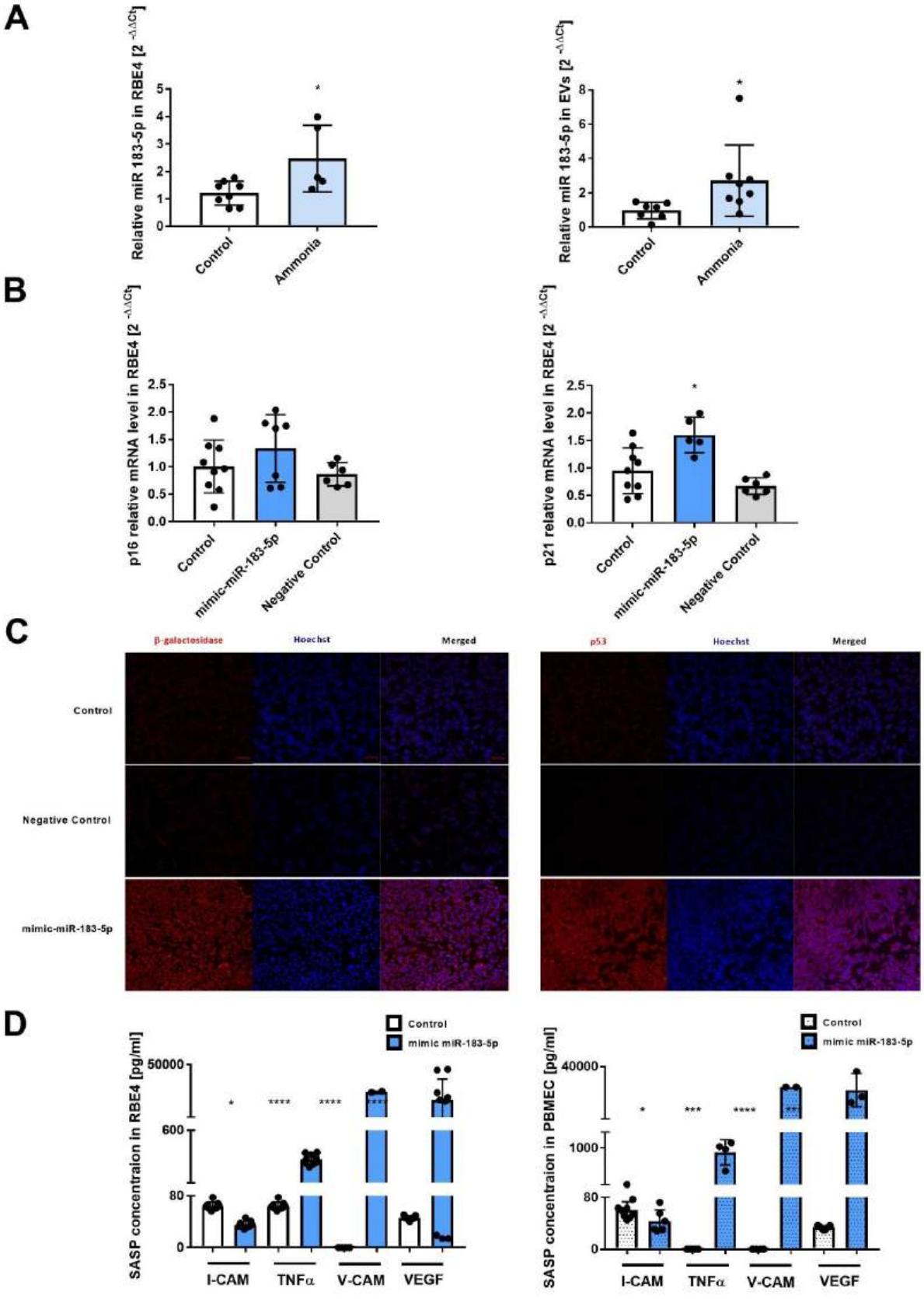

.

Unraveling Hyperammonemia-Induced Brain Saga: The Role of miRNA-183-5p in the Endothelial Senescence and Cerebrovascular Density Decline

Karolina Orzeł-Gajowik[1*], Krzysztof Milewski[2], Marta Obara-Michlewska[1], Aleksandra Ellert-Miklaszewska[3], Aneta Karpińska[4], Karina Kwapiszewska[4], Magdalena Zielińska[1*]

[1]Department of Neurotoxicology, Mossakowski Medical Research Institute, Polish Academy of Sciences, Pawińskiego St. 5, 02-106 Warsaw, Poland
[2]Laboratory of Cellular Metabolism, Nencki Institute of Experimental Biology, Pasteur St. 3, 02-093 Warsaw, Poland
[3]Laboratory of Molecular Neurobiology, Nencki Institute of Experimental Biology, Pasteur St. 3, 02-093 Warsaw, Poland
[4]Department of Soft Condensed Matter, Institute of Physical Chemistry PAS, Kasprzaka St. 44/52, 01-224 Warsaw, Poland
*Corresponding authors: Magdalena Zielińska (mzielinska@imdik.pan.pl), Karolina Orzeł-Gajowik (korzel@imdik.pan.pl)

Declaration of interests

☒ The authors declare that they have no known competing financial interests or personal relationships that could have appeared to influence the work reported in this paper.

☐ The author is an Editorial Board Member/Editor-in-Chief/Associate Editor/Guest Editor for *[Journal name]* and was not involved in the editorial review or the decision to publish this article.

☐ The authors declare the following financial interests/personal relationships which may be considered as potential competing interests:

Zrealizowane Niepodległe

Warsaw 11.05.2021

Oświadczenia autorów

Instytut Medycyny Doświadczalnej i Klinicznej
im. Mirosława Mossakowskiego
Polskiej Akademii Nauk

Zakład Neurotoksykologii

Instytut Medycyny Doświadczalnej i Klinicznej

Im. M. Mossakowskiego PAN

02-106 Warszawa ul. A. Pawińskiego 5

mgr Karolina Orzeł-Gajowik

E-mail: korzel@imdik.pan.pl

Warszawa, 15.07.2024

Oświadczenie współautora

Niniejszym poświadczam swój wkład w powstanie następującej publikacji:

PUBLIKACJA I

Orzeł-Gajowik K., Milewski K, Zielińska M. miRNA-ome plasma analysis unveils changes in blood-brain barrier integrity associated with acute liver failure in rats. Fluids Barriers CNS. 2023 Dec 8;20(1):92. doi: 10.1186/s12987-023-00484-7. PMID: 38066639; PMCID: PMC10709860.

PUBLIKACJA II

Milewski K, Orzeł-Gajowik K., Zielińska M. Mitochondrial Changes in Rat Brain Endothelial Cells Associated with Hepatic Encephalopathy: Relation to the Blood-Brain Barrier Dysfunction. Neurochem Res. 2024 Jun;49(6):1489-1504. doi: 10.1007/s11064-022-03698-7. Epub 2022 Aug 2. Erratum in: Neurochem Res. 2024 Jun;49(6):1505. doi: 10.1007/s11064-022-03780-0. PMID: 35917006; PMCID: PMC11106209.

PUBLIKACJA III

Orzeł-Gajowik K.; Gajowik, T.; Rówieniec, Ł.; Zielińska, M. The Ohm-Azing Custom-Made Transendothelial Electrical Resistance Measuring Device (and Why Is It a Current Sensation?). Sensors and Actuators B: Chemical 2024, 404, 135192, doi: 10.1016/j.snb.2023.135192.

PUBLIKACJA IV

Orzeł-Gajowik K.; Milewski, K.; Zielińska, M. Insight into microRNAs-Mediated Communication between Liver and Brain: A Possible Approach for Understanding Acute Liver Failure? Int. J. Mol. Sci. 2022, *23*, 224. https://doi.org/10.3390/ijms23010224

Wkład obejmuje:

Realizację badań, analizę wyników, przygotowaniu manuskryptów, odpowiedzi na recenzje.

Karolina Orzeł-Gajowik

Instytut Medycyny Doświadczalnej i Klinicznej
im. Mirosława Mossakowskiego
Polskiej Akademii Nauk

Zakład Neurotoksykologii

Instytut Medycyny Doświadczalnej i Klinicznej

Im. M. Mossakowskiego PAN

02-106 Warszawa ul. A. Pawińskiego 5

Prof. dr hab. n. med. Magdalena Zielińska

E-mail: mzielińska@imdik.pan.pl

Warszawa, 15.07.2024

Oświadczenie współautora

Niniejszym poświadczam swój wkład w powstanie następującej publikacji:

PUBLIKACJA I

Orzeł-Gajowik K., Milewski K, Zielińska M. miRNA-ome plasma analysis unveils changes in blood-brain barrier integrity associated with acute liver failure in rats. Fluids Barriers CNS. 2023 Dec 8;20(1):92. doi: 10.1186/s12987-023-00484-7. PMID: 38066639; PMCID: PMC10709860.

PUBLIKACJA II

Milewski K, Orzeł-Gajowik K., Zielińska M. Mitochondrial Changes in Rat Brain Endothelial Cells Associated with Hepatic Encephalopathy: Relation to the Blood-Brain Barrier Dysfunction. Neurochem Res. 2024 Jun;49(6):1489-1504. doi: 10.1007/s11064-022-03698-7. Epub 2022 Aug 2. Erratum in: Neurochem Res. 2024 Jun;49(6):1505. doi: 10.1007/s11064-022-03780-0. PMID: 35917006; PMCID: PMC11106209.

PUBLIKACJA III

Orzeł-Gajowik K.; Gajowik, T.; Rówienicz, Ł.; Zielińska, M. The Ohm-Azing Custom-Made Transendothelial Electrical Resistance Measuring Device (and Why Is It a Current Sensation?). Sensors and Actuators B: Chemical 2024, 404, 135192, doi: 10.1016/j.snb.2023.135192.

PUBLIKACJA IV

Orzeł-Gajowik K.; Milewski, K.; Zielińska, M. Insight into microRNAs-Mediated Communication between Liver and Brain: A Possible Approach for Understanding Acute Liver Failure? Int. J. Mol. Sci. 2022, *23*, 224. https://doi.org/10.3390/ijms23010224

Wkład obejmuje:

Opiekę merytoryczną i nadzór nad realizacją badań. Udział w planowaniu badań, tworzeniu koncepcji badań i założeń merytorycznych prac, analizie wyników, przygotowaniu manuskryptów, odpowiadaniu na recenzje. Pozyskiwanie środków na badania.

Wyrażam zgodę na wykorzystanie wyżej wymienionej publikacji w przewodzie doktorskim mgr Karoliny Orzeł-Gajowik

Instytut Medycyny Doświadczalnej i Klinicznej
im. Mirosława Mossakowskiego
Polskiej Akademii Nauk

Zakład Neurotoksykologii

Instytut Medycyny Doświadczalnej i Klinicznej

Im. M. Mossakowskiego PAN

02-106 Warszawa ul. A. Pawińskiego 5

Dr n. med. Krzysztof Milewski

E-mail: k.milewski@nencki.edu.pl

Warszawa, 11.07.2024

Oświadczenie współautora

Niniejszym poświadczam swój wkład w powstanie następującej publikacji:

Orzeł-Gajowik K., Milewski K, Zielińska M. miRNA-ome plasma analysis unveils changes in blood-brain barrier integrity associated with acute liver failure in rats. Fluids Barriers CNS. 2023 Dec 8;20(1):92. doi: 10.1186/s12987-023-00484-7. PMID: 38066639; PMCID: PMC10709860.

Milewski K, Orzeł-Gajowik K., Zielińska M. Mitochondrial Changes in Rat Brain Endothelial Cells Associated with Hepatic Encephalopathy: Relation to the Blood-Brain Barrier Dysfunction. Neurochem Res. 2024 Jun;49(6):1489-1504. doi: 10.1007/s11064-022-03698-7. Epub 2022 Aug 2. Erratum in: Neurochem Res. 2024 Jun;49(6):1505. doi: 10.1007/s11064-022-03780-0. PMID: 35917006; PMCID: PMC11106209.

Orzeł-Gajowik K.; Milewski, K.; Zielińska, M. Insight into microRNAs-Mediated Communication between Liver and Brain: A Possible Approach for Understanding Acute Liver Failure? *Int. J. Mol. Sci.* 2022, *23*, 224. https://doi.org/10.3390/ijms23010224

Wkład obejmuje:

Planowanie doświadczeń, koncepcji badań (publikacja 1, 2, 3), nadzór nad realizacją badań (publikacja 1, 2, 5), wykonywanie doświadczeń (praca 1, 2) analiza wyników (publikacja 1, 2, 3), napisanie manuskryptu (publikacja 1, 2, 3), przygotowanie rycin (publikacja 1, 2, 3), odpowiedzi na uwagi recenzentów.

Wyrażam zgodę na wykorzystanie wyżej wymienionej publikacji w przewodzie doktorskim mgr Karoliny Orzeł-Gajowik

IMDiK Instytut Medycyny Doświadczalnej i Klinicznej im. Mirosława Mossakowskiego Polskiej Akademii Nauk

Zakład Neurotoksykologii

Instytut Medycyny Doświadczalnej i Klinicznej

Im. M. Mossakowskiego PAN

02-106 Warszawa ul. A. Pawińskiego 5

Dr n. med. Marta Obara Michlewska

e-mail: mobara@imdik.pan.pl

Warszawa, 15.07.2024r.

Oświadczenie współautora

Niniejszym poświadczam swój udział w przygotowaniu materiału do sekwencjonowania nowej generacji.

Wyrażam zgodę na wykorzystanie wyżej wymienionej publikacji w przewodzie doktorskim mgr Karoliny Orzeł-Gajowik

Marta Obara-Michlewska

Instytut Medycyny Doświadczalnej i Klinicznej
im. Mirosława Mossakowskiego
Polskiej Akademii Nauk

Zakład Neurotoksykologii
Instytut Medycyny Doświadczalnej i Klinicznej
Im. M. Mossakowskiego PAN
02-106 Warszawa ul. A. Pawińskiego 5

Mgr inż. Łukasz Rówienicz
E-mail: lukasz.rowienicz@pw.edu.pl

Warszawa, 15.07.2024

Oświadczenie współautora

Niniejszym poświadczam swój wkład w powstanie następującej publikacji:

Karolina Orzeł-Gajowik, Tomasz Gajowik, Łukasz Rówienicz, Magdalena Zielińska, The Ohm-azing custom-made Transendothelial Electrical Resistance measuring device (and why is it a current sensation?), Sensors and Actuators B: Chemical, Volume 404, 2024, 135192, ISSN 0925-4005, https://doi.org/10.1016/j.snb.2023.135192.

Wkład obejmuje:
Zaprojektowanie i wykonanie części mechanicznej urządzenia TEER.

Wyrażam zgodę na wykorzystanie wyżej wymienionej publikacji w przewodzie doktorskim mgr Karoliny Orzeł-Gajowik

Instytut Medycyny Doświadczalnej i Klinicznej
im. Mirosława Mossakowskiego
Polskiej Akademii Nauk

Zakład Neurotoksykologii

Instytut Medycyny Doświadczalnej i Klinicznej

Im. M. Mossakowskiego PAN

02-106 Warszawa ul. A. Pawińskiego 5

Mgr inż. Tomasz Gajowik

E-mail: tomasz.gajowik@pw.edu.pl

Warszawa, 20.06.2024

Oświadczenie współautora

Niniejszym poświadczam swój wkład w powstanie następującej publikacji:

Karolina Orzeł-Gajowik, Tomasz Gajowik, Łukasz Rówienicz, Magdalena Zielińska, The Ohm-azing custom-made Transendothelial Electrical Resistance measuring device (and why is it a current sensation?), Sensors and Actuators B: Chemical, Volume 404, 2024, 135192, ISSN 0925-4005, https://doi.org/10.1016/j.snb.2023.135192.

Wkład obejmuje:
Zaprojektowanie i wykonanie części elektronicznej urządzenia TEER, przeprowadzenie badań kompatybilności elektromagnetycznej, oprogramowanie urządzenia.

Wyrażam zgodę na wykorzystanie wyżej wymienionej publikacji w przewodzie doktorskim mgr Karoliny Orzeł-Gajowik

Tomasz Gajowik

Instytut Medycyny Doświadczalnej i Klinicznej
im. Mirosława Mossakowskiego
Polskiej Akademii Nauk

Zakład Neurotoksykologii

Instytut Medycyny Doświadczalnej i Klinicznej

Im. M. Mossakowskiego PAN

02-106 Warszawa ul. A. Pawińskiego 5

Mgr inż. Aneta Karpińska

e-mail: akarpinska@ichf.edu.pl

Warszawa, 11.07.2024r.

Oświadczenie współautora

Niniejszym poświadczam przygotowanie oraz przeprowadzenie pomiarów spektroskopii korelacji fluorescencji pęcherzyków zewnątrzkomórkowych wraz z analizą uzyskanych wyników i przedstawieniem ich w formie graficznej.

Wyrażam zgodę na wykorzystanie wyżej wymienionych wyników w przewodzie doktorskim mgr Karoliny Orzeł-Gajowik.

11.07.24 Aneta Karpińska

Instytut Medycyny Doświadczalnej i Klinicznej
Im. Mirosława Mossakowskiego
Polskiej Akademii Nauk

Zakład Neurotoksykologii

Instytut Medycyny Doświadczalnej i Klinicznej

Im. M. Mossakowskiego PAN

02-106 Warszawa ul. A. Pawińskiego 5

Dr inż. Karina Kwapiszewska

e-mail: kkwapiszewska@ichf.edu.pl

Warszawa, 11.07.2024r.

Oświadczenie współautora

Niniejszym poświadczam przygotowanie oraz przeprowadzenie pomiarów spektroskopii korelacji fluorescencji pęcherzyków zewnątrzkomórkowych wraz z analizą uzyskanych wyników i przedstawieniem ich w formie graficznej.

Wyrażam zgodę na wykorzystanie wyżej wymienionych wyników w przewodzie doktorskim mgr Karoliny Orzeł-Gajowik.

K. Kwapiszewska